

ESTABLISHMENT OF DURABILITY DESIGN
TECHNIQUES TO PREVENT SPALLING OF
FACADE CLADDING IN RC BUILDINGS

RC 建築物の外装仕上げ材の剥離防止に関する耐久設
計技術の確立

2023 年 3 月

広島大学大学院先進理工系科学研究科 建築学専攻

張 沛怡

SUMMARY

The largest non-structural element in buildings, facade cladding, expresses design aesthetics while protecting structural components from weather. The most common cladding for RC buildings in Japan is rendered and ceramic tiles; however, it faces severe durability issues due to poor design, material selection, and inadequate maintenance, causing a high degree of deterioration. Typically, this cladding is composed of numerous layers of cementitious materials, with delamination being the predominant anomaly, especially between the rendering mortar and the concrete substrate. Cladding delamination can cause public safety incidents and shorten the building's lifespan. The lack of reliable methodologies and indications for assessing the durability of facade cladding makes it difficult to raise the standard of such material.

In this sense, the purpose of this study is to develop durability design techniques that can be implemented to prevent the facade cladding from peeling and spalling over time. Pre-construction performance design and in-operation preventative maintenance are crucial facade's life cycle stages.

For the performance design phase, proposed a lab-scale durability assessment method for rendering mortar/concrete adhesion that enables stakeholders to choose specifications based on predetermined targets. In this technique, a cyclic thermal load is applied to a part of the rendering mortar surface to accelerate the degradation; this part represents an external wall subjected to solar radiation. Numerical simulation and experimental results support the effectiveness of the proposed accelerated degradation method. The rate of bond strength loss can be used to rank the parameters that affect durability. This technique deviates from the norm in that it does not employ a combination of hot-cold and dry-wet cycles and only applies "partial" loads. Both are necessary for the accurate reproduction of the degradation mechanism; the former prevents erroneous reproduction of the collaborative action of the degradation agents and guarantees deterioration, while the latter offers sufficient constraints.

For the preventative maintenance phase, developed a delamination detection technique with Fibre Bragg grating sensors. Based on the relationship between the strain behavior of the materials, the technique identifies the delamination. The adhesive interface of any two cladding composition materials (concrete, rendering mortar, tiles, and tile adhesives) was examined. The moment of damage at any adhesive interface can be observed together with delamination. This technique's advantage is that continuous detection prevents early or late repairs, accidental cladding peeling, and high maintenance expenses.

While establishing the above techniques, the debonding evolution of rendering mortar was investigated. Debonding progresses on an "S-shaped" pattern, stalling at a "plateau" period. During this time, the bond strength does not diminish with the aging cycle. The bond strength test has hysteresis, requiring debonding to cumulatively approach a threshold before it can be characterized. This finding supports the need for continuous damage detection.

This dissertation summarizes a series of studies on durability design techniques. The goal is to give practitioners tools to improve the execution efficiency of a building's life cycle, extending its service life.

ACKNOWLEDGEMENTS

Since October 2017, I have spent five and a half unforgettable years at Hiroshima University. I would like to express my sincere appreciation to everyone who has and continue to offer me support.

To my supervisors, Prof. Ohkubo Takaaki and Prof. Teramoto Atsushi. I cannot adequately express how much they have helped me. In addition to my academic success, I have also received strong emotional and spiritual support from their confirmation. Thank them for their time, expertise, and comments regarding this dissertation. Being their student has been a beneficial experience that will continue to pay off for the rest of my life. I am grateful for the opportunity.

To Prof. Kawai Kenji and Prof. Tagawa Hiroshi, for the assistance and insightful remarks they provided during the process of completing my dissertation.

To the Yahata Memorial Scholarship Foundation, for providing financial support during my study for the period of six months.

To the Next-Generation of Innovative Researchers Scholarship Foundation, for awarding me a study grant for a year and a half.

To all the personnel of the Building Materials & Components Laboratory, for their assistance and moral support during the experiments, which considerably facilitated the research, and especially to my seniors, Qu Fei-Fei and Zhang Yu-Lu, who assisted me in every way upon my arrival in Japan.

To the entire Department of Architecture faculty and staff for their tremendous assistance.

Special gratitude to my close friend, Assist. Prof. Chen Xing-Chen, for her support and encouragement throughout my academic and life.

Finally, I'd like to express my gratitude to my family and friends. My father, Zhang Bin, has always had a positive outlook on education, and he instilled in me a desire for academics from an early age. Huang Ji-Hong, my mother, is the most supportive person I know. Her love and encouragement have carried me through thick and thin.

CONTENTS

SUMMARY	i
ACKNOWLEDGEMENTS	ii
CONTENTS.....	iii
LIST OF FIGURES	vi
LIST OF TABLES	x
NOMENCLATURE LIST	xi

CHAPTER I. INTRODUCTION

1.1 Background.....	1
1.1.1 Facade claddings anomalies.....	4
1.1.2 Design interventions for facade durability	6
1.1.3 Objective-based durability design.....	8
1.2 Objectives	9
1.2.1 Establishing a lab-scale method to assess the durability of mortar and concrete adhesion systems.....	10
1.2.2 Developing non-destructive testing (NDT) techniques for detachment.....	12
1.3 Scope of Work.....	12
1.4 Dissertation outline	13

CHAPTER II. LITERATURE REVIEW

2.1 Adhesion failure of facade cladding	16
2.1.1 Adhesion of the rendering mortar to the substrate	16
2.1.2 Assessment and measurement of adhesion	21
2.1.3 Environmental effects on facades	24
2.2 Approach to constructing durability assessment systems	27
2.2.1 Degradation mechanisms of rendering mortars	27
2.2.2 AT methods for studying mortar adhesion durability	30
2.2.3 Degradation patterns of mortars.....	33
2.2.4 Assessment of rendering mortar/substrate adhesion	36
2.3 NDT delamination detection techniques.....	37
2.3.1 Field-applicable NDT methods.....	37
2.3.2 Laboratory-applicable NDT methods	42
2.4 Summary	44

CHAPTER III. ESTABLISHING A LAB-SCALE DURABILITY ASSESSMENT METHOD FOR MORTAR/CONCRETE ADHESION

3.1 Proposed lab-scale durability assessment method	46
3.1.1 Proposed AT method	47
3.1.2 Dimensional design of specimens and adhesion testing	48
3.2 Numerical simulation.....	50
3.2.1 Modeling the mortar/concrete composites	49
3.2.2 Application of numerical model.....	52
3.3 Experimental test of the PTL method	54
3.3.1 Specimen preparation.....	54
3.3.2 Accelerated degradation effect tests.....	56
3.3.3 Results and discussion	58
3.4 Rendering mortar degradation pattern under PTL cycles.....	60
3.4.1 Methods	61
3.4.2 Results and discussion	62
3.5 Summary	67

CHAPTER IV. APPLICABILITY OF THE DURABILITY ASSESSMENT METHOD

4.1 Durability comparison of mortar/concrete composites	69
4.1.1 Specimen preparation.....	69
4.1.2 Durability assessment	70
4.2 A continuity approach for assessing mortar adhesion.....	74
4.2.1 Monitoring the strain behavior of specimens with FBG sensors	74
4.2.2 Experimental results and discussion	76
4.2.3 Analysis of debonding evolution based on strain monitoring results.....	83
4.3 Summary	85

CHAPTER V. DELAMINATION DETECTION WITH FBG SENSORS UNDER PTL AGING CYCLE

5.1 Experiment on small-scale specimen with tiles	87
5.1.1 Tile specimen preparation	88
5.1.2 Temperature monitoring of tile specimens.....	90
5.1.3 Strain monitoring of tile specimens	90
5.1.4 Analysis of strain amplitude.....	94
5.1.5 Response of strain behavior to adhesion state.....	97
5.2 Experiment on large-scale wall specimen.....	98

5.2.1 Specimen preparation.....	99
5.2.2 Aging cycles and delamination detection.....	100
5.2.3 Results of the bonding mortar.....	102
5.2.4 Results of the organic adhesives.....	106
5.2.5 Delamination detection of organic adhesives under freezing-thawing cycles.....	108
5.3 Summary.....	110
 CHAPTER VI. CONCLUSION AND FUTURE STRATEGIES	
6.1 Conclusion.....	112
6.1.1 A laboratory-scale durability assessment method.....	112
6.1.2 The key parameters affecting the durability of rendering mortar.....	114
6.1.3 Debonding evolution of rendering mortars under the thermal load.....	115
6.1.4 Detecting adhesion damage in tilings with FBG sensors.....	116
6.2 Future strategies.....	117
 Appendix A. Cohesive Zone Material (CZM) Mode Mixed-Mode Debonding law in AYSYS.....	
	119
 Appendix B. Effect of Curling Behavior of Mortar Due to Drying Shrinkage on Mortar-Concrete Adhesion System.....	
	121
B.1 Free curling of rendering mortar.....	122
B.1.1 Experimental procedure.....	123
B.1.2 Experimental result.....	123
B.1.3 Numerical analyses.....	125
B.2 Study of restrained shrinkage by numerical analyses.....	127
B.2.1 FE Model.....	127
B.2.2 Interfacial stress estimation under restraint conditions.....	128
B.3 Study of restrained shrinkage by DIC.....	128
B.3.1 Experimental procedure.....	129
B.3.2 Post-processing result.....	131
B.4 Effect of curling deformation on the proposed durability assessment method.....	132
B.5 Summary.....	133
 REFERENCES.....	135

LIST OF FIGURES

Figure 1-1 Average estimated service life obtained for façades claddings, considering the climatic conditions of the region in which the study was carried out, according to [11].....	3
Figure 1-2 Contribution of anomalies to the evolution of facade degradation, according to [15] ...	5
Figure 1-3 Conceptual framework for extending the service life of facades	7
Figure 1-4 Conceptual framework for objective-based durability design.....	8
Figure 1-5 Dissertation outline.....	13
Figure 2-1 Factors which exert influence on bond, according to [41]	19
Figure 2-2 The schematic illustration of the locations of the rupture surfaces during the pull-off test, according to [64].....	21
Figure 2-3 Schematic description of different experimental tests to assess the bond strength between two materials, according to [63]	22
Figure 2-4 Schematic of differences in pull-off test vs. slant shear test with respect to directions of gravity and loading, according to [50].....	23
Figure 2-5 Transition zone models of bonding interfaces in the literature.....	24
Figure 2-6 Deformation of rendering mortar	27
Figure 2-7 Failure of adhesive unity under daily solar radiation	28
Figure 2-8 Peeling and cracking due to drying shrinkage in the mortar/concrete composite specimen, adapted from [81].....	29
Figure 2-9 Debonding due to curling deformation of the overlayer, corner lift (a) and example of debonded edges (b), according to [82].....	30
Figure 2-10 Hygrothermal aging cycle, the two most used AT methods, according to [84]	31
Figure 2-11 Evolution of the adhesive strength of the specimens during the hygrothermal aging cycle, according to [85].....	31
Figure 2-12 Hygrothermal aging cycle according from Japanese Society of Finishing Standards M101	32
Figure 2-13 Four typical patterns of deterioration paths, according to [87].....	34
Figure 2-14 Evolutionary pattern of debonding of one tile, according to [89]	35
Figure 2-15 Evolution of adhesion under cyclic mechanical loading (shear stress amplitude from left to right: 1.21 MPa, 0.97 MPa, 0.81 MPa.), according to [91]	36
Figure 2-16 Monitoring of interlayer strains in composite tile-rendering-concrete specimens under artificial aging cycles, according to [13].....	41
Figure 3-1 Application of partial heating to reproduce the actual degradation condition	47
Figure 3-2 Rubber heaters for applying PTL	48

Figure 3-3 Specimen dimensions	49
Figure 3-4 Devices for bond strength tests.....	49
Figure 3-5 Mortar/concrete composites geometry	51
Figure 3-6 Modelling the mortar/concrete adhesive interface, according to [143].....	51
Figure 3-7 Thermal load conditions.....	52
Figure 3-8 Equivalent (von-Mises) stress (MPa) at the FEM model interface at 120 min	53
Figure 3-9 Maximum deformation (mm) and maximum principal stress direction of the mortar in the FEM model	53
Figure 3-10 Thermal load cycle and application.....	56
Figure 3-11 Temperature history of the mortar surface during 50 cycles	56
Figure 3-12 Contrast zones for the bond strength.....	57
Figure 3-13 Change of bond strength in both directions.....	58
Figure 3-14 Shear strength of specimens under different thermal load lengths.....	60
Figure 3-15 Aging cycles for studying degradation patterns	62
Figure 3-16 Evolution of the bond strength in the specimens submitted to the aging cycles – Peak temperature of 80 °C.....	63
Figure 3-17 Cracks on the mortar surface after thermal loading.....	64
Figure 3-18 Evolution of the bond strength in the specimens submitted to the aging cycles – Peak temperature of 70 °C.....	65
Figure 3-19 Rate of bond strength change with 70 °C aging cycles (vs. 0 cycles).....	66
Figure 3-20 Average bond strength variation for each cycle between two shear tests.....	66
Figure 4-1 Shear strength of the four types of specimens.....	71
Figure 4-2 Change rate of shear strength of specimens after degradation	72
Figure 4-3 Comparison of dimensions for FBG sensors and strain gauges	75
Figure 4-4 Arrangement of FBG sensors in the specimen	75
Figure 4-5 Temperature history of the ST specimens	77
Figure 4-6 Strain history of the SS specimens	78
Figure 4-7 Residual strain of mortar and concrete at the end of each cycle.....	79
Figure 4-8 Definition of the strain amplitude per cycle	81
Figure 4-9 Evolution of strain amplitude and strain amplitude ratio of mortar and concrete with aging cycle	81
Figure 4-10 Change rate of shear strength of SD specimens after aging cycle.....	83
Figure 5-1 Outline of tile specimen and ID of detection points	88
Figure 5-2 Tile specimens in operation and PTL ageing cycle manipulations.....	88
Figure 5-3 Temperature history of the tile specimens.....	89
Figure 5-4 Strain history of the tile specimens.....	91

Figure 5-5 Residual strain of each detection point at the end of each cycle	92
Figure 5-6 Comparison of strain behavior before and after accelerated degradation.....	94
Figure 5-7 Evolution of strain amplitude of each detection point with aging cycle	95
Figure 5-8 Evolution of strain amplitude ratio with aging cycle, (a) rendering mortar to concrete, (b) tile to rendering mortar.....	96
Figure 5-9 Outline of wall specimen.....	99
Figure 5-10 Schematic of the operation of the PTL aging cycle experiment.....	100
Figure 5-11 Temperature history of bonding mortar side.....	102
Figure 5-12 Value (left), change rate (right) of maximum SPL of impact sound.....	103
Figure 5-13 Fourier amplitude spectrum of impact sound.....	103
Figure 5-14 Strain history of concrete and tile surface	104
Figure 5-15 Strain difference between tile and concrete, (a) in the heated zone, (b) in the non-heated zone, (c) details of 33rd to 37th cycle in the heated zone	105
Figure 5-16 Ratio of the strain amplitude of the tile to concrete during each aging cycles	106
Figure 5-17 Comparison of the strain behaviour of the tiles and substrate before and after delamination.....	106
Figure 5-18 Temperature history of organic adhesives side.....	107
Figure 5-19 Acoustic diagnostic results on the organic adhesive side.....	107
Figure 5-20 Strain history of organic adhesives side	107
Figure 5-21 Strain relationship between the tiles and substrate on the organic adhesives side ...	107
Figure 5-22 Sensor configuration (left) and temperature history of concrete and tile surface (right)	108
Figure 5-23 Strain history of concrete and tile surface under freeze-thaw cycles.....	109
Figure A-1 Mixed-Mode Debonding law in ANSYS, according to [143].....	119
Figure B-1 Displacement measurement system	123
Figure B-2 The displacement of each point changes with time	124
Figure B-3 Curling deformation over 72 hours.....	125
Figure B-4 Mass loss over 72 hours.....	125
Figure B-5 Free shrinkage model.....	126
Figure B-6 Displacement results on the axial path, comparison between the experimental and numerical response.....	127
Figure B-7 Restrained shrinkage model.....	127
Figure B-8 Maximum deformation of mortar	127
Figure B-9 Equivalent (Von-Mises) Stress (MPa) in the interface.....	128
Figure B-10 DIC Specimen dimensions.....	129
Figure B-11 Measurements of the displacement field at the interface between the mortar layer and	

the concrete in the vertical direction, DIC procedure 129

Figure B-12 AOI and subset size (40×40 pixels) 130

Figure B-13 Strain distributions [μ] (in the out-of-plane direction) exhibited by specimens M-1 and T-1 at each moment 130

Figure B-14 Comparison of partial thermal loading and drying shrinkage effect on the stress state at the mortar/concrete interface 132

LIST OF TABLES

Table 3-1 Model material parameters.....	52
Table 3-2 Mix proportions of base concrete.....	55
Table 3-3 Mix proportions of rendering mortar.....	55
Table 4-1 Impact factors of the adhesion strength between mortar to concrete [145].....	70
Table 4-2 Specification of rendering mortar specimens.....	70
Table 4-3 Initial shear strength (MPa) result for each group of specimens.....	71
Table 4-4 Rate of decrease of the adhesion at the heated parts and the ends.....	73
Table 4-5 Specimen for different measurements.....	73
Table B-1 Specifications of mortar specimens.....	122

NOMENCLATURE LIST

AT	Acceleration test
ACU	Air-coupled ultrasonic
AE	Acoustic emission
CPFC	Component performance in failure conditions
CZM	Cohesive Zone Model
DIC	Digital image correlation
ET	Electromagnetic testing
EVA	Ethylene-vinyl acetate
FBG	Fiber Bragg grating sensors
FEM	Finite element model
GPR	Ground penetrating radar
IE	Impact-echo
IRT	Infrared thermography
LT	Laser testing
NDT	Non-destructive testing
NMF	Non-negative matrix factorization
NSC	Non-structural components
PCA	Principal component analysis
PSD	Power spectral density
PTL	Partial thermal load
RH	Relative humidity
SHM	Structural Health Monitoring
UAV	Unmanned aerial vehicle
UT	Ultrasonic Testing

Chapter I

INTRODUCTION

1.1 BACKGROUND

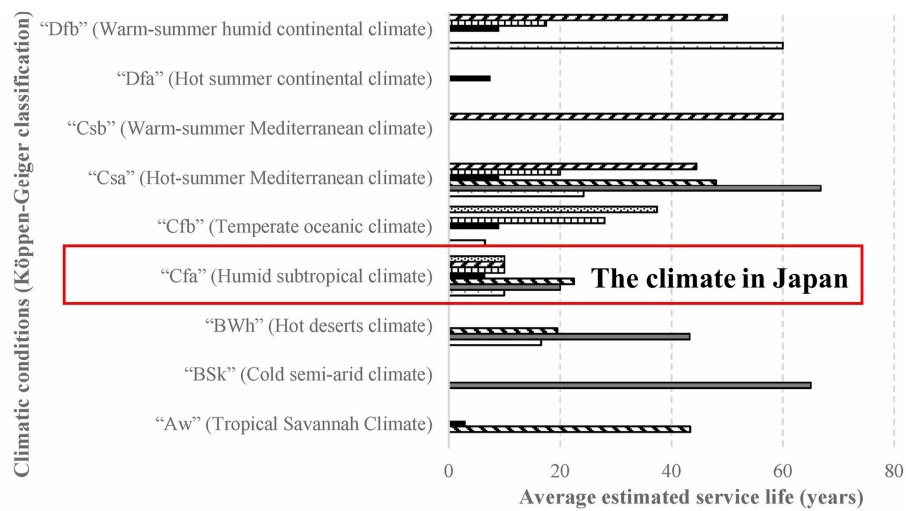
The construction materials sector is dependent on concrete and cement products. It is widely utilized in house building, bridges, airports, highways, railroads, industrial mining, and military defense projects. It is one of the most vital materials and components of infrastructure and engineering construction. Significant amounts of energy are consumed at each stage of a building's life cycle, from design and construction through maintenance and decommissioning. As the primary cementitious material used, approximately 90% of the carbon footprint of concrete comes from Portland cement [1]. Total cement production in 2021 is estimated at 4,400,000 tons [2]. Each ton of cement produced generates 0.8-1.0 tons of CO₂ (depending on kiln operation), consumes 1,700 kWh/ton of energy, and requires 1.5 tons of raw materials [3]. World construction demand is expected to remain high for a long time, and cement and other cementitious materials will remain the primary material for meeting global housing and modern infrastructure needs. Therefore, extending the service life of reinforced concrete (RC) structures and maximizing cementitious materials' use will benefit material and energy savings and reduce CO₂ emissions.

Durability is the most fundamental performance requirement of buildings. Durability is defined as "The ability of a building or its components to perform their necessary functions during a specified service life under the influence of the agents expected" [4]. It is worth pointing out that the term "service life" here refers to the physical (technical) service life, which is related to the deterioration of the building elements due to natural aging and deterioration factors. The physical service life ends when the probability of failure of a building element is more significant than a predetermined acceptable level of risk [5]. Some researchers have also introduced the concepts of functional and economical service life. The former relates to the expectations and requirements of building users. The motivation to replace materials is related to aesthetics and trends rather than a decline in technical performance. The latter is motivated by cost-efficiency considerations, as it is better to introduce new building solutions than to maintain the existing state. These two types of service life are outside the scope of this work [5].

In addition to the need to optimize the use of scarce resources, high durability guarantees to build quality and safety. These combined factors have encouraged the development of durability design techniques for buildings and components and the study of service life prediction models. Most countries in the world also have regulations that require the service life of RC structures, such as 50 years for general civil buildings in Japan. Theoretically, each component should have the same service life as the building. However, this is not the case. Structural elements, such as beams and columns, do not have the same frequency of deterioration as non-structural elements (NSEs), such as equipment, suspended ceilings, and interior and exterior finishes.

Many of the RC buildings in Japan were constructed during the period of rapid economic growth in the 1970s, and some of them have reached their required service life but are still maintained to good use. In those buildings that did not experience severe disasters (e.g., earthquakes and floods) during their service life, the durability of structural elements performed beyond expectations. In contrast, NSEs often exhibit significant degradation behavior early in their service life, even requiring several renovations and repairs throughout their life cycle, resulting in substantial public property expenditures. In addition to economic losses, the safety risks associated with low-durability NSEs are of concern, with damage to NSEs far more likely to cause injury or death in safety incidents caused by damage to building's components than structural elements [6] [7]. During the Tohoku earthquake in March 2011, injuries caused by falling ceilings in seismic shelters across Japan increased public awareness regarding the safety of NSEs. Multiple spalling accidents due to the deterioration of building facade elements are reported annually worldwide. Frequent safety accidents have increased public awareness of the importance of NSEs, and considerable attention has been paid to the performance design and safety monitoring of nonstructural components in recent years [6] [8] [9]. However, research on testing and assessment methods, design and construction, and management and maintenance techniques for the performance of NSEs are still open, and most countries have yet to establish perfect rules and indicators.

The building envelope (exterior wall cladding, sloped roof cladding, and window frames) is the NSEs that receive the most attention. Because of their role in safety, thermal and acoustic insulation, air and water infiltration/mitigation, solar energy, daylight and glare control, and aesthetics [10]. Moreover, the building envelopes are considered the first durable layer of the building, they are highly susceptible to defects that have a direct impact on the performance of the building, the comfort and quality of life of the users, and the cost of repair and maintenance [11]. The facade claddings are the NSEs with the largest application area. Facade claddings provide aesthetic expression and protect



Climatic conditions (Köppen-Geiger classification)	Average estimated service life (years)						
	Renderings	Stone claddings	Ceramic claddings	Painted surfaces	ETICS	Architectural concrete façades	Timber claddings
"Aw" (Tropical Savannah Climate)			43	3			
"BSk" (Cold semi-arid climate)		65					
"BWh" (Hot deserts climate)	17	43	20				
"Cfa" (Humid subtropical climate)	10	20	23	7	10	10	10
"Cfb" (Temperate oceanic climate)	7			9	28		37
"Csa" (Hot-summer Mediterranean climate)	24	67	48	9	20	45	
"Csb" (Warm-summer Mediterranean climate)						60	
"Dfa" (Hot summer continental climate)				8			
"Dfb" (Warm-summer humid continental climate)	60			9	18	50	

Figure 1-1 Average estimated service life obtained for façades claddings, considering the climatic conditions of the region in which the study was carried out, according to [11].

architectural elements from climatic and environmental conditions. As the "skin" of a building, it can be said that its durability directly affects the durability of the building. However, the durability of facade cladding in practice is far below what is expected for the building. Silva and Brito (2021) analyzed 107 publications and built a database on the service life of building envelope elements. They classified the average estimated service life of the facade coverings according to the climatic conditions of the study area, as in **Fig. 1-1** (Fig. 6 in [11]).

The average estimated service life of seven facade claddings (renderings, painted surfaces, ceramic and stone claddings, External Thermal Insulation Composite Systems (ETICS), architectural concrete surfaces, and timber claddings) are listed in the references, which are derived from literature reviews and expert opinions, field sampling surveys, and standards and guidelines. The facade claddings in the humid subtropical climate ("Cfa") in which Japan is located obtain the lowest average estimated service life. It is widely accepted that even the most durable ceramic and stone claddings require intensive maintenance and partial renovation/replacement after 20 to 30 years of construction

[6], making it difficult to match the 50-year service life demand for RC buildings. Therefore, the design technology for high durability of facade claddings has become a challenging and demanding task.

Mortar is essential in any facade cladding. Mortar is used in many applications and can be classified according to its use as plaster, render, tile adhesive, grout, waterproofing slurry, restoration materials, insulation and finishing systems, and others. These are usually dry-mixed mortars from specialist production plants prepared according to the application. Rendering mortars are the basis for applying all finishing materials, providing a solid, level surface for the external walls of RC buildings, and ensuring good adhesion of finishing coatings. The cementitious adhesives for ceramic tiles are known as adhesive mortar. Renderings and ceramic claddings are the two common types of facade claddings in Japan [12] and many countries worldwide, such as China [13], Portugal [14], Brazil [15], Poland [16], etc. Consequently, rendering mortars and adhesive mortars are the most produced and consumed prefabricated dry-mix mortars. World production of ceramic tiles reached 16.093 billion sqm in 2020. Consumption is 16.035 billion sqm, of which Asia accounts for around 70% [17]. Assuming an average use of 3 kg/m² for both rendering and adhesive mortars for tile coverings (a conservative estimate), this implies a world production of over 96 million tons of both types of mortar. Generally, these mortars have a service life of about 20 years and fail even after five years of use. Overcoming the non-sustainability of mortars is an important research topic and an academic aim of the authors.

1.1.1 Facade claddings anomalies

Degradation starts when the building is built, and the various anomalies that arise during the degradation process can be understood simply as defects in the facade claddings. There are many types of defects, the frequency, and severity of which depend on the geographical characteristics of the building and its use and maintenance. Researchers have generally classified facade claddings damage into the following four types [15] [18]:

- Detachment/Debonding, "Delamination" occurs when the claddings lose adhesion. (High thermomechanical stress due to sunlight exposure, joint failure, water penetration, moisture expansion, and excessive building deformation).
- Cracks, single line or interwoven, involving only the finish layer or through the entire thickness of the exterior wall. (Deformation caused by the movement of the building structure, thermomechanical stresses by the direct action of the sun).

- Joint failure, occurs in voids in the grout between the ceramic claddings and excessive joints between floors. (Inadequate grout specification, high thermomechanical stress, and interlayer shift).
- Stains, color changes on the surface of the covering, deposition of salts, microbial adhesion. (High humidity, high content of soluble salts in bricks and mortar, mold, rusting of metal elements).

The extent of damage to the facade claddings varies from defect to defect. Among them, stains and minor degrees of cracking can be classified as visual degradation [19], as they have not developed to the extent that they would lead to actual physical failure and loss of durability of the facade but still require appropriate maintenance strategies to avoid further development. Stains are usually located in areas where more rainwater is exposed, and the accumulation of rainwater in the texture of the claddings and the recesses of cracks helps microorganisms to multiply, allowing dirt to be deposited on the surface [20].

Cracking in both the cladding material and the joints can evolve toward debonding and are anomalies requiring immediate intervention. The leading cause of cracking is the movement of the substrate, which in turn is subjected to thermal solid or mechanical deformation. A high incidence of cracks is found in external walls or where there are significant dimensional changes or pressures, such as at the borders of buildings, between floors, and openings. Joint grout failures in ceramic cladding, such as cracks, and material voids, can be precursors to serious mechanical failures such as debonding. Cracks through the thickness of the facade are the most dangerous situation, which can lead to direct exposure of the structure to the environment, where water intrusion may trigger reinforcement

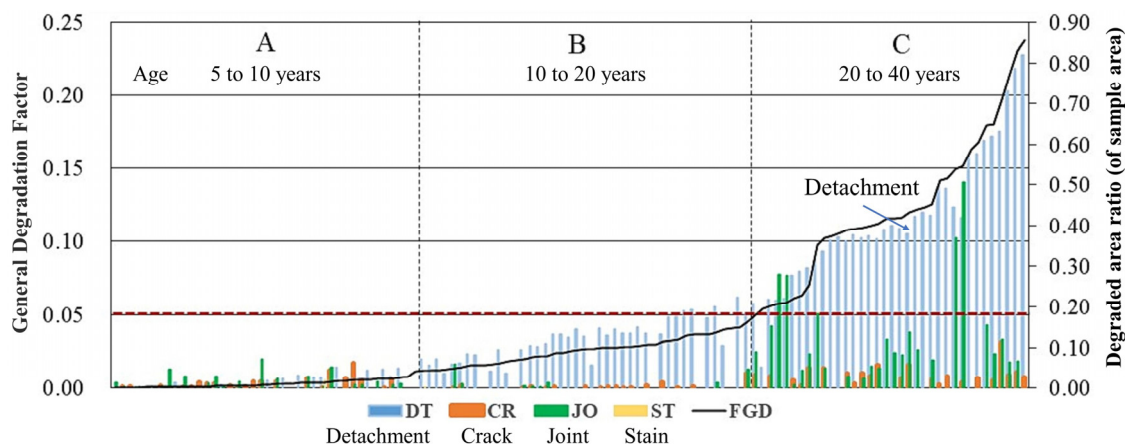


Figure 1-2 Contribution of anomalies to the evolution of facade degradation, according to [15].

corrosion and threaten the structure's safety.

These failures may eventually evolve into detachment, which depends on the progressive increase in the action of degradation agents (radiation, stormwater) and is directly related to more specific degradation mechanisms, such as thermal stress, fatigue, and deformation of the facade. Detachment represents the most severe damage to facade claddings, "peeling" leads to the failure of the protective layer and impairs the performance of the structural elements. In the worst-case scenario, a deboned cladding loses its restraint and falls from high altitudes causing accidents to people and property.

Fig. 1-2 shows the contribution of various anomalies in the degradation process of the facade, according to Bauer and Souza's investigation of a group of buildings in Brasilia with ceramic claddings. It is important to note that Brasilia does not have the same climate as Japan [15]. There is a Tropical Savannah Climate, with distinct dry and rainy seasons, where the expected service life of ceramic cladding is longer. Detachment explodes near the limit of service life. In other words, adhesion failures accelerate the overall degradation process.

Therefore, the prevention of debonding is an important research topic. A cement-rendered facade is essentially a multi-layer structure composed of different materials and ensuring the bonding integrity between the layers is essential to the durability performance. The first consideration in the durability design of a building facade is the prevention of peeling and flaking of the claddings from the concrete substrate during its life cycle.

1.1.2 Design interventions for facade durability

The facade of a building is affected by changes in the environment and the physical properties of building materials at every stage of the building's life cycle. Despite significant developments in mortar manufacture and bonding technology in recent years, facade anomalies persist, related to the poor design of construction details, inappropriate selection or/and application of materials, and inadequate maintenance [21]. Facade design decisions can interfere with service life. In the absence of a systematic approach to developing a facade design process that considers performance and durability [22], designers are often reluctant to implement novel solutions with improved durability and low maintenance requirements because the performance is difficult to prove. At the same time, high costs and technical barriers do not guarantee the efficient implementation of regular maintenance.

The current design methodology for the durability of facade cladding systems is mainly empirical. It is based on an initial value that meets the minimum requirements of the project and the codes and standards ((e.g., bond strength after construction) and empirical assumptions. If these rules are met,

the system is considered to achieve an acceptably long but unspecified life. Further consideration of durability may lead to an increase in building durability. However, this is a short-sighted and controversial approach. Because a design approach that only meets the initial performance required by standards without sufficient consideration and subsequent issues (such as environmental impact and sustainability of performance, inspection needs, and maintainability) does not allow for the definition of whole life costs, i.e., there is no way to prove that future maintenance and repair costs will be reduced. In particular, defects require immediate intervention and can bring repair costs even higher than the initial costs (because of the inclusion of a removal step). Properly designed and applied durability is entirely worthwhile if maintenance costs are considered [22].

Fig. 1-3 shows a conceptual diagram for extending the service life of a facade, where durability design is essential to achieve the desired tile performance. At this stage, full consideration should be given to the details of material degradation, including degradants-atmospheric, biological, loading, incompatibility and use, and maintenance actions [23]. According to Chew et al. [24], identifying materials with improved durability gradients is the solution to resist natural aging. Applying highly durable materials and construction techniques can slow down the degradation rate. Secondly, the life of a facade depends on environmental factors or extreme events beyond the designer's control. Regular inspection, maintenance, repair, or timely replacement of facades can significantly improve building performance and owner satisfaction. Durability design is about establishing methodological procedures that balance intended function, investment costs, and maintenance efforts to maintain the building at a high performance [5].

1.1.3 Objective-based durability design

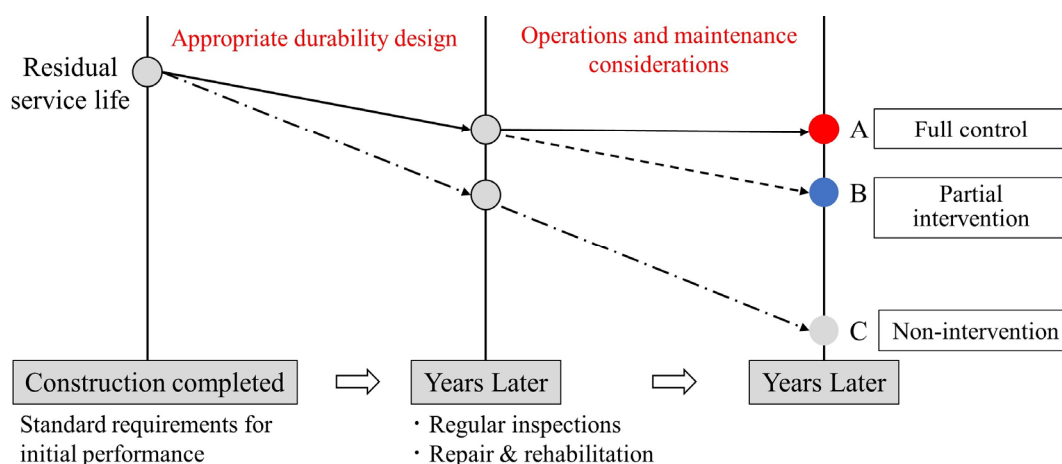


Figure 1-3 Conceptual framework for extending the service life of facades.

Concept “Objective-based durability design” is built on the Concept “Performance-based durability design” [25] [26]. Performance approaches are based on the measurement of material properties that can be linked to deterioration mechanisms under prevalent exposure conditions. The measurement of actual concrete material properties of the as-built structure allows accounting for the combined influences of material composition, construction procedures, and environmental influences and therefore forms a rational basis for durability prediction and service life design [26]. Applying this concept to the durability design of facades, we wanted to establish clear service life objectives. Durability design techniques are developed around the purpose required by the user, and such procedures allow specifications to be selected according to the purpose set. **Fig. 1-4** presents an overview of the proposed conceptual framework.

The designer first needs to define the service life objectives. Designing durability depends on the erosion of the environment in the area where it is applied and should be carefully identified and classified. Once the degradation agents have been identified, the degradation mechanisms and patterns need to be clarified, and a deterioration model developed. It is important to note that different degradation models should be developed for other building parts. According to the “layering principle” proposed by Brand [27], different parts of the same building degrade at different rates and patterns.

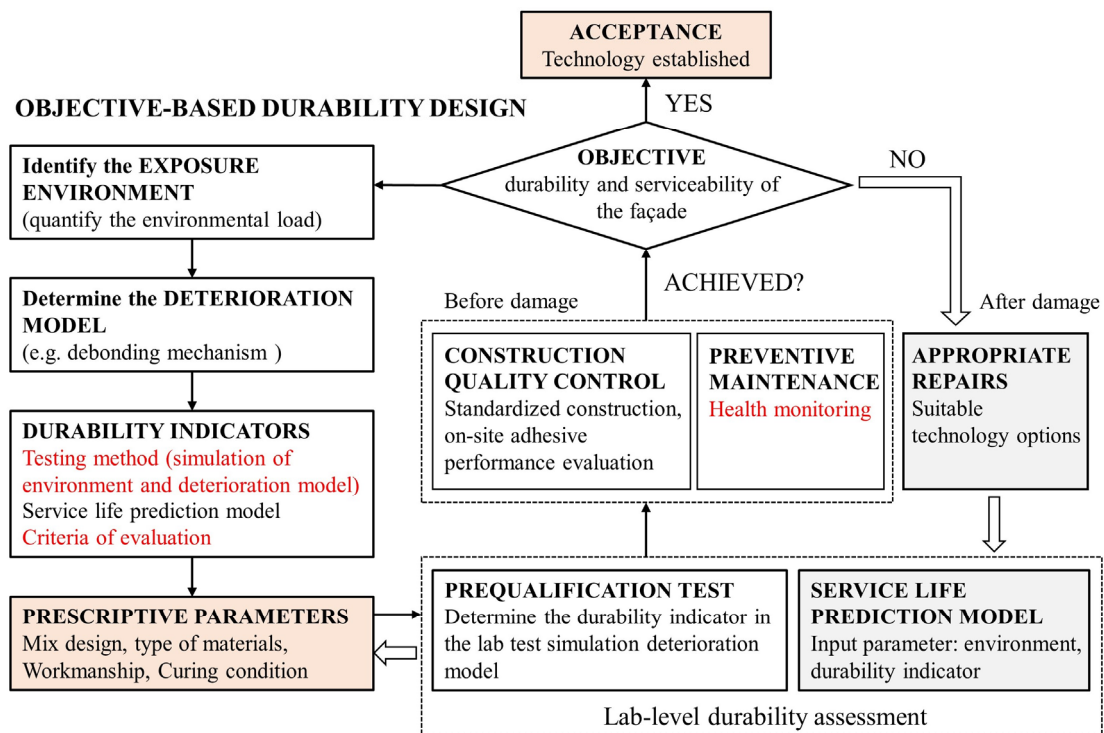


Figure 1-4 Conceptual framework for objective-based durability design.

High exposure to degradation agents does not necessarily mean higher levels of degradation, and other conditions are needed to allow degradation mechanisms to develop. This mechanism action is a process that involves chemical reactions, deformations, and mechanical efforts, among others [15]. Next, a lab-scale durability test method needs to be established. The method should be able to reproduce the impact and degradation mechanisms of the degradation agent. Further, a predictive model for service life is based. Durability metrics are related to the predicted service life and need to integrate the results of laboratory tests with long-term practical applications. Controllable durability influencing factors are specified as normative parameters and are optional specifications. The proposed technology can be applied in practice once it has passed the lab-level durability assessment. In addition, the control of construction quality, preventive management, and the expected scope of repairs are all mandatory considerations of the durability design. After all the necessary interventions have been completed, the techniques/specifications used in the design can be standardized if the product can meet the service life objectives.

Although it may take decades to establish a complete program, it has long-term implications. The objective-based design provides stakeholders with a reliable alternative because it uses realistic environmental and material models and can predict the future behavior of concrete structures, thereby quantifying the design life.

-Design based on total life cycle costs will be possible - Reduced material and energy consumption by optimizing the use of materials.

-Provides an objective basis for user-tailored design, primarily when the design is based on industry-specific material properties.

-The proposed durability testing procedures can be extended to new materials and applications. The framework for design procedures can provide an objective basis for predicting the behavior of new materials in use.

-Predictions of service life will be more reliable, thereby reducing premature dismantling and repair of components.

1.2 OBJECTIVES

The rendering mortar in the facade cladding of RC building is the chosen object of this work. As the first cementitious material comes into direct contact with the concrete substrate, the rendering mortar is responsible for connecting the concrete substrate and the finishes, but detachment frequently

occurs. Therefore, a series of studies have been carried out to maintain the adhesion integrity between the rendering mortar and the concrete, to improve the durability of facade claddings.

As shown in **Fig. 1-4**, the efficiency of the implementation of three phases determines the service life of a building: 1) pre-construction durability design, 2) preventive maintenance, and 3) appropriate and timely repair. The authors' research during my Ph.D. was distributed in two phases, 1) and 2), with separate research objectives established. The research objective for the durability design phase was to establish a laboratory-scale durability assessment system. The preventive management phase aimed to develop efficient non-destructive damage (detachment) detection techniques.

1.2.1 Establishing a lab-scale method to assess the durability of mortar and concrete adhesion systems

Reliable lab-scale durability evaluation methods are a prerequisite for selecting durable design techniques and material specifications based on objective service life. Research on high-adhesion rendering mortars has been significant gains, but some obstacles still make it challenging to apply them in practice. First, for commercial dry-mix mortars, current Japanese regulations only provide requirements for initial performance after construction and acceptance and do not have complete durability evaluation indicators like concrete. Therefore, manufacturers generally cannot offer accurate product durability and operational details required about durability. Second, the durability assessment methods for rendering mortars recommended by national codes are less convincing, as poor consideration of degradation mechanisms. This makes improving the durability of rendering mortars in actual projects challenging. Therefore, the establishment of durability assessment methods is an urgent research task.

Durability assessment methods generally consist of two tests, 1. Accelerated testing can reproduce the impact and degradation mechanisms of degradants in the laboratory. 2. Performance tests. Therefore, this study can be further divided into the following two objectives.

(1) Elucidate the degradation mechanisms and degradation patterns of adhesion integrity between rendering mortar and concrete

Determining a performance degradation model is the first step in establishing a durability assessment methodology. The characteristics of the degradation model depend on identifying current degradation mechanisms, anomalies, and external mechanical, electromechanical, thermal, chemical, and biological agents [21] and contain three key parameters, degradation agents, deterioration

mechanisms, and deterioration patterns.

Degradation agents are necessary factors (mainly climatic factors) that trigger the deterioration process. The material's response to the degradation agent is defined as the degradation mechanism, which depends on the agent as well as on the materials itself and its location (interference of other elements). In the case of rendered mortar-concrete bonding systems, the loss of adhesion is a phenomenon caused by the failure or rupture of the interface between mortar and substrate due to the generation of tensions that exceed the resistance of the connection. The leading cause of interface damage is the hygrothermal effect, and radiation and rain are key degradation agents. Several studies using both agents to reproduce degradation mechanisms in the laboratory have been conducted, but no satisfactory results were obtained, proving the complexity of the synergistic mechanisms between agents. Therefore, elucidating the relationship between degradants and degradation mechanisms on a case-by-case basis is an introductory approach.

A deterioration pattern is the pattern of performance evolution over time under a specific deterioration mechanism, which a qualitative curve can generally represent. The deterioration pattern determines the scheduling of performance tests and durability evaluation results and is essential for establishing durability evaluation methods. Therefore, it is a sub-objective to plot the degradation curves of the adhesive properties of rendered mortars based on specific degradation agents and degradation mechanisms.

(2) Determine the Accelerated testing (AT) and bonding performance test methods.

AT can be expressed as "compressed time within a reasonable test time to accelerate the failure mechanism so that product reliability can be evaluated." Increasing the frequency of use and the load level of the test equipment is a common model for AT. Since there is usually more than one degradation mechanism, combined models are recommended. But it is difficult to simulate all degradation mechanisms and the way they interact with each other. Therefore, selecting the most representative degradation mechanisms for the specific application conditions of the material to develop a particular AT is a solution. As mentioned previously, temperature and humidity are essential parameters for mortar degradation. Therefore, this study investigated the two parameters separately to establish the most suitable AT for rendered mortars.

Directing the durability assessment to the desired performance will ensure a more durable solution. This study considers the bond between the rendering mortar and the concrete substrate as the most critical parameter, but the bond strength is highly variable depending on the test method. Several

representative bonding performance test methods were investigated to obtain a bonding performance reflecting durability.

1.2.2 Developing non-destructive testing (NDT) techniques for detachment.

Effective damage detection techniques are critical to developing maintenance strategies, and timeliness and accuracy are crucial. Timeliness requirement prevents missed inspections and reduces and avoids the presence and evolution of defects. Accuracy requires reducing premature repairs due to incorrect judgments and reducing maintenance and repair costs. As mentioned earlier, detachment is the most dangerous form of failure; therefore, delamination detection is a crucial technology. This is particularly the case where delamination cannot be directly observed, as it can lead to lowered vigilance by managers and further deterioration in the form of crack formation and tile spalling. NDT is the ideal method for detecting subsurface damage and is desired by building owners. The authors investigated several common NDT techniques and concluded they have difficulty balancing timeliness and accuracy. Therefore, the development of efficient layered inspection techniques became a research objective.

1.3 SCOPE OF WORK

This study is part of establishing the durability design procedure, and the work scope is marked in red in **Fig. 1-4**. The degradation mechanisms of the rendered mortar were investigated, and the effects of temperature and humidity on the adhesion properties were discussed separately. A lab-scale durability assessment method is proposed, consisting of two tests, the AT and the adhesion strength test. Numerical simulations and experiments verified the validity of the AT. Based on the AT, investigated the deterioration pattern of the mortar. The decrease rate of the bond strength was used as a critical durability parameter to determine the best performance evaluation pattern.

Several influencing factors were investigated using the proposed durability evaluation method, including the mortar's water-cement ratio, admixtures, thickness, workmanship, and curing conditions. Previous studies investigated the effects of these parameters on the initial bonding performance, and this study further evaluated their impact on durability.

Several non-destructive methods of delamination detection are investigated, and a technique for strain monitoring using fiber Bragg grating (FBG) sensors is proposed. The technique was piloted in two overlays: rendered mortar and ceramic tile. The scope of the study includes the feasibility,

sensitivity, limitations, and development potential of the technique.

This study aims to ensure that the proposed durability assessment method enables a comparison of the durability of several different product specifications. Predicting the actual service life is not considered, as this would involve another complex area of research. Furthermore, although rendered mortar is the subject of this study, the proposed method can be extended and adapted to include different cladding and coating solutions in RC building facades.

1.4 DISSERTATION OUTLINE

The outline of this dissertation is shown in **Fig. 1-5** and consists of six chapters. The following is a summary of each chapter's content.

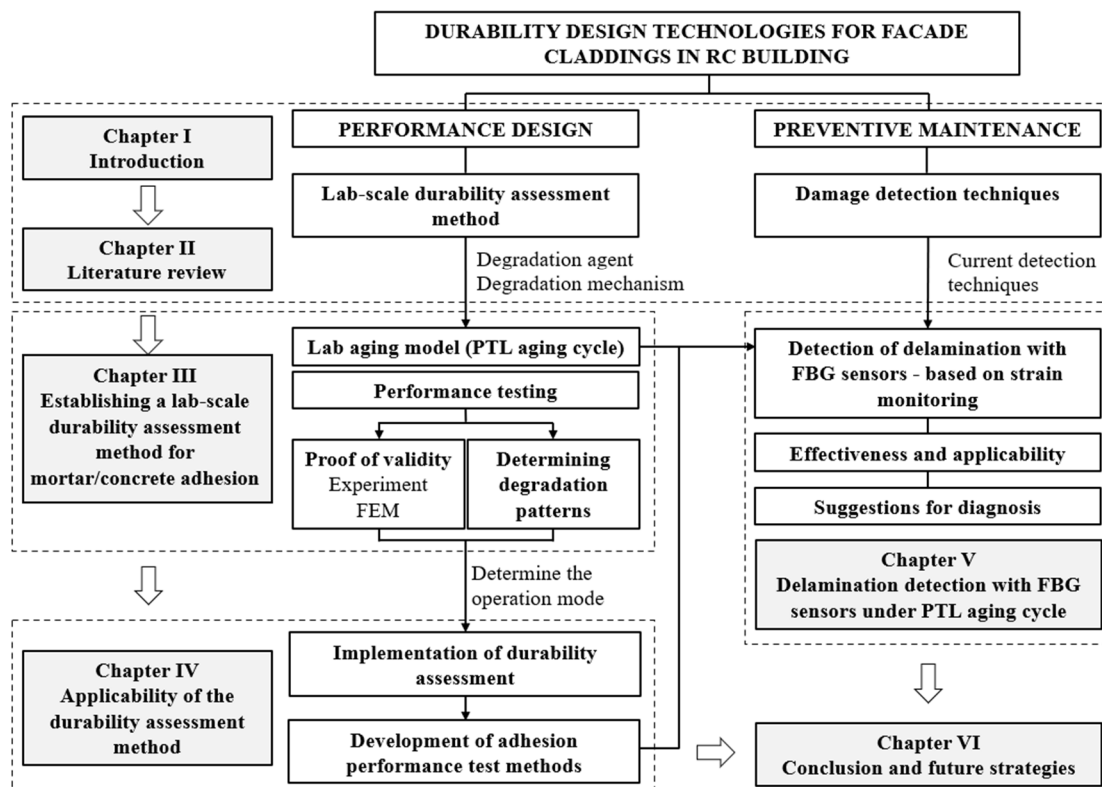


Figure 1-5 Dissertation outline.

Chapter 1

This chapter outlines the study's background, subjects, and goals. Describes the durability problems and societal requirements of facade claddings for RC buildings, along with the significance of establishing objective-based durability design methodologies. This work is focused on performance design and preventive maintenance technologies.

Chapter 2

This chapter reviews exceptional previous studies in the relevant field. Factors impacting adhesion, adhesion failure, degradation agents and degradation mechanisms, and damage detection techniques for rendered and tiling facades are the main topics covered. The fundamental procedure for constructing a durability evaluation method is described, along with the rationale for solar radiation as the principal environmental degradation agent.

Chapter 3

This chapter describes the development phase of the durability assessment method for rendering mortar/concrete adhesion. An artificial aging model is defined. The degradation mechanism under solar radiation is reproduced by applying partial thermal load (PTL aging cycle) to the rendered mortar surface. Experimental and numerical results prove this method works. PTL aging cycles were used to examine the debonding evolution of rendering mortars, confirming the unsteady nature of this process. It is concluded that continuous detection technology is necessary to improve execution efficiency as there is a risk of missed detection with the periodic damage detection methods. Furthermore, the influence of curling deformation caused by drying shrinkage on mortar adhesion was investigated (Appendix B). It was determined that the detrimental effects of curling deformation should not be ignored, and several procedures (wet curing and application of SRA) to ensure uniform drying of the mortar during curing are useful countermeasures.

Chapter 4

This chapter describes the implementation phase of the durability assessment method proposed in Chapter 3. It is possible to rank the durability of four types of specimens created utilizing distinct processes. The proposed durability assessment method benefits product development, especially for items lacking application history. It shows the material's response to solar radiation. It can be rapidly tested for durability by comparing it to a reference material with a long application history. Moreover,

discussed the limits of the bond strength tests for measuring adhesion performance; hence a strain-monitoring approach is developed to analyze adhesion loss continually. The experimental results demonstrate the method's growth potential because of its ability to capture the instant damage that occurs precisely.

Chapter 5

Based on the findings presented in Chapter 4, this chapter investigates further the application of the strain monitoring method to the damage detection of facade tilings. On tile specimens of two distinct sizes and compositional materials, FBG strain sensors were used to measure the layer strains. Observed the instant of damage at any interface. Information was provided regarding the viability of this procedure, its applicability, and the interpretation of the test results. Strain monitoring methods can minimize unnecessary or delayed repairs and, as a result, significantly reduce the danger of inadvertent tile spalling.

Chapter 6

This chapter includes the major conclusions from Chapters 1 through 5 of the dissertations, as well as recommendations for further research.

Chapter II

LITERATURE REVIEW

2.1 ADHESION FAILURE OF FACADE CLADDING

Ceramic cladding facades consist of a substrate, a render, an adhesive layer, tiles, and grout between the tiles. The properties of each layer result in different responses to environmental activities and aggressive factors. As each layer in the system adheres to the other, the response of each layer also affects the behavior of adjacent layers. Such differences in behavior are known as “differential movement” between layers. If differential movement is restricted, internal stresses accumulate, leading to adhesion failure in debonding and cracking. Adhesion failure is a natural degradation process, and several factors influence its progression, for example, the bond quality of the rendered mortar and concrete, environmental exposure, service conditions, and maintenance frequency [37] [39]. Without interference from maintenance strategies, the adhesion quality represents the initial resistance to degradation. The degradants provided by environmental exposure trigger the operation of the degradation mechanism (differential movement) and determine the degradation pattern. Initial bond quality can be improved in various ways, and much effort has been made to do so. Although environmental conditions are uncontrollable, understanding the effects of various environmental factors on facades can help decision-makers suit durability design to local needs and are essential for establishing lab-scale durability assessment methods. The following is a survey of the relevant published studies.

2.1.1 Adhesion of the rendering mortar to the substrate

Adhesion failure can occur at the bonding interface of the layers of material, and some researchers have suggested that the interface between the bonding mortar and the tiles may be the weakest in the entire tiling system [30] [31]. The authors offer a different view, suggesting that adhesion failure mainly occurs at the bonding interface between the two cementitious materials, i.e., between the rendering mortar and the concrete substrate or between the rendering mortar and the tile adhesive. Firstly, special tile adhesive mortars add more polymers to meet the bonding requirements and lead to a higher modulus of elasticity. The thickness of the bonding mortar is usually 1/5 to 1/10 of that of the rendering mortar, and the more excellent deformability and smaller thickness reduce the

difference in movement between the layers. Secondly, to increase the contact area with the adhesive, manufacturers create textures on the underside of the tiles, and these grooves form a solid mechanical fit. In addition, organic adhesives with strong deformability have been used extensively in recent years. Conversely, rendered mortars are more prone to bond failure due to their lower performance requirements (mainly to provide a smooth surface for the facade).

Rendering mortars made with Portland cement have some disadvantages. These disadvantages include 1) low tensile, flexural, shear, impact, and adhesive strengths, 2) large drying shrinkage, 3) tendency to crack with changes in temperature and moisture, 4) relatively high moisture absorption and permeation, 5) low resistance to corrosive agents, and 6) rapid loss of gauging water in thin surfacing by evaporation and substrate absorption [32]. The dominance of rendering is mainly due to its low cost and the relative lack of expertise in execution compared to other claddings and coatings [33]. Low investment often means an unacceptable level of degradation due to restricted performance and execution defects.

Weak adhesion can significantly accelerate the degradation process. Hence the adhesion behavior of mortars has been extensively studied. This section investigates the adhesion mechanisms of mortars and discusses the factors influencing the adhesion between rendering mortars and concrete substrates. However, the understanding of adhesion mechanisms is not limited to concrete substrates. It can be extended to the adhesion of mortars to all porous materials such as stone, ceramics, masonry, and even wood.

(1) Adhesion mechanism of mortars

“Adhesion” describes joining two materials with the same interface in a boundary layer. Kinloch [34] proposed five theories to explain the mechanism of the formation of intrinsic adhesion, including mechanical interlocking, diffusion theory, chemical bonding, electronic and adsorption theories. In any adhesion system, several adhesion mechanisms often act in concert, and it is difficult to identify the individual contribution of each mechanism. The interpretation of the adhesion mechanisms between two contacting materials is complex, with the structure and properties of the object and the adhesive determining how these mechanisms occur [35]. The mechanical interlocking and chemical bonding theories are the commonly proposed adhesion mechanisms on mortar to concrete.

- The theory of mechanical interlocking, where fresh mortar penetrates defects (porosity and roughness) in the surface of the concrete substrate, occurs after hydration.

- In chemical bond theory, where the degree of adhesion of a mortar is defined by the primary

and secondary chemical bonds formed at the interface. The bond strength depends on the contact between the phases. The greater the contact, the greater the bond strength.

Mechanical interlocking is considered to be the main contribution to bonding forces [36] [37] [36]. Based on the magnitude of concrete surface defects in mechanical interlocking theory, the researchers divided the adhesion of mortar into microscopic adhesion and macroscopic adhesion. Microscopic adhesion means that the mortar penetrates the pores on the surface of the substrate and forms a tiny "anchor" after hydration. Macroscopic adhesion is where the mortar fills the texture on the surface of the substrate, and the substrate holds the mortar projections in place, creating a macroscopic "bite." [36] The adhesion effect depends on the ability of the mortar to penetrate the substrate and the contact area of the interface.

Chemical bond also contributes to adhesion and, in particular, can explain the enhanced bond strength effect of adding re-dispersible powders polymers. Adhesion is understood to be the result of molecular attraction between the phases. Van der Waals forces are mainly formed between material molecules and are responsible for the bonding of multiphase materials [38]. Sakai and Sugita [39] investigated polymer-modified cement and mortar's microstructure and compounding mechanism. It was concluded that the improvement of mortar adhesion ability was related to the formation of polymer films at the interface. Mansur et al. [40] investigated the effect of EVA (poly (ethylene-co-vinyl acetate)) re-dispersible powders content on the mortar/tile interface by concluding that the enhanced adhesion was attributed to the formation of a hybrid ceramic-polymer interface based on hydrogen bonding between the silanol groups on the tile surface and the hydroxyl groups of the hydrolyzed EVA. The researchers concluded that the chemical interaction between the cement and the polymer compound, the formation of polymer films, and the formation of hydroxyl groups during hydrolysis in the polymer are beneficial for adhesion.

(2) Factors affecting the bond between mortar and concrete

Adhesion results from the interaction between two materials and are subject to many material parameters and environmental conditions. Carasek et al. [41] divided the proven factors into five main categories, as shown in **Fig. 2-1**. These are a) the characteristics and properties of the substrate, b) the characteristics of mortars and their constituent materials, c) the mortar's application technique, d) the climatic conditions at the time of execution and the lifetime of the render, and e) the time span after mortar application.

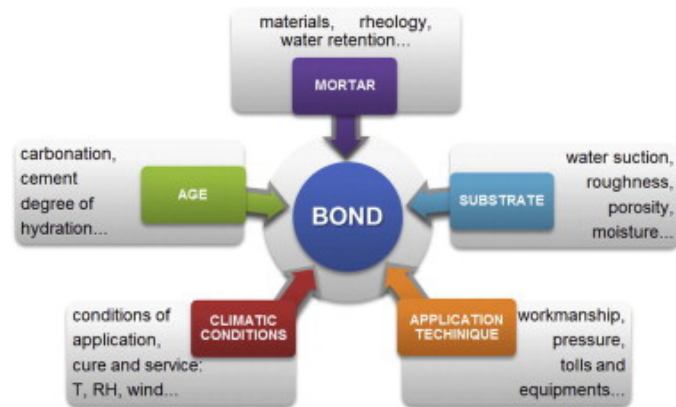


Figure 2-1 Factors which exert influence on bond, according to [41].

These factors act in two directions, one affecting the strength of the mortar and the substrate themselves and the other involving the contact between the mortar and the substrate. The strength of the substrate and the mortar itself also influences the bonding properties, but it is inefficient. Based on the mechanical interlocking theory, the contact form bonding interface is the decisive factor.

i) Short-term bond strength

The formation of microscopic adhesion depends on the water absorption of the substrate, the porosity, and the water retention capacity of the mortar. The balance between the water absorption of the substrate and the water retention of the mortar has a strong influence on the bond strength. In combinations of highly absorbent substrates and low retention mortars, excessive water release from the mortar leads to insufficient hydration of the mortar near the interface and a reduction in strength [42] [37]. In the combination of a low absorbent substrate and a high retention mortar, the low intrusion rate of the mortar into the substrate hinders the formation of microscopic adhesion [37]. In addition, a low absorbent substrate means that the bonding interface will have a water-secreting layer and a high water-to-cement ratio at the interface, resulting in a meager mortar strength close to the interface area [43]. The water retention capacity of mortars is mainly influenced by the volume of fines in the mixture. Paes et al. [44] concluded that mortars produced with larger aggregate particles retain water poorly and favor water transport from the mortar to the substrate.

The macroscopic adhesion depends on the ratio of the effective adhesion area to the potential contact area [36]. It is directly related to the interface roughness and the rheological properties of the mortar. The interface texture determines the possible contact area, while the rheological properties of the mortar determine its ability to penetrate the interface texture, i.e., the effective contact area. A

mortar with low workability will have difficulty filling irregular parts of the substrate, and voids and microcracks at the interface will significantly reduce the bond strength [45]. Furthermore, insufficient contact area accelerates degradation and adversely affects long-term bonding performance. Melo et al. [46] state that a 30% reduction in contact area may reduce the system's ability to withstand deformation by more than 70%.

The application technique of the mortar is also a decisive factor. The vast majority of short-term bond failures are the result of poor construction. These aspects include the amount of mortar per unit area, plastering pressure [47], open time [45] [47], curing method of the mortar [48] [49], pre-treatment of the interface (degree of wetting and cleaning) [50] [51], and bond agent use [37]. The five main factors that Silfwerbrand [52] identifies as affecting bonding performance are almost all related to the construction technique; the microcracking, laitance, and cleanliness of the concrete, and the compaction and curing procedures of the overlayer. The first three parameters are related to the pre-treatment of the interface. The treatment of concrete substrates is usually used for cleaning, removing scaling layers, and roughening the interface. However, improper handling can induce microcracking [53], [54], [55], such as hammering and pickling [56]. The use of the correct tools and quality control during execution is critical.

ii) Long-term bond strength.

Most studies mentioned above relate only to short-term bond strengths, which are generally tested within six months of the mortar curing. This may be because long-term bond performance is influenced by the factors mentioned above, but also by environmental factors that must be considered. The inherent stochastic nature of natural phenomena makes studies relating to assessing and predicting long-term bonding performance involve much uncertainty. At the same time, environmental exposure experiments are limited by geographical characteristics and are time-consuming. However, from studies relating to repair mortars and bond degradation, it is possible to summarize the two properties that are most influential in long-term bond performance, the ability of the substrate and mortar to resist “differential movement” and the resistance of the mortar to crack. [7] [57] [58] [59] [60].

Wetzel et al. [59] observed the development of bond failure at the glass-bonded mortar interface through glass blocks. They concluded that interface damage was caused by initial shrinkage and thermal cycling and was exacerbated by wet thermal cycling and water ingress. Tran et al. [61] simulate debonding propagation at the interface between a matrix of old concrete and a thin cementitious bond. Granju [60] also concluded that adding fibers inhibited the thin overlayer's

cracking, thereby increasing the adhesion durability to the substrate. Jenni et al. [45] suggest that using a low modulus of elasticity polymer-modified mortar between the finishing material and the substrate can significantly reduce the stress concentration at the bonding interface. Al-Ostaz et al. [62] investigated the durability of the bond between the repair material/concrete using hot-cold cycle aging tests. It was concluded that there was a strong correlation between the incompatibility of the thermal expansion and the modulus of elasticity and the reduction in bond strength. In particular, the modulus of elasticity and the coefficient of thermal expansion of the overlay are critical properties affecting the long-term bond performance under temperature fluctuations compared to the base concrete.

It is considered that mortar cracking also results from the fact that its deformation is constrained by the substrate, whether by drying and shrinking or by thermal expansion and contraction. It can therefore be argued that the "followability" of the mortar to the substrate's deformation determines the adhesion durability.

2.1.2 Assessment and measurement of adhesion

Descriptions of the factors influencing adhesion are often contradictory in the literature, which the authors consider dependent on the adhesion assessment method. Generally, testing the bond strength, i.e., the stress required to separate the substrate from the overlayer. There are various methods of testing the bond strength, e.g., whether to assess the shear strength or the tensile strength of the interface. It also depends on the location of the fracture, i.e., inside the mortar (mortar cohesion failure), at the interface (adhesion failure), or inside the concrete (concrete cohesion failure), corresponding to (a), (b), and (c) in Fig. 2-2 [64], respectively.

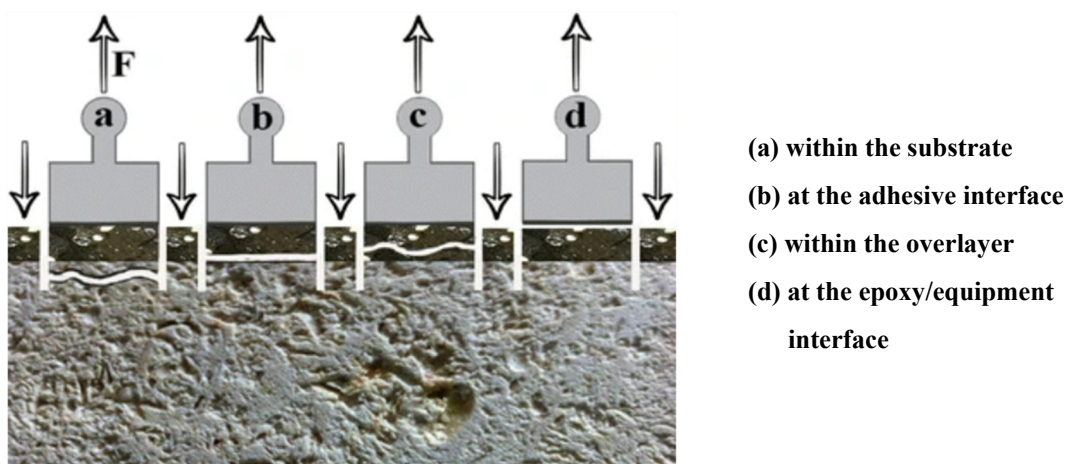


Figure 2-2 The schematic illustration of the locations of the rupture surfaces during the pull-off test, according to [64].

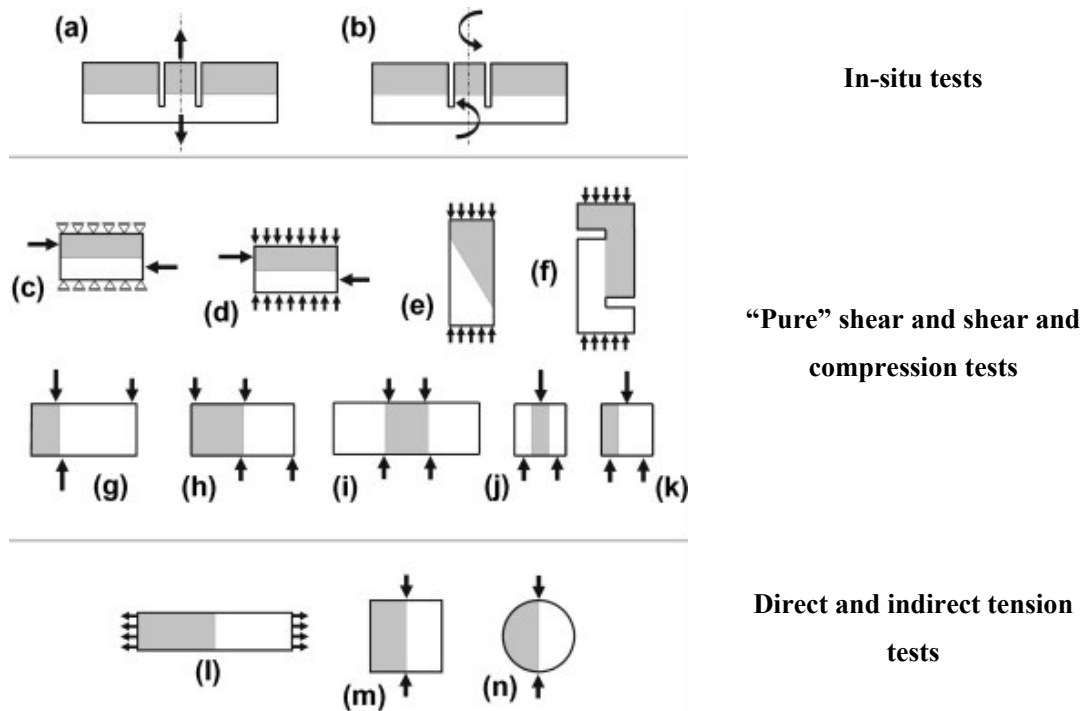


Figure 2-3 Schematic description of different experimental tests to assess the bond strength between two materials, according to [63].

(1) Bond strength test method

Common bond strength test methods include interfacial shear, torsion, and tensile testing. Bond strength values obtained by different test methods can vary considerably, as the results depend on specimen size, test set-up, loading rate, etc. In the literature, these methods are often used in combination to study the response of a bond interface subjected to different stress states. Espeche and León [63] summarize the commonly used method. There are three main groups: tension, ‘pure’ shear, and shear and compression-based tests (**Fig. 2-3**). The first group includes the pull-off test (a), the direct tension test (l), and the splitting tension test (m, n). The second group is broader and includes the torsion bond test (b), the direct shear test (c), the modified vertical shear bond test or compact shear test (f), the push-out test or push-through cube (j), the bi-surface shear test (k), and the guillotine test (g, h, i). The third group consists of the slant shear test (e) and the shear-compression test (d) [63]. The direct pull-off test (a) is the most popular because it can be performed in situ. However, the test results often show a large dispersion because the coring process and fracture location influence them, as shown in **Fig. 2-2** [64]. Shear tests are usually performed in the laboratory and the results are relatively stable. The disadvantage of most common shear test methods is the presence of interfacial bending moments due to the eccentricity of the force [65].

Different views have been presented in the literature regarding the correlation between the results

obtained by different test methods. Júlio [55] et al. reported a linear convergence between the results obtained by the slant shear test and those obtained by the pull-off test. The torsional bond strength test developed by Silfwerbrand [66] (**Fig. 2-3 (b)**) is considered a situ-applicable shear strength test method. And reported that the ratio between torsional shear bond strength and tensile pullout strength was between 2 and 3. Bentz et al. [50] suggested that the differences in results between the different testing methods were related to the microstructure at the bonding interface of the samples tested. As shown in **Fig. 2-4**, when the substrate surface was in a relatively dry state, the friction provided by the cement particles that were not fully hydrated in the overlay was able to increase the slant shear strength but contributed less to the tensile strength. In contrast, a wet substrate surface contributes more to enhanced bonding under tensile loading.

(2) Fracture location - transition zone at the bonding interface

Dispersion of fracture locations is mainly seen in drawing tests, where the fracture is thought to occur at the most vulnerable location of the specimen. However, in the case of “interface failure,” the actual fracture location is often not examined [65]. Considering the mechanical interlocking theory, it is almost impossible for the separation of the overlayer and the substrate material to occur without damage. Bond failure is also not really to occur at the interface because the mortar can't be pulled out of its original anchoring position after it has cured and formed a mechanical bond. Therefore, researchers have investigated the bonding interface of composites at a microscopic level to get information on the weakest points.

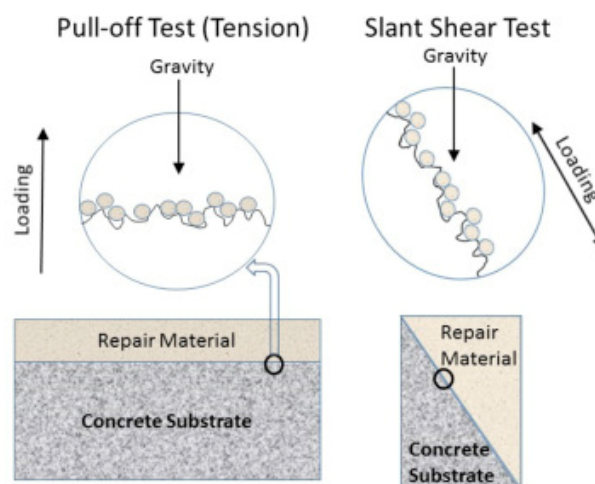


Figure 2-4 Schematic of differences in pull-off test vs. slant shear test with respect to directions of gravity and loading, according to [50].

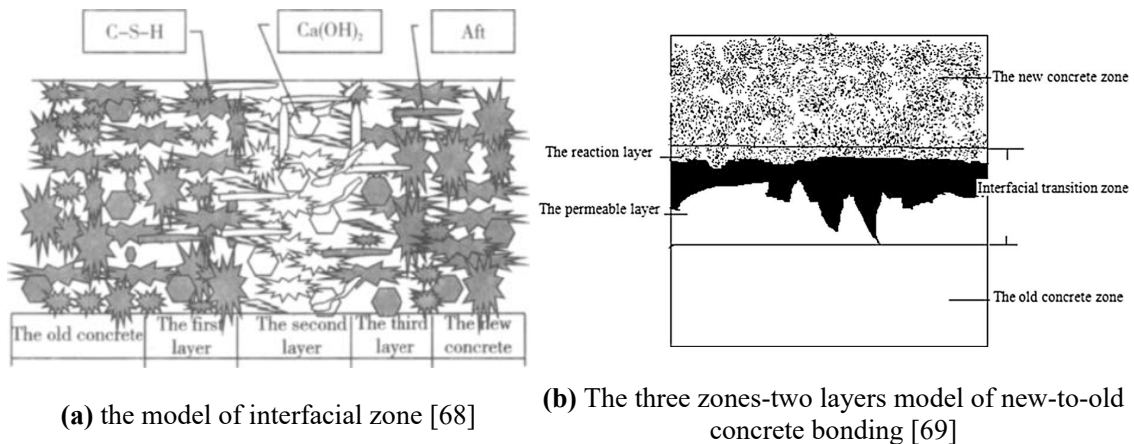


Figure 2-5 Transition zone models of bonding interfaces in the literature.

Pigeon and Saucier [67] point out that the interface between old and new concrete is very similar to the bond between aggregate and cement paste. Due to the wall effect, a transition zone similar to an interfacial transition zone should also exist between the overlay and the substrate. Xie et al. [68] further explained the microstructure of the transition zone and proposed a model, as shown in **Fig. 2-5(a)**. The hardened paste at the bonding interface was divided into a penetrating layer, a strongly affected layer, and a weakly-affected layer at the microscopic level. The first and third layers are part of the substrate and overlayer, respectively, and have a small influence on the bond strength properties. The second strongly influenced layer is located at the interface and is considered the weakest link. The local increase in the w/c ratio induced by the wall effect results in the porous qualities of this layer, with Ca(OH)_2 and needle-like Aft crystals being the main product phases. The thickness of this layer is influenced by the age and porosity of the matrix and the w/c ratio of the overlayer. Yan et al. [69] distinguished the transition zone into a reaction layer and a permeable layer on the overlay and substrate sides, respectively, as shown in **Fig. 2-5(b)**. The enhancement of the bond strength by interfacial roughness and interfacial adhesives was explained accordingly. An increase in interfacial roughness thickens the permeable layer. The bond agent applied to the interface forms a polymer film, making the reaction layer denser and stopping the cracks' extension. Beushausen et al. [70] investigated the effect of the wetting of the substrate surface on the microstructure of the transition zone. An overlayer of approximately 100 μm in thickness at the interface is defined as the transition zone, and this part of the pore structure is distinct from the cover layer. It is considered to be the weakest part. Beushausen et al. pointed out that the conventional practice of pre-wetting the substrate leads to an increase in the porosity of the transition zone. This reduces the bond strength.

The observation of the microstructure of the transition zone can explain the mechanism of action

of the factors influencing bond strength. The location of the fracture in shear bond strength tests almost always occurs in the transition zone, except in the case of microcracks in the substrate caused by improper handling. The present authors believe that the shear bond strength is more representative of the actual situation in the structure.

2.1.3 Environmental effects on facades

The environmental factors with the most significant impact on the facade correspond to the local climate. In this thesis, we focus on those studies in areas with an environment similar to Japan's, with clear seasonal distinctions. Except for some particular domains (e.g., extreme proximity to pollutants and the sea), most studies support sunlight and rainfall as the main degradation agents. Still, the weighting of these two degradation agents is controversial.

Silva and Brito [11] analyzed 107 reports summarizing the influence of climate on the estimated service life of facades. The subtropical monsoon climate (where Japan is located) was the lowest. They attributed this to the high frequency of rainfall (no significant dry season), with higher humidity being the leading cause of defects in rendered facades. Gaspar and de Brito [19] classified the impact of defects in rendered facades into five classes to determine their condition level and overall degradation. The area of the facade affected by rainwater infiltration determines the severity level, and the area involved in the worst condition should exceed 30% of the cladding area. Rainwater erosion largely influences the level of building degradation.

Pereira [71] argues that the mere moisture absorption of the material does not cause severe defects to the facade. Problems related to humidity do not occur independently. Weathering is due to salts carried by rainwater absorbed by the mortar, which attacks the composition of the cementitious material (through carbonation, chloride, or sulfate attack), destroying its physical properties. Wetzel [59] et al. conducted a long-term field study on the evolution of the damage mechanism of bonded tiles under naturally occurring combinations of moisture and thermal loads. They proposed three steps of bond failure: 1) initial cracking, 2) crack extension, and 3) crack enlargement. The initial drying shrinkage and thermal cycling caused cracking, followed by water entry, allowing rapid crack extension and enlargement under wet and thermal cyclic loading. Maranhão [72] et al., however, argued that even in the absence of defects, the increase in mortar water content due to condensation is sufficient to cause a substantial reduction in deformability and modulus of rupture. They analyzed polymeric mortars used for tiling, where a moisture content of more than 6% was sufficient to reduce the deformability of the mortar by 50%, which would significantly reduce the resistance of the mortar to other degradation agents.

The influence of humidity and temperature is difficult to discern with an extensive range of statistical results. But the frequent observation that different parts of the same building deteriorate at different rates provides some information. A statistical analysis based on tile failure incidents across Japan concluded that wall orientation and the application of dark tiles were the main risk factors for bond failure. North-facing tiles are less likely to fail than other orientations, which may depend on the maximum temperature difference between the tile surface and the bonding interface. The north wall is typically 1 °C, while the other orientations can reach a maximum of 6 °C [73]. Zurbruggen and Herwegh [31] studied the failure evolution of a typical tile system under daily and seasonal thermal loads. It was clearly shown that tile bond integrity depends on exposure to solar radiation and diurnal temperature differences. The fastest crack propagation rates were observed for southern walls with intensive solar radiation and early spring and winter when temperature variations were most significant. Bauer and Souza [15] et al. reported a clear orientation dominance of facade degradation for buildings in Brazil. Degradation rates were more blocky for north-facing walls exposed to a large amount of solar radiation. Consoli [23] et al. noted similar behavioral phenomena between facade failures of buildings, where the highest frequencies and strengths were located at the top and southern facades of the buildings. Rashid [74] et al. investigated the effect of moisture and temperature on the adhesion between polymer cement mortar/concrete in the laboratory. The interfacial tensile strength of the composites decreased significantly with increasing temperature, while the effect of moisture was minimal.

The literature shows that there is an interpenetrating relationship between the effects of temperature and humidity. One defect is a consequence of the former phenomenon and, simultaneously, a cause of the latter. Macroscopically solar radiation seems to be the more critical degrader, and the thermal expansion mismatch between materials significantly influences adhesion failure. However, a distinction must be made between the main degradation agents in different building parts. According to investigations by Gaspar and de Brito [19], continuous facades (without opening sections) do not have the same degradation pattern as corners and edges. Corners and edges are susceptible to the differential movement of the whole building and are more likely to lead to cracking than to load concentration problems. On the other hand, different parts of the same building react differently to the same degradant. Zurbruggen and Herwegh [31] pointed out that for the case of slow long-term cooling/heating (not exposed to direct sunlight), since no thermal gradient in the cross-section is formed, the expansion/contraction between the different parts depends directly on the difference in the thermal expansion coefficient. In contrast, when only the tiles are allowed to cool rapidly,

cooling/heating, the addition of temperature difference brings about a more intense differential movement.

2.2 APPROACH TO CONSTRUCTING DURABILITY ASSESSMENT SYSTEMS

According to Lewry and Crewdson [75], the critical steps in durability assessment include: 1) Factors affecting durability; 2) Defining key degradation factors for accelerated testing, and the mechanism of that degradation; 3) evaluation of the significant causes of degradation in the proposed end use environment; 4) construction of models and damage functions for the material's response to the environment based on the accelerated test results and the environmental measurements. Lab-scale durability assessments are done by simulating degradation mechanisms and accelerated aging cycles. Under normal use conditions, building components usually do not fail or considerably degrade within a reasonable testing time. Therefore, accelerated testing methods (ATs) are used in the laboratory to promptly assess or demonstrate the component or subsystem reliability. Specifically, AT experiments are performed to accelerate the failure mechanisms to ensure that the product can reach the aging state within a reasonable test period [76].

2.2.1 Degradation mechanisms of rendering mortars

Environmental degradation agents have already been discussed in Section 2.1.3. Rendering mortars are more susceptible to environmental influences than concrete substrates due to their thinner

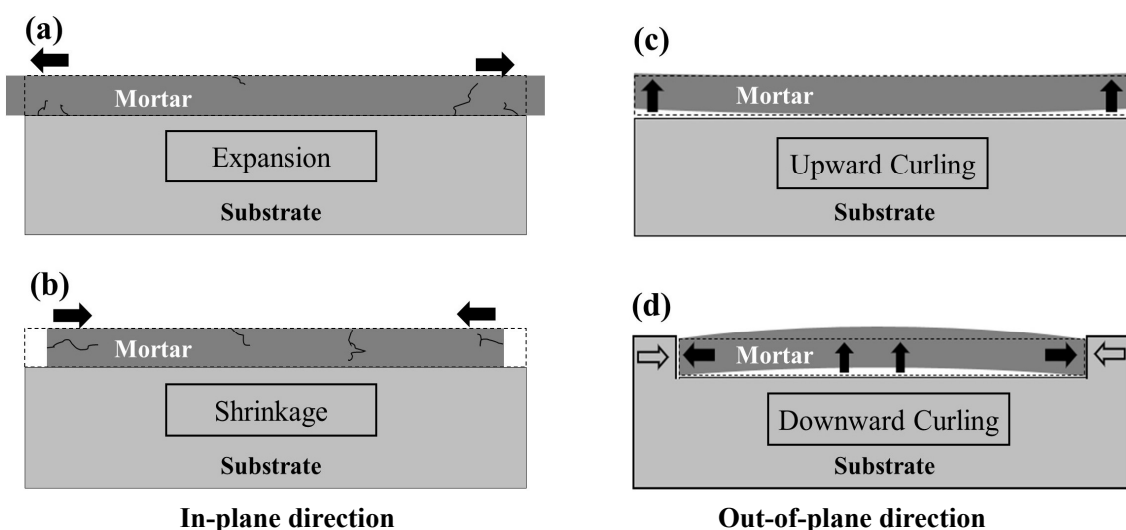


Figure 2-6 Deformation of rendering mortar.

cover thickness and greater modulus of elasticity. The differential movement is, therefore, mainly due to the deformation of the rendering mortar itself. In the case of adhesion failures, drying shrinkage and thermal expansion under solar radiation are considered to be the causes of initial interface damage [59]. **Fig. 2-6** shows the four modes of rendering mortar deformation. In practice, these types of deformation often occur simultaneously. Deformation in the in-plane direction will lead to cracks and reduce the adhesion of the mortar. Deformation in the out-of-plane direction may lead directly to debonding.

(1) Effects of solar radiation and temperature variations

Facades in actual structures are constrained by structural elements such as beams and columns. It isn't easy to have deformations that occur purely in the in-plane direction, as in **Fig. 2-6 (a)** and **(b)**. In the case of rendered mortars exposed to solar radiation, for example, when the rendering mortar expands but is restricted in the plane direction, the deformation tends to develop in a less restrictive sequence. It protrudes from the substrate due to the local temperature increase caused by sunlight, as shown in **Fig. 2-7**. As the temperature rises during the day, the mortar and substrate begin to move differently due to a mismatch in thermal expansion caused by two factors, the temperature difference between the layers and the difference in material properties. Although this deformation recovers at night as the temperature decreases, the reduction in bond strength between mortar and concrete caused by the deformation is irreversible, and the cumulative damage will lead to fatigue failure. In the worst-case scenario, due to the low tensile strength of Portland cement, cracks from expansion lead to the intrusion of rain and condensation into the interior, and the mortar can quickly spall.

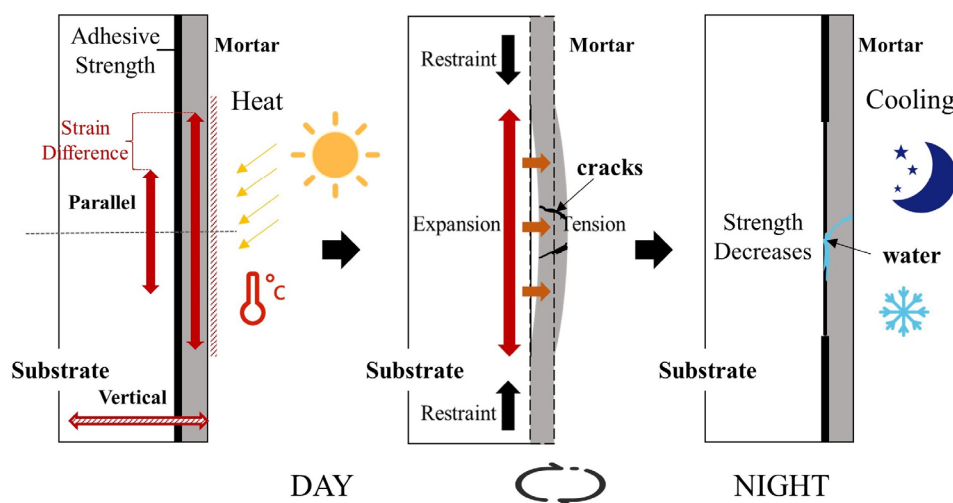


Figure 2-7 Failure of adhesive unity under daily solar radiation.

(2) Effects of drying shrinkage

The change in the volume of cementitious composites due to water loss is defined as drying shrinkage [77]. The alternation of wet and dry environments has little effect on mortars without surface defects. However, long-term drying shrinkage can have a detrimental impact on mortars. Drying shrinkage does not usually directly affect bond integrity, abnormally manifested by cracking, but can reduce bond durability. To provide good workability, rendered mortars often have a sizeable water-to-cement ratio and contain much more water than is required for the hydration of the cement, which also leads to more severe drying shrinkage. Both external and internal constraints hinder the drying shrinkage of rendered mortar. External restraint is due to its bond with the concrete. Internal restraint is caused by the moisture gradient present in the mortar (as drying usually occurs on only one face) until equilibrium with the humidity of the surrounding environment is reached. Local shrinkage is directly related to pore moisture; therefore, a shrinkage deformation gradient exists throughout the drying process [78] [79], causing the rendering mortar to deform in an out-of-plane direction, with deformation often manifesting itself as upward curling (**Fig. 2-6(c)**). This anomaly was frequently observed in the corners and edges of external walls and floor slabs.

As shown in **Fig. 2-8(a)**, the top surface of the mortar dries and shrinks, while the bottom surface remains wet with a much smaller amount of dimensional change. As the shrinkage gradient rises, the curling moment of the mortar increases, inducing tensile stresses in the mortar and substrate and may eventually overcome the material's tensile strength, leading to cracking and debonding of the mortar [80]. To quantify the effect of curling deformation, Mauroux et al. [81] have proposed an evolutionary test device for monitoring shrinkage during drying, quantifying the extension of cracks in mortars (location, opening, depth). They investigated the "free" drying shrinkage of mortars and the cracks in mortar/substrate composite specimens due to the limitation of drying shrinkage using the Digital image

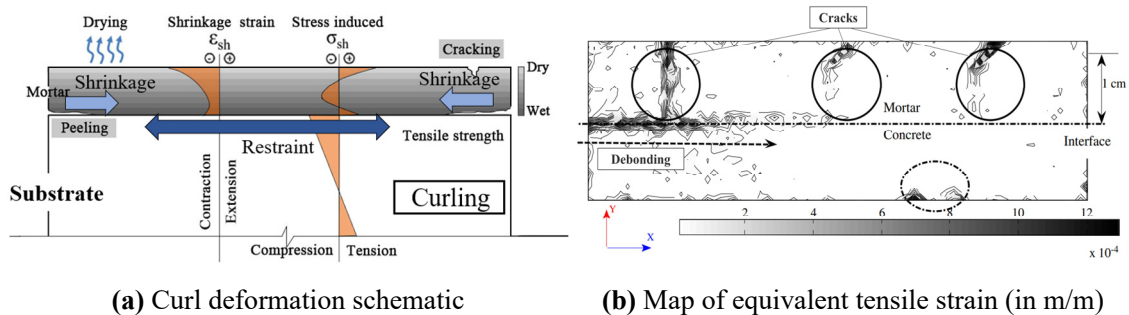


Figure 2-8 Peeling and cracking due to drying shrinkage in the mortar/concrete composite specimen, adapted from [81].

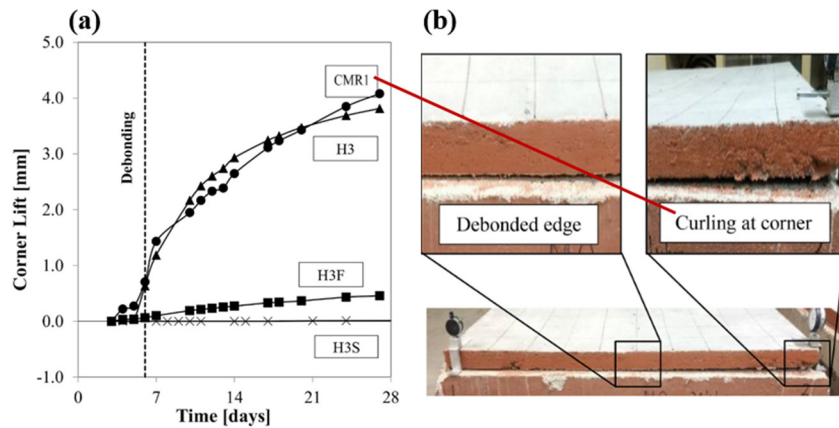


Figure 2-9 Debonding due to curling deformation of the overlayer, corner lift (a) and example of debanded edges (b), according to [82].

correlation (DIC) technique. As shown in **Fig. 2-8(b)**, cracks were observed in the mortar constrained by the substrate at a temperature of 25°C and a relative humidity of $30 \pm 5\%$. Microcracks were observed on the surface of the mortar and at the adhesive interface (arrow). The shear stresses induced by the shrinkage of the mortar result in debonding.

Chilwesa et al. [82] investigated four cementitious overlayer materials, applying them to a concrete slab with dimensions of $1150 \times 1050 \times 200$ mm, providing information on edge curling and debonding. As shown in **Fig. 2-9**, significant debonding was observed along with curling of the corners of the overlay (displacement in the out-of-plane direction). The most severely debanded specimen, CMR1, showed debonding on the 6th day after the end of casting and debanded 82% of the overlay area after 28 days (examined by hammering.) Chilwesa et al. noted that the incorporation of fibers and SRA significantly inhibited the deformation of the overlayer and alleviated cracking and debonding.

2.2.2 AT methods for studying mortar adhesion durability

Humidity and temperature are considered relevant factors in the degradation of facades. Therefore, many studies have established artificially accelerated aging cycles to assess the effect of temperature and humidity on the durability of mortar bonds. The main ones are dry-humidity, freeze-thaw, cold-heat, and hygrothermal cycles combining both factors. Some representative work is presented below.

Pigeon and Saucier [80] investigated the effect of different interfacial binders on the durability of new and old concrete bonds under three other aging conditions. The AT methods included the freeze-thaw cycle, dry-wet cycle, and drying conditions. They suggested that specimens subjected to the combined aging cycle showed durability problems not found when exposed to a single aging cycle.

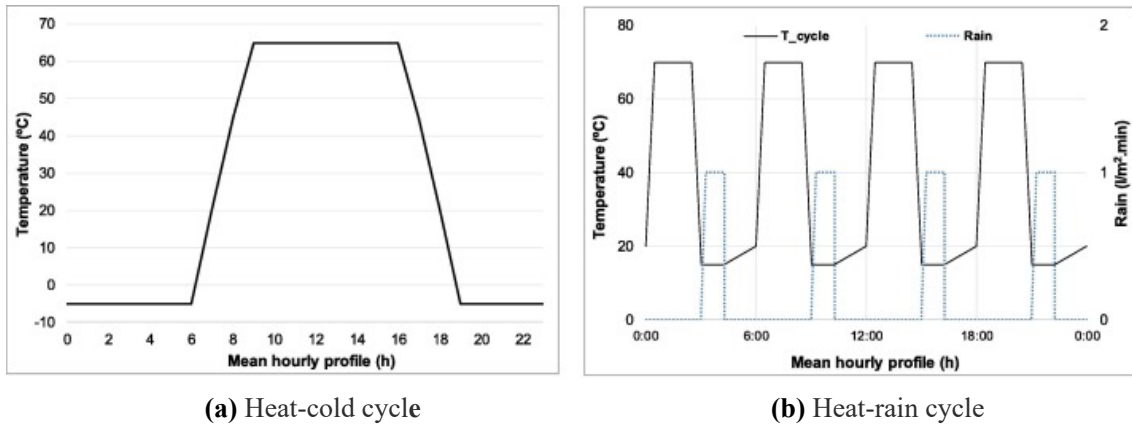


Figure 2-10 Hydrothermal aging cycle, the two most used AT methods, according to [84].

Yiu et al. [13] conducted a laboratory study on the weathering effects of external tile systems. For the mortar-tile interface, heating-cooling plus wetting-drying cycles may reduce the shear strength by more than 50% in the first 100 cycles. However, there was no significant difference in the samples before and after weathering for the render-concrete interface. Curci et al. [83] assessed the behavior of a tile system when subjected to temperature changes by applying a heating-cooling cycle to a large-scale wall to accelerate aging. The heating was performed by emitting 450 W/m² of thermal radiation from 15 halogen lamps onto the outer surface of the tiles, and the cooling was achieved by projecting cold water at approximately 20°C from the specimen's top surface. Maia et al. [84] proposed a durability assessment method for thermal mortars applicable to multi-layer systems. Two ATs were established based on specific European climatic conditions, including heat-cold (HC) and heat-rain (HR) cycles, as shown in **Fig. 2-10**. According to the results reported, the amount of water penetration was more significant for the HC-only mortar than after HC+HR. This indicates that comparing the hot-wet combination, the temperature-only load resulted in more material rupture.

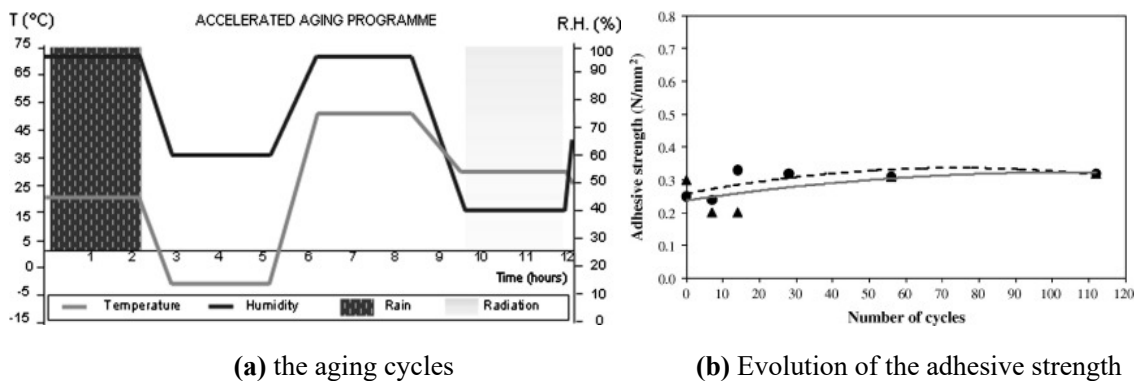


Figure 2-11 Evolution of the adhesive strength of the specimens during the hydrothermal aging cycle, according to [85].

The study by Freitas et al. [85] also suggests that the moist heat cycle may not act as the degradation agent. After the specimens were exposed to the aging cycle depicted in **Fig. 2-11(a)**, an increase in bond strength behavior was observed, as shown in **Fig. 2-11(b)**. This may be due to the dispersion of the pull-out test results and may also indicate that the provided hygrothermal cycle does not act as a degradation agent. Al-Ostaz et al. [62] proposed a thermal cycle-only AT method to exclude the effect of humidity. The average bond strength between the repair mortar/concrete decreased by 17%, 25%, and 33% after 60, 120, and 180 cycles, respectively.

Most of the studies mentioned above have used a combination of aging cycles. The standardized AT method specified in the Japanese Society of Finishing Standard M-101 [86] also combines temperature and humidity degradation agents, as shown in **Fig. 2-12**.

- 1) Irradiate the infrared lamp for 105 minutes until the surface temperature of the specimens reaches 70°C.
- 2) Sprinkle for 15 minutes (water temperature 15±5°C).
- 3) 1) and 2) as one cycle and lasting 300 cycles

This experiment was originally performed to evaluate the quality of the adhesion promoters used in plastering mortars by testing the adhesive strength between the mortar and concrete. However, several problems have been identified in practice. Specifically, the entire specimen is subjected to a high-temperature history and water supply, which may favor the hydration of the mortar. In other words, instead of acting as a degradation agent, the hygrothermal cycle may increase the bond strength. Similar AT methods have the same type of limitations. Even if the original intention of the researcher was to assess the aging behavior under temperature changes, it is difficult to strip out the moisture factor by heating through thermal radiation and cooling through dispersed water. Even though they

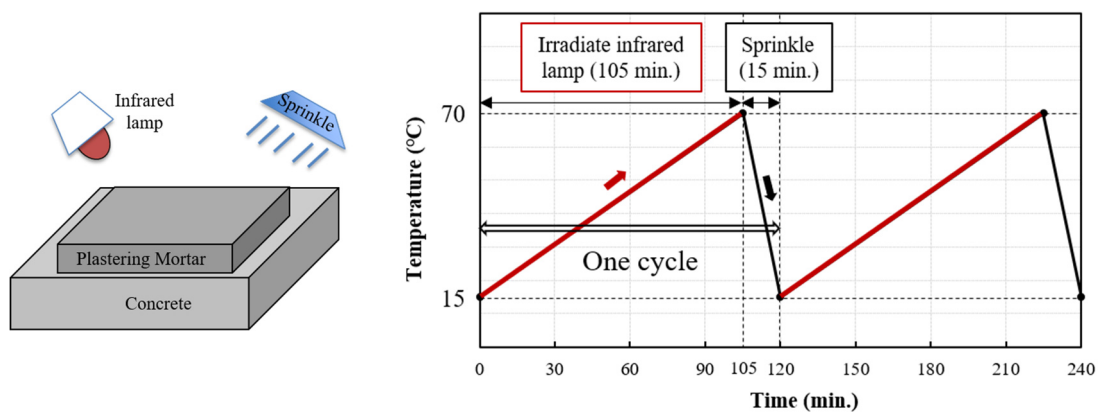


Figure 2-12 Hygrothermal aging cycle according from Japanese Society of Finishing Standards M-101.

can simulate the various degradation agents, artificial aging cycles have difficulty reproducing their synergistic mechanisms of action. At the level of the degradation mechanisms of rendered mortars, the synergistic mode of action of temperature and humidity still needs to be clarified.

Furthermore, existing AT methods are unsuitable for studying solar radiation's effects on facades, as no actual degradation mechanisms are reproduced. As shown in **Fig. 2-7**, the distribution of solar radiation on a facade must be uneven, with temperature differences arising in both out-of-plane and in-plane directions. This means that the rendering mortar subjected to solar radiation is bounded by the substrate, columns, and beams and by the mortar in the surrounding unheated areas. In this case, the thermally loaded mortar tries to deform in the out-of-plane direction, causing cracking and debonding. In the literature, composite specimens of overlayer/substrate or surfaces of the overlayer are often exposed to cyclic loading in their entirety, in which case the overlayer is only constrained from the substrate. This results in the stresses generated at the interface being mainly in the in-plane direction, with the edges of the specimen being the most affected by differential movement.

2.2.3 Degradation patterns of mortars

The general model for the durability assessment is that all specimens are tested for the extent to which their performance degrades after a certain number of aging cycles. However, it is challenging to elucidate the correlation between the rate of degradation at the laboratory level and the actual rate of structural aging. Although the different physical, chemical, and microstructural processes associated with the formation and evolution of the debonding mechanism of mortars have been studied in detail, the change in bonding properties with aging time has not yet been elucidated. Ideally, bond strength would decrease linearly with the aging cycle, but this pattern is almost impossible in natural degradation. In addition, the degradation pattern may be inconsistent from specimen to specimen, and the choice of which stage of performance testing is critical, which may alter the outcome of durability evaluations. Current research into degradation patterns has focused on two levels, the degradation pattern of the whole facade and the evolution of mortar adhesion failure, with some of the prominent work described below.

(1) Degradation pattern of the facade

The study of facade degradation patterns is mainly based on visual and empirical judgment, considering the action of various degradation agents and anomalies. Shohet et al. [87] systematically assessed the pathological cases of existing building facades (including render cladding, ceramic

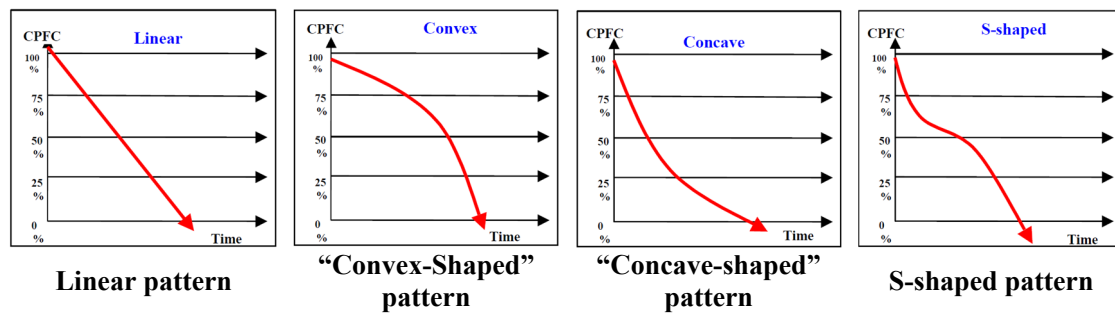


Figure 2-13 Four typical patterns of deterioration paths, according to [87].

cladding, and stone cladding). They proposed four typical patterns of facade deterioration, linear, convex, concave, and S-shaped patterns, as shown in **Fig. 2-13**. The independent variable is time, the dependent variable is the component performance in failure conditions (CPFC), and 100% represents a perfect condition.

Linear pattern – This pattern is typical in situations where a permanent deterioration agent exerts a continuous and consistent impact on the cladding. Shohet et al. suggested that this pattern is representative of weathering effects, such as damage from solar radiation.

“Convex-Shaped” pattern – Indicates physical failure of the entire facade system due to physical or chemical phenomena. For example, degradation due to differences in shrinkage between mortar and substrate.

“Concave-shaped” pattern – represents the action of chemical and physical agents on claddings. Such impact appears in cases of microorganisms or cyanobacteria development on render and on natural stone.

S-shaped pattern – represents a deterioration mechanism that changes its intensity over time. This pattern represents the possibility of some design flaws in the facade, with visually observable degradation occurring shortly after construction is completed. The primary mechanism then becomes a physical reaction that takes longer to affect the strength of the material, and the degradation enters a period of peaceful development. When this process matures, the rate of deterioration suddenly accelerates.

Other researchers prefer an 'S-shaped' pattern to describe the degradation process of the facade [19] [88]. Three distinct phases of cladding performance over time are considered. 1) the first phase is premature degradation, which occurs rapidly due to defects caused by the quality of materials and or/and construction; 2) the second phase is a slow development phase, which occurs due to the natural aging process associated with exposure to environmental degradation agents, influenced by the conditions of use and frequency of maintenance actions; 3) the third phase is a rapid development

phase, which occurs rapidly due to synergies between different degradation agents and the simultaneous presence of defects; and 4) the third phase is a rapid development phase. Agents and the simultaneous presence of defects, degradation progresses rapidly until complete failure.

(2) Degradation pattern of the adhesion

Considering debonding as a severe failure requiring immediate intervention, several studies have focused on understanding, quantifying, and describing debonding damage mechanisms. Feldfogel and Rabinovitch [89] [90] investigated the evolution of debonding mechanisms in the square, rectangular, and round tiles in porcelain cladding under uniform heating. In all cases, two threshold loads played a turning role in the evolution of the debonding mechanism. After the first threshold load is reached, the debonding mechanism starts abruptly and is accompanied by a slow and steady growth phase. Until the second threshold load is reached, debonding is rapid but steady. After the second threshold load, the debonding propagation becomes unstable, and the system will quickly break down and lose static equilibrium.

Fig. 2-14 depicts the debonding area ratio Ad (debonding area / initial bonding area) about the uniform thermal difference $\Delta\theta$. Until about 40 °C, no debonding seems to occur. Between 40 and 55 °C (point A1), a steady and slow evolution of debonding can be seen. From points, A1 to A2, a stable but "fast" debonding process is observed. A fracture occurs at the critical load $\Delta\theta = 75.53$ °C. As the enlarged view in **Fig. 2-14**, between points A2 and A3, there is an increase in the debonding area ratio but a decrease in temperature, indicating the unstable nature of the reaction at this stage. From a physical point of view, the break at point A2 means that the structure is no longer in static equilibrium for the same $\Delta\theta$. The response becomes intrinsically unstable, and the structural system fails. After point A3, the debonding process seems to stabilize and become slow again, and after the debonded

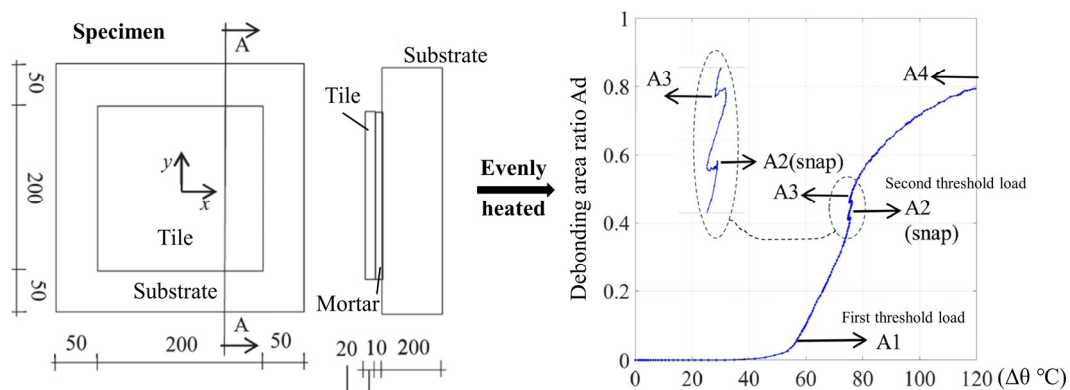


Figure 2-14 Evolutionary pattern of debonding of one tile, according to [89].

area reaches 80% (point A4), the authors do not follow it again.

This finding is consistent with the “S-shaped” degradation pattern described above. The degradation rate is unlikely to be uniformly linear even when the specimen is subjected to a single degradation agent. In another study, Cao and Chung [91] monitored the degradation of the bond between old and new mortar by contact resistance measurements under cyclic shear loading. **Fig. 2-15** depicts the fractional change in contact resistance with the number of cycles for a cyclic shear load with a shear stress amplitude of 1.21 MPa, 0.97 MPa, and 0.81 MPa with the adhesion becoming smaller with larger values on the left vertical axis. The degradation of the bond under mechanical loading also shows a three-stage “S-shaped” characteristic. It is therefore assumed that the rendered mortar will show a similar degradation pattern during the artificial aging cycle.

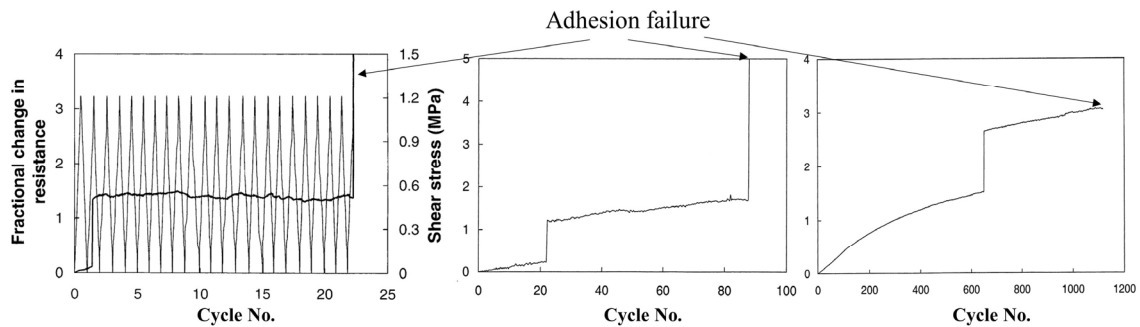


Figure 2-15 Evolution of adhesion under cyclic mechanical loading (shear stress amplitude from left to right: 1.21 MPa, 0.97 MPa, 0.81 MPa.), according to [91].

2.2.4 Assessment of rendering mortar/substrate adhesion

For the bonding of rendered mortar to concrete, the rate of reduction in bond strength before and after ATs is the basis for evaluating durability. The various bond strength test methods have been described in detail in Section 2.1.2. It can be summarized from the literature that mechanical adhesion under tension is very different from adhesion under shear. For example, high interfacial roughness increases the shear strength, while mechanical bond strength in tension depends mainly on the transverse anchoring in pores and textures [65]. When establishing a durability evaluation method, it is essential to correctly select the bond strength test method for a given test parameter based on the AT being designed.

In addition, almost all of the studies presented in Section 2.1.2 used overlayer and substrate of comparable thickness to produce the specimens. It is not a suitable sample pattern for evaluating long-term bonding performance. As described in Section 2.1.1, long-term adhesion is strongly influenced

by the differential movement, in which case the same thickness would result in an impractically small degree of substrate restraint on the deformation of the overlayer. In addition to the issue of thickness, the researcher also pointed out the influence of the geometry of the samples on the results of the adhesion strength tests. For a pull-off test, the concentration of tensile stresses at the edges of square samples compared to the more uniform distribution in round samples resulted in higher adhesion values for the latter [92]. This shows that the dimensional design of the specimens has a significant influence on the results of the performance assessment.

While laboratory-scale studies often use destructive strength tests to assess adhesion, destructive testing is not appropriate in many situations in the field. And, because destructive tests cannot be performed on the same specimen in succession, the results often exhibit a high degree of dispersion. To overcome these drawbacks, researchers have developed several non-destructive testing (NDT) techniques capable of assessing adhesion. This methodology is described in detail in Section 2.3.

2.3 NDT DELAMINATION DETECTION TECHNIQUES

The essential technique for maintaining and managing facade cladding is "delamination detection." Claddings usually begin deteriorating with the delamination of tiny areas between them and the substrate. The potential for the delaminated areas to spall under sustained fatigue loading conditions increases due to reduced adhesion; however, this minute degree of delamination is difficult to detect by visual inspection alone. NDT is an ideal approach to detect damage beneath the surface. Several researchers have applied NDT techniques to detect hidden delamination beneath facade cladding. This detection method is essential for assessing the continued availability of facade cladding after an earthquake, especially in areas that are difficult to reach. The following section describes some of the methods that have been proven to be applied in the field and those that currently remain at the laboratory scale.

2.3.1 Field-applicable NDT methods

(1) Impact acoustic inspection

Among the various NDT methods, the acoustic method offers the advantages of convenience and cost-effectiveness [93]. The method has been widely adopted owing to its high equipment and environmental compatibility and its relative reliability. In general, acoustic methods can be divided into two main categories: acoustic emission (AE) and impact echo (IE). The difference between these

two categories is the source of the sound waves, with the AE method measuring elastic waves generated by changes within the building. In contrast, the impact-echo method is based on monitoring echoes generated by external impacts, which do not cause any internal changes.

The impact sound detection method is based on the impact sound signal generated by a small hard object striking the surface of a concrete structure [94]. In facade inspection, the conventional way uses the information conveyed by the acoustic signal produced by a hammer or similar metal object striking the surface of a tile, also known as “percussion inspection.” The inspector detects abnormalities through the ear based on acoustic characteristics, such as sound pressure and frequency. This method is prevalent because of its cost-effectiveness and operability. However, diagnosis is highly dependent on the experience of the practitioner, and individual variation leads to a risk of accuracy and difficulty in quantitative assessment. In addition, this inspection method has a limited scope of practice, as the scaffolding and gondola required to survey large areas result in prohibitive costs.

In recent years, the rapid development of climbing robots [93] [94] [95] [96] has broadened the range of applications for impact acoustic inspection. Several attempts toward automation have been reported [93] [94] [97] [98] [99] [100] [101] [102]. The research has been focused on the extraction of effective parameters for characterizing defects from acoustic signals and their automated identification. The bonding integrity of the object under test can in principle be evaluated with information from both the time-domain and frequency-domain [99]. The former is based on the amplitude–time waveform of the impact sounds, while the latter is a power spectral density (PSD) distribution pattern obtained by performing a fast Fourier transform calculation on the time–amplitude waveform. Furthermore, the frequency-domain features based on PSD distribution for the identification of defects is a general method, however is sensitive to environmental noise and the roughness of the measured object surface. Tong et al. [99] proposed a method for defect characterization by time-domain features extracted from the initial acceleration peak of the impact sound, which can not only identify defects and is not easily affected by the texture of the test object surface. Luk et al. [93] proposed an evaluation method based on wavelet packet decomposition that overcomes the interference of environmental noise by identifying the outline features that constitute the PSD pattern. The researchers inspected the facades of high-risk buildings with a cable-driven climbing robot that examined 400 specimens. When the signal-to-noise ratio was greater than 2 dB, a successful detection rate of more than 80% could be achieved. In these previous studies, machine learning techniques such as artificial neural networks [93] [99] and support vector machines [94] [100]

have been applied to extract features from the collected signals to achieve automatic recognition.

Although percussion inspection in Japan relies primarily on manual work, the research and practice of automatic percussion detection systems are receiving attention. Non-contact acoustic inspection techniques using unmanned aerial vehicles (UAV) have been developed [103] [104]. Although they have not yet been practically applied, it is foreseeable that acoustic inspection has a promising future.

(2) Infrared thermography

The intensity of infrared radiation emitted by an object is related to its absolute temperature. In infrared thermography (IRT), the infrared specific wavelength signal of thermal radiation is detected from the surface of the facade. Then the temperature distribution of the wall is converted into a visually distinguishable image for human eyes. The voids created by debonding are filled with air or water, resulting in the varied overall thermal properties of the wall [105]. Thereby, healthy and delaminated areas are detected.

Unlike percussion inspection, IRT is non-contact. This method is widely employed for the quantitative evaluation of building diagnostics because of its suitability for recording and reporting, enabling non-contact detection of large areas, and providing visual images and numerical results [105] [106] [107] [108]. Most importantly, the ability to simultaneously detect large areas makes IRT appropriate for timely post-disaster assessment. The IRT approaches qualitative and quantitative evaluations for building diagnostics to vary from passive to active [105] [108], the difference being whether manual heating excitation is required. For multi-layered structures, active IRT provides more reliable results. However, for post-earthquake or high-rise buildings, conventional passive IRT using optical excitation is generally preferred for both safety and cost considerations. This makes the detection results inevitably subject to conditions, such as obstruction of the camera's view by adjacent buildings or difficulties in creating a significant temperature gradient on the observed wall due to objective circumstances (e.g., variations in natural heat sources, such as orientation and weather). In addition, measurement accuracy is reduced by: variations in emissivity, color, and stain of the finishes; air conditioning in the room; and contact elements between different materials, such as window frames and balustrades [109]. Another restriction of IRT is that interpreting post-processing results requires considerable experience, intuition, and judgment [110].

Multiple studies have reported factors that influence detection accuracy and estimated the extent of influence for these factors, such as wind speed [108], indoor and outdoor temperature differences

[111] [112], tile type [113] [114], and surface color [115]. Meanwhile, the development of thermal image analysis techniques has improved the detection accuracy of passive IRT. Lourenço et al. [105] reviewed several studies addressing the latest IRT as a diagnostic technique for building facades. Effective diagnostic methods, both quantitative and qualitative, were revealed, affirming the feasibility of detecting facade defects through passive IRT techniques. Sato et al. [116] analyzed thermal images obtained by passive IRT using self-reference lock-in thermography (lock-in processing of random temperature fluctuations). They verified the improvement in the detection accuracy of tile delamination. Edis et al. [117] analyzed the time-dependent thermal behavior of defective areas by simple image subtraction, principal component analysis (PCA), and non-negative matrix factorization (NMF) as different quantitative methods and compared the potential of these approaches in detecting delamination. They concluded that PCA and NMF have great potential for the time-dependent analysis of IRT data, as almost all stratifications were checked. Moreover, techniques have been proposed that verifiably reduce reflected noise and help interpret results [114] [118].

In recent years, with the maturity and usability of UAV technology, the difficulty in inspecting high-rise buildings is expected to be overcome. Pan et al. [119] applied forward-looking infrared technology and high-resolution photographic equipment to a UAV to develop a system suitable for the initial visual assessment of exterior walls. Such advancements in UAV technology have increased the range of IRT applications, specifically those in unsafe and inaccessible locations. However, the fundamental problem is that sufficient temperature variation in the target wall is a prerequisite for implementing IRT.

(3) Strain monitoring method

As described in Section 2.1, strain differences between each layer induce delamination of facade cladding; moreover, the occurrence of delamination can theoretically be detected by monitoring the strains in the components.

Several studies have been conducted to measure strain in ceramic claddings. Yiu et al. [13] measured strain at the tile-rendering-concrete interface using strain gauges in a laboratory AT. Although the aim of this experiment was not to investigate adhesive degradation by monitoring strains, the response of the layers of material to weathering could be observed from the strain histories, as shown in **Fig. 2-16**. Murai et al. [120] measured the ultimate strain in concrete using strain gauges and concluded no risk of tile delamination below this limit. Tanigaki et al. [121] assessed the delamination of the tiles from the concrete substrate during loading using strain differences. They reported that the

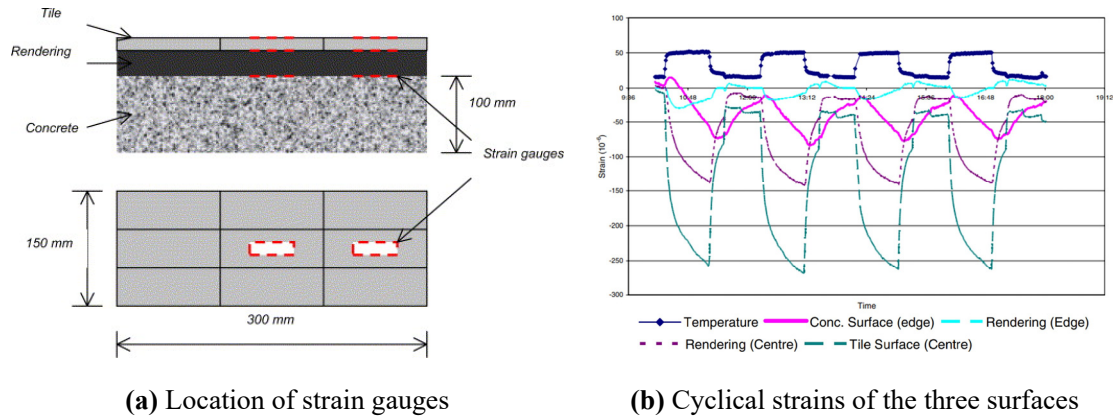


Figure 2-16 Monitoring of interlayer strains in composite tile-rendering-concrete specimens under artificial aging cycles, according to [13].

deformation consistency of the tiles to the substrate decreased as the specimens underwent wet-dry cycles. Nachi et al. [122] proposed the deformation-compatibility capability of tiles as a design indicator, which was obtained from the strain transmissibility between the concrete substrate and the tile surface. Okihashi et al. [123] monitored the strain behavior of concrete substrates and tile surfaces in exterior-exposed environments on real-scale wall specimens. They showed that the repeated strain differences between the two were caused by wet-dry and heat-cool cycles. Moreover, a method to assess the future exfoliation risk of existing wall tiles has been proposed by assessing the strain on tiles in existing buildings, as measured by strain release tests [124]. Chang et al. [125] [126] demonstrated the applicability of strain measurement techniques to measure the deterioration of tiled facades. They combined strain measurement results with acoustic diagnosis to map the deterioration symptoms diagram of square tiles, affirming the feasibility of this technique for future smart building development.

(4) Vibration

In this approach, the target structure is impacted, and the movement of claddings is integrated if adhesion is adequate. Conversely, if delamination exists, the vibration response of claddings likely differs from that of the substrate. Therefore, the delamination of facade claddings can be determined by detecting differences in the vibration response.

Ohgishi et al. [127] showed that the degree of delamination for the finishing material can be identified by the vibration acceleration index. Iwase [128] showed that the peak frequency of vibration for delaminated tiles is approximately 20 to 30 dB higher than that for healthy tiles. That partially delaminated tiles showcased such vibration characteristics only in debonded areas. Takano et al. [129]

visualized the vibrational state of a tile surface using wavelet analysis and proposed a threshold for the delamination state. Soeda et al. [130] derived the relative maximum amplitude from the impact sound waveform. They noted that the relative maximum amplitude in a healthy region is greater for tiles adhered with organic adhesives than for tiles with mortar, which may alter the threshold.

This method of detecting delamination based on vibration characteristics is well-proven, but it has the same disadvantages as the percussion method in terms of its limited detection range. When inspecting ceramic coverings, for example, current practice requires that all individual tiles are vibrated.

2.3.2 Laboratory-applicable NDT methods

The NDT methods described in Section 2.3.1 are, of course, also applicable in the laboratory. Still, a part of the measurement accuracy is often sacrificed to meet the operability in the field. For this reason, researchers have also developed other NDT methods for internal damage detection. Although these methods have some drawbacks that make them temporarily unsuitable for field diagnosis, their potential cannot be ignored as they perform well in laboratory tests, characterizing internal concrete damage and detecting reinforcement corrosion and adhesion failure in composite materials.

(1) AE method

AE is another commonly used method of acoustics. Mechanical energy is generated whenever any object or building is subjected to pressure; this energy is emitted from elastic waves. Usually, cracks in a structure emit some characteristic frequency of "unhealthy sound" as they propagate, which can be tracked to determine the location and extent of crack development. In some cases, AE in a structure needs to be detected using an ultrasonic detector.

AE is often used to follow the transition from a solid to a damaged state and to provide a damage assessment of concrete and cementitious composites [131]. Grazzini et al. [132] conducted static compressive tests on composite specimens of stone-repair mortar. They analyzed the evolution of the mortar shedding process in a coupled stone-block-mortar system by triangulation of the AE signal, assessing the adhesion surface energy released by fracture propagation. They report that the AE signal is related to the energy emitted by the specimen during the delamination phase between mortar and stone. The variation of the AE parameters depends entirely on the specimen of the fracture pattern. The AE signatures are effective for detecting early damage propagation but are also limited by cost

and detection area, with few examples of application to facade cladding.

(1) Ultrasonic Testing (UT) method

UT is one of the most widely used NDT methods for damage assessment. Although both require the use of an ultrasonic detector, what distinguishes UT from AE is that it is an active process in which high-frequency sound is transmitted into the object by the instrument, interacting with the attenuation or reflection characteristics present in the material. Tan et al. [133] evaluated the bonding state of cement and tiles using the reflected signal amplitude of pulse echoes, which was able to correspond to the results of strength tests. Meola et al. [134] compared the ability of IRT and ultrasonic techniques to inspect internal defects using simulated debonded plaster-marble specimens. In addition, ultrasonic tomography was widely applied to locate the thickness and defect areas of concrete and to assess the effectiveness of the masonry structures repair [135]. Wave velocity variations in tomograms were found to be able to reflect damage or changes in brick and mortar, specifically voids and cracks. Conventional ultrasonic testing should use a coupling fluid or gel to ensure good contact between the probe and the structure's surface, making it more suitable for the laboratory. Recently, the air-coupled ultrasonic (ACU) technique has attracted much attention due to its being more feasible for both material characterization and defect detection [136]. It removes the inherent limitation of contact ultrasonics by using air as the coupling medium and provides an efficient, noncontact inspection resolution. However, probably due to the complexity of the thickness and composition of facades, the ACU field has not explicitly focused on the application of damage detection to facade claddings.

(2) Other methods

In addition to these methods, electromagnetic testing (ET), ground penetrating radar (GPR), laser testing methods (LT), and electrical resistance measurement have also been attempted to assess the adhesion of cementitious composites. Osaki et al. [137] examined the adhesion of tiles to concrete walls using radar reflectometry. The basic principle of the measurement is that electromagnetic waves incident on the surface of a tile obtains different reflectivity due to differences in the physical properties of the layers of material. The reflectivity between tiles and the air is much greater than between tiles and adhesive and between adhesive and concrete; GPR is mainly used to detect underfloor damage in historic buildings; The amount of deformation of the finish material in the out-of-plane direction (bumps represent delamination) can be obtained using laser scanners to profile the surface of the cladding, a technique often combined with UAV for virtual reconstruction and

restoration of large and complex cultural sites [138] [139] [140]; Cao and Chung [91] measured the contact resistance between old and new mortar to estimate the bond strength under cyclic loading, where the contact resistance increases abruptly upon bond failure, as shown in **Fig. 2-15**.

2.4 SUMMARY

This chapter reviews the literature and research relating to adhesion between mortar/concrete, focusing on three main areas covered by the objectives of this thesis, namely 1) degradation factors of rendering mortars and adhesion failure mechanisms; 2) durability assessment models for mortar/concrete composites; and 3) non-destructive debonding detection techniques. The adhesion mechanism of mortars, the factors affecting adhesion, and the adhesion failure mechanism are explained, and the basis for solar radiation as the leading environmental degradation agent is determined. In addition, the general process of establishing a durability assessment method is described, and the components of the durability assessment method are detailed. The AT methods currently employed to simulate weathering, as well as their effectiveness and potential misconceptions, are outlined. The advantages and limitations of generic bond strength testing methods are also presented. The application of NDT methods for delamination detection, particularly for building envelopes, is also reviewed, with several examples of published works and an overview of future trends in the application of NDT in facade maintenance. The following conclusions can be drawn:

(1) The initial interface damage is caused by differential movement between the rendering mortar and the adjacent material, resulting from a mismatch in the amount of expansion/shrinkage caused by solar radiation and the drying and shrinking of the material. Subsequently, rainwater can intrude along defects in the material surface, further exacerbating the interface damage. Therefore, while solar radiation and rainwater are important environmental degraders, this work focuses on the initial degradation mechanisms, examining both solar radiation and drying shrinkage (ignoring the external moisture factor).

(2) The factors influencing short-term bond strength and long-term bond strength are different. The former depends on forming a strong mechanical bond between mortar and concrete; the latter relies more on the mortar's ability to follow the concrete's deformation. The dry-mix mortar industry is now mature enough to achieve adequate short-term bond strengths, provided that the quality of the process is up to standard. Manufacturers should consider long-term bond strength as part of their

product design, but there currently needs to be a standard method for assessing long-term bond strength.

(3) In the part of the study presented, the AT method for simulating weathering did not achieve the expected accelerated degradation. However, the two variables of ambient temperature and humidity were adequately considered. This is mainly related to two factors, 1) needing to adequately consider the constraining conditions in the actual structure and 2) failing to reproduce the collaborative mechanism of temperature and humidity. A new AT method needs to be proposed to improve these deficiencies.

(4) When selecting a bond strength test method, it's essential to consider the prevailing interfacial stress conditions caused by each method, which may or may not be representative of the general stress conditions encountered in the actual structure. Also, consideration must be given to whether the specimen is dimensionally designed to produce an appropriate stress state. Ideally, a test method should be developed to measure important bond strength parameters based on a relatively simple test set-up and commonly used molds.

(5) Regardless of the loading conditions, the bond failure process of mortars does not proceed steadily and goes through three distinct phases. In the last stage, the rapid development phase, debonding may occur suddenly. Therefore, the maintenance management model of periodic assessment of the adhesion of claddings may lead to missed inspections. Technology needs to be developed to continuously monitor the adhesive integrity of facade claddings.

(6) Only the strain monitoring method can satisfy continuous monitoring and field applicability in the NDT methods presented. During the research phase, it is possible to study the degradation process of mortar/concrete composites by monitoring the strain differences between the materials. The study cases in the literature use resistive strain gauges to monitor strain. However, the physical size of the strain gauges can be the starting point for bond failure, which is rarely discussed. A more suitable sensor to monitor interlaminar strain should be selected.

Chapter III

ESTABLISHING A LAB-SCALE DURABILITY ASSESSMENT METHOD FOR MORTAR/CONCRETE ADHESION

3.1 PROPOSED LAB-SCALE DURABILITY ASSESSMENT METHOD

Durability assessment methods may consist of one or more of the following four tests [75]:

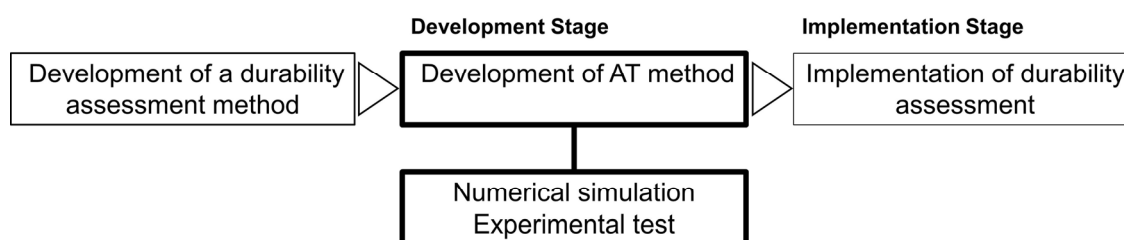
-Benchmark testing; The criteria for passing or failing durability of a material under test after AT is determined using historical data on the material's performance in a given environment.

-Reference material/comparative testing; When AT of unknown new materials is required, a durability ranking can be quickly obtained by comparing reference materials with known properties.

-Environmental/stress testing; a) attempts to simulate and accelerate the entire service environment; b) attempts to limit the material by enhancing its susceptibility to environmental factors.

-Site testing; a) exposure to the field for testing; b) in situ monitoring of buildings.

This work has been designed for accelerated aging cycles based on principle (b) in environmental/stress testing, i.e., to enhance the most susceptible environmental factors. The assessment of durability is done utilizing reference material/comparative tests. The methodological process for developing a durability assessment method applicable to rendering mortar/concrete composites went through two phases, the development and implementation phases. This chapter describes the development phase, where the validity of the proposed AT method is verified through numerical simulations and experimental testing. The implementation phase is described in detail in Chapter 4.



3.1.1 Proposed AT method

The investigation of facade anomalies reported in the literature is reviewed in Chapter 2, and solar radiation is considered the most critical environmental factor. Therefore, the proposed AT method aims to simulate the degradation mechanisms triggered by solar radiation. At the same time, the summary in Chapter 2 describes the shortcoming of the AT method used in the literature to simulate solar weathering; that is, the method of applying thermal loads does not take into account the actual conditions of the facade, resulting in a degradation mechanism that cannot be reproduced.

Considering the facade situation, the rendering generates temperature gradients in both planar and cross-sectional directions after being subjected to thermal loads. The temperature gradient in the plane direction arises from the uneven distribution of sunlight (from shading and the limitation of the solar height angle). The temperature gradient in the cross-sectional direction results from the difference between indoor and outdoor temperatures and the difference in thermal properties between materials. The methods used in previous studies to apply thermal loads to mortar/substrate composites were unable to create temperature gradients in both directions simultaneously, either by heating an entire specimen [13] [62] or by heating the whole surface of the mortar [80]. Therefore, it is necessary to provide an appropriate restraint for the rendering mortar subjected to thermal load. As shown in **Fig. 3-1**, the uneven heating due to solarization will cause a temperature difference in the wall. The temperature difference not only exists between the different layers but also exists in the in-plane direction of each layer. The temperature difference combined with the physical difference of various materials to occur the differential movement between layers. The rendering mortar in a real structure is restrained not only by the substrate, columns, and beams but also by the mortar in the surrounding unheated area. Therefore, it is necessary to mimic this limited state in an artificial aging model, which has been overlooked in previous research. To reproduce this state, in the proposed approach, a thermal

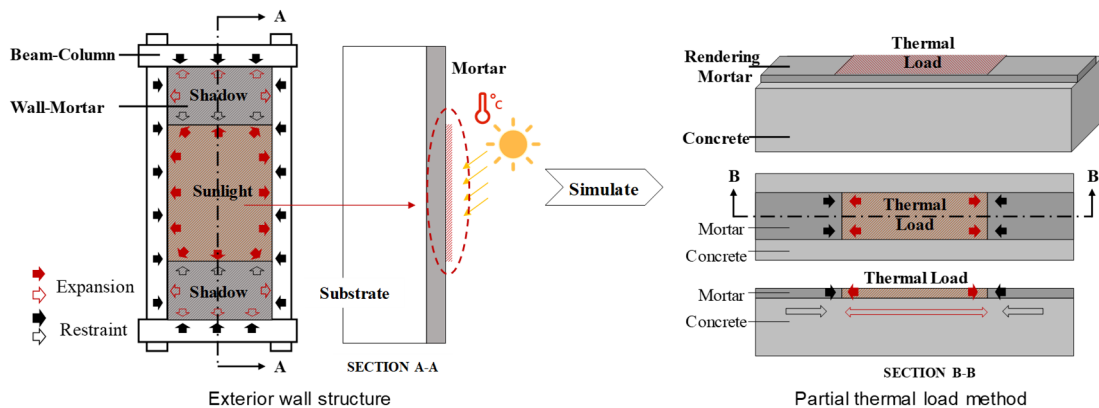


Figure 3-1 Application of partial heating to reproduce the actual degradation condition.

load is applied only in the central part of the mortar, and consequently, the unheated surrounding mortar provides restraint. The author has named this method the "partial thermal load (PTL) method."

Applying a thermal load to the specimen in a non-contact manner often results in an uncontrollable temperature, such as halogen lamp irradiation [80], as the distance between the specimen and the heat source is thus a key parameter. Ideally, the concrete substrate should be heated purely by heat transfer from the mortar, creating a temperature gradient across the thickness of the specimen, which is similar to the condition of an actual building facing exposure to solarization. To realize this, silicone rubber heaters with wire-wound elements can be placed directly in contact with the mortar to provide thermal loading. Such heaters exhibit excellent physical strength and can withstand repeated flexing without considerable deterioration in the service life and performance. Consequently, such heaters can be placed in close contact with the specimen and cut into any shape. In this work, high temperature-resistant double-sided tape was used to attach the rubber heater to the mortar's surface to avoid gaps. The setup was connected to the control equipment to control the

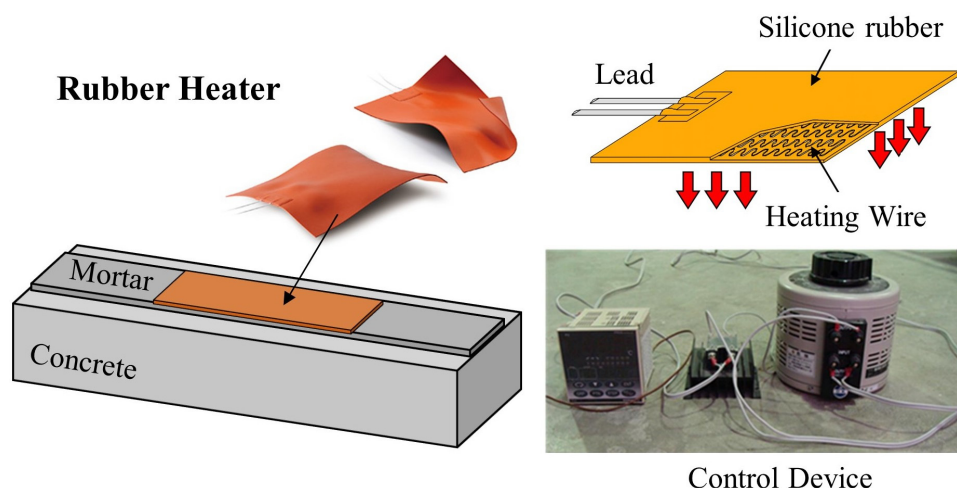


Figure 3-2 Rubber heaters for applying PTL.

temperature, heating time, and the number of cycles, as shown in **Fig. 3-2**.

3.1.2 Dimensional design of specimens and adhesion testing

As described in Section 2.2.4, the dimensional design of the specimens had a significant impact on the results of the adhesion assessment. The difference in material thickness between the mortar/substrate composite specimens in the literature surveyed is too small, resulting in an unrealistically small degree of substrate constraint on the deformation of the cover layer during the artificial aging cycle. The dimensional proportions of the specimens should be close to the actual

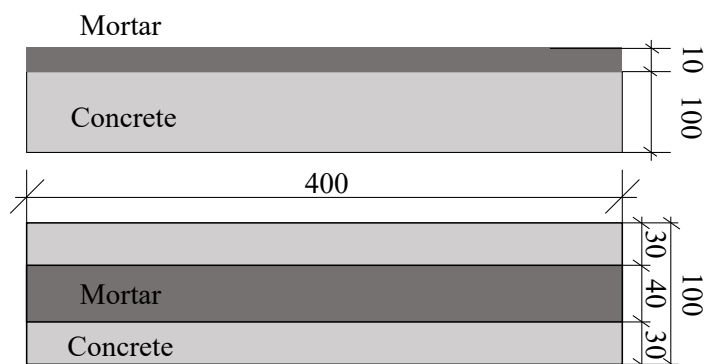


Figure 3-3 Specimen dimensions.

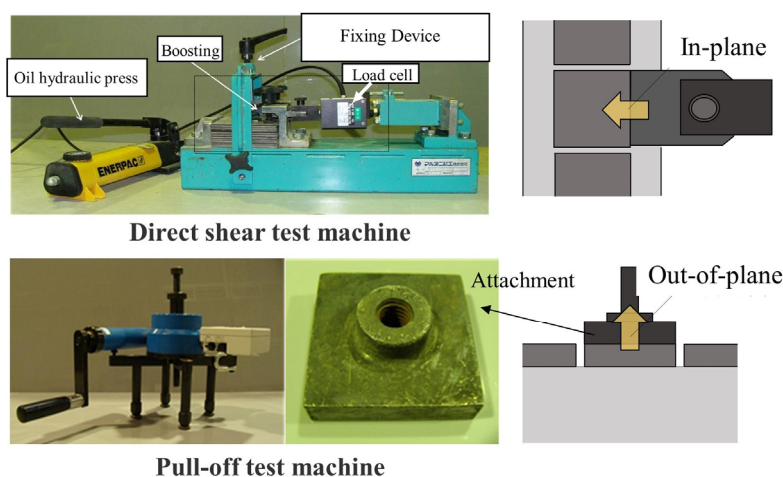


Figure 3-4 Devices for bond strength tests.

structure and based on commonly used molds. Therefore, specimens like those shown in **Fig. 3-3** are proposed. The concrete substrate was cast in the most used rectangular cast iron mold with dimensions of 100x100x400 mm, the standard size for bend strength testing of concrete in Japan. The rendering mortar had dimensions of 40×10×400 mm. The thickness of the overlayer was designed to be 1/10th of the substrate, which corresponds to the actual structure and may allow for a more reasonable magnitude of stresses generated at the adhesive interface under load. The width of the rendering mortar was designed to be 40 mm to facilitate the bond strength test. It should be noted that the findings obtained from small-sized specimens are difficult to use directly as an engineering design reference but are valuable for fast comparison and screening of samples during the product development phase.

When selecting a bond strength test method, the main interface stress conditions caused by the proposed AT need to be considered. The peeling of the mortar is caused by the restraint stresses that act both in-plane and out-of-plane; consequently, strength tests in both directions should be performed. Although tensile stress perpendicular to the interface is rare in structural design. Under solar radiation,

the interface in the structure undergoes a mixed mode involving tensile and shear stress, but the shear stresses were more dominant than the tensile stresses. Rumbayan et al. [141], who examined a wall tile structure, reported that for a tile surface temperature of 50 °C, the shear stresses generated at the tile-mortar interface were 2.6 MPa. In contrast, the tensile stresses were only 0.008 MPa. During the development phase of the durability assessment method, pull-out tests and direct shear tests were carried out to assess the degrading effect of the PTL method on the mortar/concrete adhesion. The purpose was to clarify the effect of the bond strength test method on the results of the durability assessment. The test machine was in accordance with the Japan Society for Finishing Technology standard requirements, as shown in **Fig. 3-4**.

For both tests, the rendering mortar had to be cut to 40x40 mm before the operation, which is why the mortar was 40 mm wide. In the pull-off test, the attachment is glued (e.g., epoxy resin) to the mortar surface, and care is taken to prevent the bond from bridging the cut area. The testing machine is connected to the attachment, and a perpendicular tensile load is applied; slowly rotate the handle until the mortar and concrete are separated, and the failure load is recorded. The direct shear test measures the in-plane adhesion strength by separating the plastering mortar from the mixed clay substrate by applying a force from the horizontal direction. After the specimen is fixed, the handle is shaken slowly and vertically, and the hydraulic oil pump transmits force to the side of the mortar until the mortar slides against the substrate.

3.2 NUMERICAL SIMULATION

As discussed in Chapter 2, the adhesion failure between the rendering mortar and concrete is a result of interlayer stress accumulation. The numerical model can be used to help investigate the state of interfacial stresses for a given load condition and the contribution of some factors to the development of adhesion of the mortar on the substrate. The variables can be quickly filtered by changing the properties of the material. This section validates the rationality of the proposed PTL method by performing numerical simulations by comparing it with the method of applying loads to the specimen as a whole in the literature. Comparison of the expected deterioration effect of heating the whole and part of the mortar by the stress state at the adhesive interface. The analysis was performed using ANSYS Workbench, which is a 3D finite element method (FEM) program.

3.2.1 Modeling the mortar/concrete composites

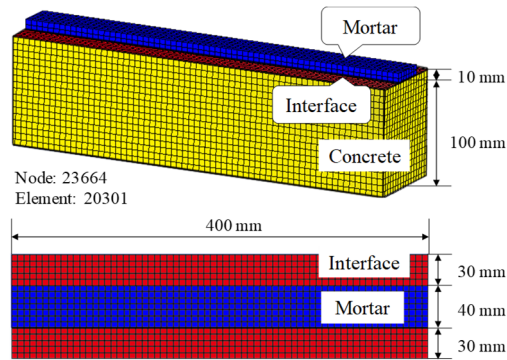


Figure 3-5 Mortar/concrete composites geometry.

As shown in **Fig. 3-5**, the 3D-FEM model consists of three components, concrete with dimensions of 100×100×400 mm, mortar with dimensions of 40×10×400 mm, and the adhesion interface. The primary purpose of this section is to validate the soundness of the proposed AT approach. Therefore, the material behavior of these elements has been simplified. In this case, the rendering mortar and concrete behavior are assumed to be linearly elastic. The ANSYS Workbench element library includes interfacial finite elements representing the cohesion zone between two elements, considering the separation across the interface. The 3-D 8-Node contact element CONTA174, schematically represented in **Fig. 3-6(a)**, is selected. The CONTA174 is a surface-to-surface contact element. The contact detection point uses a Gaussian integration point by default, which usually provides more accurate results than when using the node itself as an integration point [142]. Cohesion zone models (CZMs) have been chosen to describe interface problems. CZMs are widely used to model discrete fracture processes in some homogeneous and inhomogeneous material systems. The CMZ model is defined by introducing a critical fracture energy, which is the energy required to break the adhesive interface between the adherent and the adhered. The traction acting on the interface and the corresponding interfacial separation (displacement jump across the interface) depends on the element and material model [143]. The form of the constitutive relationships and parameters varies from model

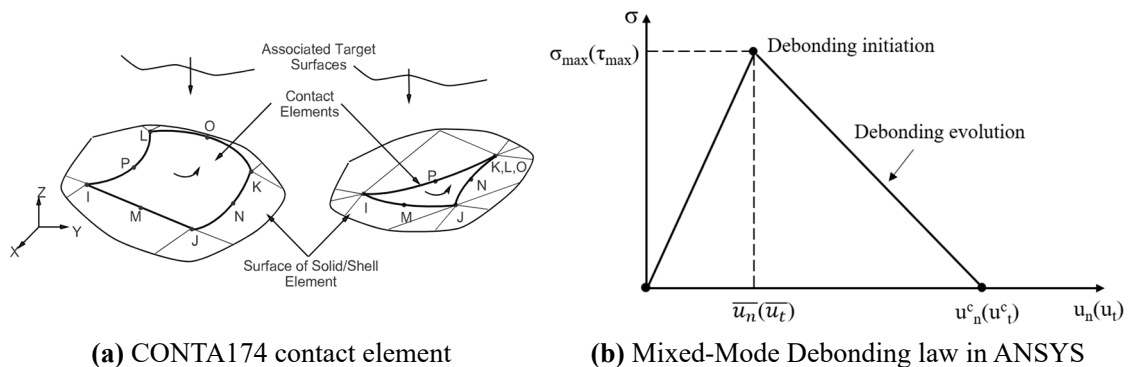


Figure 3-6 Modelling the mortar/concrete adhesive interface, according to [143].

to model. In this work, a mixed fracture model (Mode I and Mode II) of CZM is used, as shown in **Fig. 3-6(b)**, considering that the debonding of the mortar is caused by stresses in both the normal and tangential directions.

σ_{\max} , τ_{\max} , u_n^c , and u_t^c are the inputs of the interface elements. Where, σ_{\max} is the maximum normal contact stress; τ_{\max} is the maximum equivalent tangential contact stress; u_n^c is the contact gap at the completion of debonding; u_t^c is the tangential slip distance at the completion of debonding. The parameters were set based on the results of bond strength tests obtained under the same conditions in the laboratory, as detailed in Section 3.3. In addition, a theoretical reference to the CZM used is supplemented in **Appendix A** of the dissertation. The material parameters of the concrete and mortar components were set according to the JSCE recommendations [144], as summarized in **Table 3-1**.

Table 3-1 Model material parameters

Parameter	Concrete	Mortar	Interface
Density (kg/m ³)	2300	2100	-
CTE (1/°C)	1.10E-05	1.50E-05	-
Young's Modulus (GPa)	28	20	-
Poisson's Ratio	0.2	0.2	-
Tensile Yield Strength (Pa)	2.78E+06	3.50E+06	-
Compressive Yield Strength (Pa)	3.00E+07	3.96E+07	-
Isotropic Thermal Conductivity (W/m·°C)	1.6	1.5	-
Specific Heat (kJ/kg·°C)	0.7	0.6	-
Maximum Normal Stress (Pa)	-	-	1.05E+06
Maximum Tangential Stress (Pa)	-	-	9.73E+05
Normal separation distance (μm)			400
Tangential slip distance (μm)			400
Artificial Damping Coefficient (s)	-	-	0.001

3.2.2 Application of numerical model

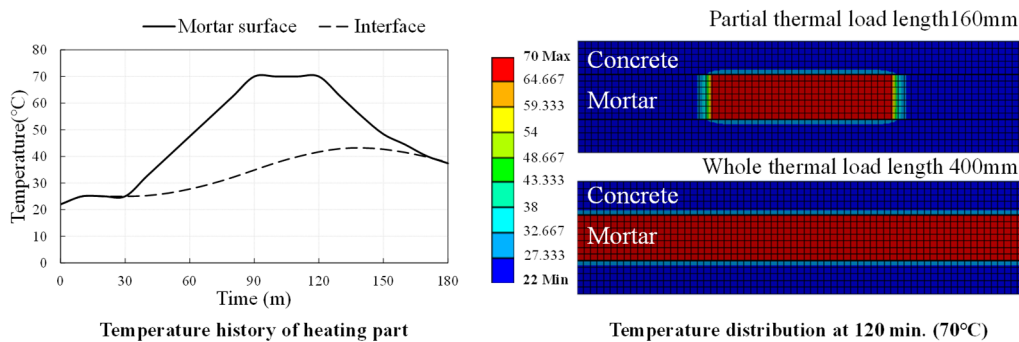


Figure 3-7 Thermal load conditions.

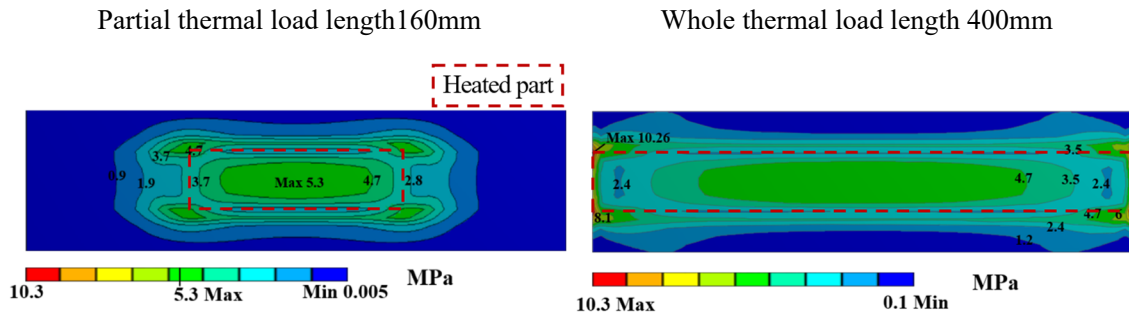


Figure 3-8 Equivalent (von-Mises) stress (MPa) at the FEM model interface at 120 min.

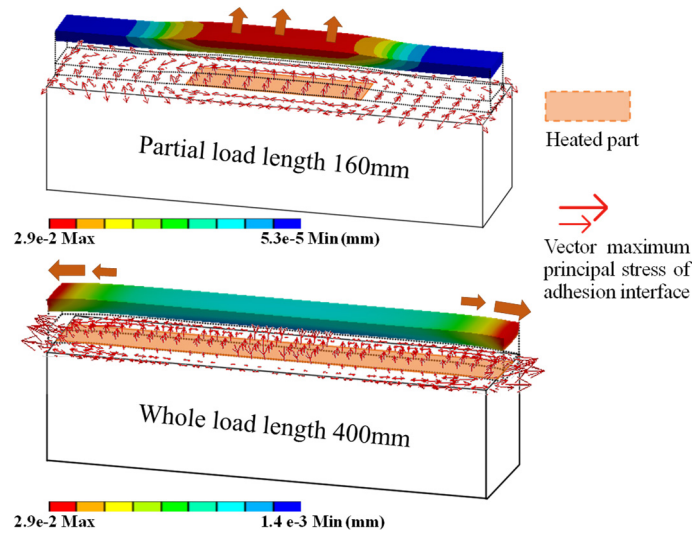


Figure 3-9 Maximum deformation (mm) and maximum principal stress direction of the mortar in the FEM model.

The model was evaluated by performing transient thermal and structural analyses. The concrete bottom surface in the model was set as a fixed constraint, similar to that in the actual conditions. One thermal load cycle was applied to the entire and central part of the mortar surface with a load length of 400 mm and 160 mm, respectively. **Fig. 3-7** shows the temperature history of the mortar surface and the adhesion interface below the thermal load zone. It can be noted that after the peak temperature load of 70 °C was maintained for 30 min., the temperature increased only around the loaded portion owing to the low thermal conductivity of the concrete. The purpose is to obtain the stress distribution of the adhesion interface at high temperatures to verify the rationality of the proposed partial thermal load method. The dry shrinkage effect, cracks, and decrease in the adhesive strength owing to the cyclic thermal loads were not considered.

Fig. 3-8 shows the equivalent stress at the interface of the FEM model under thermal load lengths of 160 mm and 400 mm, at the 120th minute of a cycle (after heating at 70 °C for 30 min). It can be noted that in the case of the model subjected to a partial thermal load, the stress is concentrated at the

center of the mortar; in contrast, in the model subjected to the whole load, the stress is concentrated at the ends, in accordance with the movement trend of the mortar. **Fig. 3-9** shows the maximum deformation of the mortar under one thermal loading cycle, the red arrow represents the direction of the maximum principal stress of the adhesion interface at that moment. The maximum principal stress of the heated part of the interface is directed in the out-of-plane direction, and the mortar and concrete have a tendency to delaminate. However, the maximum principal stress of the interface subjected to the whole thermal load is located at the end, and the direction is almost parallel with the interface. From the deformation results, the expansion caused by the heating of the mortar constrained by the surrounding area tends to deform the material in the vertical direction. Therefore, the stress is concentrated on the loaded part. In contrast, the mortar not constrained by the surroundings tends to deform toward both ends, and the stress is concentrated at the ends.

The FEM analysis results indicate that the deformation of the mortar subjected to partial thermal load is consistent with that of the actual rendering mortar for external walls. The complete heating method cannot reproduce the degradation mechanism of the actual walls owing to the thermal expansion of the mortar not being sufficiently constrained. Therefore, it is considered that providing thermal load at the center, which can degrade the target location by realizing an appropriate constraint for the heated part, is a superior accelerated deterioration approach compared to the complete heating approach.

3.3 EXPERIMENTAL TEST OF THE PTL METHOD

It has been verified by numerical analysis that the damage pattern caused by the PTL method is more representative of what happens when the facade is exposed to solar radiation. In this section, the actual degradation effect of the PTL method is verified experimentally, i.e., by comparing the change in mortar adhesion before and after loading.

3.3.1 Specimen preparation

The dimensional design of the specimens is described in Section 3.1.2. The mixture proportions of the concrete substrate and rendering mortar are listed in **Tables 3-2** and **3-3**, respectively.

The concrete substrate for all the specimens was prepared by demolding the concrete the day after casting and subsequently curing it in 20 °C water for more than two months. The concrete was sufficiently dried to reduce the errors caused by drying shrinkage. Specifically, before plastering, the substrates were dried for more than one week at 40 °C.

The specimens were prepared with reference to the Japanese Architectural Standard Specification—JASS15 Plastering Work [145]. Generally, to achieve higher adhesive strength, a series of pretreatments, such as polishing, cleaning, and adhesive application, are performed on the plastered surface. There are different technique classifications according to the concrete removal depth [56].

Table 3-2 Mix proportions of base concrete.

Strength (N/mm ³)	Slump (cm)	Water- cement ratio, W/C (%)	Weight (kg/m ³)				
			Water	Cement	Fine	Coarse	Admixture
36	18	44	180	410	798	887	3.32

Table 3-3 Mix proportions of rendering mortar.

Mortar	Cement	Fine aggregate	Cement: Fine aggregate (by Weight)	W/C (%)
Pre-mixed mortar	Ordinary Portland cement 80% Blast furnace slag 20%	S: Crushed sand	1: 2.5	50/60

Sand blasting, shot blasting, grinding, low-pressure/high-pressure water demolition and manual/mechanical milling are the common methods used to create rough concrete surfaces. However, some of the more destructive methods increase the roughness while also increasing the risk of micro-cracking on the substrate surface, thereby reducing the bond [54], [56], [146]. This study aimed to validate the proposed AT method; therefore, the initial bond strength was not deliberately optimized. In this work, 60-grit sandpaper was used to clean up the substances generated during curing and the residual release agent on the substrate surface until the surface of the substrate exposed the fine aggregate, and no visible texture can be observed visually. The roughness was between 1 and 2 according to the International Concrete Repair Institute (ICRI) standard [147]. Acetone was used to remove dust and grease, which improved the adhesion of the mortar. Finally, ethylene-vinyl acetate (EVA), which is an adhesion promoter, was applied to the surface two hours prior to plastering. This step is necessary to prevent the water in the mortar from being absorbed excessively by the concrete. The effect of the degree of dryness of the interface on adhesion has been subject to debate. Traditional treatments recommend pre-wetting the surface of the substrate, but some researchers consider this practice detrimental to adhesion. In this case, it peels off the concrete very easily. The specific reasons for this have been discussed in Section 2.1.1. Lukovic and Ye [148] also state that dry substrates result in more voids at the interface as the water loss from the substrate reduces the effective W/C and the hydration of the applied material. Therefore, adequate drying of the substrate before the mortar is cast,

then using EVA to control water transport may be a compromise; meanwhile, the formation of polymer films and the formation of hydrogen bonds during hydrolysis in the polymer favor adhesion [38] [40].

The rendering mortar used in this work is a commercial ready-mixed mortar developed to plaster and repair fracture surfaces. This type of mortar is usually described in terms of the strength grade and is reasonably stable. According to the manufacturer's data, this rendered mortar has a compressive strength of 30 N/mm² after 28 days of curing. Because rendering mortar is fragile in the early stage of curing, it was maintained in a stationary state for two days after pouring and then moved to an environment with a temperature of 20 °C and relative humidity of 60% for 28 days until the degradation experiment was performed.

3.3.2 Accelerated degradation effect tests

(1) Accelerated degradation

The same thermal load as that in the FEM analysis described in Section 3.2.2 was used in the experiment. One cycle was divided into four temperature steps for a total of three hours: 25 °C (30 min) → 25 °C to 70 °C (60 min) → 70 °C (30 min) → 70 °C to 25 °C (60 min), as shown in Fig.3-10(a). Notably, the cycling pattern is not unique, as alternative cycles with varied peak temperatures and temperature gradients have been utilized in subsequent research. The influence of the cyclic mode of thermal loading is outside the scope of this dissertation and will be studied in the

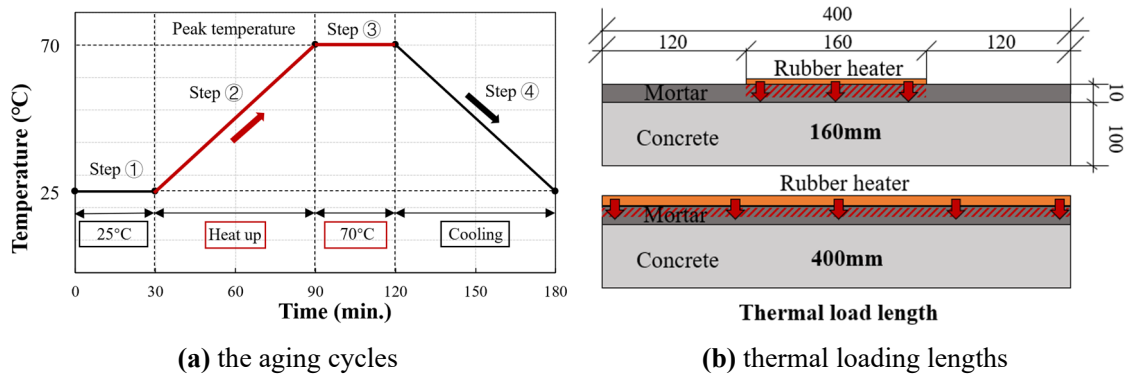


Figure 3-10 Thermal load cycle and application.

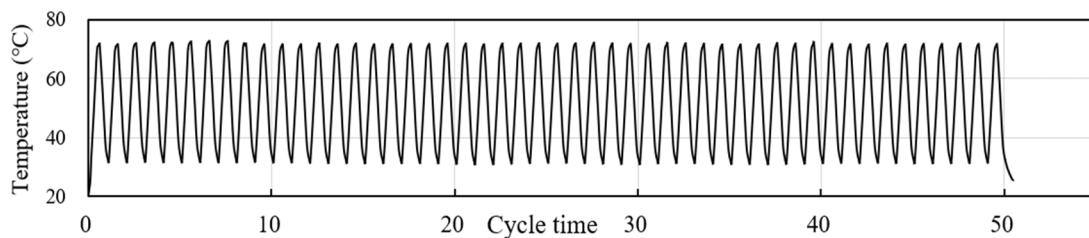


Figure 3-11 Temperature history of the mortar surface during 50 cycles.

future. During the heating experiment, the surface temperature of the rubber heater and mortar was monitored in real-time by using thermocouples. The laboratory temperature was maintained at 20 °C because the rubber heater could only be operated when the set temperature was higher than the room temperature. The peak temperature of 70 °C was determined based on the most severe load conditions that an exterior wall may be subjected to in summer. The number of cycles was set to 50 based on the tolerance of the weakest part. In particular, it was necessary to ensure that the specimen with the weakest adhesion strength in the degradation experiment did not peel. **Fig. 3-11** shows the temperature history of the mortar surface of a specimen under 50 thermal loading cycles. It was confirmed that the desired temperature could be applied to the mortar surface by the rubber heater.

To validate that the partial heating method could degrade the adhesion, the entire specimen was heated using the same rubber heater, and the temperature history was recorded. As shown in **Fig.3-10(b)**, the two thermal load lengths (160 mm and 400 mm), as in the FEM analysis, were applied to the specimens by controlling the length of the rubber heater.

(2) Bond strength test

After the specimen was cured (after 50 load cycles) and cooled to room temperature, the mortar was evenly cut into 10 parts with dimensions of 40 mm×40 mm×10 mm using a grinder and tested sequentially before testing. The adhesive strength was defined as the ratio between the failure load and the test area:

$$S = N/A_o \tag{3-1}$$

where S is the adhesion strength, N is the maximum shear/tensile failure force, and A_o is the test area (16 mm²).

Owing to the symmetry of the specimen, the average value of the strength at a location equidistant

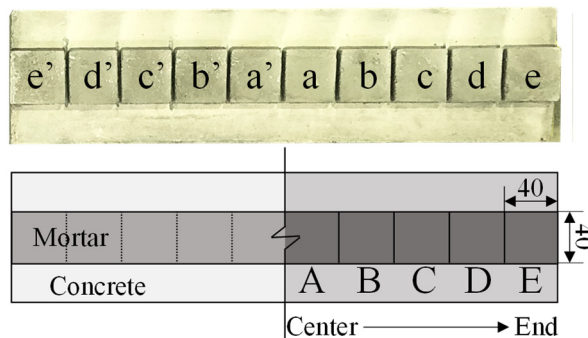


Figure 3-12 Contrast zones for the adhesive strength.

from the heated part was used. For example, the average of a and a' was considered the adhesive strength of the middle part A. The adhesive strength of the specimen was divided into five parts from the center to the end as A–E for the evaluation, as shown in **Fig. 3-12**. Because the adhesive strength test was destructive, at least two specimens were prepared (not heated after curing) to obtain the initial values for each group. The average value was considered the experimental result.

3.3.3 Results and discussion

(1) Degradation effect of PTL aging cycle on adhesion

Fig. 3-13 shows the adhesion of the specimens in the tension and shear tests after degradation over 50 cycles of thermal loading compared to the initial value. It can be noted that the adhesive strength of the central part (A, B) of the specimens subjected to the thermal load is significantly reduced, whereas that of the unloaded part (C, D, E) remains nearly constant. The decrease in the adhesive strength of the loaded boundary area B is slightly larger than that for the load center A in both the shear and tensile tests. Mahaboonpachai et al. [12] reported that under a temperature gradient and thermal expansion mismatch, shear stress occurs along the interface between the concrete and adhesive mortar. In particular, high shear stress occurs at the two edges of the specimen along the interface between the concrete and adhesive mortar. In addition, the stress state of the adhesive interface subjected to high temperatures, as shown in **Fig. 3-8**, can also explain the large decrease in the adhesive strength of region B. The stress concentration occurs not only in the central part of the load but also in the edge region. The high correlation between the experimental and numerical results supports the reliability of the numerical model. Moreover, it can be speculated that as the adhesive strength of the central part gradually decreases with the increase of the number in thermal cycles, the stress concentration part moves from the load center to the load edge.

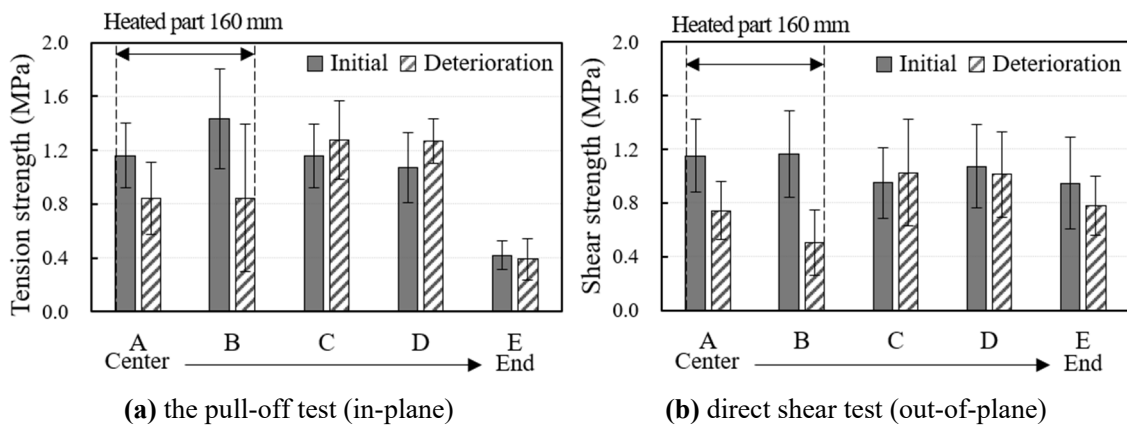


Figure 3-13 Change of bond strength in both directions.

It can be considered that regardless of the employed strength test method, it is possible to evaluate whether the adhesive strength of the specimen decreases after the specimen is subjected to accelerated deterioration through the thermal cycle loading method. However, during the pull-off test, it was observed that the attachment attached to the mortar (used to connect the tester) peeled off from the specimen before the adhesion failure. In contrast, the damage in the shear tests essentially occurred in the interface transition zone, where a thin layer of mortar was observed to cover the damaged interface, which is more comparable to the situation in the actual structure. Therefore, in the proposed durability evaluation system, the direct shear test was selected to evaluate the adhesion.

In both the tests and especially in the tensile test, the adhesive strength of the end of specimen E was lower than that of other parts. According to Georgin et al. [149], mortar can undergo curling deformation (deformation in the out-of-plane direction) owing to drying shrinkage. This phenomenon's causes are detailed in full in Section 2.2.1, the moisture gradient present in the rendering mortar thickness during the curing process thus likely caused a differential shrinkage in the thickness. **Appendix B** of the dissertation documents a series of studies to assess the effect of curling deformation on mortar adhesion. Using laser sensors and the digital image correlation (DIC) technique, respectively, the curling of mortar in the free drying shrinkage and constrained shrinkage states were studied. The stresses at the adhesive interface between mortar and substrate were anticipated by numerical simulation. The research confirmed that curling had a negative effect on adhesion. DIC revealed out-of-plane deformation of the mortar/concrete specimens' ends. Nevertheless, according to numerical models, the PTL offers a significantly more potent force for debonding than drying shrinkage even under extreme drying circumstances. Furthermore, effective countermeasures, such as the use of shrinkage reducing agents (SRA) and the placement of an overlayer on the mortar surface, which both promote uniform drying of mortar, can be used. Although curling distortion of mortars is a non-negligible factor affecting adhesion, it does not interfere with the evaluation of durability, it is found. Effective countermeasures can be implemented, such as using shrinkage reducing agents (SRA) and applying an overlayer on the mortar surface, both of which promote uniform drying of mortar. It is concluded that although curling deformation of mortars is a non-negligible factor impacting adhesion, it does not interfere with the durability assessment.

(2) Degradation effect of the thermal load lengths

To verify the degradation effect of the partial thermal loading experiment on the adhesion, the complete thermal loading experiment was performed as a control group. **Fig. 3-14** shows the shear

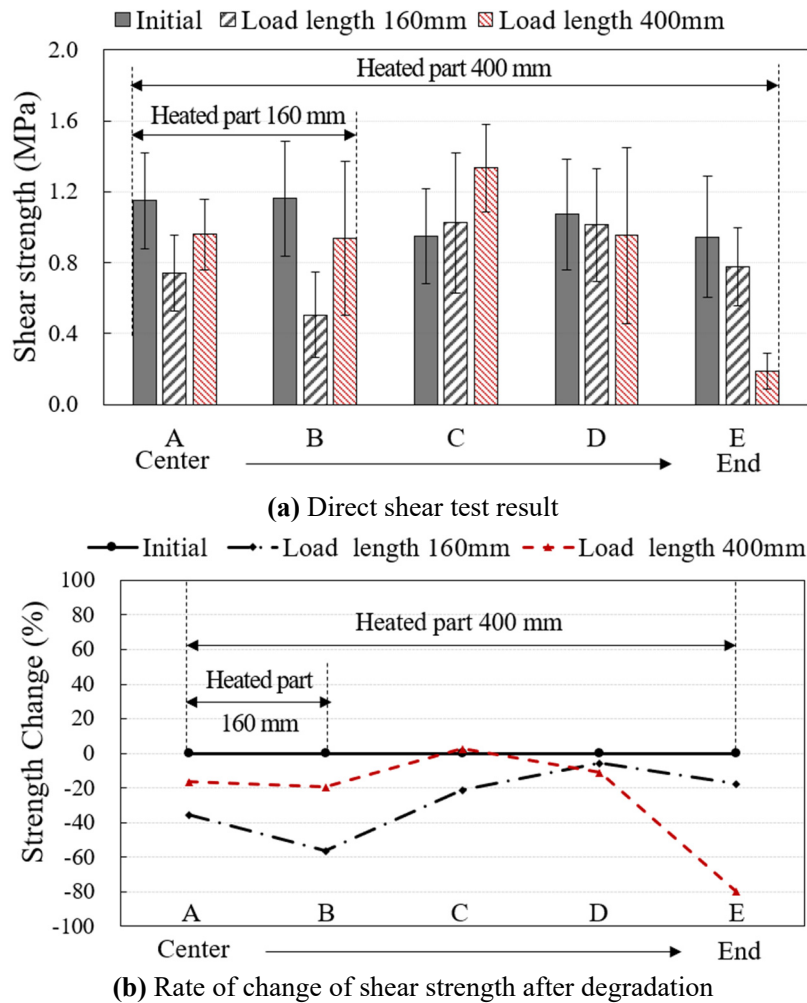


Figure 3-14 Shear strength of specimens under different thermal load lengths.

test result and change rate of the specimens before and after degradation, induced by the change in the thermal loading lengths (160 mm and 400 mm). The results indicate that the partial heating method can significantly degrade the adhesion of the target location. The adhesion of the middle part (A, B) of the specimens subjected to a partial thermal load significantly decreased, whereas that of the other parts only decreased slightly. In contrast, the complete load specimens exhibited more obvious damage only at the end.

The experimental and FEM analysis results indicate that the proposed partial thermal load method can simulate the actual degradation mechanism and is a reasonable and effective means to realize accelerated degradation. The direct shear test gives more consistent bond strength results than the pull-out test. A high correlation exists between stress generation and the mechanism of reduction in adhesive strength. It is necessary to monitor the interfacial stress in future experiments.

3.4 RENDERING MORTAR DEGRADATION PATTERN UNDER PTL CYCLES

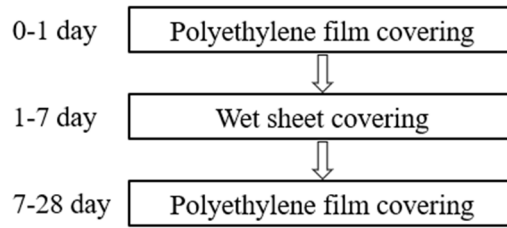
The health status of a structure can be determined by analyzing the features extracted from continuous or periodically spaced measurements. Where continuous monitoring is not possible, it is a question of how to set the periodicity of the measurements. In section 2.2.3 of Chapter 2, two studies on the degradation pattern of the adhesive properties of mortars are presented. The debonding process of the mortar is accompanied by two crucial inflection points, both under thermal loading in the uniform warming mode and under cyclic mechanical loading. Before the first inflection point, debonding proceeds slowly and is even difficult to observe; after the first inflection point, debonding develops rapidly but steadily; after the second inflection point is encountered, stability is lost and soon progresses to destruction. However, the pattern of change in debonding behavior before and after the inflection point is influenced by the loading pattern. Furthermore, according to Cao and Chung [91] (**Fig. 2-15**), the amplitude of the cyclic mechanical load (maximum load) also affects the location of the inflection point and the pattern of development of debonding. The degradation pattern of adhesion may be correlated with the load's form and magnitude.

The decision on the measurement period is, therefore, crucial for the results of the durability evaluation. In section 3.3, the testing of the adhesion state was carried out after 50 thermal load cycles. On the one hand, there is no basis to justify this as good timing for the test, as it is difficult to determine at which stage of debonding evolution after 50 cycles. On the other hand, the durability comparison was only carried out after a given load cycle, whether this mode of assessment is justified. Whether it is necessary to output combined results after parallel testing in multiple dimensions. All these questions need to be judged based on the degradation pattern of mortar adhesion under the proposed AT method.

This section, therefore, investigates how the bond strength of the mortar decreases along with the PTL cycle.

3.4.1 Methods

The specimens were prepared according to the method described in Section 3.3.1. The only difference is that the curing method of the rendering mortar was adjusted to reduce curling deformation due to drying shrinkage; according to previous studies [150], curling deformation occurs mainly in the week after mortar casting. Therefore, the surface of the mortar was covered with a wet sheet for the first 7 days of curing:



The mortar adhesion degradation pattern was obtained through bond strength tests every six PTL cycles. The thermal load was applied in the same way described in Section 3.3.2. The difference is that the bond strength of one set of specimens is tested every six cycles until the bond strength in the heated area falls below 0.4 MPa, which is the minimum permissible value in the specification for the bond strength of exterior rendering mortars. Direct shear tests obtained the bond strength. Each group contains three specimens, and given the symmetry, six data can be obtained from the same position.

The thermal cycle is shown in **Fig. 3-15**. As mentioned earlier, the degradation pattern is related to the loading magnitude and the loading form. By adjusting the peak temperature, experiments were carried out in two cyclic modes with different loading magnitudes and loading rates (warming and cooling rates). In this study, one cycle was 4 hours: 25 °C (60 min) → 25 °C to 70/80 °C (60 min) → 70/80 °C (60 min) → 70/80 °C to 25 °C (60 min). It is worth mentioning that the experimental environment was slightly different between the 80 °C cycles and the 70 °C cycles. The 70 °C cycles were carried out at a temperature of 20 °C and 60% humidity, whereas the 80 °C cycles only controlled the room temperature (20 °C) and not the humidity.

3.4.2 Results and discussion

As the plastering was done by hand, the results of the bond strength tests were inevitably highly scattered, although the variables were controlled as far as possible. In discussing the results, the bond strength for each group of specimens was calculated as follows; the average of the six results from the

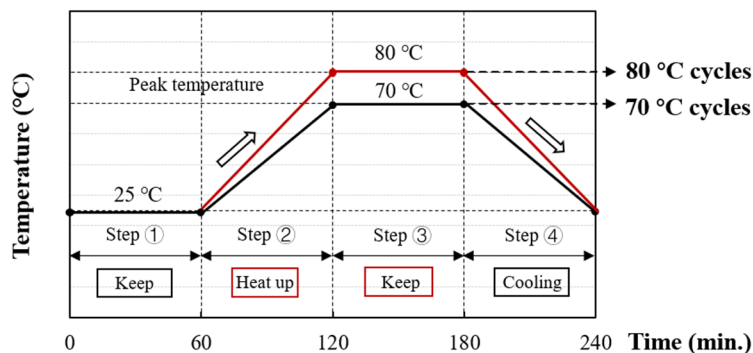


Figure 3-15 Aging cycles for studying degradation patterns.

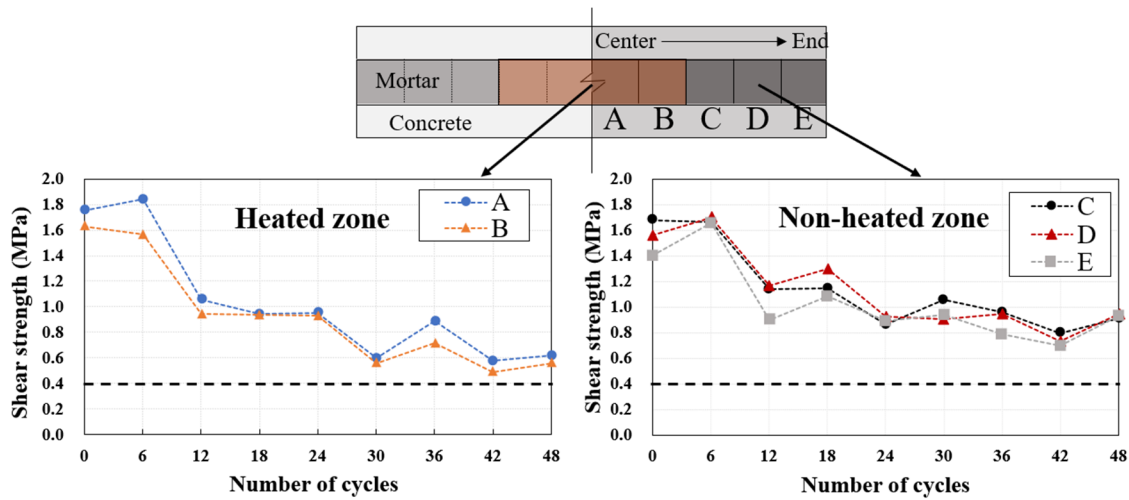
exact location after the maximum and minimum values had been removed.

(1) Accelerated degradation at 80 °C cycles

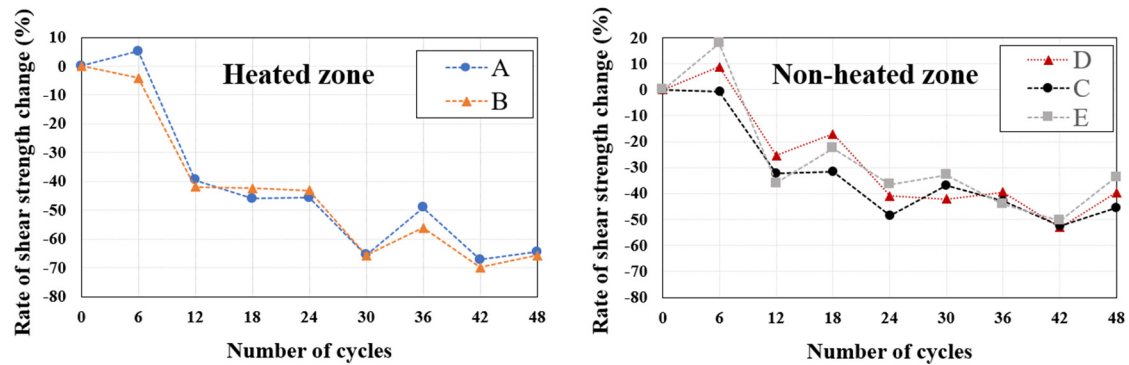
In the first study, the specimens were subjected to a maximum of 48 load cycles. Evolution of the bond strength in the specimens submitted to the aging cycles is shown in **Fig. 3-16**, **(a)** **(b)** shows the bond strength value and the rate of bond strength change, respectively. The following equation obtains the rate of bond strength change:

$$R_D = (S_D - S_0)/S_0 \tag{3-2}$$

where R_D is the rate-of-change of the bond strength, S_0 is the bond strength before load, and S_D is the bond strength at the same position after degradation.



(a) Variation of bond strength values with aging cycles



(b) Rate of bond strength change with aging cycles (vs. 0 cycles)

Figure 3-16 Evolution of the bond strength in the specimens submitted to the aging cycles
– Peak temperature of 80 °C.

First, for the heated regions (A and B) in the left column of **Fig. 3-16**, the bond strength of the concrete and mortar gradually decreases with PTL cycles. However, the rate of decrease was not uniform and was significant between 6 and 12 cycles at a maximum temperature of 80°C for the PTL cycle. In other words, the first inflection point of the degradation process occurs between 6 and 12 cycles when debonding suddenly starts to develop. Subsequently, debonding gradually evolved between the 12th and 24th cycles but showed a steady trend. No decrease in bond strength was observed at this stage, which could be due to two reasons; 1) debonding proceeds so slowly at this stage that the bond strength test cannot observe it. 2) the variability of the initial bond quality of the specimens. **Fig. 3-17** (left) represents the results of the bond strength test in area A. The results of the 12-30 cycles show a large dispersion. There was another significant drop in adhesion between cycles 24-30. Although the test results fluctuated in cycle 36, combining the results from cycles 42 and 48, the debonding process appeared to stabilize and slow down again after cycle 30 until cycle 48, when half of the specimens already had bond strengths below 0.4 MPa, and loading was terminated.

In addition, after the 30th cycle, cracks were observed on the surface of the heated mortar in some specimens, and the morphology of the cracks is marked in **Fig. 3-17**. Complete debonding of the mortar in part with cracks (area A) occurred at the time of cutting, which was because the tensile force generated by the expansion of the mortar in the out-of-plane direction under thermal load exceeded its tensile strength, resulting in fracture damage. This may indicate that the cracks on the surface of the rendered facade represent a small area where the rendering mortar has debonded.

A decrease in bond strength was also observed for the non-heated areas. After 48 cycles, the rate of decrease in bond strength in the non-heated areas was approximately half that in the heated areas, with an average reduction of 39% in parts C, D, and E and 65% in parts A and B. The most significant decrease in bond strength was also observed between cycles 6 and 12. The most significant reduction in bond strength throughout the process also occurred between cycles 6 and 12, with the difference that no second inflection point was observed afterward. In fact, the decrease in the strength of the C,

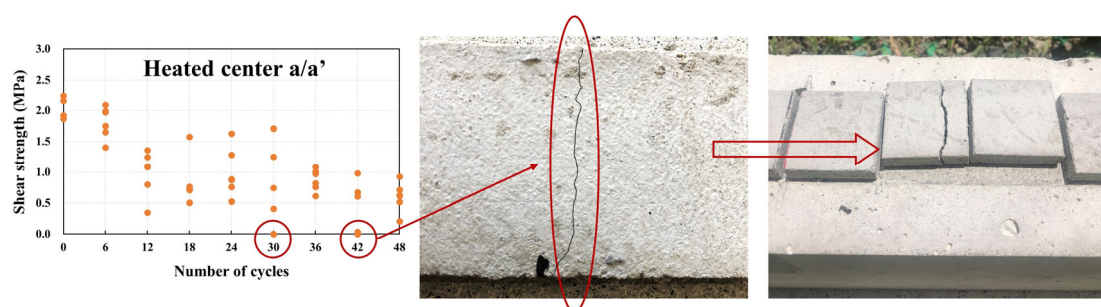


Figure 3-17 Cracks on the mortar surface after thermal loading.

D, and E parts was around 35% in both the 12th and 48th cycles. Therefore, it can be assumed that debonding hardly evolves in the non-heated region after cycle 12. This 35% loss of adhesion is most likely due to the drying shrinkage of the mortar.

(2) Accelerated degradation at 70 °C cycles

In the second study, the specimens suffered a maximum of 78 cycles due to a decrease in peak temperature. Evolution of the bond strength in the specimens submitted to the aging cycles is shown in **Fig. 3-18**, which shows the trend lines for each variable. The degradation pattern of mortar adhesion changes as the peak temperature of the thermal load decreases. For the heated zone, unlike the "stepwise" decrease observed at the 80 °C cycles, the delamination between mortar and concrete at the 70 °C aging cycles proceeded in a relatively steady and gradual manner. The overall decrease in adhesion for B, representing the edge of the heated area, was more significant than for the center of the heated area (part A), with complete debonding observed at the earliest, consistent with the description in section 3.3. Part A's shear strengths were 1.65 MPa and 0.36 MPa after 0 and 78 accelerated aging cycles, respectively, with a shear strength loss of about 78%. While for part B, the shear strengths were 1.76 MPa and 0.23 MPa, respectively, with a shear strength loss of about 87%.

In both thermal loading modes, the non-heated and heated zones had similar degradation patterns,

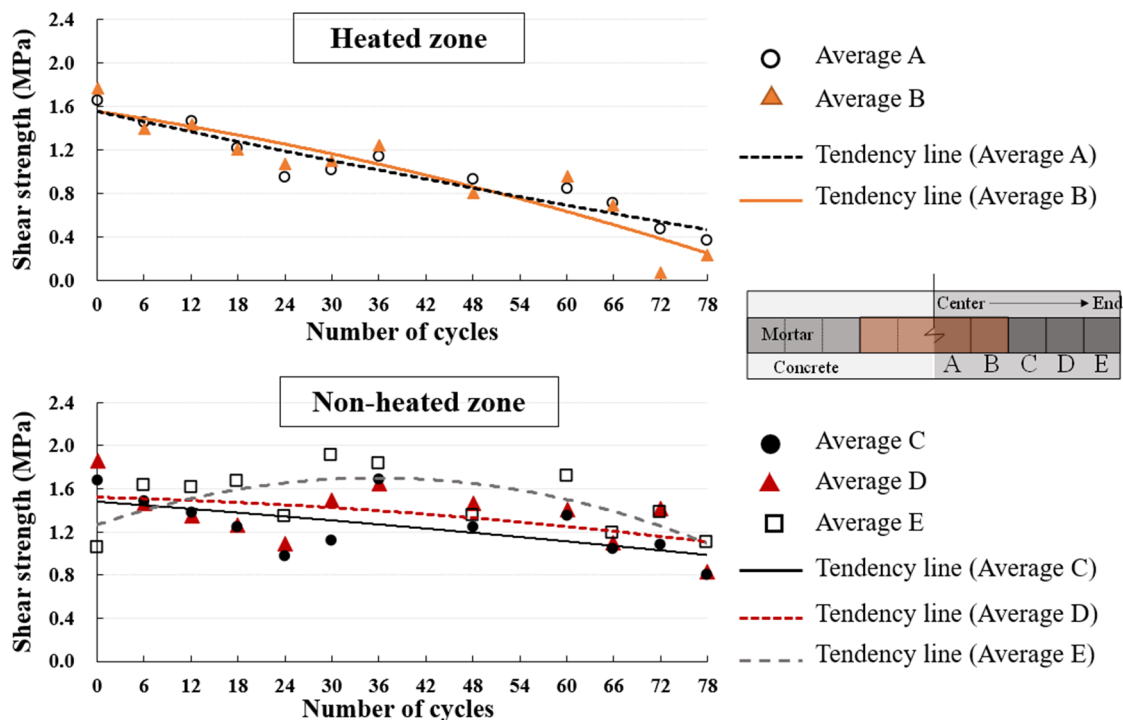


Figure 3-18 Evolution of the bond strength in the specimens submitted to the aging cycles – Peak temperature of 70 °C.

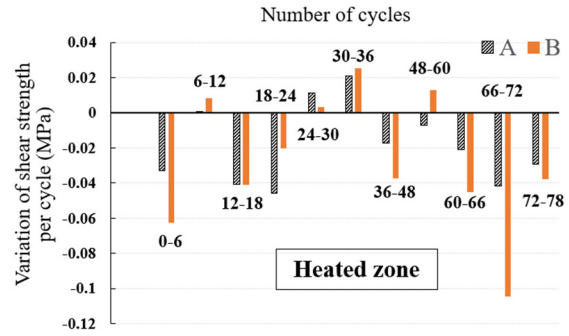
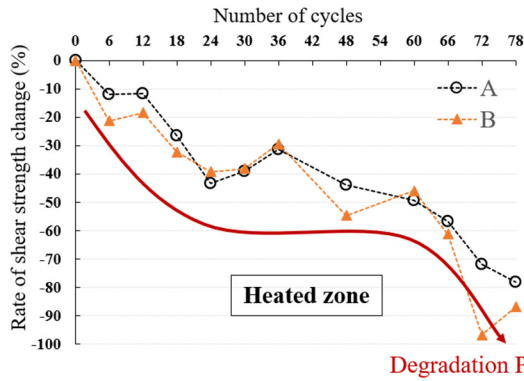


Figure 3-19 Rate of bond strength change with 70 °C aging cycles (vs. 0 cycles) **Figure 3-20** Average bond strength variation for each cycle between two shear tests.

except that the overall loss of shear strength was less in the unheated area. From the center of the specimen to both ends (C→E), 36%, 23%, and -5% were lost, respectively. The rate of shear strength loss shows that the non-heated region is also affected by thermal loading to some extent, and the closer to the thermal loading zone, the greater the trend of shear strength loss. In addition, there is almost no strength loss in the end E of the specimens, which may be related to the humidity control in this experiment. The increase in ambient humidity and the change in the curing method reduced the curling deformation of the mortar.

Fig. 3-19 depicts the rate of change in bond strength with 70 °C cycles of heating the region. Since there are no results for cycles 42 and 54, **Fig. 3-20** shows the average shear strength change per cycle between the two shear tests to observe the adhesion evolution more clearly. Calculated from the following equation,

$$\bar{S} = (S_i - S_j)/(i - j) \quad (3-3)$$

where \bar{S} is the average shear strength change per cycle, S_i is the shear strength after the i -th cycle, and S_j is the shear strength after the j -th cycle.

From **Fig. 3-19** and **Fig. 3-20**, it is observed that cycles 0-6, 12-24, and 60-78 are the phases with the fastest shear strength reduction. The overall degradation pattern is similar to that observed in the 80 °C cycles, which an "S" curve can represent. Three phases characterize the evolution of debonding, and cycles 24 and 60 can be considered crucial inflection points. After a certain percentage of shear strength is lost, the debonding process tends to slow down and develops rapidly only when the next

critical point is reached. Although the fluctuation of shear strength between cycles 24 and 60 is significant, the evolution of debonding in this phase can be considered slow when viewed as a whole. This "S-shaped" degradation path is consistent with that reported in the two studies presented in the literature review [89] [91] (**Fig. 2-14** and **Fig. 2-15**). Therefore, it is considered that this is not a chance result but a general pattern of mortar debonding evolution.

Interestingly, similar shear strength losses were observed in both loading modes before the slow progression of debonding. In the 80 °C cycles, the inflection point occurs at cycle 12 when the shear strength loss is A (40%) and B (42%). In the 80-degree cycle, the inflection point occurs at cycle 24 when the shear strength loss is A (43%) and B (40%). It can be concluded that after a loss of about 40% of shear strength, the evolution of debonding enters a slow development phase until the next critical point, which may be due to fatigue accumulation. This slow development phase is referred to as the "plateau" in this paper. The plateau is prolonged as the load strength (peak temperature) decreases. This means that more aging cycles need to be run to pass the plateau of debonding evolution before the shear strength continues to decrease. Conversely, it might be inferred that the lower the durability of the mortar/concrete adhesion, the shorter the plateau.

Based on these results, the author concludes that an adequate number of aging cycles should be set according to the cycling pattern when comparing the durability of the two specifications of mortar/concrete composites. At the very least, it should be guaranteed that the debonding evolution of the less adhesive specimen has passed the plateau after accelerated degradation. If the debonding of both specimens happens to have progressed to the plateau when the loading is stopped, each has likely lost 40% of its initial strength, making it difficult to compare durability. A better approach might be to perform a multi-dimensional durability test, that is, to compare the loss of bond strength after different cycles to obtain a comprehensive durability evaluation result.

3.5 SUMMARY

This chapter describes the development process of the durability assessment method. In this study, an AT method was proposed to evaluate the durability of the rendering mortar in terms of adhesion to concrete substrates. Experimental results and numerical analysis demonstrated the validity of the AT method. Based on the proposed AT method, the debonding evolution of the rendering mortar was investigated. The main conclusions of this work are:

(1) The effectiveness of the partial thermal load conditions was demonstrated, and it was noted that the restraints provided by the surrounding parts of the mortar must be considered to reproduce the real degradation environment in the laboratory.

(2) Loss of bond strength between the heated mortar and the concrete was observed in both the pull-off tests and direct shear tests. It is considered that the thermal load will cause stress in both the in-plane and out-of-plane directions at the adhesion interface between the mortar and concrete.

(3) Results of the numerical analysis performed using a 3D-FEM model confirmed that the in-plane and out-of-plane stresses were concentrated in the area in which the adhesive strength was reduced by the partial heating method, and the stress generation and mechanism of the adhesion failure were reasonably correlated.

(4) The stress concentration occurred at the edge of the load portion at which the joint strength decreased most during the experiment. Presumably, the weakest areas for plastering the mortar correspond to the junctions subjected to both sunlight and darkness, instead of those subjected only to direct sunlight.

(5) Under cyclic thermal loading, the mortar adhesion deteriorates in an "S-shaped" path. A "plateau" period can be observed in the debonding evolution, during which the bond strength does not decrease as the aging cycle runs. The debonding evolution hit a plateau when the loss of bond strength reaches about 40%. The duration of the plateau is related to the load strength. After the plateau, the debonding develops rapidly until the adhesion failure.

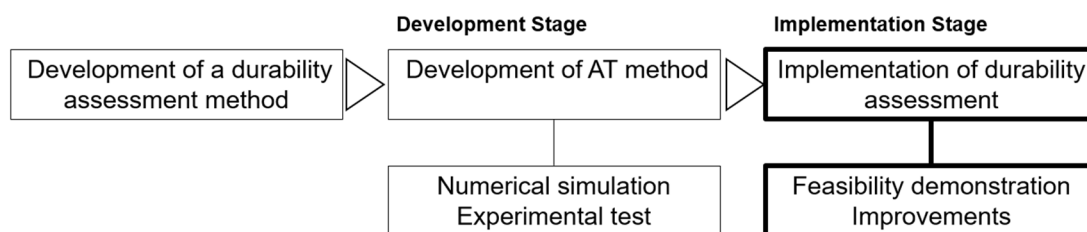
(6) Adhesion at the specimen ends is lost due to curling deformation caused by drying shrinkage, which can be improved by wet curing. For durability assessment, the drying shrinkage resistance of mortar can be determined by the loss of adhesion at the specimen ends.

Together with the above conclusions, it is concluded that the proposed durability assessment method can conduct the next step for implementation testing.

Chapter IV

APPLICABILITY OF THE DURABILITY ASSESSMENT METHOD

This chapter describes the implementation phase of the process for establishing a durability assessment method. After the feasibility of this method is proved, some upgrading attempts are made. First, the proposed AT method was applied to several mortar/concrete specimens prepared according to different specifications, and their durability was compared by shear strength tests. Secondly, an approach to continuously monitor the adhesion is proposed to provide higher accuracy of the adhesion test results in place of the shear strength test.



4.1 DURABILITY COMPARISON OF MORTAR/CONCRETE COMPOSITES

A durability assessment is run by comparing tests with reference material. This means that specimens prepared in strict accordance with the methods recommended by the code are used as the reference material. After performing the same AT, the durability ranking of the new material is determined by comparison with the reference material. This approach does not correlate with actual service life but allows for rapid comparison and parameter selection at the beginning of product development. Meanwhile, the reference material as a standard value, according to the actual service life of the reference material, can roughly estimate the expected service life of the new material.

4.1.1 Specimen preparation

Specimens prepared according to the method described in Section 3.3.1 were used as reference material (control group) and designated SV. Three experimental groups were set up, each varying only one parameter based on the SV specimen, that is, the water-cement ratio (W/C) of the mortar, the use of a shrinkage reducing admixtures (SRA), and the thickness of the mortar to prepare specimens with different adhesion between mortar and concrete. These parameters were selected as

they influence the bond strength of the mortar and concrete, as specified in the Japanese Architectural Standard Specification—JASS15 Plastering Work (2019) [145], as shown in **Table 4-1**. Although no recommendations are given in the code, according to the research in Chapter 3, drying shrinkage is also a factor in the decrease of bond strength. Therefore, the use of SRA is set as a parameter. SRA was invented by Goto et al. in the 1980s [151] and has been proven by numerous studies to effectively reduce the shrinkage and cracking of cement-based materials [152] [153]. The experimental parameters of the four types of specimens are listed in **Table 4-2**.

On specimen SV basis, the W/C of the L-1 specimens is 0.6, which is higher than the W/C of 0.5 recommended by the manufacturer. The mortar thickness of the L-2 specimens was set as 15 mm instead of 10 mm (an increase of 50%). In addition, because dry shrinkage influences the adhesion strength, the amount of SRA was set as a parameter, and the mortar of the L-3 specimens was mixed with 1% SRA. Theoretically, group L-3 should have the best adhesion, SV second, and groups L-1 and L-2 are worse because of the selection of unfavorable parameters to the adhesion.

Table 4-1 Impact factors of the adhesion strength between mortar to concrete [3.7].

			Adhesion strength		
			Lower		Lower
Factors	Adhesive interface	Roughness	Smooth	<	Rough
		Adhesion promoter	Water	<	EVA
	Mortar	W/C	Large	<	Small
		Thickness	Thick	<	Thin

Table 4-2 Specification of rendering mortar specimens.

Experimental parameter	Specimen notation			
	SV	L-1	L-2	L-3
W/C (%)	50	60	50	50
Thickness (mm)	10	10	15	10
Admixture	-	-	-	SRA

4.1.2 Durability assessment

The PTL-based aging cycle model is shown in **Fig. 3-10(a)**. The principles for setting the aging cycles are discussed in the conclusions in Section 3.4. The degradation of AT should allow the worst adhesion specimens to pass the "plateau" in the evolution of debonding; that is, the specimens should lose at least 40% of their bond strength after AT. According to the results in Chapter 3.3, the bond strength loss of SV specimens after 50 aging cycles has met this requirement, with heating centers A at 35.5% and B at 56.4%. Therefore, 50 aging cycles with a peak temperature of 70 °C is considered a reasonable choice in this study. The bond strength was obtained by direct shear test.

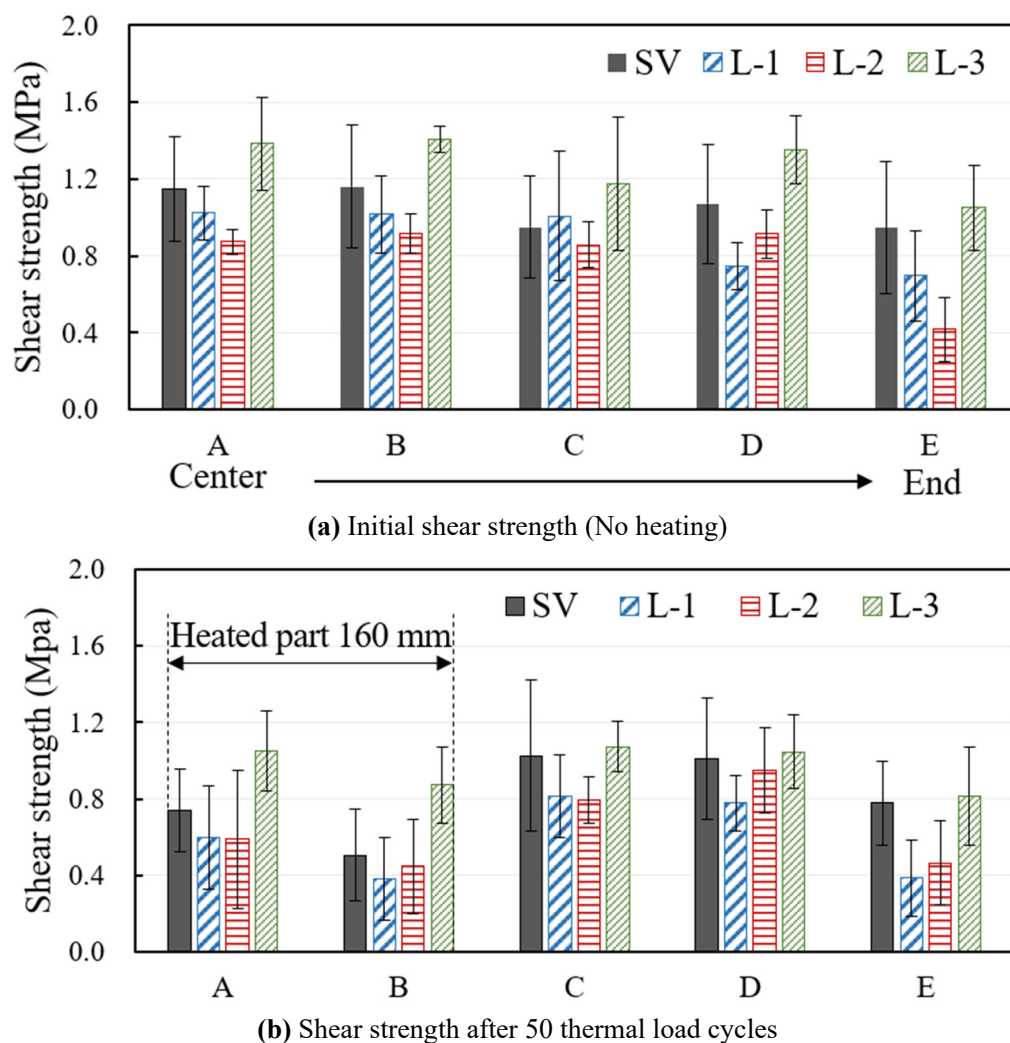


Figure 4-1 Shear strength of the four types of specimens.

Fig. 4-1 shows the shear strength results for the four groups of specimens before and after being subjected to 50 partial thermal load cycles. The strength without heating decreases in the following order: L-3 (mortar mixed with SRA) > SV (standard value) > L-1 (mortar W/C is 60%) > L-2 (mortar thickness is 15 mm).

Table 4-3 Initial shear strength (MPa) result for each group of specimens.

Specimen notation	Center				End
	A	B	C	D	E
SV	1.15 (100%)	1.16 (100%)	1.30 (100%)	1.07 (100%)	0.95 (100%)
L-1	1.02 (89%)	1.02 (88%)	1.01 (78%)	0.75 (70%)	0.70 (74%)
L-2	0.88 (77%)	0.92 (79%)	0.86 (66%)	0.91 (85%)	0.42 (44%)
L-3	1.38 (120%)	1.41 (122%)	1.18 (90%)	1.35 (126%)	1.05 (110%)

The values obtained in the shear tests are presented in **Table 4-3**. The influence of each

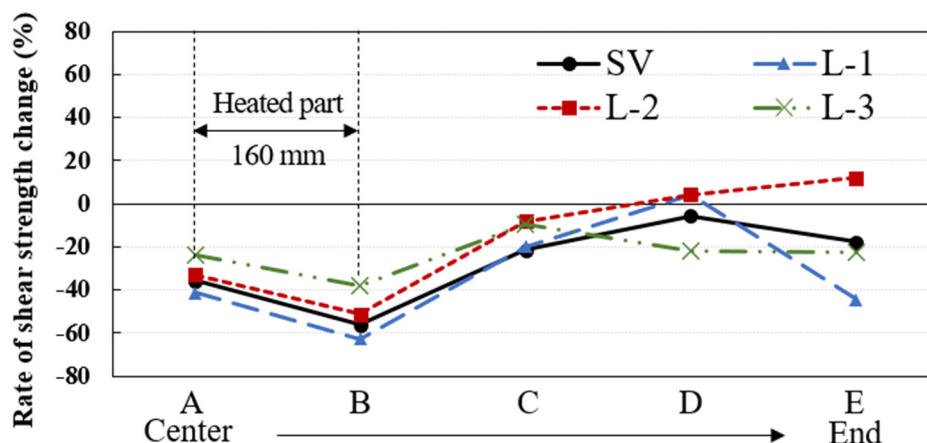


Figure 4-2 Change rate of shear strength of specimens after degradation.

parameter on the strength of the adhesives is presented as a percentage of the SV group (this latter is assigned 100%, from which the others follow), making it possible to observe the gain or loss of resistance as a function of the adopted plastering process, considering the recommended of the code as the reference value.

As speculated, the L-3 specimens exhibited a higher adhesion strength than that of the SV specimen. As mentioned in Section 2.2.1, the mortar produces a moisture gradient in the thickness during the curing. Because the moisture loss at the top of the mortar is higher than that at the bottom, the shrinkage at the surface is greater, and an upward curl deformation occurs at the edge. Thus, compared to SV specimens, L-3 specimens with the addition of SRA showed a 10-20% increase in shear strength, especially at the ends most affected by drying shrinkage. In contrast, specimens with thicker mortar (L-2) had lower shear strength due to a more significant difference in shrinkage between the upper and bottom surfaces, with only 44% of the shear strength of SV specimens at the ends. This result demonstrates the notable effect of dry shrinkage on the mortar–concrete adhesion system. Thus, dry shrinkage should be considered a key factor influencing the failure mechanism.

Fig. 4-2 shows the rate-of-change of the shear strength of the four specimen groups after 50 aging cycles, as calculated by **Equation 3-2**. All the specimens exhibit a higher reduction in the shear strength in part B than in part A. This was due to the higher stress levels at the edges of the heated region, as described in Section 3.3. Subsequently, another significant loss of shear strength occurred at the end of the specimens. This was due to the accelerated moisture loss from the mortar surface caused by the heating, and drying shrinkage again led to a reduction in bond strength at both ends.

In this work, the criterion to evaluate the durability of the rendering mortar–concrete adhesion system was as follows: A lower decrease rate of the thermal loaded parts (A and B) was considered to correspond to a higher durability of the specimen. **Table 4-4** presents the decrease rate of the

shear strength at the heated parts (A and, B). The durability was noted to decrease in the following order: L-3 > L-2 > SV > L-1. The average decrease ratio of the shear strength of the specimens (L-1) with a 10% increase in water-cement ratio was 1.13 times that for the SV group. In contrast, the decrease ratio of the L-3 specimens (mixed SRA) was 0.67 times that of the SV group, indicating that the mortar–concrete adhesion system under this treatment method exhibited superior stability. On the other hand, the resistance of mortar to curling deformation can be obtained by comparing the shear strength change rate of part E. Here, the strength increase exhibited by specimen L-2 at the end may be due to the lower initial value (shear strengths of 0.42 MPa and 0.47 MPa before and after degradation, respectively). Specimens with larger w/c (L-1) are more susceptible to drying shrinkage. This may also indicate that the low durability of L-1 specimens under thermal loading may be due to their more significant drying shrinkage rate. The specimen with SRA added (L-3) did not show excellent resistance to drying shrinkage but obtained high durability evaluation results. This may indicate that SRA does not improve durability only by reducing dry shrinkage but most likely by changing other physical properties of mortar, such as elastic modulus and linear expansion coefficient, a hypothesis that requires more research.

Table 4-4 Rate of decrease of the adhesion at the heated parts and the ends.

Specimen notation	Rate of decrease of shear strength (%)		
	Heated zone		Both ends
	A	B	E
SV	35.7	56.0	17.9
L-1	41.2	62.7	44.2
L-2	33.5	51.1	-11.9
L-3	23.9	38.3	22.9

Moreover, the factors affecting the adhesion and durability of plastering mortar are ranked. A comparison of the absolute value of the difference between the average initial shear strength of each experimental group and the SV group, the influence of the parameters on the initial adhesion in the following order: mortar thickness (10/15 mm) > W/C ratio (0.5/0.6) > addition of admixture (yes/no). Similarly, by comparing the absolute value of the difference in the decrease ratio of the adhesive strength between the SV specimens and other specimens, under the conditions set in this experiment, indicated that the influence of the parameters on the durability decreased in the following order: addition of admixture (yes/no) > W/C ratio (0.5/0.6) > mortar thickness (10/15 mm).

The initial adhesion strength comparison results and durability evaluation results of the specimens indicate that although satisfactory short-term adhesion can be obtained with the plastering methods recommended by existing specifications for external walls, the durability of the system, i.e., the long-term adhesion, cannot be guaranteed. Consequently, it is necessary to evaluate

the durability of the materials when evaluating or developing new plastering/rendering mortar materials or workmanship techniques.

4.2 A CONTINUITY APPROACH FOR ASSESSING MORTAR ADHESION

The validity of the proposed durability assessment method has been verified in the previous section. The method can be used to compare the durability of mortar/concrete adhesion made in different ways and to obtain a general idea of the influence of various factors on durability. However, the method still has some shortcomings, in particular, the bond strength test used to obtain the loss of adhesion. Regardless of which bond strength test method is used, the results show a high degree of dispersion and variability. This is because the plastering is carried out by hand, the same as in the actual construction. The low durability of rendered is often caused by poor construction quality [22]. The destructive bond strength tests may influence the judgment of durability due to the variability in the construction quality of the specimens, as the bond strength before and after degradation was obtained on different specimens. On the other hand, the degradation pattern of the adhesion was investigated in Section 3.4, and it was determined that debonding does not occur at a uniform rate. Therefore, the testing period of bond strength may affect the evaluation result of durability. In summary, developing a method that can continuously monitor adhesion on the same specimen is necessary. The strain-tracking method described in Section 2.3.1 was considered suitable as a non-destructive test method capable of monitoring the whole process of mortar debonding.

4.2.1 Monitoring the strain behavior of specimens with FBG sensors

As discussed in Section 2.3.1, significant strain differences are expected between the elements when the adhesion between two materials fails. In other words, the response of the composite to an external force impacts changes from an integrated behavior to a dispersed behavior. Theoretically, it is possible to detect debonding by analyzing the characteristics of the strain behavior of the rendering mortar and concrete. At the same time, this method allows continuous monitoring of the same specimen and may help to study the evolution of debonding. Therefore, the work in this section investigates the strain behavior of mortar/concrete specimens under PTL cycles.

(1) FBG sensors

Strain gauges are typically used to obtain the strain in each component element. However, not only can the gauge sections reduce adhesion, but also the effect of an approximately 1–2 mm thick

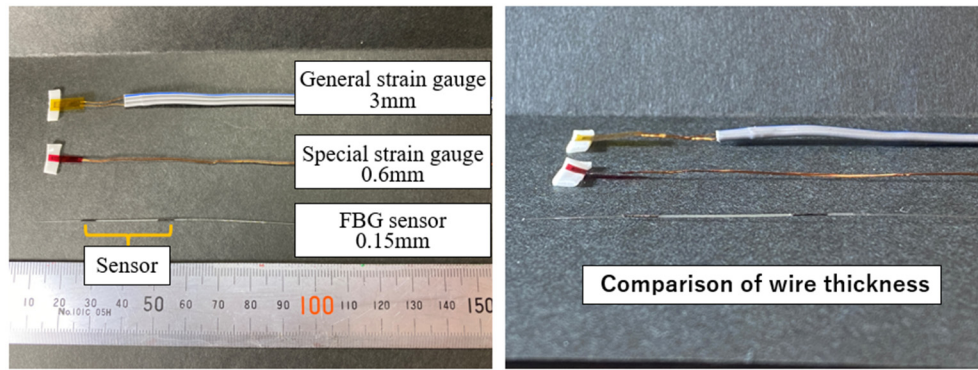


Figure 4-3 Comparison of dimensions for FBG sensors and strain gauges.

wire cannot be ignored. This implies that the application of strain gauges can potentially contribute to delamination. In this study, FBG sensors are attached to the concrete substrate and mortar surface to measure strain.

FBG sensor is a grating-based point fiber optic sensor. Unlike distribution fiber optic sensors, the measurement range is limited to the distance where the grating is carved. FBG reflects a portion of the incident light of a specific wavelength, called the Bragg wavelength, which is determined by the refractive index of the fiber and the grating spacing. When local deformation occurs, the grating period and reflected wavelength change accordingly, allowing the local strain to be detected [154].

The FBG sensor used in this experiment is a polyimide-coated sensor with a diameter of approximately 0.15 mm. As shown in **Fig. 4-3**, the FBG sensor limitedly affects the bonding properties of the tiles compared to the strain gauge. By virtue of their small size, signal stability and suitability for multiplexing, FBG sensors have been widely used for damage monitoring of composite materials [155]. Moreover, there are practical reports that FBG sensors should be suitable for long-term health monitoring of real structures [156]. FBG sensors can be set with intensive sampling periods (1 kHz), allowing the tracking of strain behavior during earthquakes. In addition, compared to traditional sensing techniques that require many strain gauges and protective cables,

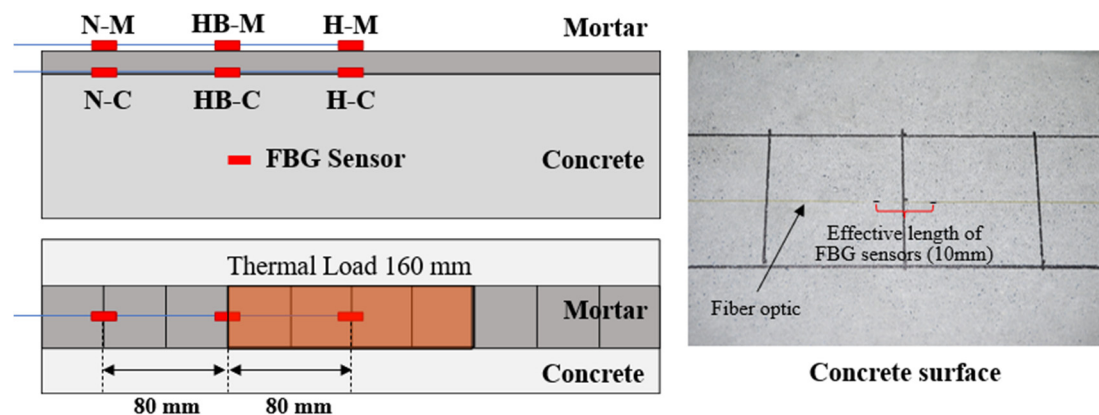


Figure 4-4 Arrangement of FBG sensors in the specimen.

FBG enables the integration of many sensors in a single fiber and the ability to measure from either end of the fiber. However, the slim dimensions of FBG sensors are similar to those of a double-edged sword, with a high risk of wire breakage. Therefore, the FBG sensors used in this experiment are coated with glass-fiber-reinforced plastics (approximately 1 mm outside diameter) on the wire (away from detection points) to increase the stiffness and prevent wire breakage encountered during the experiments.

(2) Specimen preparation

The specimens were prepared according to the procedure in Section 3.4. The difference was that FBG sensors were attached to the concrete substrate surface (adhesive interface) before the mortar was poured. The three most representative locations for measurement were chosen, the center of the heated area, the edge of the heated area, and the center of the unheated area. At each location, two FBG sensors with an effective length of 10 mm are installed parallel to the surface of the concrete substrate and mortar to obtain the strain on each element. To refer to the degradation paths obtained through the bond strength tests, the thermal load cycles applied in this work were the same as the 70 °C cycles in Section 3.4. The thermal load was applied to the central 160 mm x 40 mm area of the mortar; in one cycle: 25 °C to 70 °C (60 min) → 70 °C (60 min) → 70 °C to 25 °C (60 min) → 25 °C (60 min). **Fig. 4-4** shows the installation of the FBG sensor.

In addition to the specimens used for strain measurement (SS), other specimens of the same specification were prepared for different measurements, as shown in **Table 4-5**. ST specimens were used to measure the temperature change at the corresponding position of the FBG sensor for temperature compensation calculations. SI and SD specimens were used for shear strength tests to measure the change in bond strength before and after the load, respectively. All specimens were subjected to the same temperature load, and the experiments were carried out at constant temperature and humidity (20 °C and 60% relative humidity).

Table 4-5 Specimen for different measurements

Specimen notation	Measurement
ST	Temperature
SS	Strain
SI	Initial shear strength
SD	Degradation shear strength

4.2.2 Experimental results and discussion

As shown in **Fig. 4-4**, the detection points are named as follows; the center of the heated area, the boundary of the heated area, and the unheated area are named H, HB, and N, respectively; C

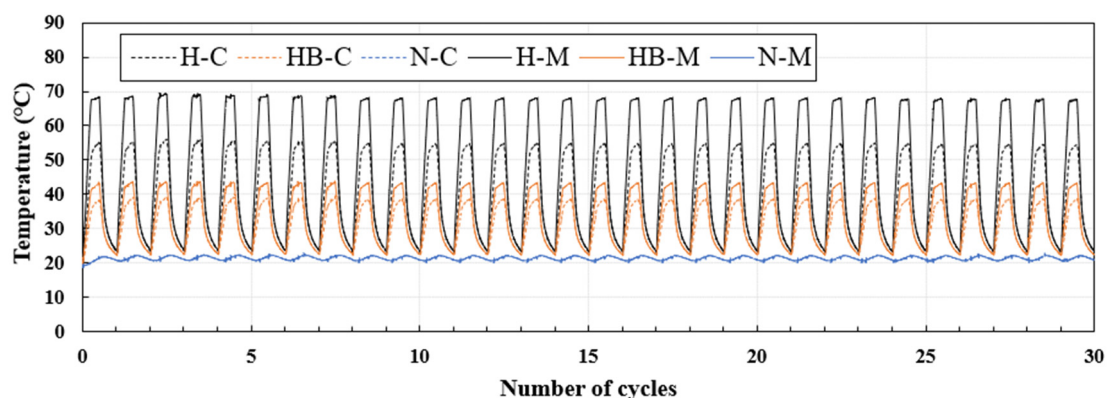


Figure 4-5 Temperature history of the ST specimens.

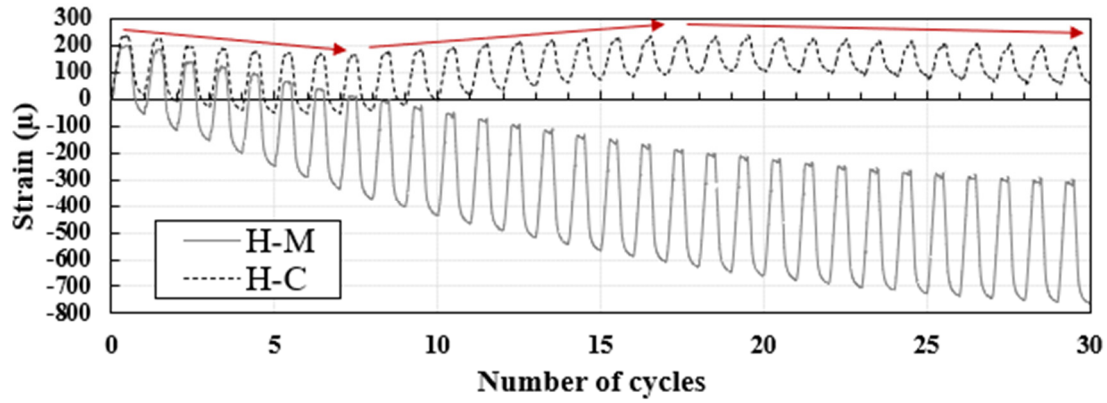
represents the sensor located on the concrete surface and M represents the sensor located on the mortar surface. For example, H-M stands for a mortar surface located in the center of the heated area.

(1) Temperature monitoring

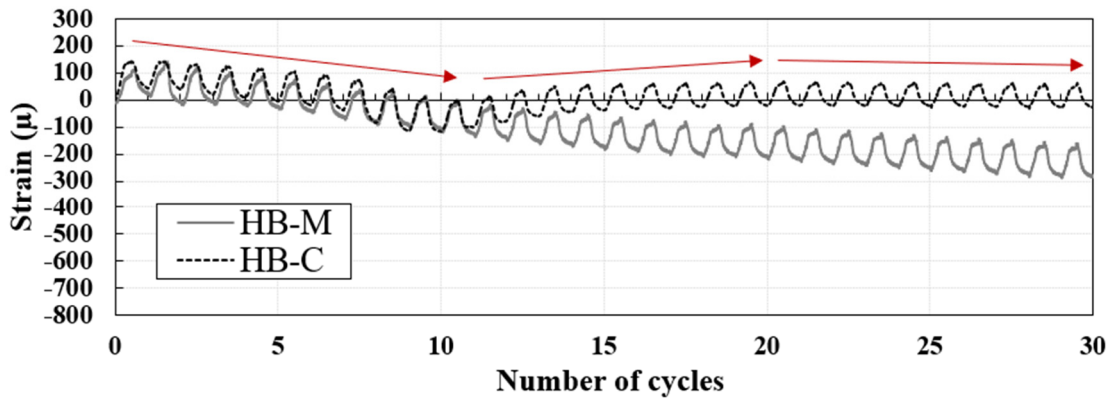
Fig. 4-5 depicts the measured temperature evolution at each detection point during aging cycles for the mortar/concrete composites. Notably, for point H-M, the temperature curve (black solid line) displayed relevant fluctuation at 70 ± 2 °C (equilibrium level). The automated temperature control system of the rubber heaters causes this effect. The system switches the heater on/off depending on the thermocouple detection of the mortar surface temperature, i.e., if the mortar is cooling down or heating up by over ± 1 °C. During the high-temperature plateau (about 1 hour) of each cycle, there is a temperature difference of about 15 °C between the concrete and the mortar at the thermal loading center, which is sufficient to cause the expected differential movement. The temperature at HB-M, which straddles the boundary between the heated and unheated areas, is approximately 30 °C lower than the center of the heated area (H-M), which could explain the loss of adhesion in part C in **Fig. 4-2**. In contrast, the temperature at N-M in the non-heated region is almost the same as room temperature, which can ensure that this region is not damaged by the thermal load while providing the expected restraint for the heated part.

(2) Strain monitoring

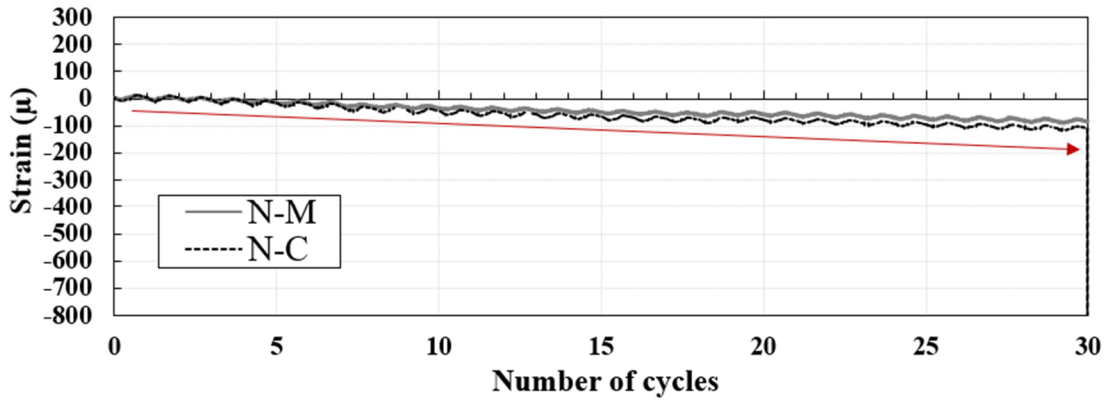
Fig. 4-6 reveals the cyclical strain induced in different layers by the thermal cycles detected by the FBG sensors; (a) (b) (c) lists the strain results comparing the mortar surface and the concrete surface in parallel positions at the area subjected to different thermal load levels, respectively. To observe the strain development trend more clearly, **Fig. 4-7** shows the strains of mortar and concrete at the end moment of each cycle, defined as the residual strain per cycle.



(a) Thermal loading center



(b) Thermal loading boundary

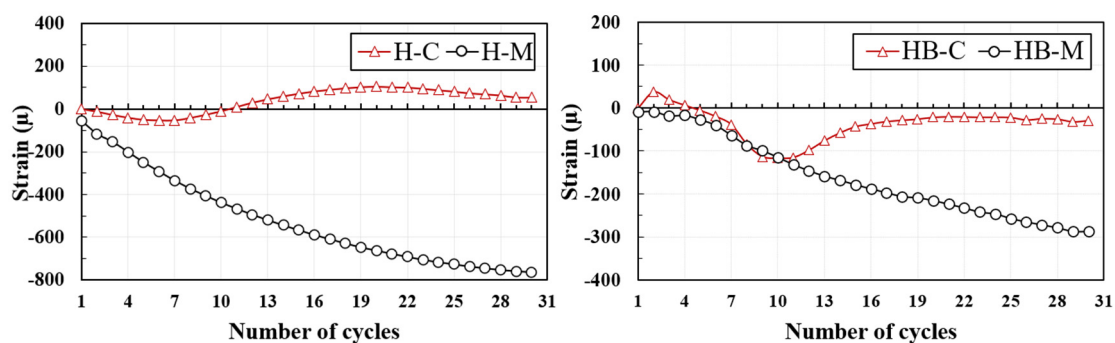


(c) Non-heated area

Figure 4-6 Strain history of the SS specimens.*i) Thermal loading center (H-C & H-M)*

In the center of the heated area, the strain trajectories of H-C and H-M overlap only in the first cycle and then gradually separate. In the 1st-7th cycles, the strains of H-C developed toward the shrinkage side, and from the 8th cycle onward, it turned to the tensile until the 17th cycle, when it started to develop slowly toward the shrinkage side again. On the contrary, the strain of H-M keeps growing toward the contraction side.

According to the strain trajectory, cycles 1-7, the concrete follows the mortar towards the



(a) Thermal loading center

(b) Thermal loading boundary

Figure 4-7 Residual strain of mortar and concrete at the end of each cycle.

shrinkage side with the same strain behavior. The bond integrity may still be maintained during this period. However, the gradual increase in strain difference indicates that degradation is ongoing. Starting from cycle 8, the concrete shows a strain behavior opposite to that of the mortar, and it is presumed that debonding may have occurred at this moment when the concrete loses the restraint from the mortar and the prestress applied initially to the FBG sensor starts to relax (H-M installed at the adhesive interface). This speculation is also supported by the residual strains in **Fig. 4-7(a)**, where the residual strains of the concrete increase from cycle eight at a constant temperature, indicating that the pressure on point H-C is gradually lost. The gap between the strain trajectory of the concrete and the mortar becomes progressively larger in cycles 8-17, and the extent of debonding is slowly expanding. From cycle 17 onwards, the concrete gradually develops towards shrinkage again, probably because the debonding within the detection range of the FBG sensor has been completed (complete release of prestress) and the drying shrinkage becomes the dominant factor in the strain trajectory. Penetration cracks were observed on the mortar surface in the heating center after 24 aging cycles, and it can be inferred that debonding has occurred.

ii) Thermal loading boundary (HB-C & HB-M)

The strain trajectories of mortar and concrete located at the thermal load boundary follow a pattern similar to that of the center of the heated area. HB-M progresses toward shrinkage with the aging cycle, while HB-C undergoes a three-stage transition from shrinkage-tension-shrinkage. Due to the lower strength of the thermal load applied and the minor temperature difference between mortar and concrete, HB-C has been following the strain trajectory of HB-M in cycles 0-11. Starting from cycle 12, the strains of HB-C and HB-M gradually separate, indicating that the debonding evolution begins from this moment. From the residual strains of **Fig.4-7(b)**, the debonding develops until the 20th cycle, until the residual strains of H-C cease to change. After the 20th cycle, the residual strains of HB-C show only a weak decreasing trend due to drying shrinkage. It can be

expected that, without further increasing the strength of the thermal load, the debonding will not continue.

iii) Non-heated zone (N-C & N-M)

According to the strain history in the non-heated zone, there is no damage to the bond integrity of mortar and concrete here. The strain trajectories of N-C and N-M maintain a good following, both towards shrinkage. However, there is a slight separation between the strain trajectories of N-C and N-M with drying shrinkage, which may indicate a partial loss of adhesion. It can be expected that the strain trajectories of mortar and concrete will further separate as the drying shrinkage increases.

iv) Effect of drying shrinkage

Comparing the shrinkage trends of the mortar in the three regions, the drying shrinkage was strongly influenced by the temperature. Since the temperature in the room was constant, the mortar temperature did not ever fall below 20 °C during the experiment, which means that the shrinkage came only from drying. After 30 cycles, the residual strains in the mortar at the thermal load center, thermal load boundary, and unheated area were -763μ , -287μ , and -118μ , respectively. At the thermal load center, PTL leads not only to an expansion deformation of the mortar in the out-of-plane direction but additionally to a drying shrinkage of about 645μ in the in-plane direction. This phenomenon can explain the results of the durability evaluation in section 4.1. In the heating center (part A), L-1 (larger w/c) specimens obtained the maximum loss in adhesion, while L-3 (with SRA added) specimens showed the least adhesion loss. This may indicate that the drying shrinkage does not counteract the thermal expansion but rather exacerbates the differential movement of mortar and concrete and accelerates the debonding evolution.

(3) Cyclic strain amplitude analysis

The strain amplitudes of mortar and concrete were calculated for each cycle, as shown in **Fig. 4-8**, where the strain amplitude is defined as the difference between the maximum and minimum strain values. **Fig. 4-9** shows the strain amplitudes at each detection point (left column) and the ratio of the strain amplitudes of the mortar to that of the concrete (right column). The "strain amplitude ratio" is given as follows:

$$\text{Strain amplitude ratio} = \frac{A_M}{A_C} \quad (4-1)$$

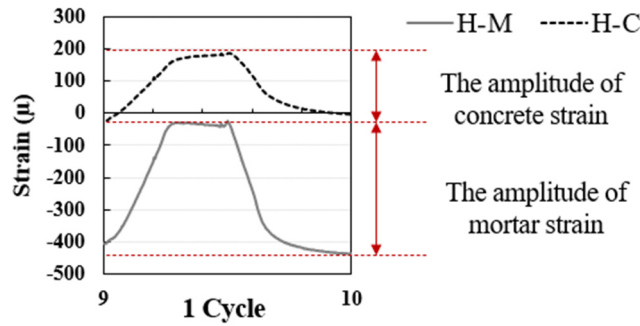
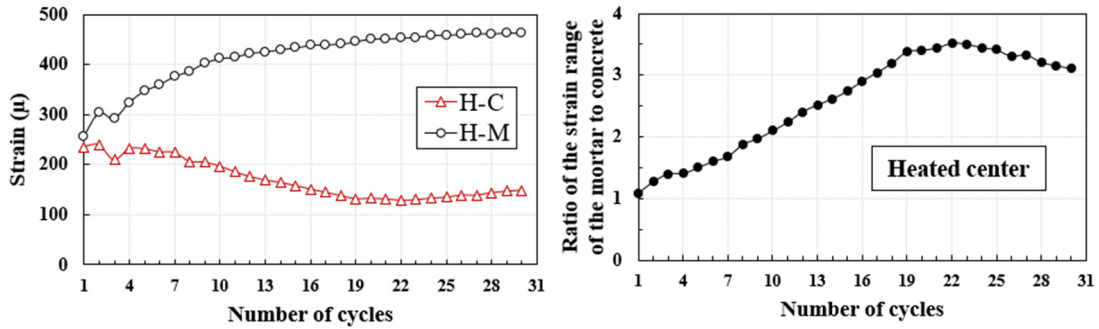
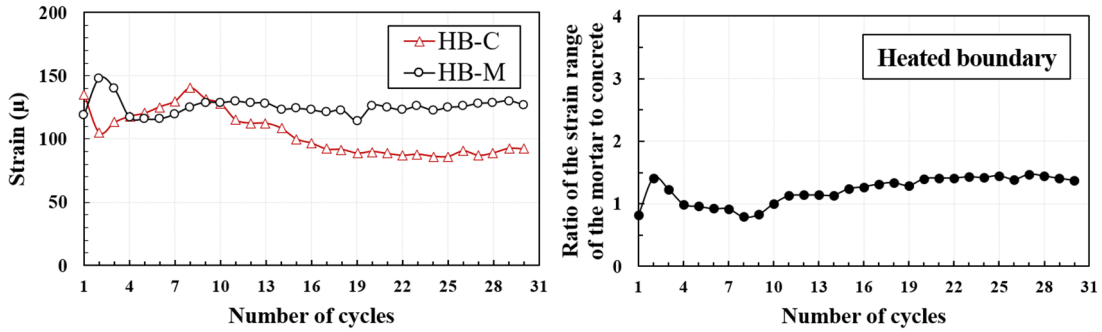


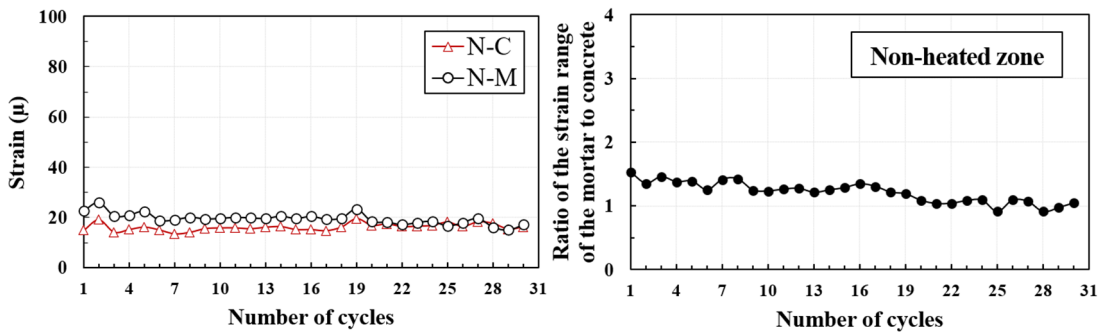
Figure 4-8 Definition of the strain amplitude per cycle.



(a) Thermal Load center



(b) Thermal load boundary



(c) Non-heated area

Figure 4-9 Evolution of strain amplitude and strain amplitude ratio of mortar and concrete with aging cycle.

Where A_M is the strain amplitude of mortar, A_C is the strain amplitude of concrete at the corresponding position.

The strain amplitude reflects the magnitude of the deformation of the element at each cycle with constant thermal loading cyclic pattern and represents the variation of the constraint condition to which the element is subjected. At the center of the thermal load, the strain amplitude of H-M increases cycle by cycle, with a faster growth rate from 0-10 cycles, a slower growth rate from 10-20 cycles, and no change after 19 cycles. The growth of the strain amplitude implies that the confinement imposed on the mortar is gradually decreasing; that is, the adhesion of the mortar to the concrete is slowly lost. The growth rate of strain amplitude may also represent the rate of debonding evolution. After 19 cycles, the strain amplitude of the mortar stops growing as debonding does not continue to develop. For H-C, the strain amplitude is stable from cycles 0-7 (the fluctuation in the 3rd cycle may be due to the temperature control variation), decreases from cycle 8, and returns to stability after cycle 19. From the 8th cycle onwards, the restrained equilibrium of the concrete is broken and gradually returns to "free." Due to the lower temperature of the concrete, the strain amplitude gradually decreases after losing the traction of the mortar until reaching the next equilibrium condition (cessation of the debonding evolution). Observing the strain amplitude ratio, the strain amplitude ratio shows an increase from cycles 0-19 as the deformation of the mortar increases and the concrete decreases. This phase represents the debonding evolution. After 19 cycles, the strain amplitude ratio shows a slight decrease as the strain amplitude of H-C slowly increases (H-M remains constant). This may be due to the reduction of elastic modulus due to the decline in moisture content of concrete with drying shrinkage [157].

At the thermal loading boundary (note that the difference between the range shown in the vertical axis of **Fig. 4-6(a)(b)(c)**, HB-C and HB-M show fluctuations at cycles 2 and 3. Comparing the strain histories in **Fig. 4-6(b)**, it can be assumed that this phenomenon is not due to debonding but to some measurement errors. Apart from this, the strain amplitude of the mortar did not show a massive increase. The strain amplitude of HB-C gradually decreased from cycle 9, indicating that debonding probably started from this moment. From cycles 19-30, the strain amplitudes of HB-M and HB-C maintained a relatively stable state, indicating stagnation in the evolution of debonding. In addition, a slight increase in the strain amplitude ratio was observed in cycle 9, but the overall change was not significant.

In the non-heated area, the strain amplitudes of the mortar and concrete and the strain amplitude ratio between the two always remained stable, so it was possible to reconfirm that the adhesion integrity at this location had not been damaged.

(4) Shear strength results

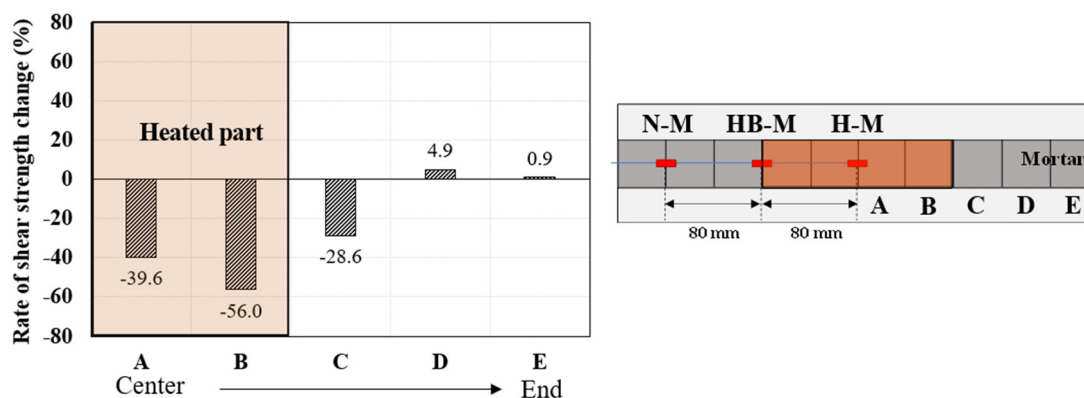


Figure 4-10 Change rate of shear strength of SD specimens after aging cycle.

Fig.4-10 shows the average rate-of-change of the shear strength of the SD specimens after 30 cycles (versus 0 cycles), as calculated by **Equation 3-2**. Sensors H-C and H-M are located at part A, HB-M and HB-C are located at the junction of part B and part C, and N-M and N-C are located at the intersection of parts D and E. A significant decrease in bond strength was observed for part A. Although the average shear strength loss of SD specimens did not reach 100%, complete debonding was observed on one of the specimens, and penetration cracks were also observed on the mortar surface of this specimen (the same as those observed on the SS surface). Thus, the shear strength results support that complete debonding of H-C from H-M occurred.

Based on the strain measurement results, HB-M and HB-C are believed to have delaminated. However, parts B and C retain some shear strength. Two reasons could cause this, 1) variation in the initial bonding of SD to SS; 2) Delamination at the thermal loading boundary occurred only in a small area near the FBG sensor. Although the FBG sensor is small, the adhesive used may have affected the initial bond strength. However, the delamination of the small area was insufficient to cause adhesion failure in the 40 mm × 40 mm area. This illustrates the limitations of the bond strength test.

4.2.3 Analysis of debonding evolution based on strain monitoring results

Section 3.4 studies the debonding evolution based on the shear strength test. In the 40 mm × 40 mm range, the debonding evolution follows an "S-shaped" path, characterized by three stages with two critical inflection points. As mentioned before, the strength tests are periodic, the results show dispersion and variability, and the "S-shaped" degradation path is based on statistical findings. The strain monitoring approach focuses on the evolution of debonding over a tiny area (effective length of the FBG sensors). The strain histories of H-M and H-C provide insight into the whole mortar/concrete adhesion process, from health to damage. The strain trajectory of the 1st cycle represents a healthy state of adhesion, where the strains of H-C and H-M almost overlap, and the

gap is shown only at the peak strain. In cycles 2-5, the strain trajectories gradually separate, but observing the residual strains, the tilt direction of H-C and H-M is the same (toward shrinkage), and the strain behavior of the two materials maintains mutual follow-through during this period; hence that adhesion integrity is not damaged. However, the gradual separation of strain trajectories may represent that debonding is developing. As mentioned earlier, cementitious materials are bonded to each other primarily by mechanical interlocking, which means that the separation of strain trajectories may represent the breakage of some mechanical bonds, and the bond integrity can be maintained before these breaks are joined into a small debonding area. Thus, although the materials move in the same direction, their connection becomes weaker. In cycles 5-7, the residual strain in H-M continued to become larger in the negative value, but H-C did not follow this trend. In this period, debonding has developed to the extent that concrete is not allowed to follow the deformation of mortar, more mechanical bonds break, and small areas of debonding gradually form. In cycles 7-19, H-C moves in the opposite direction of H-M, and the growth rate of residual strain goes through a fast-to-slow process.

The 7th cycle can be considered an inflection point in the debonding evolution, where the broken mechanical bonds within the sensor's detection range form a small debonding area. The mortar and concrete in this area lose their restraining effect on each other, and the strain behavior of each element tends to a "free" state. Subsequently, the debonded area gradually increases. **Fig. 4-9(a)** shows that the cycle-by-cycle increase in the deformation of mortar and concrete leads to an increase in the strain amplitude ratio, which indicates that the constraint between the two becomes weak. After the delamination of point H-C, the evolution of debonding in the surrounding area continues, and the growth of the residual strain slows down. Nineteen cycles later, a complete adhesion failure is reached within the sensing range of the FBG sensor (as evidenced by the penetration cracks observed on the mortar surface), and the stagnation of the strain amplitude ratio indicates a dynamic equilibrium between the movement of the mortar and that of the concrete.

The initial shear strength of the specimens in this work is low, and the evolution of debonding in the thermal loading center is accompanied by the beginning of the aging cycle. However, more details can be observed at the thermal loading boundary where the temperature applied is lower. According to the HB-C and HB-M residual strains (**Fig.4-7(b)**), the debonding evolution starts abruptly in the 11th cycle and develops rapidly in cycles 11-17. After 20 cycles, the strain amplitudes of both HB-C and HB-M (**Fig. 4-9(b)**) no longer change, and it is considered that, at this moment, the two have regained equilibrium. According to Feldfogel and Rabinovitch [89] [90], the debonding mechanism initiates abruptly after encountering a threshold load. After rapid but stable development until the next threshold load, debonding propagation becomes unstable, and the system breaks

rapidly. Only similar first two phases (initiation phase and stable propagation phase) could be distinguished in this study. This may be because this study focused on a tiny area, while their study was conducted on a tile. The final unstable propagation phase may represent the accumulation of small areas of debonding. On the other hand, adhesion failure may not have occurred where HB-C and HB-M are located (refer to the shear strength after 30 cycles). If the aging cycle continues, fatigue-induced adhesion failure may occur.

In contrast to Section 3.4, no plateau period for the evolution of debonding (bond strength does not decrease with the aging cycle) was observed in this work. The initiation of the debonding mechanism on a tiny area maintains a steady propagation until the bonding failure. The assumption can be made that a plateau period during the degradation of adhesion over a large area may represent that some tiny delamination is accumulating in the area and that the shear strength continues to decrease only after a certain threshold is reached, e.g., if the debonded area gets to a certain percentage.

The application of FBG sensors to monitor the debonding evolution of mortars has proven feasible. Moreover, the embedding of the FBG sensor had almost no effect on the adhesive properties of the tested material compared to previous studies using strain gauges. By monitoring the strain of each element, it is possible not only to capture the moment when delamination occurs but also to estimate the progress of degradation based on the change in strain behavior. In durability assessment tests, a combination of strength tests and strain monitoring can be considered to assess the loss of adhesion of specimens, which may improve the accuracy of durability assessment results.

4.3 SUMMARY

This chapter describes the implementation process of durability assessment methods and proposed improvements. In the first study, the durability assessment was run by comparing the loss rate of bond strength with four types of specimens prepared using different techniques. The feasibility of the durability evaluation method is verified, which consists of the PTL aging cycles and a direct shear test. The second study proposed a method for continuous assessment of adhesion loss. The purpose is to improve the accuracy of adhesion measurement, thus, the reliability of durability evaluation. The strain behavior of mortar and concrete under the PTL aging period was monitored with FBG sensors, and the debonding evolution process was analyzed. Several strain characteristics representing the adhesion loss were put forward. The following conclusions were derived:

(1) The durability assessment method can be used to compare the durability of mortar–concrete adhesion systems made using different methods and to approximately understand the influence of various factors on the durability.

(2) Assessing adhesion loss by shear strength tests can yield statistically significant durability assessment results, but there is a risk of accuracy. This is especially true when comparing two specimens with small differences in durability. More valid parameters need to be defined for durability assessment.

(3) Essential parameters affecting the long-term adhesion of mortar to the concrete are the drying shrinkage, modulus of elasticity, and thermal expansion coefficient of the materials. These three physical properties combine to determine the difference in deformation between mortar and concrete.

(4) The strain monitoring method enables observation of adhesiveness from health to damage on the same specimen. The degradation progress of the adhesion can be estimated from the characteristics of the strain behavior. When the adhesion is intact, overlapping mortar and concrete strain trajectories can be observed; during the cumulative stage of adhesion loss, strain trajectories gradually separate but progress in one direction; strain trajectories lose their followability to each other, representing the occurrence of delamination.

(5) According to the strain monitoring results, the degradation effect of the PTL aging cycle comes not only from the thermal expansion mismatch between materials but also from the drastic drying shrinkage under the influence of high temperature. Therefore, the durability evaluation results represent the combined ability of the specimens to resist solar radiation and drying shrinkage.

At present, the prototype of the durability evaluation method has been formed. The method is valuable for achieving evaluation in the early stages of product development. Still, it is only suitable for comparing several specimens with widely varying specifications at the laboratory level. Some improvements are needed to make it universally usable. The definition of valid parameters is an issue that deserves to be studied. After an experimental study, it was concluded that a combination of strength testing and strain monitoring could be considered to assess the loss of adhesion of specimens. The combination of continuous monitoring and periodic testing can improve the reliability of the durability assessment results. However, the small sample size is insufficient to have an explicit knowledge of the strain behavior of the composites, and further studies are needed. On the other hand, the volume of specimens is small. The reference value of the results of durability evaluation of mortar/concrete composites on a small scale for practical engineering design is one of the issues that must be considered in the future.

Chapter V

DELAMINATION DETECTION WITH FBG SENSORS UNDER PTL AGING CYCLE

In Section 1.2 of Chapter 1, the three crucial phases that determine the service life of a structure are outlined, namely pre-construction durability design, preventive maintenance, and appropriate and timely repair. For the first stage, Chapters 3 and 4 establish a laboratory-scale durability assessment method. This chapter discusses a study to achieve preventive maintenance with high implementation efficiency, including the development of effective NDT techniques for detecting facade cladding damage.

Preventive maintenance refers to periodic damage detection and maintenance work on buildings. As a building element directly exposed to environmental erosion, the efficiency of the preventive maintenance of facade cladding materials is also a matter of public safety. The Building Standard Law in Japan, revised in 2008, emphasizes the maintenance and management of exterior tiles on specific buildings (designated by government decree or by specific administrative bodies), requiring a report on diagnostic results every ten years. Similar to Japan, in Singapore [158], Hong Kong [97], the United States, and Canada [159], periodic inspection laws for buildings in service have been enacted to prevent the spalling of building finishes. In this context, researchers have made efforts to develop efficient damage detection techniques.

The basic technique for maintaining and managing facade cladding is "delamination detection." Section 2.3 describes several field-applicable methods and laboratory-applicable methods. Among them, the strain monitoring method can meet high accuracy and field applicability. Moreover, it is a pre-embedded sensor method, meaning the inspection can be carried out continuously. According to previous studies on the evolution of mortar debonding, the debonding mechanism is abruptly initiated. It develops rapidly, and the continuity detection technique can be used to minimize missed detections. On the other hand, this technique can determine the safety, extent of damage, and continued availability of building facades as soon as possible after a major disaster such as an earthquake. The strain monitoring method is therefore considered to have the potential for development.

In Chapter 4, the strain monitoring method was practiced on mortar/concrete specimens using FBG sensors. The debonding evolution was reflected in the strain behavior of the mortar and concrete. The possibility of monitoring strains by means of FBG sensors to detect damage to facade

cladding materials was initially validated. However, it must be acknowledged that the insufficient sample size and the simple composition of the specimens of the study are mentioned above. Further research is needed in this area if strain behavior is to be fully understood and appreciated. Therefore, in this chapter, the application of FBG sensors for damage detection on facade cladding materials is further investigated using tiles as the object of study and the proposed PTL aging cycle to simulate natural degradation. The aim is to clarify the feasibility of the strain monitoring method, its applicability, and the interpretation of the detection results.

5.1 EXPERIMENT ON SMALL-SCALE SPECIMEN WITH TILES

The first study was carried out on a small scale with tiled specimens. The aim was to investigate the applicability of the strain monitoring method in simulating multilayer composite structures with tile finishes.

5.1.1 Tile specimen preparation

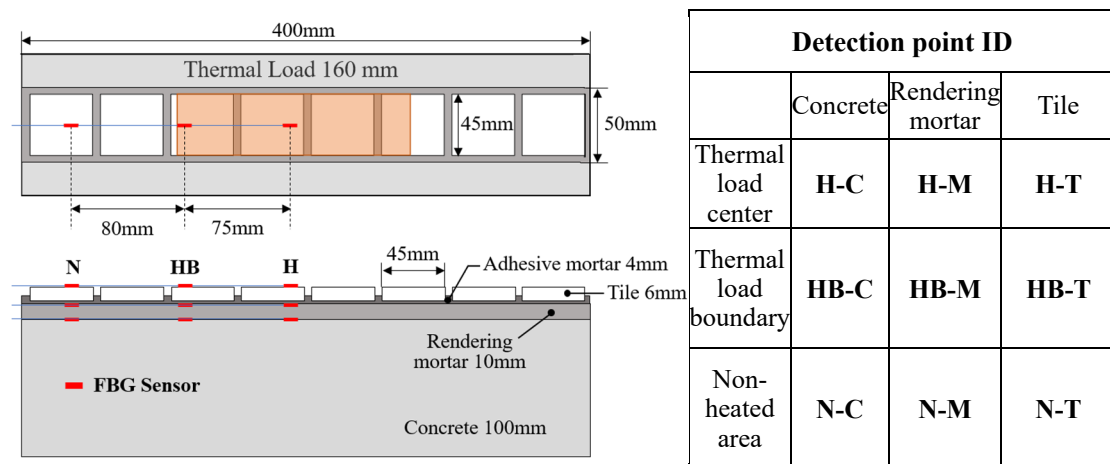


Figure 5-1 Outline of tile specimen and ID of detection points.

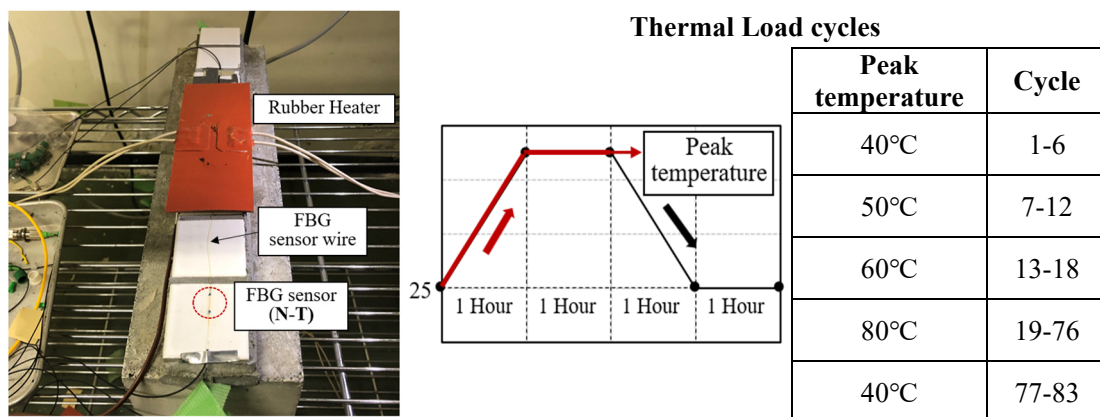
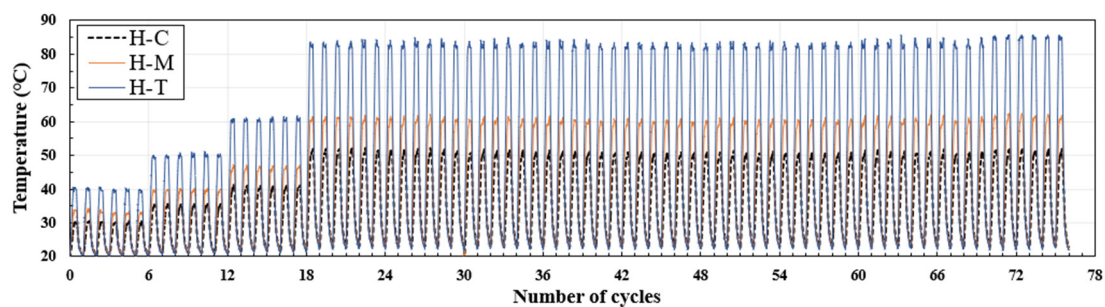
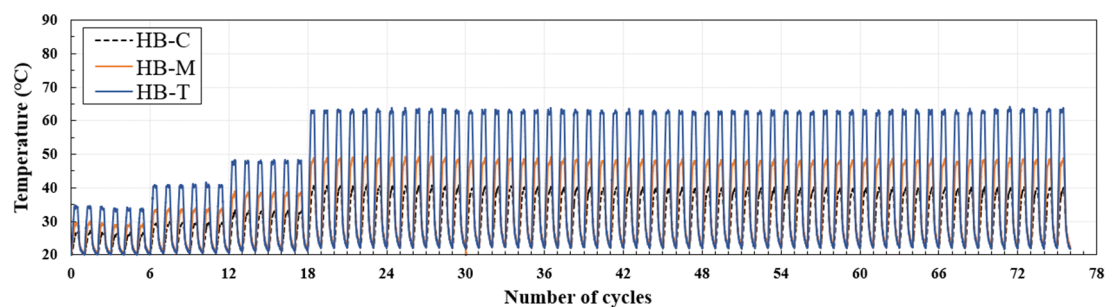


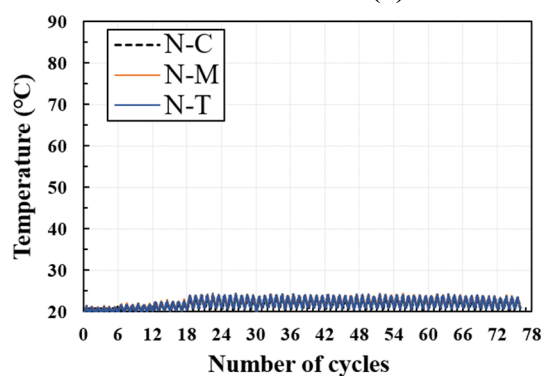
Figure 5-2 Tile specimens in operation and PTL ageing cycle manipulations.



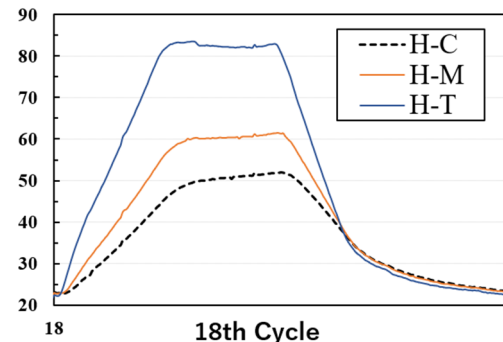
(a) Thermal loading center



(b) Thermal loading boundary



(c) Non-heated area



(d) Enlarged view of the 18th cycle

Figure 5-3 Temperature history of the tile specimens.

The dimensions of the specimens are shown in **Fig. 5-1**. The materials and preparation procedures for the specimens (concrete and rendering mortar) were identical to those in previous studies, except for the parts other than adhesive mortar and tiles, referring to standard specifications (SV specimens). The concrete substrate has dimensions of 100 mm × 100 mm × 400 mm, and the rendering mortar has dimensions of 10 mm × 50 mm × 400 mm. After the rendering mortar had cured for 7 days, mosaic tiles (45 mm × 45 mm × 6 mm) were installed on the upper surface with adhesive mortar. Adhesive mortar is a pre-mixed commercial product with high water retention and viscosity. The adhesive mortar was applied according to the manufacturer's specifications and JASS 19 [160], which establishes the execution procedures and ceramic tile installation control with organic and cementitious adhesives on facades.

Fig 5-1 shows the configuration and ID of the FBG sensors for the specimen. FBG sensors

were attached to substrate surfaces (between concrete and rendering mortar), rendering mortar surfaces (between rendering mortar and adhesive mortar), and tile surfaces. As in Section 4.2, the strain and temperature evolution were monitored in the thermal loading center, thermal loading boundary, and non-heated areas. **Fig. 5-2** shows the programmed settings of the rubber heater. The aging cycle pattern is essentially the same as in the previous study, with the difference that the setting temperature of the rubber heater is gradually increased from 40°C to 80°C to maintain a relatively long healthy period. After the last cycle at 80 °C, the peak temperature was dropped again to 40 °C, and the strain response of specimens before and after accelerated degradation was compared.

5.1.2 Temperature monitoring of tile specimens

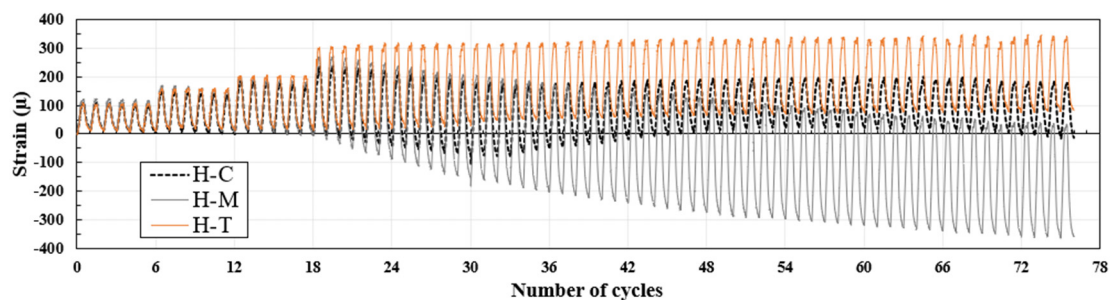
The temperature history of the detection points is shown in Figure 5-3. At the thermal loading center, the maximum temperature difference between H-T and H-M is about 20 °C, and that between H-M and H-C is about 10 °C. This is because the thermal conductivity of tiles is less than that of cementitious materials. At the thermal loading boundary, the temperature difference between HB-M and HB-C is still 10 °C, although the maximum temperature of HB-T is lower than that of H-T by about 20 °C. It can be speculated that the thermal expansion differences between rendering mortar and concrete are similar at the center and boundary of the thermal loading. In the non-heated area, the temperatures of the three materials remain almost the same, which can ensure that the thermal load does not damage the area.

Fig. 5-3(d) zooms in on the temperature history at the thermal loading center for cycle 18. The temperature evolution in the tile system is different from that in the mortar/concrete system. One effect observed is the reversal of the temperature pattern after the onset of cooling, where the temperature of the tile surface decreases faster than the temperature of the other layers. This is the same as the temperature evolution of the prototype wall tilings noted in reference [31]. The rapid warming and cooling of the tiles induce more stress accumulation at the adhesive interface.

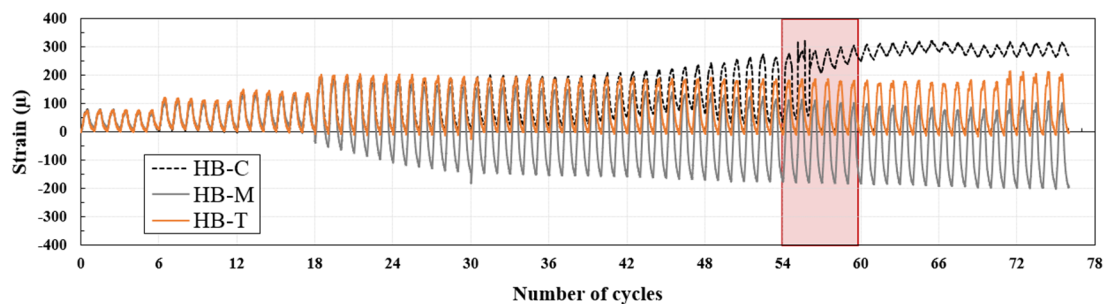
5.1.3 Strain monitoring of tile specimens

Fig. 5-4 shows the strain history of the tile specimens; (a) (b) (c) lists the strain evolution of the tile surface, the rendering mortar surface, and the concrete surface in parallel positions in areas subjected to different levels of thermal loading, respectively. **Fig. 5-5** shows the evolution of the residual strains of each layer (definition of residual strains in Section 4.2).

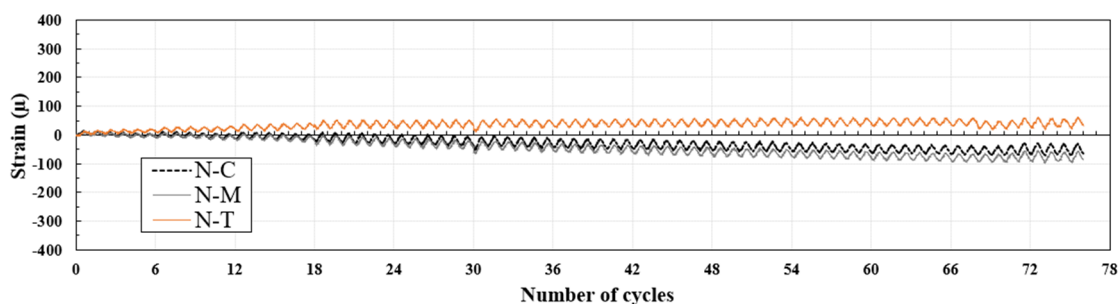
(1) Thermal loading center (H-C, H-M and H-T)



(a) Thermal loading center



(b) Thermal loading boundary



(c) Non-heated area

Figure 5-4 Strain history of the tile specimens.

The strain history of the heating center shows that in the early stages of heating, there is no difference in the strains of the tiles, rendering mortar and substrate, which move as a whole. However, when the heating temperature was increased to 80 °C, they each began to behave differently. For the tile/rendering mortar interface, the direction of motion of H-T and H-M diverged from cycle 18, with H-T moving toward the tensile side and H-M moving toward the compressive side. This indicates that the adhesion between the tiles and the rendering mortar starts to lose after 18 cycles. As for the rendering mortar/concrete interface, the debonding evolution starts from cycle 33. the motion directions of H-C and H-M diverge from cycle 33, with H-C turning around and moving toward the tensile direction.

The variation of residual strain shows more clearly (Fig. 5-5(a)) the point of divergence in the strain behavior of the layers. Starting from cycle 18, the adhesion between the tiles and the rendering mortar becomes less and less able to restrain the drying shrinkage. The residual strain of the tiles

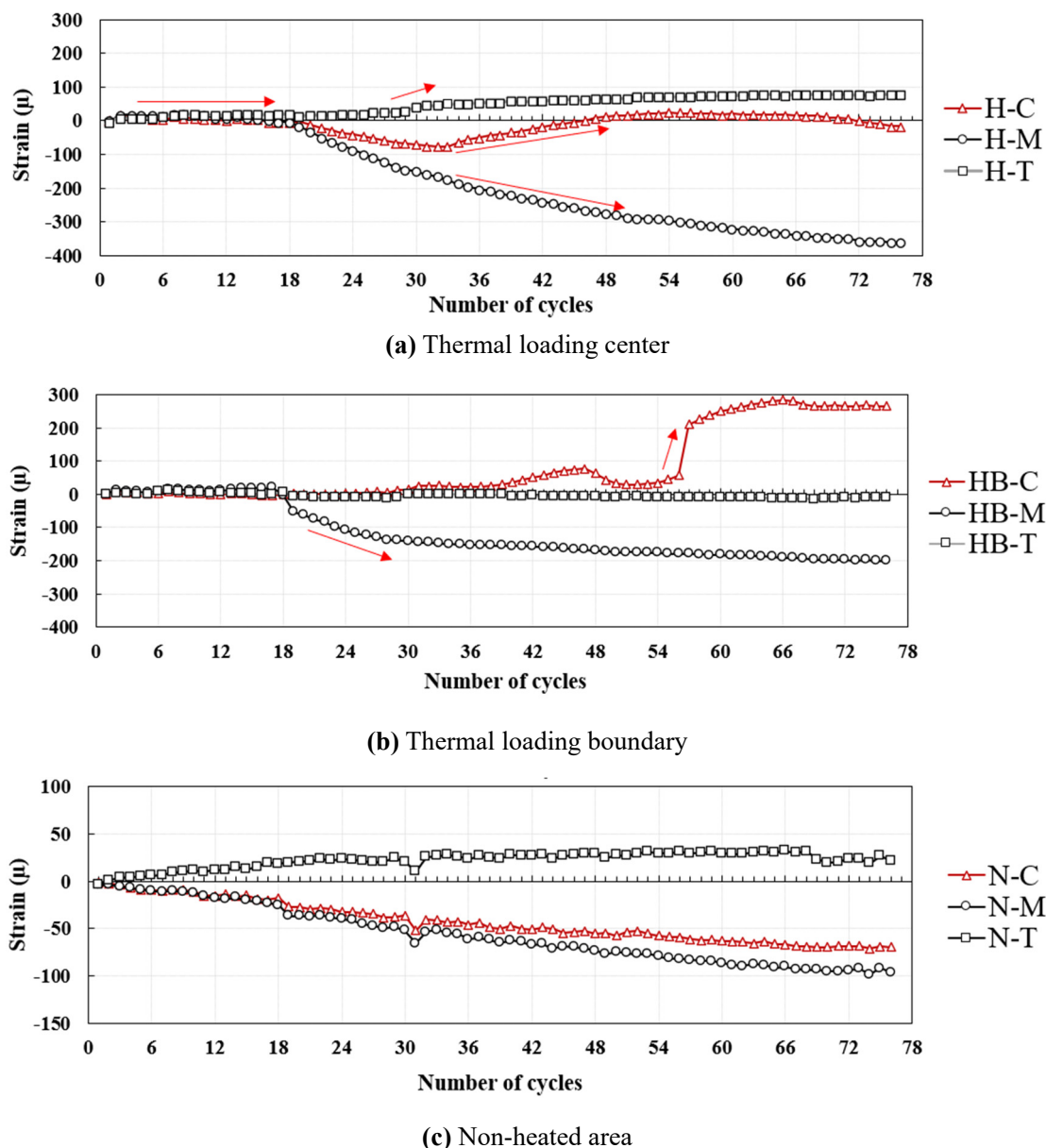


Figure 5-5 Residual strain of each detection point at the end of each cycle.

was observed to show an abrupt gain at cycle 29 and then started to increase gradually (with constant residual temperature). This may be due to the voids at the interface causing the tiles to protrude in the out-of-plane direction. The debonding evolution of the concrete/mortar interface is the same as in Section 4.2. During the damage accumulation (cycles 18-33), the concrete follows the mortar towards the shrinkage side, but the gradual increase of the strain difference indicates that the adhesion is degrading. Starting from cycle 33, the concrete shows a strain behavior opposite to that of the mortar. It is presumed that debonding may have occurred at this moment, rendering the mortar loses its ability to confine the concrete.

(2) Thermal loading boundary (HB-C, HB-M and HB-T)

The strain trajectories of the tiles and rendering mortar located at the heating boundary follow a pattern similar to that of the heating center. From cycle 18 onward, HB-M progressed toward shrinkage with the aging cycle and separated from the strain trajectory of HB-T. However, observing the residual strain of HB-T (**Fig. 5-5(b)**), HB-T has maintained a steady motion and showed a slight tendency to shrink. It is likely that the tile/rendered mortar interface at the boundary of the heated region did not delaminate and only partially lost its adhesion.

Interestingly, concrete (HB-C) exhibited anomalous strain behavior. The residual strain of HB-C underwent a three-phase transition from tensile-shrinkage-tensile. It gradually increased from cycle 18, showed a brief decrease in cycles 47-55, and maintained at a stable high-level position after a massive outbreak of increase in cycle 56. That is, the concrete is released from the mortar restraint from cycle 18, and cycles 18-56 represent the period of development of debonding. However, interpreting the strain anomaly behavior for cycle 56 is challenging. One reasonable speculation is that with the accumulation of debonded areas, a sudden outbreak of large debonding occurred in cycle 56, i.e., complete adhesion failure within the detection range of the FBG sensor. The loss of pressure from the overlayer kept the HB-C sensor at a tensile state. Another possibility is that the FBG sensor has been damaged along with the debonding.

(3) Non-heated part (N-C, N-M and N-T)

Based on the strain in the non-heated zone (**Fig. 5-4(c)**) and the residual strain (**Fig. 5-5(c)**) history, no debonding occurred at either interface. N-C and N-M strain trajectories maintained good follow-through, both towards shrinkage. N-T did not show a shrinkage tendency, which may be due to the buffering effect of the adhesive mortar layer. The adhesive mortar layer absorbed most of the traction force from the rendering mortar, and the joints allowed for more deformation of a single tile. The residual strain results indicate that even with healthy adhesion, to some extent, the tiles do not move in the same direction as the rendering mortar (note the small range of representation of the vertical axis in **Fig. 5-5(c)**).

(4) Comparison of strain behavior before and after accelerated degradation

Next, the strain responses of the specimens were compared before and after accelerated degradation at the same aging cycle (peak temperature of 40 °C). As shown in **Fig. 5-6**, there was no significant difference in the strain trajectories of the layers of material before degradation. In the thermal loading center, the peak strain of the mortar showed a difference of about 15 μ . The maximum temperature difference between mortar and tile at this moment is about 7 °C, but the coefficient of thermal expansion of mortar is much larger than that of tile. After subjecting to 76

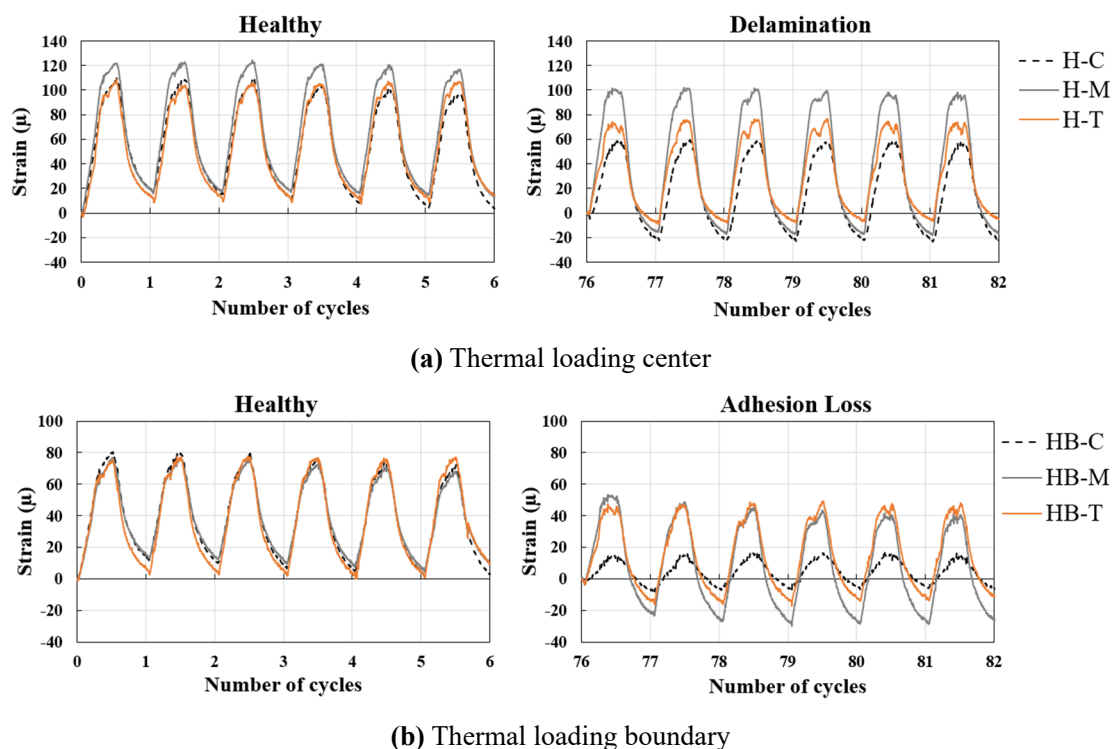


Figure 5-6 Comparison of strain behavior before and after accelerated degradation.

aging cycles, the strain trajectories of the layers of the material showed dispersion. The dispersion increased to 30μ between mortar and tile and more than 40μ with concrete. This indicates that the mortar is bound by the tiles and concrete before deterioration but has the highest thermal expansion coefficient and can expand freely after the adhesion loss.

At the thermal load boundary, the strain trajectories of the layers before degradation almost overlap. After degradation, the mortar and tiles maintain a healthy adhesion, but the concrete exhibits a different strain behavior. Combined with the previous speculation, it is believed that an adhesion failure occurred at HB-C and that a construction defect may exist at this location.

5.1.4 Analysis of strain amplitude

The evolution of the strain amplitude for each layer after 18 cycles was calculated (for the definition of strain amplitude, refer to **Fig. 4-8**) as shown in **Fig. 5-7**. Notably, the difference in the range of vertical coordinates in **Fig. 5-7 (a) (b) (c)**. In the non-heated area, the strain amplitudes of the three materials remain stable so that it can be reconfirmed that the bond integrity is not compromised at this location.

At the thermal loading center, the strain amplitude of H-M increases cycle by cycle, with a faster growth rate from cycles 18-30, a slow growth rate from cycles 30-42, and no further change after cycle 42. As mentioned earlier, the growth of strain amplitude implies that the mortar is losing constraint, and the adhesion is slowly lost. The strain amplitude of H-T shows a slight decrease once

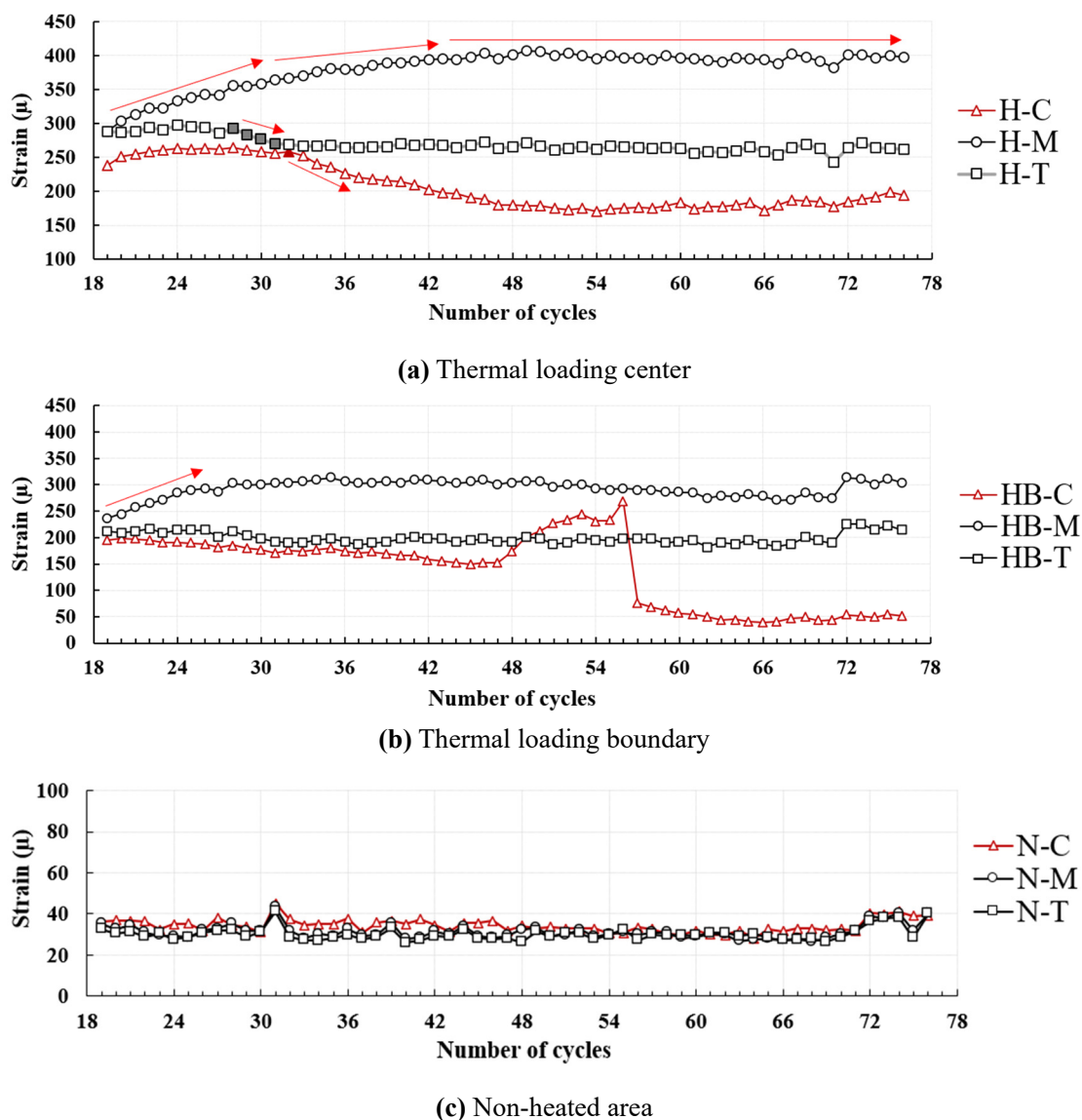
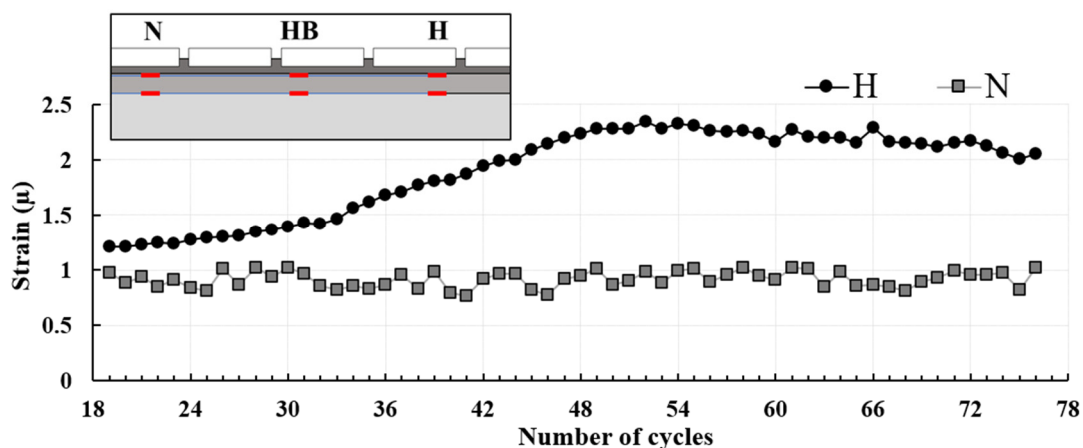


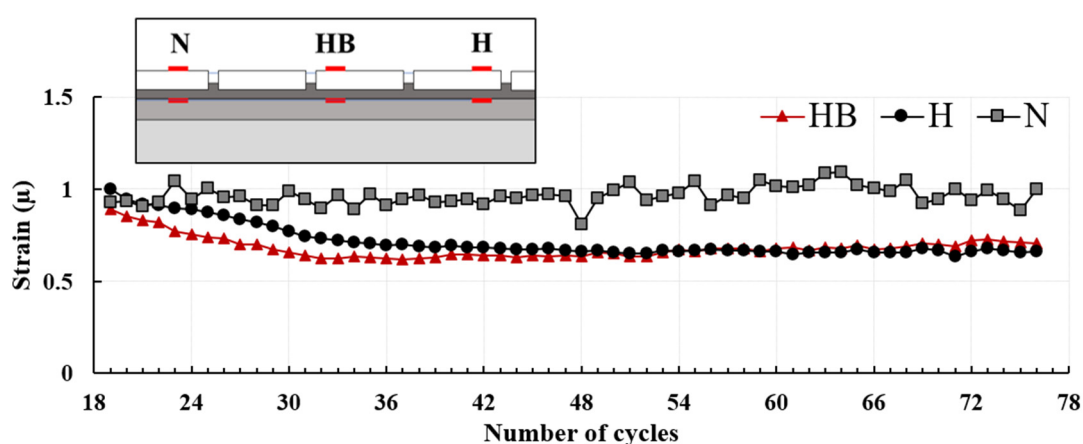
Figure 5-7 Evolution of strain amplitude of each detection point with aging cycle

at cycle 29, decreasing by about 50μ . The reduction in deformation of the tiles is accompanied by the loss of adhesion due to the smaller thermal expansion coefficient of the tiles. The decrease in strain amplitude of H-C occurs after cycle 33 for reasons similar to those of H-T. According to the above observations, the debonding evolution of the tile/rendering mortar interface starts at cycle 29, and the debonding evolution of the rendering mortar/concrete interface starts at cycle 33.

Here, "debonding evolution" represents a significant loss of adhesion, not an adhesion failure. Over the 10 mm effective length of the FBG sensor, the debonding area is gradually accumulated until bond failure is reached within the detection range. In the strain monitoring method, the damage is determined by comparing the strain response of the healthy part. This is a qualitative rather than a quantitative diagnosis. It is possible to determine the generation of debonding by the anomaly of strain response, but it is challenging to decide on the size of debonding area. The authors concluded



(a) Rendering mortar/concrete interface



(b) Tile/rendering mortar interface

Figure 5-8 Evolution of strain amplitude ratio with aging cycle, (a) rendering mortar to concrete, (b) tile to rendering mortar

that the anomalous change in strain amplitude implies the appearance of voids at the interface and therefore defined the moment of discovery of voids as the moment of initiation of debonding evolution. Comparing the strain amplitude in the non-heated region (Fig. 5-7(c)), the accumulation of damage starts from 18 cycles but does not reach the level of "debonding" yet.

At the thermal loading boundary, the strain amplitude of HB-M evolves similarly to that of H-M, but no significant decrease in HB-T is observed. Thus, the tile/rendered mortar interface does not reach the conditions for initiating the debonding mechanism, although there is a certain degree of adhesive loss. The strain amplitude of HB-C decreases in cycles 38-48, increases in cycles 48-56, and remains stable with a small amplitude after an abrupt drop in cycle 56. It is essentially certain that after 56 cycles the adhesion at the rendering mortar/concrete interface failed over a significant area. The concrete surrounding the FBG sensor returns to its "free" state, deforming only slightly under the influence of thermal loads. Interestingly, the phenomenon of temporary increase in concrete strain amplitude (48-56 cycles) prior to adhesion failure was also observed in the mortar/concrete specimens in Section 4.2, again at the thermal loading boundary. The mechanism

is not yet clear, but this phenomenon can be considered as a precursor to adhesion failure.

Fig. 5-8 (a) and (b) show the strain amplitude ratios of concrete to rendering mortar and tile to rendering mortar, respectively. The strain amplitude ratios in the non-heated regions remain stable at both interfaces, which is proof of healthy adhesion. For the mortar/concrete interface, the central amplitude ratio of the thermal load increases from 18 to 48 cycles, with a more significant increase from cycle 33 onwards. The growth rate of the amplitude ratio reflects the debonding evolution rate. After cycle 48, the mortar and concrete reach an equilibrium state, which may lead to adhesion failure due to fatigue if the loading temperature is not further increased. According to Mahaboonpachai et al. [12], damage accumulated in terms of micro-cracks at the interface when the temperature on the tile surface is around 80°C. The results of the thermal loading boundary are not discussed further due to the disturbing nature of the HB-C data.

For the tile/mortar interface, similar behavior is observed at the central and boundary of the thermal load. The amplitude ratio decreases from 18 to 36 cycles due to the increased motion of the mortar and the decrease of the tiles, reaching equilibrium after 36 cycles. Again, it can be considered that the maximum damage at this load intensity has been reached.

5.1.5 Response of strain behavior to adhesion state

Three adhesion states can be determined based on the analysis of strain behavior: healthy adhesion, adhesion damage (partial debonding), and adhesion failure (complete debonding).

- Healthy adhesion. The strain behavior in the non-heated regions (N-T, N-M, N-C) represents a healthy bond. The strain behavior between all layer materials maintains some correlation, and a stable strain amplitude ratio is maintained.

- Adhesion damage (partial debonding). Adhesion damage occurs at both interfaces in the thermal loading center, manifested by the separation of the strain trajectories of the materials. The sudden decrease/increase in strain amplitude represents a loss of correlation, and the materials lose their followability to each other's deformation.

- Adhesion failure (complete debonding). Adhesion failure occurs at the mortar/concrete interface at the thermal loading boundary. The material exhibits a different strain behavior than healthy adhesion, accompanied by a more dramatic change in strain amplitude.

Determining the boundary between adhesion damage and adhesion failure is complex, and the difference may lie in the intensity of the change in strain behavior. The anomaly exhibited by point HB-C may be due to an initial defect. If the load intensity is further increased, other test points may exhibit similar strain behavior.

Consistency in the overall deformation direction (tensile/compression) at the mortar/concrete bond interface represents a healthy adhesion, and loss of consistency implies adhesion damage. However, due to the buffering effect of the adhesive mortar, the deformation direction of the tiles is less influenced by the mortar, therefore, the correlation between the strain behavior of the tiles and the mortar needs to be interpreted with care. In addition to comparing the strain behavior in healthy conditions, more relevant data need to be accumulated. It is certain, however, that with the loss of adhesion, the material moves closer and closer to its unconstrained "free state."

In summary, strain monitoring makes it possible to clarify the degradation progress of the adhesion. The initial data (healthy state) should be retained for engineering applications. If the strain behavior shows a loss of follow-through, one should be alert and increase the frequency of inspections; if the strain behavior shows severe abnormalities, repair and replacement of components should be considered.

5.2 EXPERIMENT ON LARGE-SCALE WALL SPECIMEN

Previous studies have verified the feasibility of detecting delamination with FBG sensors on small-scale specimens. By monitoring the interlaminar strain, we can observe the adhesion degradation process of the four-layer composite (tile-adhesives-rendered-concrete) under PTL aging cycles. However, the results obtained on a small area of the adhesive interface cannot be directly used as a design reference in practical engineering, and its corresponding conclusions are flawed. For example, it is impossible to simulate the constrained behavior of structural components such as beams and columns. Firstly, due to the dimensional limitations of the small-scale specimens, the deformation due to thermal loading is only constrained to one dimension, i.e., along the length of the specimen. It is almost free in the other direction, which does not correspond to the constraint conditions of an external wall when subjected to solar radiation. Secondly, small-scale specimens are heavily influenced by drying shrinkage, which interferes with interpreting the experimental results. Therefore, validating the proposed AT method with the delamination detection method on large-scale specimens is necessary.

In this section, a specimen of the concrete substrate, consisting of beams, columns, and walls, was created to simulate a wall. PTL aging cycles were applied to the specimen, and the wall was constrained from both directions in the plane to simulate the actual solar radiation on the outer wall. To further confirm the reliability of delamination detection using the FBG sensor, we adopted the acoustic diagnosis as the circumstantial evidence for the occurrence of delamination. In addition, two types of tile adhesives commonly available on the market were tested: bonding mortar and

organic adhesives. This study contained three objectives, 1) to validate the feasibility of FBG sensor detection of delamination on a large-scale specimen, 2) to investigate the applicability of the proposed AT method, and 3) to investigate the difference in the debonding evolution between cementitious and organic adhesives.

5.2.1 Specimen preparation

As shown in Fig. 5-9, a small concrete wall specimen was prepared as the substrate with overall dimensions of 505 x 505 mm, surrounded by a beam and column with a cross-sectional area of 100

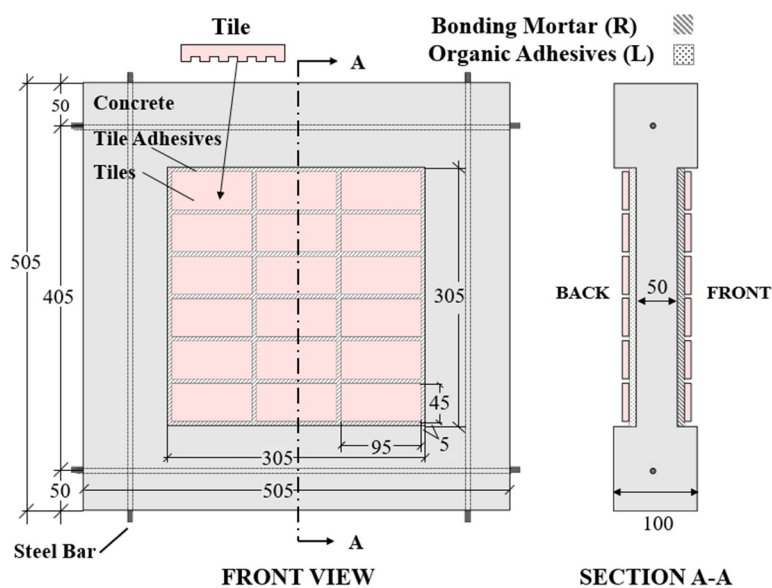


Figure 5-9 Outline of wall specimen.

x 100 mm and reinforced with 6 mm diameter steel bars. The tiles were laid in the central area used to simulate the wall, which measured 50 x 305 x 305 mm, with wire mesh inside. The mixture proportion of the concrete substrate is listed in Table 3-2. Twenty-one ceramic tiles measuring 90 x 45 mm with a jagged surface were laid on the front and back of the substrate using bonding mortar and organic adhesive, respectively.

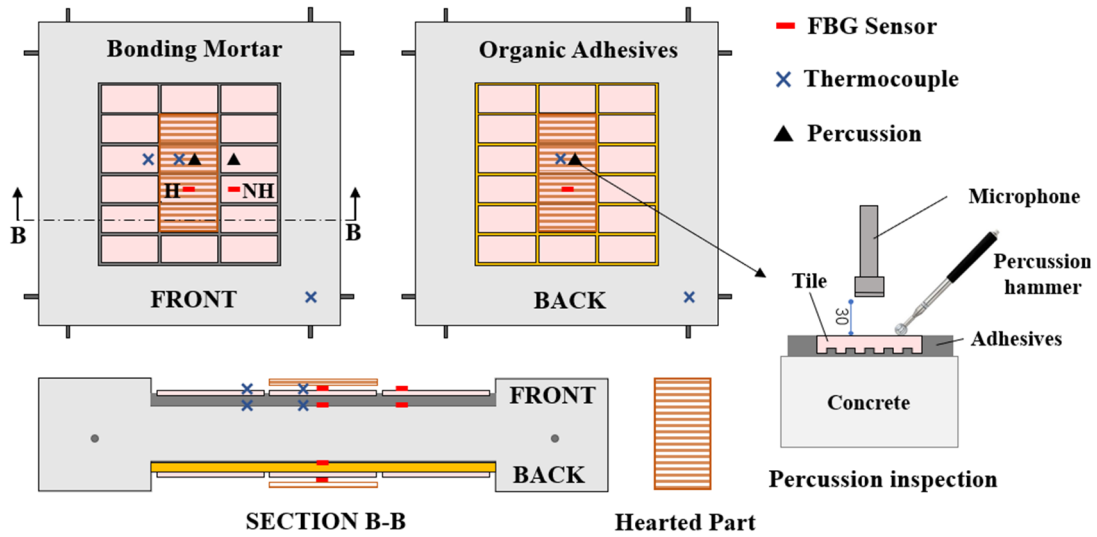
Bonding mortars and organic adhesives are two common tile adhesives currently available on the Japanese market. The former, whose main component is a polymer-cement mortar, has a long history of use and is still the most widely used. The latter, commercially known as elastic adhesives and is an organic adhesive, with urethane resin or modified silicon adhesives as the major component, which has only been used as a tile adhesive in the last 20 years but is rapidly gaining widespread development and application due to its excellent physical properties and ease of construction. The same bonding mortar as in Section 5.1 was used in this study. Organic adhesives come from the same manufacturer, both adhesives are commercially available in premixed type, and

the methods of application and mixture proportion are in strict accordance with the manufacturer's instructions.

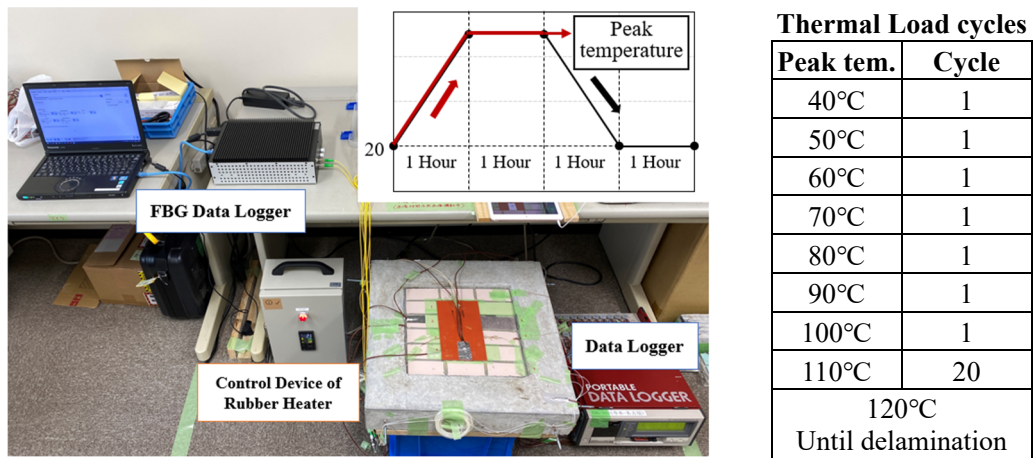
In this study, no rendered layer was applied between the concrete substrate and the bonding mortar to minimize the differences in drying shrinkage between the materials. Furthermore, the concrete substrate was allowed to cure in a general indoor environment for two months to ensure that most of the drying shrinkage had occurred.

5.2.2 Aging cycles and delamination detection

As previously mentioned, to investigate the applicability of the proposed AT method under two-dimensional constraints, the rubber heater used to provide the thermal load was secured to the surface of the four central tiles by heat-resistant double-sided tape. **Fig. 5-10(a)** shows the area of the specimen subjected to the thermal load and the configuration of the sensors. **Fig. 5-10(b)** shows



(a) arrangement of sensors in the specimen



(b) setup of the experimental device and aging cycles

Figure 5-10 Schematic of the operation of the PTL aging cycle experiment.

the setup of the experimental device and aging cycles.

The delamination detection point is set in addition to the center of the area subjected to thermal load on the front (bonding mortar) and the back (organic adhesive). There is also a detection point for the area on the front that is not heated. The detection points are named with symbols: the part subjected to thermal load is denoted by H and vice versa by NH. For example, H-Tile represents the detection point on the surface of a tile in the area subjected to thermal load. Ideally, areas subjected to thermal loads will delaminate while other areas will retain integrity. As described in Section 5.1, damage in strain monitoring methods is inferred indirectly through abnormal strain response and therefore requires reference to data from sound sites. At each detection point, two FBG sensors are placed parallel to the substrate surface and the tile surface. According to the results of the study in section 5.1, delamination was generally the first between the two cementitious materials. As the specimen was an utterly symmetrical structure, the thermocouple used to calculate the temperature compensation was set in a symmetrical position on the FBG sensor to prevent the thermocouple wires from becoming the starting point for debonding.

A gradual warming approach was still taken to run the PTL aging cycle, as shown in **Fig. 5-10(b)**. The rubber heater starts at 40 °C and rises cycle by cycle until delamination occurs. Although the temperature setting of the rubber heater was relatively high, the actual temperature of the tile surface was about 90 °C at the maximum, as shown in **Fig. 5-11**. Referring to Section 5.1 for the degradation speed of the aging cycle with a peak temperature of 80°C, the high-temperature setting for this work is intended to accelerate the degradation process. Similar to Section 5.1, a secondary cyclic thermal load was applied to the specimens diagnosed as delaminated after they had cooled, reproducing the temperature history in the sound condition to compare the trajectory of the strain occurring before and after delamination.

It is worth noting that the ATs on both sides of the specimen are not performed simultaneously but sequentially. Since the test was conducted from the mortar side, it is possible that the organic adhesive on the back side was also affected by the test on the mortar side. Still, in any case, since no delamination occurred on the organic adhesive side, there was little influence of heat transfer to the backside.

Acoustic diagnostics are performed at the end of each cycle to assist in monitoring the progress of degradation. As shown in **Fig. 5-9(a)**, the tile undergoing percussion inspection is located above the tile attached to the FBG sensor. Due to the symmetry of the specimen, tiles in symmetrical positions are considered to undergo the same degradation process. The same inspector tapped the center of the tile with a special hammer, taking an average of three measurements. A microphone was fixed 30mm above the percussion point to record the percussion audio.

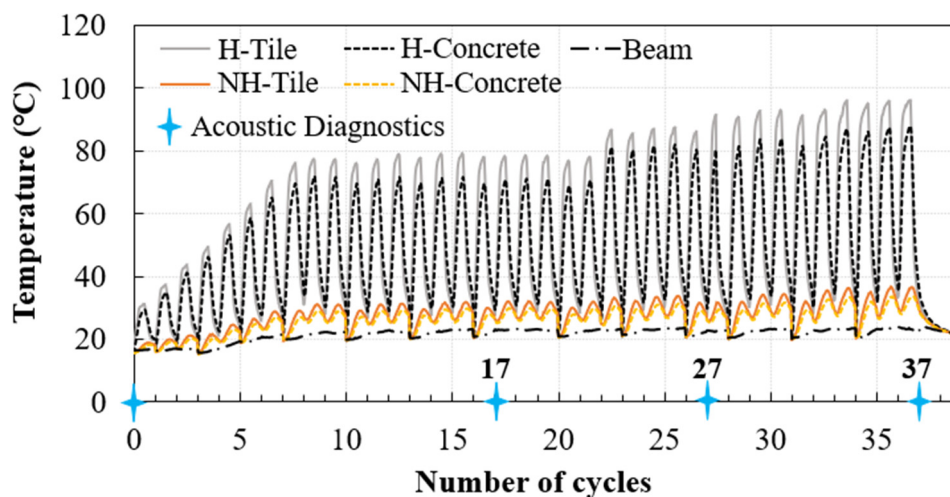


Figure 5-11 Temperature history of bonding mortar side.

5.2.3 Results of the bonding mortar

(1) Temperature monitoring

The temperature history of the detection points on the side where the bonding mortar was applied is shown in **Fig. 5-11**, with a temperature difference of around 40°C between the control temperature of the rubber heater and the actual temperature of the tile surface. The temperature variation in the tile without thermal load is minimal compared to the area subjected to the thermal load, and it can be assumed that the adhesion integrity of the area is always maintained. The framework beam column that provided the constraint in the specimen was barely affected by the thermal load and was essentially the same as the ambient temperature, providing the expected constraint conditions.

(2) Acoustic diagnosis results

The acoustic diagnostic results at the end of the 0th, 17th, 27th and 37th cycles were conducted. The sound pressure level (SPL) waveforms of the percussive audio were calculated, and a Fast Fourier Transform (FFT) was performed. As shown in **Fig. 5-12**, the maximum absolute value of the SPL is defined as the relative maximum amplitude derived from the SPL - time waveform. Soeta et al. [161] supported the reliability of using the relative maximum amplitude derived from the sound waveform as a diagnostic criterion for stratification. Considering the sensitivity of using the magnitude of sound pressure (Pa) as an evaluation metric, we converted this metric to sound pressure levels. Still, the trend in magnitude was not altered. The SPL - time waveform is calculated using the audio processing software "WavePad" as follows:

$$LP = 20\lg(P/P_0) \quad (4-1)$$

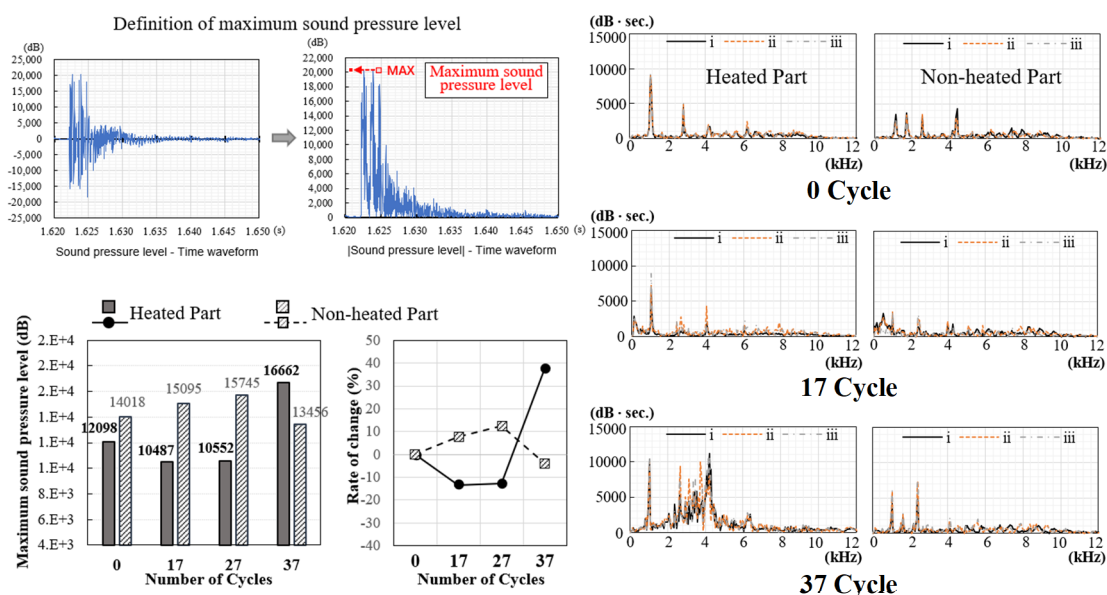


Figure 5-12 Value (left), change rate (right) of maximum SPL of impact sound. **Figure 5-13** Fourier amplitude spectrum of impact sound.

Where LP is the sound pressure level (dB), P is the sound pressure (Pa), P_0 is the reference acoustic pressure (2×10^{-5} Pa)

As a diagnostic basis, these two analysis methods of percussive audio have been validated in several previous studies in our laboratory [162]. **Fig. 5-12** and **Fig. 5-13** show the maximum SPL and the Fourier amplitude spectrum, respectively. Both diagnoses showed that at the end of cycle 37, only the impact sound of the heated area tiles showed an unusual variation. The maximum SPL increased significantly by more than 4000 dB (approximately 38%) compared to the initial period. Similarly, the Fourier amplitude spectrum results showed an unusual spectral peak. We determine that delamination of the heated tiles has occurred at this moment. It is worth noting that in this experiment, the peaks of the amplitude spectrum were shifted towards higher frequencies along with the peeling, but in other experiments, there have been shifts towards the lower frequency side. We plan to investigate the mechanism in the future.

(3) Strain monitoring

Fig. 5-14 (a) and **(b)** show the strain history of the detection points in the non-heated and heated zones, respectively. In the non-heated zone, the strain of the tiles is less than the strain of the substrate, while in the heated zone, the opposite is true. This can be explained by the temperature history, where there is a temperature difference between the tiles and the substrate in the heated zone. In contrast, in the non-heated zone, the temperature of the two mostly agrees. This is due to the tile joints preventing heat conduction between the tiles, whereas the substrate has a continuity of heat transfer. Furthermore, the tiles used in this study have a lower coefficient of thermal expansion than the substrate.

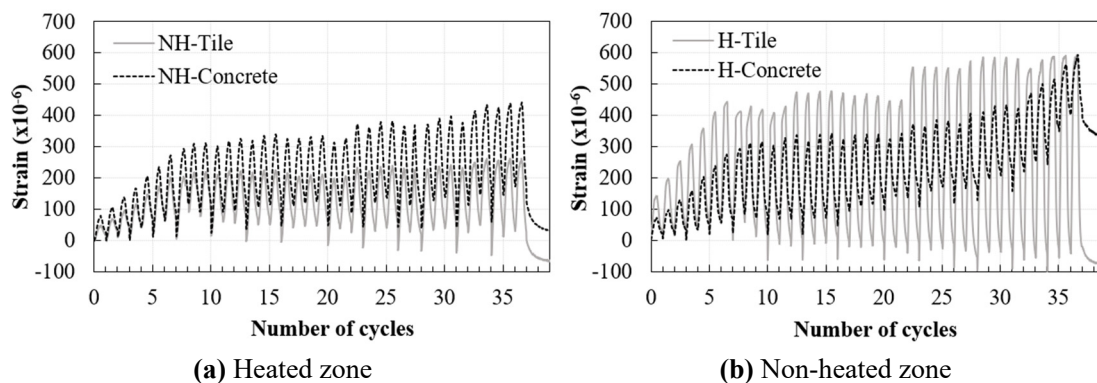


Figure 5-14 Strain history of concrete and tile surface.

As mentioned earlier, the occurrence of delamination is indirectly inferred from the observed anomalous strain response. Theoretically, some correlation should be maintained between the strain of the tiles and the concrete in a sound state. Along with the degradation process, this correlation will disappear the moment delamination occurs, when the tiles lose the restraint of the substrate. To this end, the absolute value of the strain difference between them was calculated. The “|strain difference|” is given as follows:

$$\Delta\varepsilon = |\varepsilon_T - \varepsilon_C| \quad (5-1)$$

Where $\Delta\varepsilon$ is the |strain difference|, $\varepsilon_T/\varepsilon_C$ is the strain on tile/concrete surfaces.

Fig. 5-15 shows the history of strain differences in the unheated and heated zones, respectively. At the end of each thermal cycle, i.e., when the temperature of the heated tile has dropped to its minimum, the strain difference at this moment is defined as the residual strain difference and is marked in the figures.

The strain differences at both detection points, H and NH, increase with the aging cycles, indicating degradation progression. However, the adhesion integrity of the non-heated zone was also not disrupted until the end of the experiment (which is also evidenced by the acoustic test results), as no abrupt fluctuations were observed, indicating that the linkage between the strains of the tiles and the substrate was always maintained. In contrast, there is a sharp increase in the strain difference at the detection point H, especially in the period from the 33rd to the 37th cycle in **Fig. 5-15(a)**. According to the strain history at point H shown in **Fig. 5-14 (a)**, the strain in the substrate starts to develop overall towards the tension side from the 30th cycle onwards. By the 37th cycle, the strain relationship between the substrate and the tiles has changed dramatically compared to the beginning of the heating and combined with the acoustic diagnostic results. There is a high probability of delamination between the tiles and the substrate at the end of the 37th cycle.

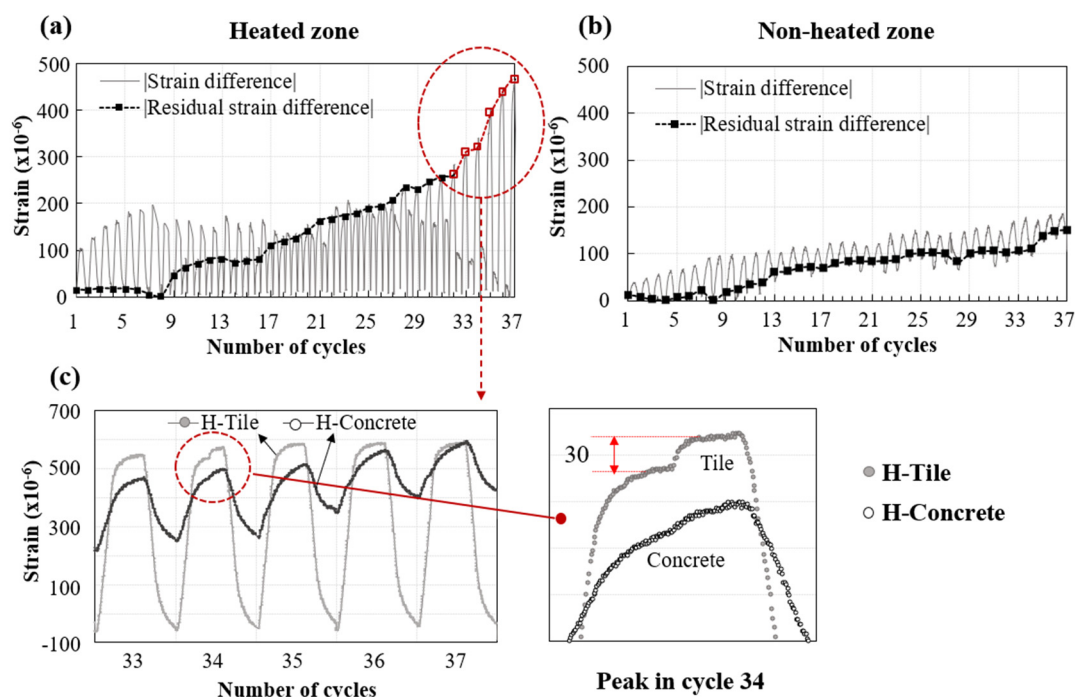


Figure 5-15 Strain difference between tile and concrete, (a) in the heated zone, (b) in the non-heated zone, (c) details of 33rd to 37th cycle in the heated zone.

It should be noted that the rubber heater relies on natural cooling, with the residual temperature at the end of each cycle also rising with the peak temperature. However, the detection point H was subjected to thermal loading, despite the peak temperature did not change during the phase from 33rd to the 37th cycle, and the residual strain difference rose intensely with each cycle. This might be regarded the process by which delamination occurs. For further investigation, the strain history for this phase was expanded, as shown in **Fig. 5-15(c)**. The strain on the tiles increased rapidly by approximately 30μ before the peak temperature was about to be reached, while the substrate strain did not follow this change. This indicates that the correlation maintained between them was suddenly lost at this moment, which is most likely the moment when delamination occurred. Subsequently, as the thermal load is cycled, the delamination gradually increases until it can be diagnosed by percussion.

In addition, **Fig. 5-16** shows the ratio of the strain amplitude of the tiles to the substrate during each cycle, calculated according to **Equation 4-1**. By monitoring the correlation between the strain tracks of the tile and the substrate, it is possible to conclude that the unheated zone always maintains a healthy adhesion, with the strain range ratio remaining relatively stable at approximately 0.75 independent of variations in peak temperature. In contrast, the strain amplitude ratio in the heated zone increased sharply after 34 cycles. This means that the strain amplitude of the tile becomes more extensive than that of the structure after delamination, as the delamination reduces the substrate constraint to which the tiles are subjected.

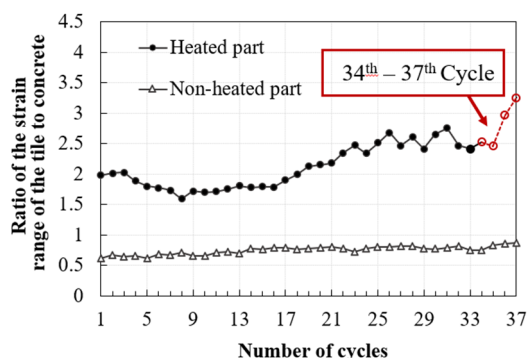


Figure 5-16 Ratio of the strain amplitude of the tile to concrete during each aging cycles.

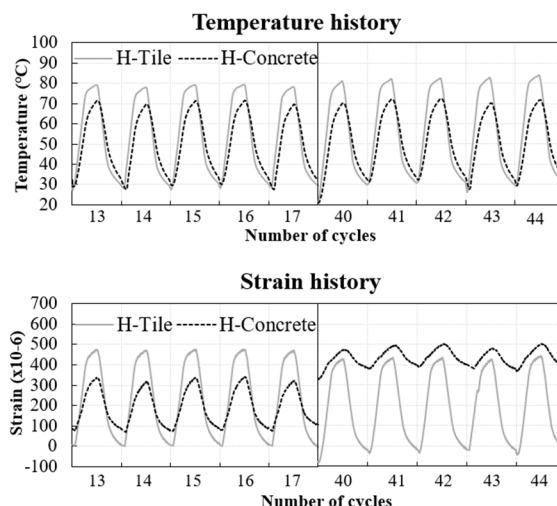


Figure 5-17 Comparison of the strain behaviour of the tiles and substrate before and after delamination.

Finally, to verify the occurrence of delamination and to observe the strain behavior between the tiles and the substrate after delamination, aging cycles were applied again, reproducing the temperature history for cycles 12-17 (the period diagnosed as sound) with a tolerance of $\pm 5^\circ\text{C}$. A comparison of the temperature and strain history is shown in **Fig. 5-17**. The secondary thermal loads were named cycles 40-44. It can be observed that despite having a similar thermal load temperature history, after being diagnosed as delaminated, the strain magnitude relationship between tile and structure reversed, showing a different strain behavior to that of the sound period. As described in Section 5.1, the shift in the strain behavior of the tiles and the substrate indicates a loss of association. It can be considered that delamination has occurred at this moment.

In summary, the proposed AT method can accelerate the degradation of wall specimens. The whole process of delamination of the tiles from the substrate under thermal loads was successfully observed by monitoring the strain with FBG sensors. The loss of correlation between the strain trajectories of the material marks the onset of delamination. In addition, a discontinuous strain response can be considered as a danger signal, which has never been observed in previous studies.

5.2.4 Results of the organic adhesives

After the test on the mortar adhesive side was completed, the rubber heater was replaced on the back side, and the same test was conducted on tiles bonded with organic adhesive. The temperature history of the other side of the specimen, the detection points on the side where the organic adhesive was applied, is shown in **Fig. 5-18**. Despite a brief temperature control anomaly (cycle 36), the rubber heater has provided sufficient high-temperature heat load. In contrast to **Fig.**

5-11, the organic adhesives reduced the temperature difference between tiles and substrate to an almost negligible level. The acoustic diagnostic results are displayed in Fig. 5-19, where no signs of delamination were diagnosed during the 45 thermal load cycles.

The corresponding strain histories are shown in Fig. 5-20. In contrast to the bonding mortar specimen, the residual strains in the tiles and substrate gradually shifted towards compression as the peak temperature increased, probably due to the physical properties of the organic adhesives. Interestingly, during cycles 38-45, only the strain in the tiles increased with the peak temperature, while the strain fluctuations in the substrate remained stable. The speculation is that the organic adhesives soften as the temperature rises, and with good elasticity, the tension from the expansion of the tiles is absorbed internally by the adhesives.

The path of the strain relationship between the tiles subjected to thermal loading and the substrate is shown in Fig. 5-21. The absolute value of the strain difference, the residual strain difference, and the strain amplitude ratio are calculated in the same way as in Section 5.2.3 (1). Based on the description above, the variation in correlation represents the occurrence of delamination, the same as in the acoustic diagnosis. No indication of delamination occurring was observed from the strain results. According to the results of the strain amplitude ratio, the strain between the tiles and the substrate maintained a stable relationship, which represents a sound

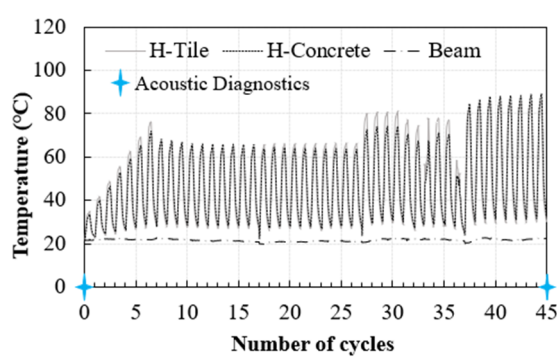


Figure 5-18 Temperature history of organic adhesives side.

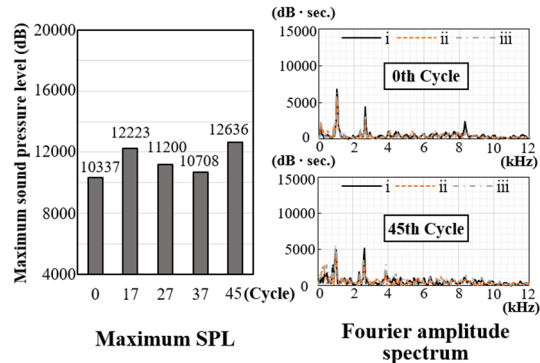


Figure 5-19 Acoustic diagnostic results on the organic adhesive side.

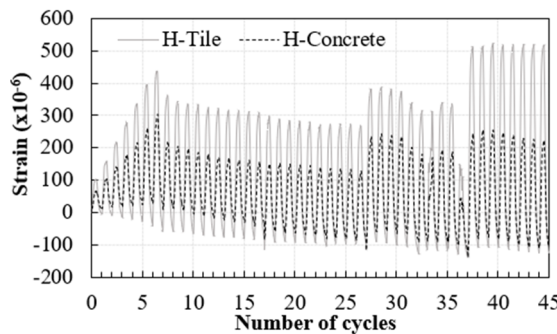


Figure 5-20 Strain history of organic adhesives side.

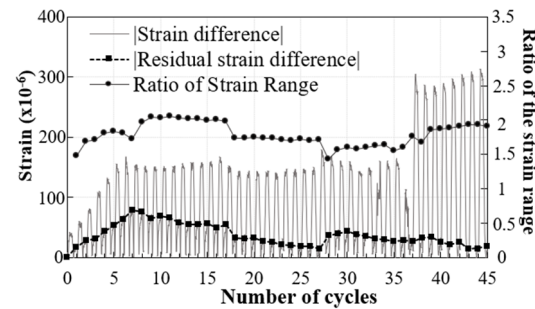


Figure 5-21 Strain relationship between the tiles and substrate on the organic adhesives side.

adhesion integrity. Thereafter, the thermal load continued to run for a number of cycles, but delamination was never diagnosed. Hereby, the organic adhesive is thought to be able to resist delamination of the tiles due to sunlight and reduce the risk of spalling.

5.2.5 Delamination detection of organic adhesives under freezing-thawing cycles

Due to their small modulus of elasticity, organic adhesives make it difficult to obtain damage information from the usual percussion methods. Although FBG sensors detected no delamination of elastic adhesive specimens due to high-temperature thermal loading, an attempt was made to induce delamination of organic adhesives by freeze-thaw cycles, given that similar organic adhesives exhibit hardening phenomena (increased modulus of elasticity) at low temperatures.

(1) Experimental procedure

The specimens were transferred to a thermostatic chamber, and after they had reached the ambient temperature of $-10\text{ }^{\circ}\text{C}$, a cyclic thermal load was again applied in the original area. This time the temperature of the tile surface subjected to the thermal load was strictly controlled. Except for the temperature, the duration and pattern of the cycle remain the same: $-10\text{ }^{\circ}\text{C}$ to $40\text{ }^{\circ}\text{C}$ (60 min) \rightarrow $40\text{ }^{\circ}\text{C}$ (60 min) \rightarrow $40\text{ }^{\circ}\text{C}$ to $-10\text{ }^{\circ}\text{C}$ (60 min) \rightarrow $-10\text{ }^{\circ}\text{C}$ (60 min). The cycle was performed 45 times, and the temperature error was controlled to $\pm 3\text{ }^{\circ}\text{C}$.

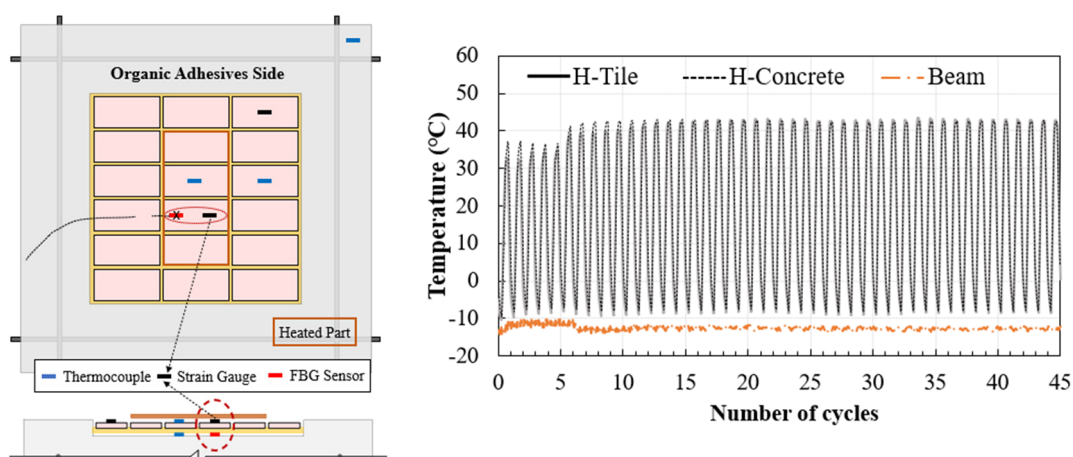


Figure 5-22 Sensor configuration (left) and temperature history of concrete and tile surface (right).

Unfortunately, the FBG sensor on the tile surface broke, and we replaced an electrical resistance strain gauge in its original position. In contrast, the substrate strain is still monitored with the original FBG sensor. The detection configuration is shown in **Fig. 5-22**

(2) Experimental result

Fig. 5-23 shows the strain histories of the tile and substrate and the strain amplitude ratios for each cycle. Similar to the **Fig. 5-18**, there is almost no temperature difference between the two materials, but the relationship between the magnitude of the strain results for the two is reversed. The temperature amplitude is also around 50 °C for cycles 10-25 in **Fig. 5-18** and **Fig. 5-20**. The strain amplitudes of the concrete measured by the FBG sensors are similar for the same temperature amplitude, but the strain amplitude of the tiles is significantly reduced (measured with strain gauges). There are two possible reasons for this: 1) the variability of the strains measured by the different

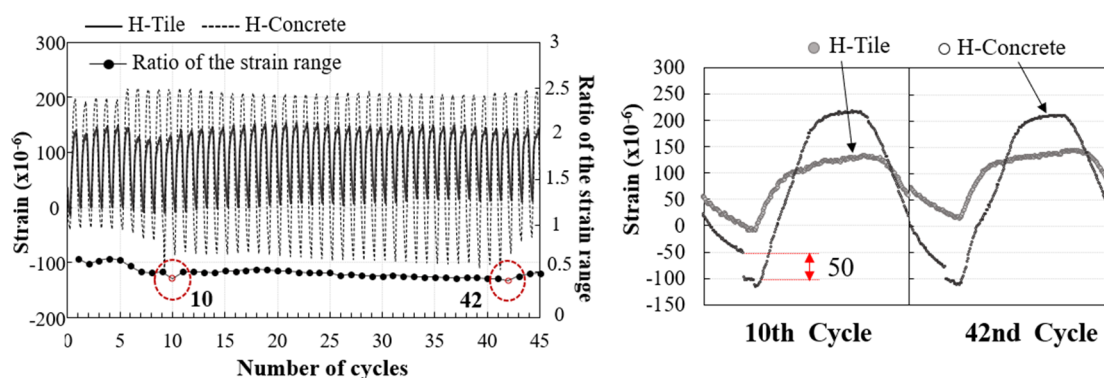


Figure 5-23 Strain history of concrete and tile surface under freeze-thaw cycles.

sensors, even though both perform temperature compensation calculations; 2) the hardening of the organic adhesive at low temperatures, which hinders the deformation of the tiles, while the substrate (without joints), the deformation is difficult to suppress by the organic adhesives.

Despite the differences between the sensors, the results of the strain amplitude ratios demonstrate the correlation between the movement of the tiles and the substrate. Overall, a stable correlation between them was maintained, but the strain amplitude of the substrate increased slightly in the 10th and 42nd cycles, expanding the strain history for these two cycles and observing a discontinuous strain response, as shown in **Fig. 5-23**. In the 10th cycle, the substrate contracted by approximately 50 μ when the temperature reached its trough, and a similar situation was observed in the following cycles. This suggests that delamination could have occurred at this moment, with the hardening of the organic adhesive at low temperatures, having been momentarily peeled from the substrate, the constraint on the substrate surface being released, and the shrinkage instantly increasing. However, the weakest temperatures provided in this study were insufficient to denature the adhesive, which softened and returned to elasticity as the temperature increased. The adhesion integrity was not damaged.

In summary, in terms of resistance to natural aging caused by sunlight, applying organic adhesives reduces the risk of delamination of tiles compared to bonding mortars. Attention should also be paid to the embrittlement of organic adhesives due to low temperatures or other factors.

Although the general level of cold weather does not cause permanent damage to organic adhesives, there is a risk that transient denaturation at low temperatures can lead to tile delamination.

5.3 SUMMARY

This chapter describes the feasibility study of the SM method for delamination detection in tile systems. PTL thermal loads were applied to tile specimens of two different scales and constituent materials, and the strains of all layers were monitored with FBG sensors. The following conclusions were derived:

(1) The application of FBG sensors for the delamination detection of tile finishes has proven feasible. Furthermore, the strain tracking of the composite material by the FBG sensor makes it possible to observe the moment of damage at any of the bonding interfaces. This gives building managers timely warnings and establishes the lowest-cost tile maintenance program.

(2) The strain response of an interface composed of different materials may differ when adhesive damage occurs and needs to be inferred by comparison with the strain response of that interface when it is in a healthy state. In general, accompanying the degradation, material deformation will increasingly converge to an unconstrained state. The disappearance of the original followability between the strain trajectories of the two materials can be used to determine adhesion damage. In the case of constant load, abnormal strain response, such as a sudden increase or decrease, can be considered a sign of pathology. Early warning can reduce the risk of accidental tile spalling.

(3) In exterior tilings, rendering mortar is the most deformable component. The response of the rendering mortar to climate may be the main factor in delamination. Therefore, performance control of rendering mortars (e.g., reducing the thermal expansion coefficient) may be an effective way to improve the durability of exterior tilings.

(4) Quality control of the application is critical to the durability of the exterior tilings. Original construction defects can lead to adhesion failure at low load strengths.

(5) Resistant to natural ageing caused by sunlight, the application of elastic adhesives reduces the risk of delamination of tiles compared to bonding mortars. However, it is still to be careful of factors that can cause the elastic adhesive to become brittle, such as low temperature conditions.

In summary, this study provides evidence on the feasibility of FBG sensors for tile delamination detection and describes simple diagnostic approaches. Pre-installation of FBG sensors in the facade claddings of new building can greatly enhance the execution efficiency of the

preventative maintenance phase. The FBG sensors are installed where the cladding is most likely to peel off, such as around openings in the building and joints between structural components. The health of these locations is used as early warning information to plan the timing of a comprehensive inspection rationally. If large strain fields need to be detected, a FBG sensor network could be considered for monitoring special buildings and high-risk areas. However, although it is possible to determine adhesion damage qualitatively, it is currently difficult to interpret the strain behavior in correspondence with adhesive properties. Further research is needed in combination with other diagnostic methods.

Chapter VI

CONCLUSION AND FUTURE STRATEGIES

6.1 CONCLUSION

This dissertation describes a series of studies conducted to establish an objective-based durability design procedure for RC building facades with rendered and tiling. A laboratory-scale durability assessment method is proposed that can be utilized during the durability design phase to evaluate mortar/concrete adhesion with different materials and application procedures. A technique for detecting delamination of facade claddings with FBG sensors is proposed. This technique contributes to the efficiency of the execution of the preventive maintenance phase. In addition, key parameters influencing the durability of the rendering mortar are investigated, as well as the debonding evolution under the thermal loads. The main conclusions of each chapter's experimental and investigative work are summarized below.

6.1.1 A laboratory-scale durability assessment method

Previous methodologies for durability assessment of rendered mortars applied to RC buildings were shown to be inadequate and unreliable. Therefore, based on the actual degradation mechanism, a reliable AT method is proposed based on the PTL aging cycle. The proposed AT method proved to be a very useful and powerful tool for assessing long-term adhesion between multiple cementitious materials. It is beneficial for rapid assessment during the product development phase.

(1) The proposed durability assessment method is applicable to the climate zone in which Japan is located, characterized by no clear distinction between dry and rainy seasons, long sunshine hours, and large daily temperature swings. The probability of damage to facade claddings in similar climatic zones differs significantly by orientation.

(2) Solar radiation is identified as the main degradation agent, and thermal expansion mismatch between materials is the main degradation mechanism of facade claddings. The proposed PTL aging cycle can simulate this degradation mechanism. "Partial" thermal loading is critical. Both thermal load and sufficient restraint must be provided to reproduce the degradation mechanism under solar radiation.

(3) The pull-off test and the direct shear test can measure the adhesion loss due to thermal loading. At the central and boundary of the thermal loading area, the shear strength decreases by 34.5% and

56.4%, and the tensile strength by 27.3% and 35.4%, respectively. Therefore, it is considered that the thermal expansion mismatch between the materials generates stresses in both in-plane and out-of-plane directions at the bonding interface, and the shear stress is greater than the normal stress, which is a realistic rule in general structures.

(4) All experimental results showed that the mortar/concrete specimens obtained the greatest loss of adhesion in part located at the thermal load boundary. The numerical analysis results confirm that the maximum concentrated stress value was obtained at this location. This indicates a reasonable correlation between stress generation and the degradation mechanism of adhesion. Moreover, it can be assumed that the weakest position of the facade claddings should correspond to the junction of solar radiation and shadows and not to the position exposed to sunlight directly.

(5) In durability assessment experiments, the adhesion of the specimen ends is decreased due to curling deformation caused by drying shrinkage. However, this does not affect the results of the durability evaluation run at average relative humidity conditions. Furthermore, the resistance of the rendering mortar/concrete composite to drying shrinkage can be determined by the adhesion loss at both ends of the specimens.

(6) Assessing the loss of adhesion through bond strength testing can yield statistically significant durability assessment results. However, it should also consider the dispersion of test results and the construction variability of specimens when referring to the assessment results. This is especially true when comparing two specimens with little differences in durability. A combination of different adhesion tests is recommended, such as the strain monitoring method mentioned below.

(7) The adhesion test cycle should be designed according to the aging cycle pattern and the specimens with the weakest adhesion. The aging cycle run should guarantee at least 50% adhesion loss for the weakest specimens. A better approach may be to perform a multidimensional test of durability, i.e., simultaneous comparison of adhesion loss after different aging procedures to obtain a comprehensive durability evaluation.

Although according to the literature survey, temperature and water are the main degradation agents. But simulating the collaborative mechanism of different degradation agents in nature is complicated. Using temperature as the only degradation agent in experimental scale durability assessment methods is reasonable and valid. For other relevant degradation mechanisms, representative aging procedures must be designed according to the applied climate zone (e.g., freeze-thaw cycles corresponding to cold climate, dry-wet cycles corresponding to wet climate, etc.).

Nevertheless, each aging procedure has advantages and limitations, and experts should choose carefully according to the climatic conditions of the proposed application.

In addition, even if the correspondence between the aging cycle and service life cannot be clarified for the time being. The proposed durability assessment methods are also of great value, especially for new products with no application history. These tests reflect how the material should behave under solar radiation. Comparing it to a reference material with a lengthy application history allows a quick determination of whether the new material has the required durability.

6.1.2 The key parameters affecting the durability of rendering mortar

Under thermal loading, the followability of the rendering mortar and concrete to each other's deformation determines the long-term adhesion performance. Some key parameters determine the followability of the rendering mortar.

(1) Material properties. Dry shrinkage, modulus of elasticity, and coefficient of thermal expansion. These three physical properties determine the deformation match of mortar to concrete. Specimens with the same mix proportion underwent 50 aging cycles, and specimens with 1% SRA added reduced the shear strength loss by about 15% (compared to specimens without SRA). Higher temperatures result in more drying shrinkage, so rendered mortars with small dry shrinkage exhibit higher durability. In tile specimens, the rendering mortar/concrete interface undergoes bond failure earlier than the tile/rendering mortar interface, although the latter was subjected to higher temperatures. It is speculated that this phenomenon is due to the low modulus elasticity of bonding mortar acting as a buffer. Adhesives with low elastic modulus can reduce the tangential and normal stresses at the bonding interface. The performance of organic adhesives in the experiments in section 5.2 regarding resistance to thermal loads supports this speculation. Similarly, rendering mortars in tile specimens showed the most intense response to temperature, and lowering the coefficient of thermal expansion of rendering mortars may help to improve durability. In conclusion, the compatibility of material's physical properties should be considered as significant aspect of durability design.

(2) Applications. Since thermal expansion mismatch is the main degradation mechanism. The temperature at which the rendered mortar is applied may be a key parameter. The optimum application temperature is the median temperature of the region throughout the year, and construction in severe cold and hot weather should be avoided. In addition, studies on curling deformation indicated that the shrinkage gradient developed on the thickness of the rendering mortar is also a key parameter affecting adhesion. A rendering mortar with a thickness of 15 mm reduced the short-term bond strength by an

average of 30% compared to a 10 mm rendering mortar. Although the former did not exhibit a more loss of adhesion than the latter after the aging cycle, the presence of initial defects also reduced the service life. Applying techniques that allow the mortar to dry uniformly can significantly reduce this effect. Reducing the thickness of the mortar for each application, providing moist curing conditions at an early stage, applying SRA, and adding an overlay to prevent evaporation can all prevent high moisture gradients from forming within the mortar.

6.1.3 Debonding evolution of rendering mortars under the thermal load

The debonding evolution of the rendering mortar was studied by periodic bond strength tests and continuous strain monitoring, representing debonding on a large scale (40 mm × 40 mm) and a small scale (0.15 mm × 10 mm).

According to the bond strength test results, the adhesion of the mortar deteriorates with the aging cycle in an "S-shaped" path, showing three characteristic phases of degradation-stagnation-degradation. A "plateau" period can be observed during the degradation process, during which the bond strength does not decrease with the running of the aging cycle. The debonding evolution enters the plateau period when the loss of bond strength reaches about 40%. The duration of the plateau period is related to the load intensity (peak temperature of the thermal load). The higher the peak temperature, the shorter the plateau period. The plateau before adhesion failure may occur more than once, but it is certain that debonding does not evolve at an even rate.

In strain monitoring experiments, debonding evolution is studied on one specimen. The debonding evolution is inferred from the characteristics of the strain behavior. The debonding evolution at the small-scale level goes through two phases: damage accumulation and debonding development. The damage accumulation phase is characterized by gradually separating the strain trajectories of mortar and concrete but in the same direction of deformation. It is assumed that some mechanical bonds break at the interface, weakening the connections between the materials but maintaining the ability to follow each other's deformation. Subsequently, these fractured connections form small areas of debonding, which gradually expand to complete delamination with the aging cycle.

In summary, these results allow the hypothesis to be made that the plateau period in the evolution of large-scale debonding may represent that some tiny debonded areas are being accumulated and that the bond strength test results will not continue to decrease until a certain threshold is reached. Therefore, for periodic damage detection methods, debonding occurs abruptly. A continuous detection scheme can improve efficiency and accuracy.

6.1.4 Detecting adhesion damage in tilings with FBG sensors

The adhesion state of facade claddings must be monitored over time to ensure their protection and correctly maintain and repair them when they begin to exhibit signs of degradation. The response of the constituent materials of a facade to climate reflects their adhesion condition, and damage detection is performed by identifying anomalies in strain behavior. FBG sensors were used to detect adhesion damage of tile specimens composed of concrete, rendering mortar, tiles, and tile adhesives (bonding mortar or organic adhesives).

The experimental findings show that the FBG sensor's ability to track the composites' strain enables the detection of damage at any adhesive interface. Based on the strain behavior, three bonding states can be distinguished.

-Healthy adhesion. A constant strain amplitude ratio is maintained, for example, and the strain behavior between the material's layers maintains some correlation.

-Adhesion damage (partial debonding) The two materials start to lose their ability to follow each other's deformation when their strain trajectories begin to diverge, and their strain amplitudes abruptly decrease or increase.

-Adhesion failure (complete debonding). With a considerable shift in strain amplitude, the relationship between the strain behavior of the materials is completely different from the first one.

The principles above are generally relevant to every adhesive interface in a tiling system; however, the strain behavior corresponding to damage may differ amongst materials and must be compared to the strain response of that interface in a healthy state. In general, the determination of adhesion damage can be based on the loss of the initial following between the strain trajectories of the two materials. When the load is constant, an aberrant strain response, such as a quick increase or reduction, indicates a lesion.

Although this is a qualitative detection strategy rather than a quantitative one, it can alert building managers when intervention is required. If strain behavior demonstrates a lack of followability, one should be cautious and increase the frequency of inspections; if strain behavior becomes severely abnormal, one should consider repairing or replacing the affected components. The strain monitoring method can prevent premature or delayed maintenance, hence reducing the danger of accidental tile spalling significantly.

6.2 FUTURE STRATEGIES

Based on the findings of this study, future development of highly durable facade cladding systems will concentrate on the following issues:

The general application of the proposed method for assessing durability still faces the following main hurdles:

- 1) Adequate identification of degradants.
- 2) Synergistic interactions between degradants
- 3) Key criteria for assessment.
- 4) Mode of performance test execution.
- 5) The connection between assessments and real service life.

Future studies will establish natural aging stations and create a database of existing structures. Determining the climate factors under which the material will be used is one of the most crucial aspects of durability assessment. Solar radiation may be the major degradation agent in many climatic zones, however, field data should be utilized to optimize the operation mode of the heat-cool cycle. The repeatability of the deterioration paths derived from artificial aging cycles must be confirmed in natural aging.

The proposed durability assessment method employs bond strength as a crucial criterion. Nonetheless, the variability of the bond strength test restricts the accuracy of the evaluation. The strain monitoring method's experimental results suggest new possibilities. In the future, it is anticipated that bonding performance will be measured by strain monitoring or other tests, along with the determination of new critical parameters. The choice of parameters must be based on the material's physical changes in natural aging. The aim is to create a system that can assess durability based on numerous criteria, allowing experimenters more selection options.

In the conclusion, the key parameters determining the durability of the rendered mortar are presented. These parameters are summarized from the experimental findings. The plan for further action is to quantify the impact of these criteria. In facade construction, rendering mortar is the most malleable and controllable substance. One of the ongoing projects investigates the optimal physical interaction between material layers based on durability evaluation tests. Furthermore, initial defects caused a significant majority of adhesion failures, and long-term goals include standardizing the

application procedure in durability design.

The strain monitoring method has proved to be an effective technique for damage detection of tilings. However, it is not yet possible to quantify the strain behavior of the material, and only the most fundamental property judgments are possible. Future plans include investigating strain behavior in various aging environments and actual structures in conjunction with other nondestructive testing techniques, such as the UT and AE methods. The objective is to quantify the relationship between strain responses and adhesion, while further investigating the reasonability of the hypothesis about the debonding evolution.

Appendix A

Cohesive Zone Material (CZM) Mode Mixed-Mode Debonding law in ANSYS

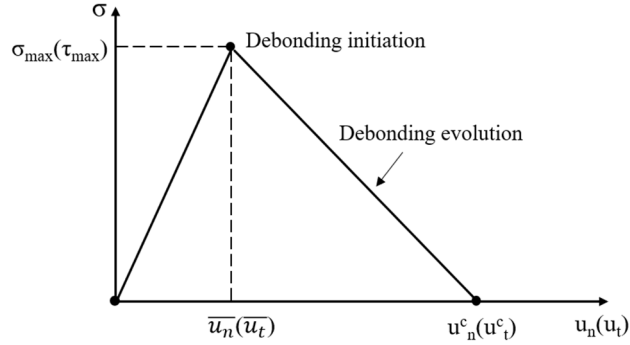


Figure A-1 Mixed-Mode Debonding law in ANSYS, according to [143].

In mixed-mode debonding the interface separation depends on both normal and tangential components. The equations for the normal and the tangential contact stresses as follows [143]:

$$P = K_n u_n (1 - d_m) \quad (1)$$

and

$$\tau_t = K_t u_t (1 - d_m) \quad (2)$$

where:

P = normal contact stress (tension)

τ_t = tangential contact stress

K_n = normal contact stiffness

K_t = tangential contact stiffness

u_n = contact gap

u_t = tangential slip distance

d_m = debonding parameter

The debonding parameter is defined as:

$$d_m = \left(\frac{\Delta_m - 1}{\Delta_m} \right) X \quad (3)$$

with $d_m = 0$ for $\Delta_m = 1$ and $0 < d_m = 1$ for $\Delta_m > 1$, and Δ_m and X are defined below.

$$\Delta_m = \sqrt{\left(\frac{u_n}{u_n} \right)^2 + \left(\frac{u_t}{u_t} \right)^2} \quad (4)$$

$$X = \left(\frac{u_n^c}{u_n^c - \bar{u}_n} \right) = \left(\frac{u_t^c}{u_t^c - \bar{u}_t} \right) \quad (5)$$

where:

\bar{u}_n = contact gap at the maximum normal contact stress (tension)

\bar{u}_t = tangential slip distance at the maximum tangential contact stress

u_n^c = contact gap at the completion of debonding

u_t^c = tangential slip distance at the completion of debonding

The constraint on X that the ratio of the contact gap distances be same as the ratio of tangential slip distances is enforced automatically by appropriately scaling the contact stiffness values.

For mixed mode, debonding is complete when the energy criterion is satisfied:

$$\frac{G_n}{G_{cn}} + \frac{G_t}{G_{ct}} = 1 \quad (6)$$

With

$$G_n = \int P du_n \quad (7)$$

$$G_t = \int \tau_t du_t \quad (8)$$

$$G_{cn} = \frac{1}{2} \sigma_{max} u_n^c \quad (9)$$

$$G_{ct} = \frac{1}{2} \tau_{max} u_t^c \quad (10)$$

where:

G_n / G_t = The normal / tangential fracture energies

G_{cn} / G_{ct} = The normal / tangential critical fracture energies

σ_{max} = Maximum normal contact stress

τ_{max} = Maximum equivalent tangential contact stress

Appendix B

Effect of Curling Behavior of Mortar Due to Drying Shrinkage on Mortar-Concrete Adhesion System

A significant shear strength loss at the free edge of the mortar/concrete adhesion specimens was observed in the experimental studies in Chapters 3 and 4, even though this part of the specimen was not affected by thermal loading. As described in Section 2.21, this phenomenon is most likely due to drying shrinkage. The difference in moisture between the upper and lower surfaces of the mortar causes it to deform in an out-of-plane direction at the unconstrained free edges in the form of a "curling" (**Fig. 2-6(c)**). Curling deformation is considered an adhesion failure mechanism, and it is necessary to evaluate the potential impact of curling deformation on the durability of mortar/concrete adhesion in establishing durability assessment methods.

Curling deformation leads to the generation of confining stresses at the bond interface. Previous studies have focused on cracking due to in-plane stresses, and researchers have described cracks due to the inhibition of drying shrinkage [81] [82]. However, stresses in both directions (in-plane and out-of-plane) affect the bond between mortar and concrete. For this reason, predicting the restraining stresses generated at the bond interface in both directions is necessary. Furthermore, the study focused on the concrete slab and pavement slabs [79] [82] [163] [164], and the overlay applied to these elements is very different from rendered facades. Therefore, it is necessary to reinvestigate the effect of curl deformation on the façade claddings.

Appendix B describes the series of studies that were conducted, the curling of mortar in the free drying shrinkage and restrained shrinkage states was investigated using laser sensors and digital image correlation (DIC) technique, respectively. The stresses at the mortar-substrate adhesive interface due to curling were predicted by numerical simulation. The purpose of this study is to understand the curling behavior of rendering mortars, thereby assessing its effect on the mortar-concrete adhesion system.

B.1 FREE CURLING OF RENDERING MORTAR

B.1.1 Experimental procedure

(1) Specimen preparation

Two mortar materials were selected for investigating the curing behavior under the non-restraint condition. One is a standard formulation for rendering (PL), according to the Japanese Architectural Standard Specification — JASS15 Plastering Work. It was the reference mortar upon SR specimens which inclusion of SRA. SRA is widely used as an admixture to reduce the drying shrinkage of cementitious materials and is beneficial in reducing curling [153]. As described earlier, curling results from the drying shrinkage gradient in the thickness of the mortar. Therefore, the thickness of specimens and the amount of drying shrinkage (with/without SRA) as two parameters to prepare multiple specimens with different curling deformations. Table B-1 reports the mixture proportion and specimen specifications.

The mortar specimens had dimensions of 10/20/30 mm × 100 mm × 400 mm, as shown in **Fig. B-1**. The specimens were demolded on the third day after casting and subsequently curing in water at 20 °C for 21 days.

Table B-1 Specifications of mortar specimens

Specimen ID	Parameter		Cement (C)	Fine aggregate	S/C (by Weight)	W/C (%)
	Thickness	SRA				
PL-1	10mm	-	Ordinary Portland cement	S: Crushed sand	2.5	50
PL-2	20mm					
PL-3	30mm					
SR-1	10mm	1% ^a				
SR-2	20mm					
SR-3	30mm					

a % by weight of the gross mass

(2) Measurements with Laser Sensors

The most common method to quantify curl deformation is to measure the vertical displacement (usually at the center and corner) of a specified detection point on the specimen (away from the substrate direction). **Fig. B-1** shows the device for measuring curling behavior, that is, the displacement of the upper surface of the mortar in the out-of-plane direction. To reproduce the curling of exterior wall mortar, the upper surface of specimens was open to the air, and the other sides were

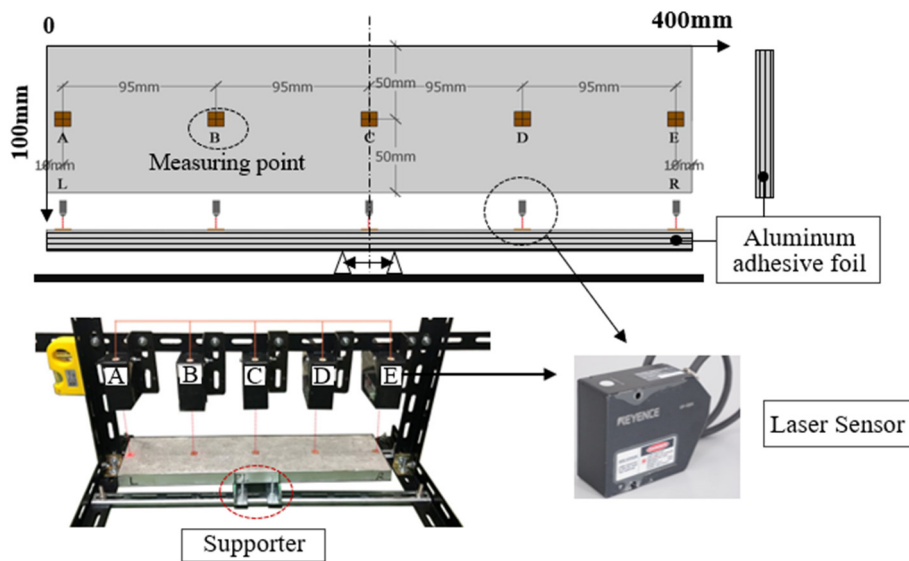


Figure B-1 Displacement measurement system.

protected from drying by adhesive aluminum tapes. Ideally, the specimen will have a parabolic shape on the section after being curled. Five symmetrical measuring points were set on the central axis of the drying surface, and a thin copper plate of 10 mm² was attached to each measuring point. The five laser sensors, whose accuracy is 0.2 $\mu\text{m}/\text{m}$, are used to measure the displacement in the vertical direction. The bottom surface was supported by two steel sheets, each 25 mm from the center of the specimen, to limit the position of the measuring points. Therefore, specimens should only occur under self-restraint caused by the drying shrinkage gradient.

To observe a more pronounced curl, the specimens were placed in an incubator at 40 °C and 3% RH for accelerated drying after the initial value was measured. The displacement and mass loss were then measured periodically over 72 hours.

B.1.2 Experimental result

(1) The curling deformation

Fig. B-2 shows the displacement of the drying surface of the mortar specimen in the out-of-plane direction. Based on the displacement results of the five symmetrical measurement points, the specimens were considered to exhibit significant curling. At point C, corresponding to the central portion of the specimen, as the drying progresses, it is displaced downward, and the others are symmetrically displaced upward. The displacement was significantly reduced from the ends to the middle (A and E at both ends, B and D at the midpoint). Measuring points A and E, B and D are in a central symmetrical position, and the displacement of the two is in an approximately symmetrical state.

On the whole, the measurement points distributed in symmetrical positions on both sides have

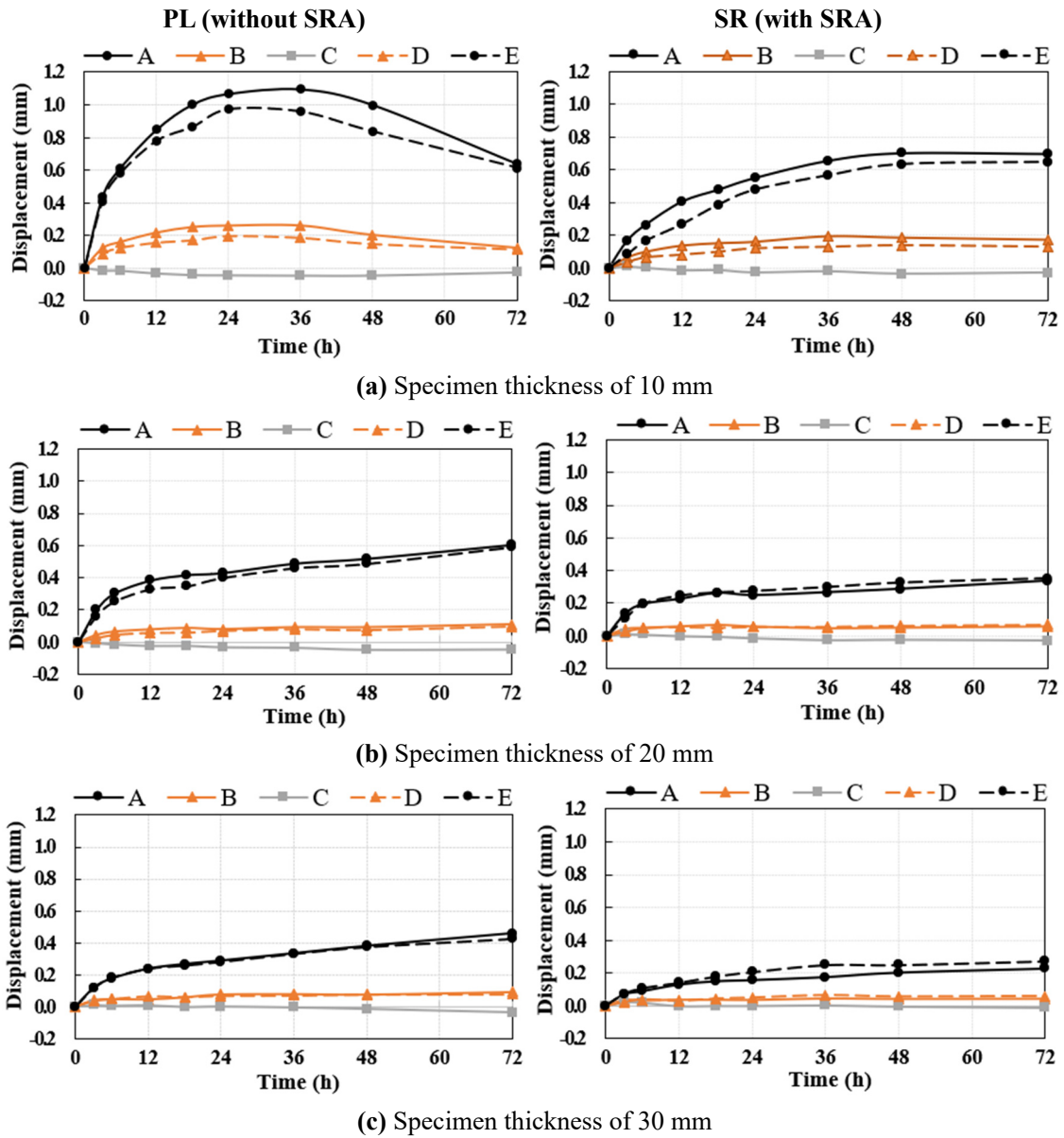


Figure B-2 The displacement of each point changes with time.

similar displacements. In the following results, the difference in displacement between the ends (A, E) and the specimen center (C) is used to calculate the curl amount. The curling deformation is given as follows:

$$C = (dA + dE)/2 - dC \quad (\text{B-1})$$

Where C is the curling deformation index [mm], dA , dE and dC is the displacement at point A, E and C [mm].

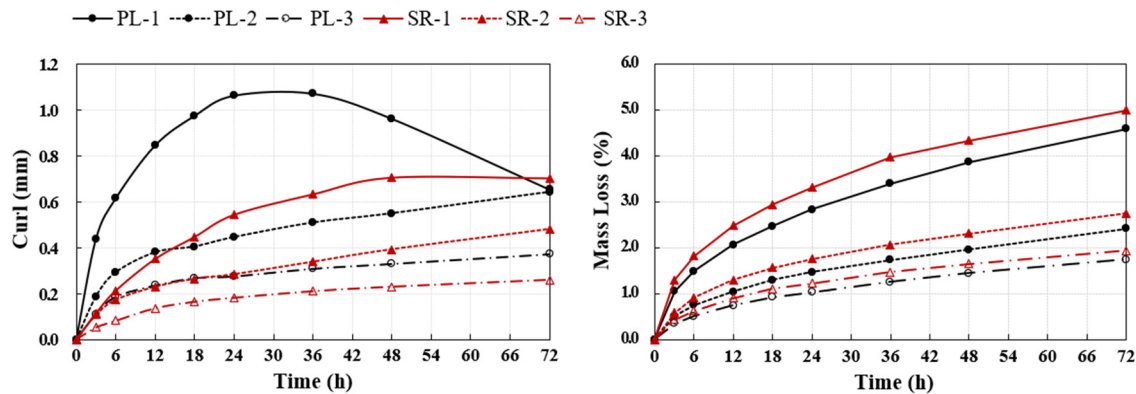


Figure B-3 Curling deformation over 72 hours. **Figure B-4** Mass loss over 72 hours.

Fig. B-3 shows the curling deformation index of each specimen over 72 hours. As the thickness increases, the curling deformation of the specimen decreases. This indicates that the thinner specimens produced a more significant shrinkage gradient due to the faster drying speed, and the non-dried part functions as a restraint in the thick specimens. The thin specimen (PL-1) reaches the maximum curling deformation at 36 hours. Then the deformation of the specimen fell back since the drying speed inside the specimen began to become uniform, and the difference in the amount of shrinkage between the surface and the bottom surface was reduced. Compared with PL specimens, the curling deformation of mortars containing SRA was significantly reduced.

(2) Mass loss rate

The mass loss rate (water loss) of mortars is shown in **Fig. B-4**. Since the specimens only evaporated water through the upper surface in the initial drying stage, it is considered that the mass loss of the specimen is dependent on the thickness. The 10mm thin specimens showed the largest decrease in mass moisture content. In particular, the specimens containing SRA showed a more significant mass loss rate regardless of the thickness. This phenomenon may be related to the mechanism of action of SRA. The SRA used in this experiment is not a type that has a water retention effect but a type that reduces capillary tension.

B.1.3 Numerical analyses

(1) FE Model

A simple numerical simulation method for curling is proposed based on the 3D FEM analyses with the program ANSYS Workbench. The results obtained by numerical analysis have been compared with the experimental results to verify mutually.

The models have the same dimensions as the specimens. Three thicknesses (10mm / 20mm / 30mm) were set, as shown in **Fig. B-5**. Corresponding to the positions of the two supporting steel sheets in the displacement measurement (each 25 mm from the center of the bottom surface of the model), two lines of 100 mm length were fixed as constraints. The material parameters are the same as in Section 3.2.1 (**Table 3-1**).

Since all specimens have the same drying area, the same type of specimens needs to simulate the same shrinkage gradient to reproduce the curl. For this purpose, we split the mortar model from 1/10 of the thickness into two elements, with the upper 1/10 as a shrinkage element. The drying shrinkage

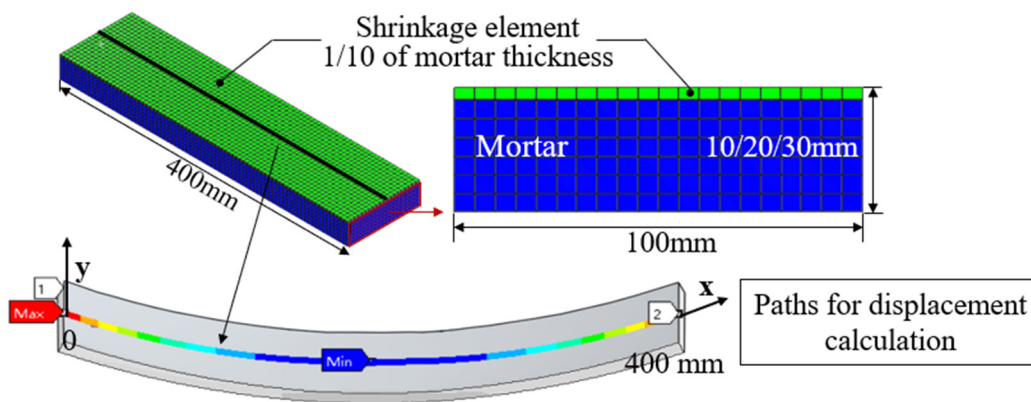
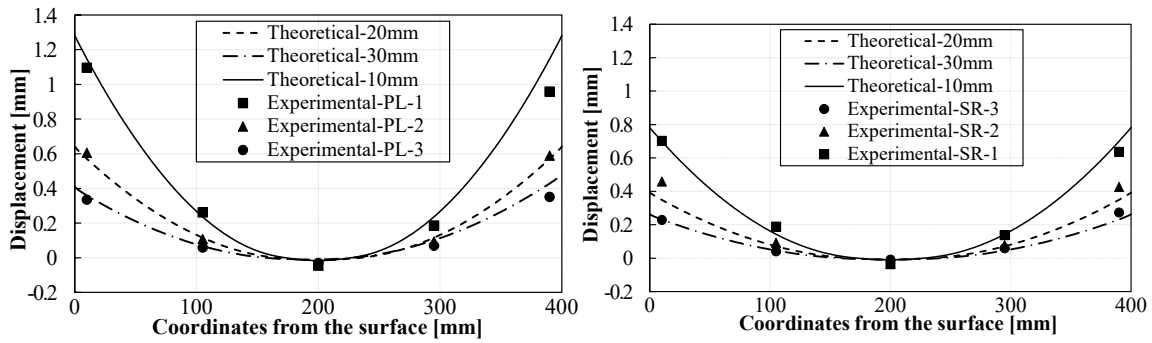


Figure B-5 Free shrinkage model.

is controlled by adjusting the thermal expansion coefficient of the shrinkage element material. According to **Fig. B-3**, both PL-1 and SR-1 specimens reached maximum deformation in the free curling test. We applied a shrinkage strain of 1300 μ and 800 μ to the shrinkage element based on the displacement of the PL-1 specimen at 36 hours and the displacement of the SR-1 specimens at 72 hours, respectively.

(2) Analysis results

The experimental and numerical displacement comparison results are shown in Fig. B-6. Corresponding to the measurement points of displacement in the specimen, the displacement path is the long central axis of the upper surface (shrinkage surface) of the model. **Fig. B-6(a), (b)** shows the results of the model given a shrinkage strain of 1300 μ and 800 μ , compared to the maximum displacement results of the PL and SR specimens, respectively. The numerical results obtained for the models with different thicknesses at quantitative shrinkage strains are well agreed with the experimental results, which indicates that all specimens almost reached peak curling within 72 hours.



(a) 1300 μ shrinkage model with PL specimen (b) 800 μ shrinkage model with SR specimens

Figure B-6 Displacement results on the axial path, comparison between the experimental and numerical response.

In this analysis, we did not give the overall distribution of drying shrinkage strain in the specimen as in reality. It just gave a shrinkage strain to some elements of the upper surface, but the experimental results can be reproduced by this analysis, which verified the model and supported the ability to characterize the curl using displacement measurements. In addition, when the same shrinkage strain is input, the experimental results are reproducible for specimens of different thicknesses. This indicates that the internal shrinkage gradients of the driving curling forces of the mortar are similar, which may be due to the severe drying conditions.

B.2 STUDY OF RESTRAINED SHRINKAGE BY NUMERICAL ANALYSES

B.2.1 FE Model

To understand the influence of curling on the mortar-concrete adhesion system, modeling the restrained condition to estimate the stress state at the adhesion interface when the concrete substrate restrained the curling of the mortar. The model consists of three components, concrete with dimensions

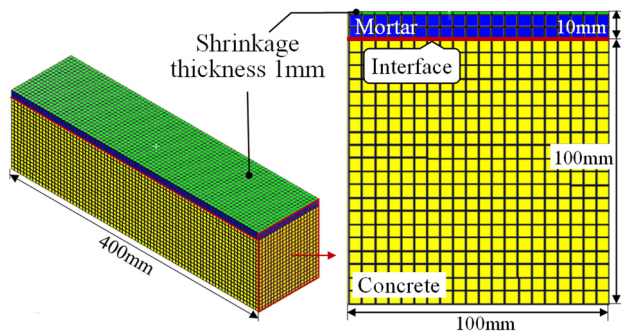


Figure B-7 Restrained shrinkage model.

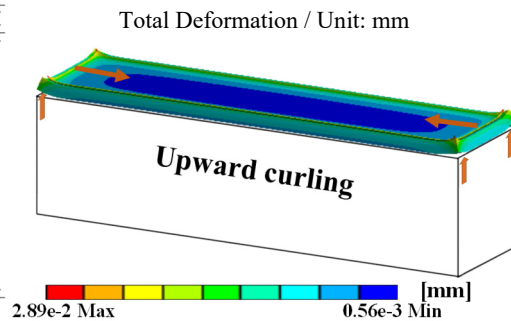


Figure B-8 Maximum deformation of mortar.

of 100 mm × 100 mm × 400 mm, mortar with dimensions of 10 mm × 100 mm × 400 mm, and the adhesion interface; the mesh adopted is shown in **Fig. B-7**. The cohesion zone model (CZM) based adhesion material was set on the adhesion interface elements. A detailed description is given in Chapter 3 and Appendix A of the dissertation. The interfacial stress state of the mortar subjected to thermal loading has been investigated using the same model.

B.2.2 Interfacial stress estimation under restraint conditions

Based on the numerical results of the free curling with the same thickness (10mm), the same method was used to apply the corresponding shrinkage strain to the restrained curling model. After applying a strain of 1300 μ to the shrinkage element, the deformation result of the mortar **Fig. B-8** and the equivalent stress distribution at the adhesive interface is shown in **Fig. B-9(a)**. The stresses are concentrated at the corners and free edges of the interface. Previous studies confirmed the correlation between stress generation and the adhesive strength reduction mechanism. We believe that the effect of this degree of stress generation on the mortar-concrete adhesion system is not negligible.

As previously mentioned, SRA has the effect of reducing the curling of the mortar. According to the numerical results of the SR-1 free curling model, a strain of 800 μ was applied to the shrinkage element of the model, and the equivalent stress distribution at the adhesive interface is shown in **Fig. 9(b)**. The interfacial stress decreases as the curling deformation decreases. Hereby, SRA is thought to be able to suppress the reduction in the mortar adhesion to the substrate due to curling deformation, which agrees with that reported by Chilwesa et al [82].

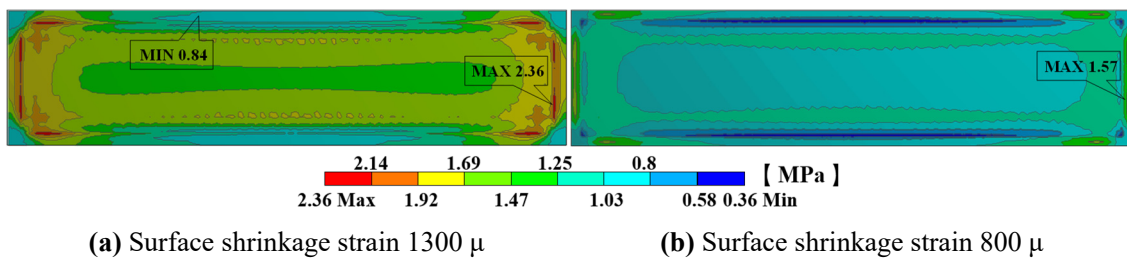


Figure B-9 Equivalent (Von-Mises) Stress (MPa) in the interface.

B.3 STUDY OF RESTRAINED SHRINKAGE BY DIC

Although the numerical simulation results have shown the potential of curling in reducing the adhesive strength of mortar to concrete, the correlation between the interlayer peeling phenomenon

and curling still needs to be supported by experimental data. To this end, we monitored the peeling of a mortar cast on a concrete substrate by Digital Image Correlation (DIC) technique, namely monitoring the relative displacement between the mortar and the substrate in the out-of-plane direction.

B.3.1 Experimental procedure

A 100×100×400 mm concrete block was used as the substrate for the specimen. Two common Japanese exterior wall finishes were investigated, mortar coating (M-1 specimen) and tile finish (T-1 specimen). All materials used in the experiments are described in the previous chapters. Materials for specimen M-1 are referenced in **Tables 3-2** and **3-2** (w/c of mortar is 0.5), and specimen T-1 was tiled on top of the rendering mortar of specimen M-1. The bonding mortar and tiles used were the same as those used in Section 5.1.

The concrete substrate was cured in water for over two months. Since the restrained curling tests were performed under the same conditions as those of free curling tests, in an incubator (40 °C and R.H. 3%), the concrete was sufficiently dried in the same environment for more than one week before plastering to reduce the effect on curling. A mortar layer of 400 mm² and 10 mm thickness was poured on these substrates. After plastering, the mortar was cured in a 20 °C and R.H. 60% environment with

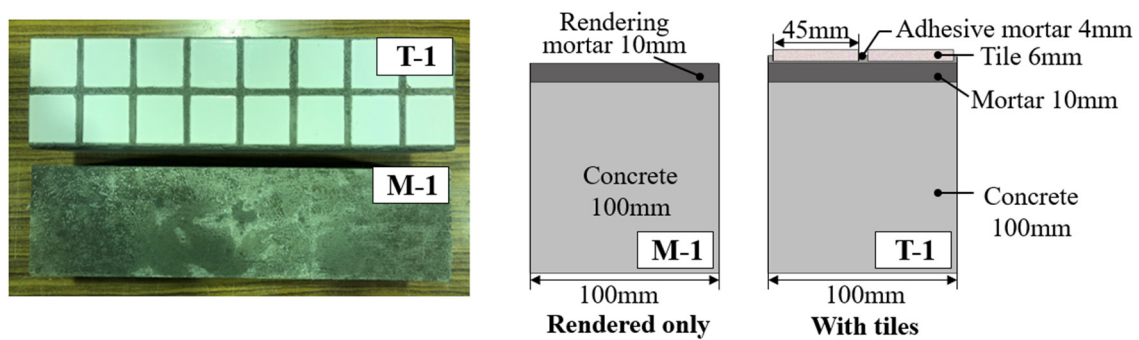


Figure B-10 DIC Specimen dimensions.

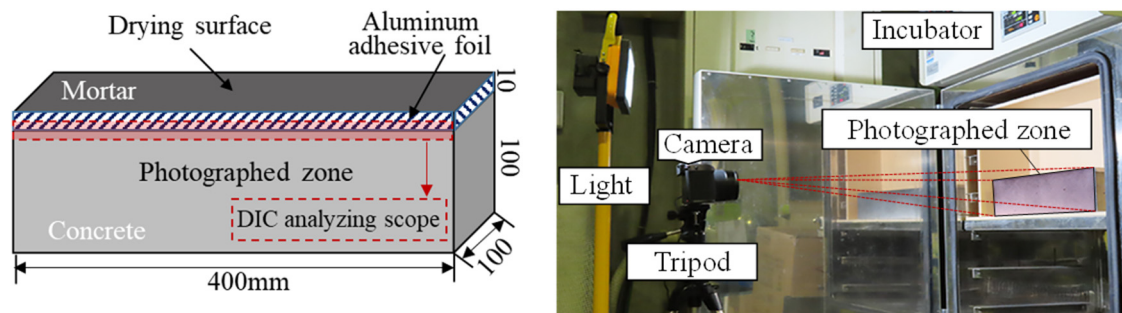


Figure B-11 Measurements of the displacement field at the interface between the mortar layer and the concrete in the vertical direction, DIC procedure.

a wet sheet covering the exposed surface for seven days. After seven days, the mold was removed, and the four sides of the mortar layer were insulated by adhesive aluminum tapes. The above is the preparation process of specimen M-1, on which the tiles (6×45×45 mm) are laid is T-1, as shown in Fig. B-10.

The DIC technique is based on the comparison of two images with two random gray levels recorded before and after a displacement. The first picture is called “reference” and the second “deformed” [81]. In order to ensure the accuracy and relevance of the results obtained by this method, these principles were followed when acquiring the images for post-processing:

- (1) Provide a suitable light source and ensure that the light source is consistent for each shot.
- (2) The relative position of the camera to the photographed object remains constant.
- (3) The parameters of the camera are the same for each shot.

The photographic procedure is shown in Fig. B-11. During the test, a LED light provides a stable light source. The camera is remotely controlled by a mobile device to ensure no change in the position

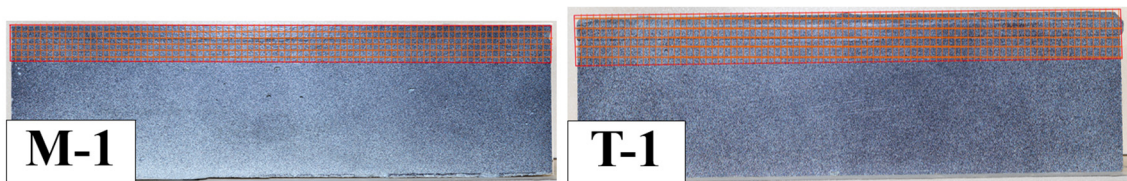


Figure B-12 AOI and subset size (40 × 40 pixels).

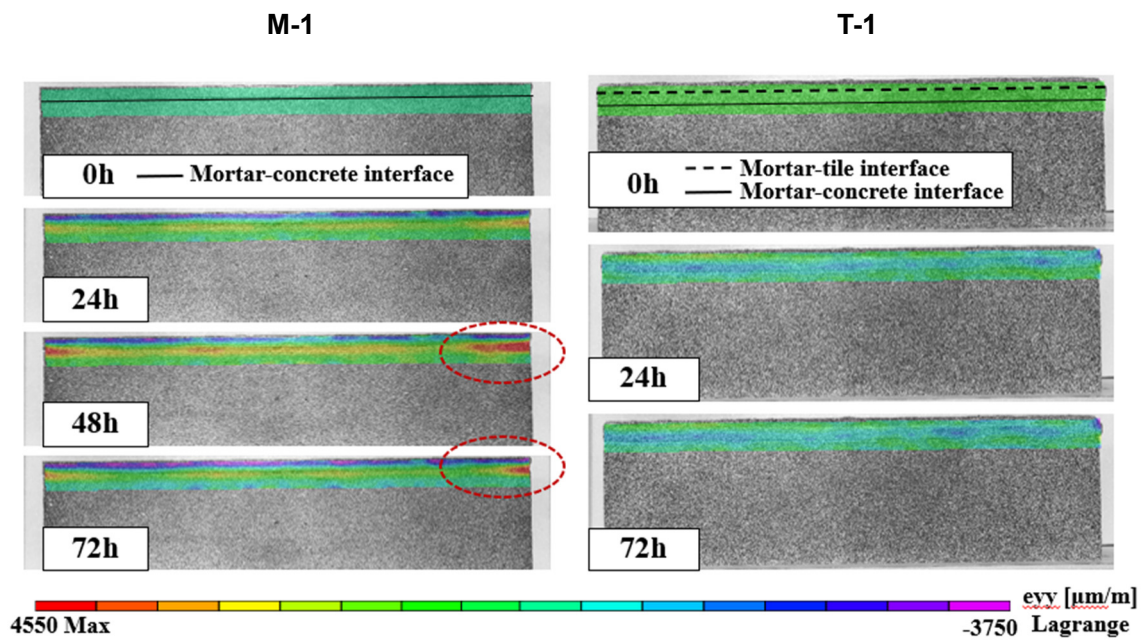


Figure B-13 Strain distributions [μ] (in the out-of-plane direction) exhibited by specimens M-1 and T-1 at each moment.

of the light source, the camera, and the specimen. In order to improve the efficiency of image post-processing, the photographed surface of the specimen was spray painted to obtain a random ink dot pattern. From the beginning of drying, images (8278×6208 pixels) of the plane were recorded every 24 hours for three days.

B.3.2 Post-processing result

In this study, DIC is carried out using Vic-2D v6, a software developed by Correlated Solutions, to measure displacement fields. In the post-processing software, the AOI (Area-of-Interest) and the size of the subset for the operation are selected. Each subset is the smallest feature image unit to estimate the deformation by matching the "deformed" image to the subset with the same characteristics in the "reference" image. The aim is to investigate the peeling behavior of the mortar-concrete adhesive interface, as shown in **Fig. B-12**, where the selected AOI contains the coating and the interface, and the subset size of 40×40 pixels is the result of several tests.

Fig. B-13 shows the strain distribution along the out-of-plane direction as calculated by the post-processing software. After 48 hours of drying, it can be observed that the M-1 specimen has a clear tendency to peel at the free edge of the adhesive interface between mortar and concrete. Compared to the M-1 specimen, no significant strain in the out-of-plane direction was observed in the AOI range of the T-1 specimen. The strain distribution at 72 hours of drying was almost identical to that at 24 hours. That is, virtually no interlaminar peeling occurred in the T-1 specimen. Based on the different material properties of ceramic and cementitious materials, the main object of evaporating moisture from T-1 specimens is the adhesive mortar layer through the tile joints and thin sides. Therefore, the strain may have occurred mainly in the in-plane direction.

B.4 EFFECT OF CURLING DEFORMATION ON THE PROPOSED DURABILITY ASSESSMENT METHOD

The studies in Chapters 3 and 4 clarified that curl deformation resulted in a loss of shear strength at the end of the specimens. Therefore, there is a need to clarify the effect of curl deformation on durability evaluation, that is, to determine the influence of ambient humidity on durability assessment. To compare the damage of mortar-concrete adhesion due to both drying shrinkage and thermal loading, the interface stress states due to these two factors were compared by numerical analysis, as shown in **Fig. B-14**. The curl deformation is the result of a shrinkage strain of 1300μ . The thermal loading

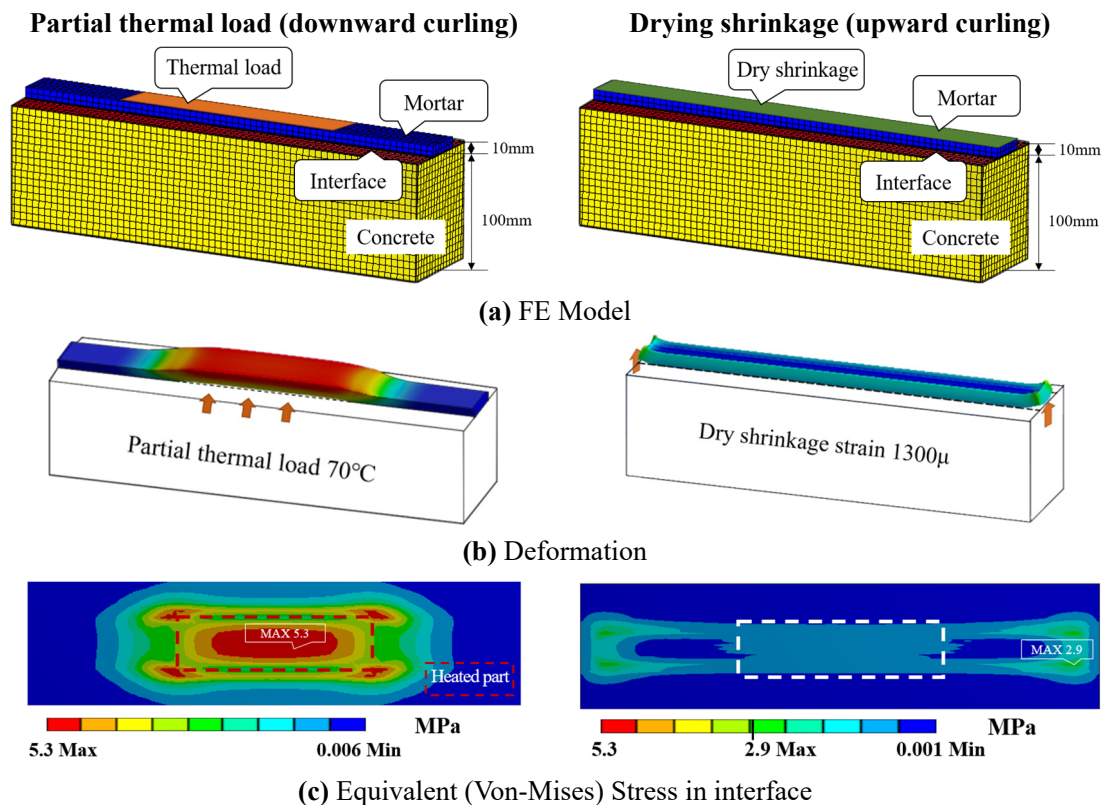


Figure B-14 Comparison of partial thermal loading and drying shrinkage effect on the stress state at the mortar/concrete interface.

conditions are the same as in Section 3.2.2 (partial thermal load at a peak temperature of 70 °C).

According to the stress results, there is almost no deformation in the middle of the mortar under the most severe drying conditions. In other words, even if the thermal load causes more severe drying shrinkage, it only reduces the bond strength at both ends and has little effect on the middle part. Because the proposed method for assessing durability is based on the loss of bond strength in the heated part (the part inside the dashed box), the adhesion loss at the end does not affect the results of the durability assessment. Although the results of the DIC experiment showed that the central part of the M-1 specimen also tended to deform in an out-of-plane direction, considering that this study was conducted under extremely severe drying conditions (40 °C, 3% RH), the durability assessment was conducted at 20 °C, 60% RH. It is considered that the actual influence of drying shrinkage in the durability assessment experiment is much less.

Conversely, the durability assessment method established for rendering mortars does not consider curl deformation as a degradation mechanism. This is because the rendered facades are minor affected by curling deformation. First, rendering mortars are generally applied in two or three passes, avoiding the formation of significant shrinkage differences in thickness. Secondly, the render layer is usually

covered with decorative coatings, such as paint and tile. In addition, there are cases where a spray-on SRA specific to the facade is applied. All of these measures have been proven to inhibit the development of curling.

B.5 SUMMARY

Rendering mortar curls due to the drying shrinkage gradient present in the thickness and the continuous monitoring of the displacement field by the DIC technique enables a clear observation of the mortar peeling due to curling, which can be considered as the mechanism of the adhesion between mortar and concrete decreases at the free edges.

The proposed numerical analysis method can simulate the curling and effectively understand the stress state generated at the interface. It is considered that curling deformation is a factor to affect the adhesive unity of mortar and concrete.

This study tried two methods to reduce the curling deformation, applying SRA and overlayer. Based on the displacement measurements and DIC monitoring results, both methods effectively suppress curling. The inhibition capacity has not been investigated in detail, but applying similar techniques that can keep the mortar uniformly dry in construction may be effective in preventing the decrease of bond strength at the free edges, and plan to develop them in the future.

This study contributes to understanding the behavior of mortar-concrete adhesion systems, thereby improving the durability of mortar coating in actual RC structures. However, this study was conducted under severe drying conditions, and further research is needed in this area if the effect of curl deformation on long-term adhesion is to be fully understood and appreciated. For example, establishing a milder experimental environment to understand curling behavior further and monitoring interfacial stresses while performing mechanical property tests.

In summary, the proposed durability assessment method does not need to consider the additional effect of drying shrinkage. The deformation of the specimen in either in-plane or out-of-plane direction is driven by the partial thermal load providing a much greater force than the drying shrinkage. Therefore, while materials with low shrinkage may show a higher durability rating, this result must be due to the resistance of the material to differential movement due to high temperatures and is a combination of all relevant properties of the material (i.e., shrinkage, modulus of elasticity, tensile strength, creep, and interfacial adhesion interactions, etc.). Therefore, the durability assessment

method proposed in this study can operate in a general humidity environment, and the possibility of errors in durability assessment results due to drying shrinkage is negligible.

REFERENCES

- [1] R. Doug Hooton, John A. Bickley. “Design for durability: The key to improving concrete sustainability” *Construction and Building Materials*, Vol. 67 Part C (2014): 422-430. <https://doi.org/10.1016/j.conbuildmat.2013.12.016>
- [2] Statista Cement production worldwide from 1995 to 2021 (Web) <https://www.statista.com/statistics/1087115/global-cement-production-volume>
- [3] World Cement Association Urges Climate Action (Web News) <https://unfccc.int/news/world-cement-association-urges-climate-action>
- [4] ISO, ISO 15686 Buildings and constructed assets – Service life planning, Part 1: General Principles (2000).
- [5] A. Sandak, J. Sandak, M. Brzezicki, A. Kutnar. “Service Life Performance”. *In: Bio-based Building Skin. Environmental Footprints and Eco-design of Products and Processes*: Springer, Singapore (2019). https://doi.org/10.1007/978-981-13-3747-5_5
- [6] A. Filiatrault, T. Sullivan. “Performance-based seismic design of nonstructural building components: The next frontier of earthquake engineering” *Earthquake Engineering and Engineering Vibration*, Vol. 13 (Suppl 1) (2014):17–46. <https://doi.org/10.1007/s11803-014-0238-9>
- [7] S. Yagi, A. Teramoto, T. Yeow, T. Seike, K. Kusunoki, I. Nakamura. “Validating Resilient Detailing of Japanese Ceilings, Windows, and Wall Tiles Using an E-defense Shake-table Test” *Journal of Earthquake Engineering*, Vol. 26(16) (2021): 8525-8551. <https://doi.org/10.1080/13632469.2021.1988764>
- [8] E. Martinelli, C. Faella. “An Overview of the Current Code Provisions on the Seismic Response of Acceleration-Sensitive Non-Structural Components in Buildings” *Applied Mechanics and Materials*, Vol. 847 (2016): 273-280. <https://doi.org/10.4028/www.scientific.net/AMM.847.273>
- [9] C. Lima, E. Martinelli, (2018). “Seismic response of acceleration-sensitive non-structural components in buildings,” *Buildings*, Vol. 9(1), 7. <https://doi.org/10.3390/buildings9010007>
- [10] Andrea Martinez, Mic Patterson, Anders Carlson, Douglas Noble. “Fundamentals in Façade Retrofit Practice” *Procedia Engineering*, Vol. 118 (2015): 934-941. <https://doi.org/10.1016/j.proeng.2015.08.534>
- [11] A. Silva, J. de Brito. “Service life of building envelopes: A critical literature review” *Journal of Building Engineering*, Vol. 44 102646 (2021). <https://doi.org/10.1016/j.jobe.2021.102646>
- [12] T. Mahaboonpachai, Y. Kuromiya, T. Matsumoto. “Experimental investigation of adhesion failure of the interface between concrete and polymer-cement mortar in an external wall tile structure under a thermal load” *Construction and Building Materials*, Vol. 22-9 (2008): 2001-2006. <https://doi.org/10.1016/j.conbuildmat.2007.07.002>
- [13] C. C. Y. Yiu, D. C. W. Ho, S. M. Lo. “Weathering effects on external wall tiling systems” *Construction and Building Materials*, Vol. 21 (2007): 594-600. <https://doi.org/10.1016/j.conbuildmat.2005.11.002>
- [14] A. Silva, J. de Brito, Pedro L. Gaspar. “A comparative multi-criteria decision analysis of service life prediction methodologies for rendered façades” *Journal of Building Engineering*, Vol. 20

- (2018): 476-487. <https://doi.org/10.1016/j.jobe.2018.08.009>
- [15] E. Bauer, A. L. R. Souza. “Failure patterns associated with facade zones and anomalies in the initiation and propagation of degradation” *Construction and Building Materials*, Vol. 347: 128563 (2022). <https://doi.org/10.1016/j.conbuildmat.2022.128563>
- [16] M. Łukasik, B. Michałowski, and J. Michalak. “Assessment of the Constancy of Performance of Cementitious Adhesives for Ceramic Tiles: Analysis of the Test Results Commissioned by Polish Market Surveillance Authorities” *Applied Sciences* Vol.10(18): 6561 (2020). <https://doi.org/10.3390/app10186561>
- [17] MECS / Acimac Research Centre. World production and consumption of ceramic tiles (2020). <https://www.ceramicworldweb.com/en/economics-and-markets/world-production-and-consumption-ceramic-tiles-2020>
- [18] J.D. Silvestre, J. de Brito. “Ceramic tiling in building façades: Inspection and pathological characterization using an expert system” *Construction and Building Materials*, Vol. 25-4 (2011): 1560-1571. <https://doi.org/10.1016/j.conbuildmat.2010.09.039>
- [19] Pedro L. Gaspar, J. de Brito. “Quantifying environmental effects on cement-rendered facades: A comparison between different degradation indicators” *Building and Environment*, Vol. 43-11 (2008): 1818-1828. <https://doi.org/10.1016/j.buildenv.2007.10.022>
- [20] M. Y. L. Chew, P. P. Tan. “Facade staining arising from design features” *Construction and Building Materials*, Vol. 17-3 (2003): 181-187. [https://doi.org/10.1016/S0950-0618\(02\)00102-2](https://doi.org/10.1016/S0950-0618(02)00102-2)
- [21] Inês Flores-Colen, J. de Brito. “A systematic approach for maintenance budgeting of buildings façades based on predictive and preventive strategies” *Construction and Building Materials*, Vol. 24-9 (2010): 1718-1729. <https://doi.org/10.1016/j.conbuildmat.2010.02.017>
- [22] J. S. Medeiros. “Why does facade ceramic tiling fail?” *VI Congreso mundial de la calidad del azulejo y del pavimento cerámico - Qualicer, Castellón: Spain* (2000):1-10.
- [23] O. J. Consoli, W. L. Repette, M. A. Cincotto. “Durability of the Facades from the Perspective of Architectural Decisions” *International Conference on Durability of Building Materials and Components, XII DBMC, Porto, PORTUGAL* (2011).
- [24] M. Y. L. Chew, N. Silva, P. P Tan, S. Das. “Grading of risk parameters for facade maintainability” *International Journal on Architecture Science*, Vol. 7-3 (2006): 77-87.
- [25] R. Folic. “Some aspects of designing concrete structures based on durability S. Grković1, R. Folić” *First scientific- applied conference with international participation reinforced concrete and masonry structures- theory and practice– Sofia* (2015).
- [26] H. Beushausen, R. Torrent, M. G. Alexander. “Performance-based approaches for concrete durability: State of the art and future research needs” *Cement and Concrete Research*, Vol. 119 (2019): 11-20. <https://doi.org/10.1016/j.cemconres.2019.01.003>
- [27] S. Brand. “How buildings learn—what happens after they’re built,” Orion Books, London, 1997. (BOOK)
- [28] M. F. S. Rodrigues, J. M. Teixeira, J. C. Cardoso. “Buildings envelope anomalies: A visual survey methodology” *Construction and Building Materials*, Vol. 25-5 , (2011): 2741–2750. <https://doi.org/10.1016/j.conbuildmat.2010.12.029>
- [29] J. Souza, A. Silva, J. de Brito, E. Bauer. “Analysis of the influencing factors of external wall ceramic claddings' service life using regression techniques” *Engineering Failure Analysis*, Vol.83

- (2018): 141–155. <https://doi.org/10.1016/j.engfailanal.2017.10.005>
- [30] A. Wetzel, R. Zurbriggen, M. Herwegh. “Spatially resolved evolution of adhesion properties of large porcelain tiles” *Cement and Concrete Composites*, Vol. 32-5 (2010): 327-338. <https://doi.org/10.1016/j.cemconcomp.2010.02.002>
- [31] R. Zurbriggen, M. Herwegh. “Daily and seasonal thermal stresses in tilings: a field survey combined with numeric modeling” *Materials and Structures*, Vol. 49 (2015): 1917-1933. <https://doi.org/10.1617/s11527-015-0623-5>
- [32] S. Ahmad, A. Elahi, S.A. Barbhuiya, Y. Farid. “Use of polymer modified mortar in controlling cracks in reinforced concrete beams,” *Construction and Building Materials*, Vol. 27-1 (2016): 91-96. <https://doi.org/10.1016/j.conbuildmat.2011.08.023>
- [33] P. Gaspar, J. de Brito. “Mapping defect sensitivity in external mortar renders” *Construction and Building Materials*, Vol. 19-8 (2005): 571–578. <https://doi.org/10.1016/j.conbuildmat.2005.01.014>
- [34] A. J. Kinloch. “Adhesion and adhesives: science and technology” *Chapman & Hall Eds.*, London and New York (1987): 441. (Book)
- [35] J. Y. Petit, B. Comelli, R. Perrin, E. Wirquin. “Effect of formulation parameters on adhesive properties of ANSI 118-15 and 118-11 compliant tile adhesive mortars” *International Journal of Adhesion and Adhesives*, Vol. 66 (2016): 73-80. <https://doi.org/10.1016/j.ijadhadh.2015.12.011>
- [36] C. M. Stolz, A. B. Masuero. “Analysis of main parameters affecting substrate/mortar contact area through tridimensional laser scanner” *Journal of Colloid and Interface Science*, Vol. 455 (2015): 6-23. <https://doi.org/10.1016/j.jcis.2015.05.028>
- [37] Zanelato, E.B., Alexandre, J., de Azevedo, A.R.G. et al. “Evaluation of roughcast on the adhesion mechanisms of mortars on ceramic substrates” *Materials and Structures* Vol. 52-53 (2019): <https://doi.org/10.1617/s11527-019-1353-x>
- [38] J. Salustio, S. M. Torres, A. C. Melo, ÂJCe Silva, A. C. Azevedo, J. C. Tavares, M. S. Leal, J. M. P. Q. Delgado. “Mortar Bond Strength: A Brief Literature Review, Tests for Analysis, New Research Needs and Initial Experiments” *Materials*. Vol. 15-6 (2022): 2332. <https://doi.org/10.3390/ma15062332>
- [39] E. Sakai, J. Sugita. “Composite mechanism of polymer modified cement” *Cement and Concrete Research*, Vol. 25-1 (1995): 127-135. [https://doi.org/10.1016/0008-8846\(94\)00120-N](https://doi.org/10.1016/0008-8846(94)00120-N)
- [40] A. A. P. Mansur, O. L. do Nascimento, H. S. Mansur. “Physico-chemical characterization of EVA-modified mortar and porcelain tiles interfaces” *Cement and Concrete Research*, Vol. 39-12 (2009): 1199-1208. <https://doi.org/10.1016/j.cemconres.2009.07.020>
- [41] H. Carasek, P. Japiassú, O. Cascudo, A. Velosa. “Bond between 19th Century lime mortars and glazed ceramic tiles” *Construction and Building Materials*, Vol. 59 (2014): 85-98. <https://doi.org/10.1016/j.conbuildmat.2014.02.043>
- [42] A. R. G. Azevedo, B. R. França, J. Alexandre, M. T. Marvila, E. B. Zanelato, G. C. Xavier. “Influence of sintering temperature of a ceramic substrate in mortar adhesion for civil construction” *Journal of Building Engineering*, Vol. 19 (2018): 342-348. <https://doi.org/10.1016/j.jobbe.2018.05.026>
- [43] A. Moropoulou, A. Bakolas, K. Bisbikou. “Physico-chemical adhesion and cohesion bonds in joint mortars imparting durability to the historic structures” *Construction and Building Materials*,

- Vol. 14-1 (2000): 35-46. [https://doi.org/10.1016/S0950-0618\(99\)00045-8](https://doi.org/10.1016/S0950-0618(99)00045-8)
- [44] I. N. Paes, E. Bauer, H. Carasek, E. Pavón. “Influence of water transportation inside a mortar/block system on bonding resistance behavior” *Revista Ingenieria de Construccion*, Vol. 29-2 (2014): 175–186.
- [45] A. Jenni, L. Holzer, R. Zurbruggen, M. Herwegh. “Influence of polymers on microstructure and adhesive strength of cementitious tile adhesive mortars” *Cement and Concrete Research*, Vol.35-1 (2005): 35–50. <https://doi.org/10.1016/j.cemconres.2004.06.039>
- [46] A. C. Melo, A. J. Costa e Silva, S. M. Torres, J. P. M. Q. Delgado, A. C. Azevedo. “Influence of the contact area in the adherence of mortar – Ceramic tiles interface” *Construction and Building Materials*, Vol. 243: 118274 (2020). <https://doi.org/10.1016/j.conbuildmat.2020.118274>
- [47] Z. Y. Zhao and W. L. Zhang. “Influence of workmanship on the bonding strength of tiles to external walls,” *International Journal of Adhesion and Adhesives*, Vol. 17-1 (1997): 47–53. [https://doi.org/10.1016/S0143-7496\(96\)00019-X](https://doi.org/10.1016/S0143-7496(96)00019-X)
- [48] J. A. Thamboo and M. Dhanasekar. “Characterisation of thin layer polymer cement mortared concrete masonry bond” *Construction and Building Materials*, Vol. 82 (2015): 71–80. <https://doi.org/10.1016/j.conbuildmat.2014.12.098>
- [49] M. Y. L. Chew. “Factors affecting ceramic tile adhesion for external cladding” *Construction and Building Materials*, Vol. 13-5 (1999): 293–296. [https://doi.org/10.1016/S0950-0618\(99\)00023-9](https://doi.org/10.1016/S0950-0618(99)00023-9)
- [50] D. P. Bentz, I. De la Varga, J. F. Muñoz, R. P. Spragg, B. A. Graybeal, D. S. Hussey, D. L. Jacobson, S. Z. Jones, J. M. LaManna. “Influence of substrate moisture state and roughness on interface microstructure and bond strength: Slant shear vs. pull-off testing” *Cement and Concrete Composites*, Vol. 87 (2018): 63-72. <https://doi.org/10.1016/j.cemconcomp.2017.12.005>
- [51] H. Beushausen. “The influence of concrete substrate preparation on overlay bond strength” *Magazine of Concrete Research*, Vol. 62-11 (2010): 845-852. <https://doi.org/10.1680/mac.2010.62.11.845>
- [52] J. Silfwerbrand, H. Beushausen “Bonded concrete overlays – bond strength issues” *Proceedings ICCRRR 2005 International Conference on Concrete Repair, Rehabilitation and Retrofitting*, (2005): 19–21.
- [53] A. Garbacz, M. Górka, L. Courard. “On the effect of concrete surface treatment on adhesion in repair systems” *Magazine of Concrete Research*, Vol. 57-1 (2005): 49-60. <https://doi.org/10.1680/mac.2005.57.1.49>
- [54] L. Courard, T. Piotrowski, A. Garbacz. “Near-to-surface properties affecting bond strength in concrete repair” *Cement and Concrete Composites*, Vol. 46 (2014): 73–80. <https://doi.org/10.1016/j.cemconcomp.2013.11.005>
- [55] E. N. B. S Júlio, F. A. B Branco, V. D. Silva. “Concrete-to-concrete bond strength. Influence of the roughness of the substrate surface” *Construction and Building Materials*, Vol. 18-9 (2004): 675–681. <https://doi.org/10.1016/j.conbuildmat.2004.04.023>
- [56] M. A. Yazdi, E. Dejager, M. Debraekeleer, E. Gruyaert, K. V. Tittelboom, N. De Belie. “Bond strength between concrete and repair mortar and its relation with concrete removal techniques and substrate composition” *Construction and Building Materials*, Vol. 230:116900 (2020). <https://doi.org/10.1016/j.conbuildmat.2019.116900>
- [57] J. Silfwerbrand. “Stresses and Strains in Composite Concrete Beams Subjected to Differential

- Shrinkage” *ACI Structural Journal*, Vol. 94-4 (1997): 347–353. DOI: 10.14359/485
- [58] N. J. Delatte, M. S. Williamson, D. W. Fowler. “Bond Strength Development with Maturity of High-Early-Strength Bonded Concrete Overlays” *ACI Materials Journal*, Vol. 97-2 (2000): 201–207. <https://doi.org/10.14359/824>
- [59] A. Wetzel, R. Zurbriggen, M. Herwegh, A. Greminger, J. Kaufmann. “Long-term study on failure mechanisms of exterior applied tilings” *Construction and Building Materials*, Vol. 37 (2012): 335-348. <https://doi.org/10.1016/j.conbuildmat.2012.07.072>
- [60] J. L. Granju. “Thin bonded overlays: About the role of fiber reinforcement on the limitation of their debonding,” *Advanced Cement Based Materials*, Vol. 4-1 (1996): 21-27. [https://doi.org/10.1016/S1065-7355\(96\)90059-0](https://doi.org/10.1016/S1065-7355(96)90059-0)
- [61] Q. T. Tran, A. Toumi, A. Turatsinze. “Modelling of debonding between old concrete and overlay: fatigue loading and delayed effects” *Materials and Structures*, Vol. 40 (2007): 1045–1059. <https://doi.org/10.1617/s11527-006-9204-y>
- [62] A. Al-Ostaz, M. Irshidat, B. Tenkhoff, P. S. Ponnappalli. “Deterioration of Bond Integrity between Repair Material and Concrete due to Thermal and Mechanical Incompatibilities” *Journal of Materials in Civil Engineering*, Vol. 22-2 (2010): 136–144. [https://doi.org/10.1061/\(ASCE\)0899-1561\(2010\)22:2\(136\)](https://doi.org/10.1061/(ASCE)0899-1561(2010)22:2(136))
- [63] Ariel D. Espeche, Javier León. “Estimation of bond strength envelopes for old-to-new concrete interfaces based on a cylinder splitting test” *Construction and Building Materials*, Vol.25-3 (2011): 1222-1235. <https://doi.org/10.1016/j.conbuildmat.2010.09.032>
- [64] B. Szemerey-Kiss, Á. Török. “Failure mechanisms of repair mortar stone interface assessed by pull-off strength tests” *Bulletin of Engineering Geology and the Environment*, Vol. 76 (2017): 159-167. <https://doi.org/10.1007/s10064-016-0964-5>
- [65] H. Beushausen, M. Alexander. “Bond strength development between concretes of different ages” *Magazine of Concrete Research*, Vol. 60-1 (2008): 65–74. <https://doi.org/10.1680/mac.2007.00108>
- [66] J. Silfwerbrand. “Shear bond strength in repaired concrete structures” *Materials and Structures*, Vol. 36 (2003): 419–424. <https://doi.org/10.1007/BF02481068>
- [67] M. Pigeon, F. Saucier. “Durability of repaired concrete structures” *Proceedings of an International Symposium on Advances in Concrete Technology* (1992): 741–773.
- [68] H. Xie, G. Li, G. Xiong. “Microstructure model of the interfacial zone between fresh and old concrete,” *J. Wuhan University of Technology*, Vol. 17-4 (2002): 64-68. <https://doi.org/10.1007/BF02838421>
- [69] Y. He, X. Zhang, R. D. Hooton, X. Zhang. “Effects of interface roughness and interface adhesion on new-to-old concrete bonding” *Construction and Building Materials*, Vol. 151 (2017): 582-590. <https://doi.org/10.1016/j.conbuildmat.2017.05.049>
- [70] H. Beushausen, B. Höhlig, M. Talotti “The influence of substrate moisture preparation on bond strength of concrete overlays and the microstructure of the OTZ” *Cement and Concrete Research*, Vol. 92 (2017): 84-91. <https://doi.org/10.1016/j.cemconres.2016.11.017>
- [71] C. Pereira, J. de Brito, J. D. Silvestre. “Contribution of humidity to the degradation of façade claddings in current buildings” *Engineering Failure Analysis*, Vol. 90 (2018): 103-115. <https://doi.org/10.1016/j.engfailanal.2018.03.028>

- [72] F. L. Maranhão, K. Loh, V. M. John. “The influence of moisture on the deformability of cement–polymer adhesive mortar” *Construction and Building Materials*, Vol. 25-6 (2011): 2948-2954. <https://doi.org/10.1016/j.conbuildmat.2010.12.004>
- [73] T. Kumagai, M. Nakamura and K. Irino. “Study on Temperature Distribution and Repetitive Thermal Stress at Interface between Tile and Bedding Mortar of Ceramic Tile Finished External Wall by Solar Radiation” *Shimizu kensetsu kenkyuu houkoku*, Vol. 60 (1994). (In Japanese)
- [74] K. Rashid, T. Ueda, D. Zhang, K. Miyaguchi, H. Nakai. “Experimental and analytical investigations on the behavior of interface between concrete and polymer cement mortar under hygrothermal conditions” *Construction and Building Materials*, Vol. 94 (2015): 414-425. <https://doi.org/10.1016/j.conbuildmat.2015.07.035>
- [75] A. J. Lewry, L. F. E. Crewdson. “Approaches to testing the durability of materials used in the construction and maintenance of buildings” *Construction and Building Materials*, Vol. 8-4 (1994): 211-222. [https://doi.org/10.1016/S0950-0618\(09\)90004-6](https://doi.org/10.1016/S0950-0618(09)90004-6)
- [76] L. A. Escobar and W. Q. Meeker. “A Review of Accelerated Test Models” *Statistical Science*, Vol. 21-4 (2007): 552–577. <https://doi.org/10.1214/088342306000000321>
- [77] K. Eguchi, K. Teranishi. “Prediction equation of drying shrinkage of concrete based on composite model” *Cement and Concrete Research*, Vol. 35-3 (2005): 483-493. <https://doi.org/10.1016/j.cemconres.2004.08.002>
- [78] B. Bissonnette, P. Pierre, M. Pigeon. “Influence of key parameters on drying shrinkage of cementitious materials” *Cement and Concrete Research*, Vol. 29-10 (1999): 1655-1662. [https://doi.org/10.1016/S0008-8846\(99\)00156-8](https://doi.org/10.1016/S0008-8846(99)00156-8)
- [79] S. Shadravan, C. Ramseyer, T. H. K. Kang. “A long term restrained shrinkage study of concrete slabs on ground” *Engineering Structures*, Vol. 102 (2015): 258-265. <https://doi.org/10.1016/j.engstruct.2015.08.018>
- [80] F. Saucier, M. Pigeon. “Durability of new-to-old concrete bondings” *Proceedings of the ACI International Conference on Evaluation and Rehabilitation of Concrete Structures and Innovations in Design*, Hong-Kong, Vol.128 (1991): 689–706. <https://doi.org/10.14359/2066>
- [81] T. Mauroux, F. Benboudjema, P. Turcry, A. Aït-Mokhtar, O. Deves “Study of cracking due to drying in coating mortars by digital image correlation” *Cement and Concrete Research*, Vol. 42-7 (2012): 1014-1023. <https://doi.org/10.1016/j.cemconres.2012.04.002>
- [82] M. Chilwesa, L. Facconi, F. Minelli, A. Reggia, G. Plizzari. “Shrinkage induced edge curling and debonding in slab elements reinforced with bonded overlays: Influence of fibers and SRA” *Cement and Concrete Composites*, Vol. 102 (2019): 105-115. <https://doi.org/10.1016/j.cemconcomp.2019.04.017>
- [83] H. C. F. Curci, R. P. de Andrade, F. L. Maranhão, H. C. Gomes, E. M.B. Campello. “Analysis of adhered tiling systems based on experimental evaluation and numerical modeling” *Construction and Building Materials*, Vol.325: 126746 (2022). <https://doi.org/10.1016/j.conbuildmat.2022.126746>
- [84] J. Maia, N. M. M. Ramos, R. Veiga. “A new durability assessment methodology of thermal mortars applied in multilayer rendering systems” *Construction and Building Materials*, Vol. 222 (2019): 654-663. <https://doi.org/10.1016/j.conbuildmat.2019.06.178>
- [85] V. P. de Freitas, H. Corvacho, M. Quintela, J. M. P. Q. Delgado. “Assessing the durability of

- mortars tiles – A contribution for a prediction model” *Engineering Failure Analysis*, Vol. 44, (2014): 36-45. <https://doi.org/10.1016/j.engfailanal.2014.04.027>
- [86] M-101, (2015). “Japan Society for Finishings Technology Specification, M-101:2015, Water absorption modifier for cement mortar coating” *Tokyo: Japan Society for Finishings Technology*. (In Japanese).
- [87] I. M. Shohet, M. Puterman, E. Gilboa. “Deterioration patterns of building cladding components for maintenance management” *Construction Management and Economics*, Vol. 20 (2002): 305-314. <https://doi.org/10.1080/01446190210125563>
- [88] R. Bordalo, J. de Brito, P. L. Gaspar, A. Silva. “Service life prediction modelling of adhesive ceramic tiling systems” *Building Research & Information*, Vol. 39-1 (2011): 66-78. <https://doi.org/10.1080/09613218.2010.532197>
- [89] S. Feldfogel, O. Rabinovitch. “Two dimensional debonding failure in adhesively bonded tiles” *International Journal of Solids and Structures*, Vol. 148–149 (2018): 94-109 <https://doi.org/10.1016/j.ijsolstr.2017.12.031>
- [90] S. Feldfogel, O. Rabinovitch. “Evolution and stability of tile detachment – Experiments and modeling” *International Journal of Solids and Structures*, Vol. 210–211 (2021): 145-161. <https://doi.org/10.1016/j.ijsolstr.2020.11.001>
- [91] J. Y. Cao, D. D. L. Chung. “Degradation of the bond between old and new mortar under cyclic shear loading, monitored by contact electrical resistance measurement” *Cement and Concrete Research*, Vol. 31-11 (2001): 1647-1651. [https://doi.org/10.1016/S0008-8846\(01\)00607-X](https://doi.org/10.1016/S0008-8846(01)00607-X)
- [92] N. M. M. Ramos, M. L. Simões, J. M. Delgado and V. P. de Freitas. “Reliability of the pull-off test for in situ evaluation of adhesion strength” *Construction and Building Materials*, Vol. 31 (2012): 86–93. <https://doi.org/10.1016/j.conbuildmat.2011.12.097>
- [93] B. L. Luk, K. P. Liu, Z. D. Jiang, F. Tong. “Robotic impact-acoustics system for tile-wall bonding integrity inspection” *Mechatronics*, Vol. 19-8 (2009): 1251–1260. <https://doi.org/10.1016/J.MECHATRONICS.2009.07.006>
- [94] B. Li, K. Ushiroda, L. Yang, Q. Song, J. Xiao. “Wall-climbing robot for non-destructive evaluation using impact-echo and metric learning SVM” *International Journal of Intelligent Robotics and Applications*, Vol. 3 (2017): 255–270. <https://doi.org/10.1007/s41315-017-0028-4>
- [95] D. Schmidt, K. Berns. “Climbing robots for maintenance and inspections of vertical structures - A survey of design aspects and technologies” *Robotics and Autonomous Systems*, Vol. 61-12) (2013): 1288–1305. <https://doi.org/10.1016/j.robot.2013.09.002>
- [96] A. Hajeer, L. Chen, E. Hu. “Review of Classification for Wall Climbing Robots for Industrial Inspection Applications” *2020 IEEE 16th International Conference on Automation Science and Engineering (CASE)* (2020): 1421-1426. <https://doi.org/10.1109/CASE48305.2020.9216878>
- [97] B. L. Luk, K. P. Liu, F. Tong, and K. F. Man. “Impact-acoustics inspection of tile-wall bonding integrity via wavelet transform and hidden Markov models” *Journal of Sound and Vibration*, Vol. 329-10 (2010): 1954–1967. <https://doi.org/10.1016/j.jsv.2009.11.038>
- [98] F. Tong, S. K. Tso, M. Y. Y. Hung. “Impact-acoustics-based health monitoring of tile-wall bonding integrity using principal component analysis” *Journal of Sound and Vibration*, Vol. 294: 1–2 (2006): 329–340. <https://doi.org/10.1016/j.jsv.2005.11.017>
- [99] F. Tong, S. K. Tso, X. M. Xu. “Tile-wall bonding integrity inspection based on time-domain

- features of impact acoustics,” *Sensors and Actuators, A: Physical*, Vol. 132-2 (2006): 557–566. <https://doi.org/10.1016/j.sna.2005.12.035>
- [100] F. Tong, X. M. XU, B. L. Luk, K. P. Liu. “Evaluation of tile–wall bonding integrity based on impact acoustics and support vector machine” *Sensors and Actuators A: Physical*, Vol. 144-1 (2008): 97–104. <https://doi.org/10.1016/J.SNA.2008.01.020>
- [101] B. L. Luk, K. P. Liu, F. Tong. “Rapid evaluation of tile-wall bonding integrity using multiple-head impact acoustic method” *NDT & E International*, Vol. 44-3 (2011): 297–304. <https://doi.org/10.1016/J.NDTEINT.2011.01.004>
- [102] S. X. Liu, F. Tong, B. L. Luk, K. P. Liu. “Fuzzy pattern recognition of impact acoustic signals for nondestructive evaluation” *Sensors and Actuators A: Physical*, Vol. 167-2 (2011): 588–593. <https://doi.org/10.1016/J.SNA.2011.03.015>
- [103] T. Sugimoto, K. Sugimoto, I. Uechi, N. Utagawa, C. Kuroda. “Noncontact acoustic inspection of outer wall by acoustic irradiation induced vibration from UAV equipped with sound source” *Proceedings of Meetings on Acoustics*, Vol. 38: 065005 (2019). <https://doi.org/10.1121/2.0001078>
- [104] Y. Nakagawa, T. Sugimoto, K. Sugimoto, I. Uechi. “Research on improvement of defect detection accuracy by resonance judgment for noncontact acoustic inspection method by acoustic irradiation-induced vibration” *Japanese Journal of Applied Physics* 61:SG, SG1035 (2022). <https://doi.org/10.35848/1347-4065/ac51bd>
- [105] T. Lourenço, L. Matias, P. Faria. “Anomaly Diagnosis in Ceramic Claddings by Thermography—A Review,” *In Proceedings of the 7th International Conference on Safety and Durability of Structures (ICOSADOS 2016)*, Vila Real, Portugal (2016): 10–12, 1–8.
- [106] R. M. D. Andrade, E. Esposito, N. Paone, G. M. Revel. “Nondestructive techniques for detection of delamination in ceramic tile: a laboratory comparison between IR thermal cameras and laser Doppler vibrometers” *Proc. SPIE 3585, Nondestructive Evaluation of Aging Materials and Composites III*, (1999). <https://doi.org/10.1117/12.339868>
- [107] C. Meola, R. Di Maio, N. Roberti, G. M. Carlomagno. “Application of infrared thermography and geophysical methods for defect detection in architectural structures” *Engineering Failure Analysis*, Vol. 12-6 (2005): 875–892. <https://doi.org/10.1016/j.engfailanal.2004.12.030>
- [108] A. Kylili, P. A. Fokaides, P. Christou, S. A. Kalogirou. “Infrared thermography (IRT) applications for building diagnostics: A review” *Applied Energy*, Vol. 134 (2014): 531–549. <https://doi.org/10.1016/j.apenergy.2014.08.005>
- [109] T. Komiyama, Y. Tanigawa. “Characteristics of thermal imager and spectral absolute reflectance of finishing materials influencing on reliability of thermographic survey” *Concrete Research and Technology*, Vol. 7-1 (1997): 109-120. (In Japanese) https://doi.org/10.3151/crt1990.8.1_109
- [110] D. S. P. Rao. “Infrared thermography and its applications in civil engineering” *The Indian Concrete Journal*, Vol. 82-5 (2008): 41–50.
- [111] T. Komiyama, Y. Nakano, Y. Tanigawa. “Experimental study on limitation of thermographic survey applied to detection of delamination of finishing materials on external wall” *Journal of Structural and Construction Engineering (Transactions of AIJ)*, Vol. 61-484 (1996): 13-20. (In Japanese) https://doi.org/10.3130/aijs.61.13_2

- [112] T. Nishikawa, A. Hirano, E. Kamada. “Experimental study on the improvement of precision in the thermography method by the subtraction processing” *Journal of Structural and Construction Engineering (Transactions of AIJ)*, Vol. 65-528 (2000) 27-32. (In Japanese)
https://doi.org/10.3130/aijs.65.27_2
- [113] T. Nishikawa. “Experimental study on thermography method for external wall removal using middle wave infrared rays” *Journal of Structural and Construction Engineering (Transactions of AIJ)*, Vol. 69-575 (2004): 31-36. (In Japanese)
https://doi.org/10.3130/aijs.69.31_1
- [114] T. Y. Cheng, T. Sakagami, S. Kubo, D. Sato. “Reduction of reflection noise in delamination detection of external building tiles by infrared thermography” *J. JSNDI*, Vol. 61-5 (2012): 235-238. (In Japanese) <https://doi.org/10.11396/jjsndi.61.235>
- [115] S. Fujimori, Y. Kurokawa, Y. Tanigawa. “Study on improvement method for infrared thermography considering surface color values” *Journal of Structural and Construction Engineering (Transactions of AIJ)*, Vol. 71-600 (2006): 23-28. (In Japanese)
https://doi.org/10.3130/aijs.71.23_2
- [116] D. Sato, T. Sakagami, T. Komiyama, S. Kubo. “Development of passive lock-in thermography technique for improvement of accuracy of internal defect” *Proceedings of Japan Concrete Institute*, Vol. 29-2 (2007): 667-672. (In Japanese)
- [117] E. Edis, I. Flores-Colen, J. de Brito. “Time-dependent passive infrared thermographic inspection of facades,” *Proceedings of 13th International Conference on Durability of Building Materials and Components*, São Paulo, Brazil (2014): 853-860.
<https://doi.org/10.13140/RG.2.1.3630.6964>
- [118] R. Marani, D. Palumbo, U. Galietti, E. Stella, T. D’Orazio. “Enhancing defects characterization in pulsed thermography by noise reduction” *NDT and E International*, Vol. 102 (2019): 226–233.
<https://doi.org/10.1016/j.ndteint.2018.12.009>
- [119] N. H. Pan, C. H. Tsai, K. Y. Chen, and J. Sung. “Enhancement of external wall decoration material for the building in safety inspection method” *Journal of Civil Engineering and Management*, Vol. 26-3 (2020): 216-226. <https://doi.org/10.3846/jcem.2020.11925>
- [120] T. Murai, M. Kakizaki, K. Ogasawara. “Study of installation on super workable concrete – Experimental study on adhesion of cement mortar to deforming concrete substrate” *AIJ Journal of Technology and Design*, Vol. 8 (1999): 29-34. (In Japanese)
https://doi.org/10.3130/aijt.5.29_1
- [121] K. Tanigaki, K. Saigusa. “Study on deformation follow properties of dry-wet cycled tile under layer mortar” *AIJ Journal of Technology and Design*, Vol. 15 (2002): 19-22. (In Japanese)
<https://doi.org/10.3130/aijt.8.19>
- [122] H. Nachi, T. Ono. “The effect of tile elements on deformational performance of tile facing at external walls,” *Journal of Structural and Construction Engineering (Transactions of AIJ)*, Vol. 563 (2003): 15-22. (In Japanese) https://doi.org/10.3130/aijs.68.15_1
- [123] T. Okihashi, M. Kono, Y. Masuda. “Movement of tile finish wall, in outdoor exposure test and heating cooling repeat test” *Journal of Structural and Construction Engineering (Transactions of AIJ)*, Vol. 76-661 (2011): 465-470. (In Japanese) <https://doi.org/10.3130/aijs.76.465>
- [124] T. Okihashi, Y. Masuda, M. Kono. “Study on estimation of exfoliation for the existing tile finish”

- Journal of Structural and Construction Engineering (Transactions of AIJ)*, Vol. 77-681 (2012): 1623-1628. (In Japanese) <https://doi.org/10.3130/aijs.77.1623>
- [125] C. Y. Chang, Y. C. Yi, S. S. Hung, Y. S. Lee, Y. C. Chang. “Applying strain-sensing technology for monitoring and diagnosing peel-based deterioration of tiled exterior walls” *International Journal of Civil, Structural, Environmental and Infrastructure Engineering Research and Development*, Vol. 7 (2017): 39–48. <https://doi.org/10.24247/ijcseierdaug20176>
- [126] C. Y. Chang, S. S. Hung, L. H. Liu, and C. P. Lin. “Innovative strain sensing for detection of exterior wall tile lesion: smart skin sensory system” *Materials*, Vol. 11(12):2432 (2018). <https://doi.org/10.3390/ma11122432>
- [127] S. Ohgishi, H. Ono, T. Oooka. “Study of the performance of the three methods infrared image, impact vibration response, percussion inspection in the detection of internal defects in reinforced concrete and the delamination of plastered mortar and tiles” *Concrete Engineering*, Vol. 27-8 (1989): 103-114. (In Japanese) https://doi.org/10.3151/coj1975.27.8_103
- [128] A. Iwase. “Vibration characteristics of tile in peeling off and a new touching diagnostic method” *Journal of Architecture and Planning (Transactions of AIJ)*, Vol. 59-455 (1994): 1-7. (In Japanese) https://doi.org/10.3130/aija.59.1_1
- [129] A. Takano, Y. Ohta, F. Inoue, R. Morato. “Research on quantitative detection of outer tile exfoliation by Wavelet analyse” *Journal of the Visualization Society of Japan*, Vol. 26-2 (2006): 189-192. (In Japanese) https://doi.org/10.3154/jvs.26.Supplement2_189
- [130] T. Soeta, T. Mikami. “Basic study into a diagnostic system for exterior tile debonding” *Journal of Structural and Construction Engineering (Transactions of AIJ)*, Vol. 81-729 (2016): 1779-1787. (In Japanese) <https://doi.org/10.3130/aijs.81.1779>
- [131] E. Tsangouri, D. G. Aggelis. “A review of acoustic emission as indicator of reinforcement effectiveness in concrete and cementitious composites” *Construction and Building Materials*, Vol. 224 (2019): 198-205. <https://doi.org/10.1016/j.conbuildmat.2019.07.042>
- [132] A. Grazzini, G. Lacidogna, S. Valente, F. Accornero. “Delamination of plasters applied to historical masonry walls: analysis by acoustic emission technique and numerical model” *IOP Conference Series: Materials Science and Engineering* Vol. 372:012022 (2018). <https://doi.org/10.1088/1757-899X/372/1/012022>
- [133] K. S. Tan, K. C. Chan, B. S. Wong, L. W. Guan. “Ultrasonic evaluation of cement adhesion in wall tiles” *Cement and Concrete Composites*, Vol. 18-2 (1996): 119-124. [https://doi.org/10.1016/0958-9465\(95\)00008-9](https://doi.org/10.1016/0958-9465(95)00008-9)
- [134] C. Meola, R. di Maio, N. Roberti, G. M. Carlomagno. “Application of infrared thermography and geophysical methods for defect detection in architectural structures” *Engineering Failure Analysis*, Vol. 12-6 (2005): 875-892. <https://doi.org/10.1016/J.ENGFAILANAL.2004.12.030>
- [135] M. Zielińska, M. Rucka. “Non-destructive assessment of masonry pillars using ultrasonic tomography” *Materials*, Vol. 11-12 (2018). <https://doi.org/10.3390/ma11122543>
- [136] Y. Fang, L. Lin, H. Feng, Z. Lu, G. W. Emms. “Review of the use of air-coupled ultrasonic technologies for nondestructive testing of wood and wood products” *Computers and Electronics in Agriculture*, Vol. 137 (2017): 79–87. <https://doi.org/10.1016/j.compag.2017.03.015>
- [137] S. Osaki, A. Mase, Y. Hirata, M. Iwakura. “Imaging Diagnostics of Inside of a Building Wall Using Millimeter-Wave Reflectometer” *Applied Sciences (Switzerland)*, Vol. 12-6 (2022).

- <https://doi.org/10.3390/app12062879>
- [138] Y. J. Hoon, S. Hong. “Three-dimensional digital documentation of cultural heritage site based on the convergence of terrestrial laser scanning and unmanned aerial vehicle photogrammetry” *ISPRS International Journal of Geo-Information*, Vol. 8-2 (2019).
<https://doi.org/10.3390/ijgi8020053>
- [139] S. Barba, M. Barbarella, A. di Benedetto, M. Fiani, L. Gujski, M. Limongiello. “Accuracy assessment of 3d photogrammetric models from an unmanned aerial vehicle” *Drones*, Vol. 3-4 (2019): 1–19. <https://doi.org/10.3390/drones3040079>
- [140] T. Bilis, T. Kouimtoglou, M. Magnisali, P. Tokmakidis. “The use of 3D scanning and photogrammetry techniques in the case study of the roman theatre of Nikopolis. Surveying, virtual reconstruction and restoration study” *International Archives of the Photogrammetry, Remote Sensing and Spatial Information Sciences - ISPRS Archives*, Vol. 42-2W3 (2017): 97–103. <https://doi.org/10.5194/isprs-archives-XLII-2-W3-97-2017>
- [141] R. Rumbayan, T. Mahaboonpachai, T. Matsumoto. “Thermographic measurement and thermal stress analysis at the interface of external wall tile structure” *Journal of applied mechanics*, Vol. 9 (2006): 1069-1076. <https://doi.org/10.2208/journalam.9.1069>
- [142] ANSYS Mechanical APDL Theory Reference. 13.174. CONTA174 - 3-D 8-Node Surface-to-Surface Contact.
- [143] ANSYS Mechanical APDL Theory Reference. 4.12. Cohesive Zone Material (CZM) Model.
- [144] JSCE, (2017). “Standard Specifications for Concrete Structures 2017 DESIGN” Tokyo: Japan Society of Civil Engineers.
- [145] JASS15, (2019). “Japanese Architectural Standard Specification—JASS15 Plastering Work” Tokyo: Architectural Institute of Japan. (In Japanese)
- [146] P. M. D. Santos, E. N. B. S. Júlio. “A state-of-the-art review on roughness quantification methods for concrete surfaces” *Construction and Building Materials*, Vol. 38 (2013): 912-923. <https://doi.org/10.1016/j.conbuildmat.2012.09.045>
- [147] ICRI (International Concrete Repair Institute) 1997. “Selecting and specifying concrete surface preparation for sealers, coatings, and polymer overlays.” Technical Guideline No. 03732, Des Plaines, IL.
- [148] M. Luković, G. Ye. “Effect of Moisture Exchange on Interface Formation in the Repair System Studied by X-ray Absorption” *Materials*, Vol. 9-2 (2016). <https://doi.org/10.3390/ma9010002>
- [149] J. F. Georgan, J. Ambroise, J. Péra and J. M. Reynouard. “Development of self-leveling screed based on calcium sulfoaluminate cement: Modelling of curling due to drying” *Cement and Concrete Composites*, Vol.30-9 (2008): 769–778.
<https://doi.org/10.1016/j.cemconcomp.2008.06.004>
- [150] P. Y. Zhang. “Research on Assessment Methodology and Influencing Factors of Durability for Plastering Mortar” *Master's Thesis*, Advanced Science and Engineering, Hiroshima University, Japan (2020).
- [151] T. Goto, T. Sato, K. Sakai. “Cement shrinkage reducing agent and cement composition” US Patent 4547223, United States Patent and Trademark Office (1985).
- [152] C. Nmai, R. Tomita, F. Hondo, J. Buffenbarger. “Shrinkage-reducing admixtures” *Concrete International*, Vol. 20-4 (1998): 31-37.

- [153] J. Mora-Ruacho, R. Gettu, A. Aguado. “Influence of shrinkage-reducing admixtures on the reduction of plastic shrinkage cracking in concrete” *Cement and Concrete Research*, Vol. 39-3 (2009): 141-146. <https://doi.org/10.1016/j.cemconres.2008.11.011>
- [154] U. M. N. Jayawickrema, H. M. C. M. Herath, N. K. Hettiarachchi, H. P., Sooriyaarachchi, J. A. Epaarachchi. “Fibre-optic sensor and deep learning-based structural health monitoring systems for civil structures: A review” *Measurement*, Vol. 199: 11154 (2022). <https://doi.org/10.1016/j.measurement.2022.111543>
- [155] K. S. C. Kuang, W. J. Cantwell. “Use of conventional optical fibers and fiber Bragg gratings for damage detection in advanced composite structures: A review” *Applied Mechanics Reviews*, Vol. 56-5 (2003): 493-513. <https://doi.org/10.1115/1.1582883>
- [156] M. Majumder, T. K. Gangopadhyay, A. K. Chakraborty, K. Dasgupta, D. K. Bhattacharya. “Fibre Bragg gratings in structural health monitoring—Present status and applications” *Sensors and Actuators, A: Physical*, Vol. 147-1 (2008): 150–164. <https://doi.org/10.1016/j.sna.2008.04.008>
- [157] B. D. Liu, W. J. Lv, L. Li, P. F. Li. “Effect of moisture content on static compressive elasticity modulus of concrete” *Construction and Building Materials*, Vol. 69 (2014): 133-142. <https://doi.org/10.1016/j.conbuildmat.2014.06.094>
- [158] M. Y. L. Chew. “Façade inspection for falling objects from tall buildings in Singapore” *International Journal of Building Pathology and Adaptation*, ISSN: 2398-4708 (2021). <https://doi.org/10.1108/IJBPA-10-2020-0087>
- [159] K. Tomita, M. Y. L. Chew. “A Review of Infrared Thermography for Delamination Detection on Infrastructures and Buildings” *Sensors*, Vol. 22(2): 423 (2022). <https://doi.org/10.3390/s22020423>
- [160] JASS19, (2022). “Japanese Architectural Standard Specification—JASS19 Ceramic tiling work.” Tokyo: Architectural Institute of Japan. (In Japanese)
- [161] T. Soeta, S. Ito, T. Fujinuma, T. Mikami. “Trial inspection of exterior-tile wall specimens with a prototyped tile debonding diagnostic device” *Journal of Structural and Construction Engineering (Transactions of AIJ)*, Vol. 85-767 (2020): 1-9. (In Japanese) <https://doi.org/10.3130/aijs.85.1>
- [162] 川口莉穂 (2021) 「センシング技術を用いた非構造建築部材の定量的評価手法の提案」、修士論文、広島大学。
- [163] W. Y. Liao, Y. Y. Zhuang, C. Zeng, W. Deng, J. Huang, H. Y. Ma. “Fiber optic sensors enabled monitoring of thermal curling of concrete pavement slab: Temperature, strain and inclination.” *Measurement*, Vol. 16: 108203 (2020). <https://doi.org/10.1016/j.measurement.2020.108203>
- [164] W. Q. Guo, Y. Wei, L. Ma. “Shrinkage-induced warping of UHPC overlay cast on hardened NSC substrate under various conditions” *Cement and Concrete Composites*, Vol. 134: 104772 (2022). <https://doi.org/10.1016/j.cemconcomp.2022.104772>